Università degli Studi di Salerno

Facoltà di Scienze Matematiche Fisiche e Naturali

Dottorato di Ricerca in Fisica – IV ciclo Nuova Serie

R&D on OPERA ECC:

studies on emulsion handling and event reconstruction techniques

Chiara Sirignano

Tutor : Prof. Giuseppe Grella A.A. 2004/2005

To Fulvio for his daily respect, love
and fruitful collaboration…

Acknowledgments

In this thesis there is a really short review of my last three years life. None of those exciting experiences and results could have been possible without help, collaboration and friendship of several people so I would like to strongly thank all of them.

First of all I am grateful to Prof. Giuseppe Grella for his continuous and friendly support and to Prof. Giorgio Romano for sharing with me his endless knowledge about nuclear emulsions and physics.

I shared my daily activities with many people and I must show appreciation to all of them for bearing, trusting and helping me.

Since the first second I entered the Salerno lab, five years ago, I found four new friends, Cristiano, Emiliano, Maurizio and Salvatore, they introduced me to neutrino physics community, computer programming, grains, tracks, vertices, TT predictions, charm decays, efficiency and …. many others interesting or just funny features !

I would like also to thank Prof. Giovanni Rosa and Ing. Salvatore Buontempo for our fruitful collaboration and discussions about many many OPERA related items.

Special thanks to Prof. Kimio Niwa and Prof. Mitsuhiro Nakamura and to all the members of Nagoya F-Ken in particular to Ariga, Naganawa, Hiramatsu and Taku Nakamura for their helpful collaboration and sharing of experiences about nuclear emulsions and refresh chambers dangerous construction … and also for their friendship during my stay in Japan.

I spent 30 % of the last three years in a dark room and I will never forget all the people that were with me, there were many heavy jobs to do! Many thanks to Romolo, Pasquale, Vito, Emilia, Claudia, Vincent, Aldo, Alessandra and Donato.

Finally I have to be grateful to my family : father, mother and sister Cristina for bearing me….it has been very hard but they had never gave up!

Introduction

I accomplished my Ph.D. research activity in Salerno Emulsion Group that is involved in the preparation of OPERA experiment: an European-Japanese project that will study neutrino oscillations. In particular it is expected to observe $\nu_\mu \rightarrow \nu_\tau$ oscillation signal via the direct reconstruction of ν_τ interactions in a target of nuclear emulsions films and lead. The experiment will use of a high energy ν_μ beam produced at CERN and of a detector placed in the LNGS underground laboratory; the sub-micron spatial resolution provided by nuclear emulsions will allow to identify oscillation signal with a very low background level. This aspect makes OPERA an inimitable challenge, in the case of neutrino oscillation direct observation there will be the conclusive verification of all the results obtained by other experiments (Kamiokande, SuperKamiokande, K2K). The OPERA detector will consists of 12 million nuclear emulsion films and in order to guarantee their analysis it has been necessary to realize an automatic scanning system having remarkable speed and precision in the reconstruction of neutrino interactions, furthermore detector construction and emulsion handling related items needed a dedicated R&D activity. In these months the OPERA collaboration is carrying out the detector assembly and the physical data acquisition is expected to start in July 2006.

Salerno Emulsion Group joined Opera Experiment since its very beginning and is mainly involved in emulsion handling and scanning; I will report about my contribution to these two activities in the following pages.

The thesis has the following structure:

- a brief history of nuclear emulsions and a description of their basic properties such has latent image formation and high energy particles tracks characteristics;
- review of neutrino physics and neutrino oscillation search experimental results;
- review of last experiments exploiting nuclear emulsion technique. Nuclear emulsions high spatial resolution allowed important results in neutrino and neutrino induced charm physics. DONUT collaboration reported the ν_τ first direct observation, their detector has an ECC structure (Emulsion/Iron target) similar to the one that will be used in OPERA. CHORUS experiment had a large emulsion neutrino target and reported the largest sample of neutrino induced charm events; Salerno Group was involved in that experiment and realized a fully automatic emulsion scanning system that inspired the one that will be used in OPERA.
- review of my work and personal experience on Opera ECC design and test. Emulsions and lead sheets are supposed to be in contact for years inside Opera detector, so it is necessary to guarantee no damage on the emulsions due to lead radioactivity or chemical reactions between lead, emulsion films, other brick components and the Gran Sasso experimental environment. All these items lead to an intense R&D activity that has been vital for the entire experiment.
- review of my work on CS detector self-refreshing studies, emulsion development and description of the gridding and labeling machine designed and realized in Salerno. The huge amount of emulsion films that will be used in OPERA requested very accurate

design of emulsion handling infrastructures foreseen at LNGS; in particular the development phase was studied in order to keep the emulsion quality suitable for fast and accurate automatic physics analyses. The large quantity of films that will be handled every day deserved to develop an automatic labeling procedure to keep ECC and Sheet unique identities; the labeling procedure will be accomplished by an optical device that has been entirely designed and realized by Salerno Group. An accurate description of this apparatus is given in this section.

- European Emulsion Scanning system is described in this section and also a detailed review of pion interaction location study is given. Results reported refer to several Pion exposures to PS beam at CERN and are the first significant OPERA rehearsal. On the basis of those test-activities it has been possible to evaluate efficiency and limits of our hardware and software tools.

Nuclear Emulsions

*"…*On April 7, 1959 a rocket carried a package containing various instruments into the lower of the van Allen radiation belts. The existence of this radiation belt was known at that time but its nature was not. The rocket's nose was recovered; in it there were a few postage-stamp size pieces of nuclear emulsion that have a story to tell. During the 15 minutes that the rocket remained at an altitude above 100 Km, the emulsion had gathered complete information about the radiation. Proton tracks in the emulsion definitely established the nature of the ionization that had been detected previously. Freden and White at the Livermore branch of the Lawrence Radiation Laboratory analyzed the tracks. They determined the proton energy spectrum, the flux density, and observed that other types of nuclei where almost completely absent*…"*[1]

This experiment is a good example of the peculiar fitness of emulsion for exploratory investigations. Nuclear emulsions were developed largely for the study of atomic nuclei and elementary particles. Most of nuclear physics can be witnessed by careful study of reactions seen to take place in the body of em
ulsions itself.

An indication of emulsions usefulness as an instrument of discovery is given by Table 1.1; there are listed the elementary particles found since 1946 when emulsion came into use for such investigations.

π^+	Emulsion
π^-	Emulsion
π^0	Counter and emulsion
Λ	Cloud chamber
K^+	Emulsion
K^-	Emulsion
K^0	Cloud chamber
Σ	Emulsion
Σ	Cloud chamber
Σ	Bubble chamber
Ξ	Cloud chamber
Ξ	Bubble chamber
p	Counters
n	Counters
Λ	Emulsion
ν_τ	Emulsion Cloud Chamber

Table 1.1

Nuclear research emulsions were first developed in the 1940s to meet the needs of physicists engaged in research on cosmic radiation. The range of materials was improved and extended throughout the following decade until workers in many fields recognized the versatility of nuclear emulsions in the recording of charged particles and ionizing radiation. Now they are extensively used in autoradiography, in medical and biological research, in metallurgy and in the study of chemically reactive surfaces [2].

Basic properties

Emulsions used for the charged particles tracks recording consist of an inorganic component, silver halide micro crystals (a few tenth of a micron in diameter), and usually about an equal volume of "gel phase", consisting mainly of gelatin with a variable quantity of water and small amounts of glycerol, sensitizes and possibly other substances. The equilibrium water content depends on the relative humidity and temperature of the air in contact with the emulsion [1].

The silver halide is usually in the form of silver bromide crystals with a small amount of iodine in the crystal lattice; there have been also attempts to replace the gelatin matrix of the emulsion by synthetic materials, but thus far without complete success.

The size of the silver halide crystals will determine the sensitivity of the emulsion; large grains are more sensitive to ionizing radiation than small ones. In general, a low sensitivity emulsion is used to detect high-energy radiation or particles, as there is plenty of energy available to free electrons. However, a more sensitive emulsion is required to detect very high-energy particles as they deposit very little energy along their tracks and travel too fast to be trapped by the silver halide crystals [3].

Nuclear emulsions are fundamentally the same as general-purpose photographic emulsions, but have several distinguishing features:

- silver halide crystals are very uniform in size and sensitivity
- there are very few crystals that may be developed without exposure to a charged particle
- the silver to gelatin ratio is much higher than in a conventional emulsion

A ionizing particle encountering a crystal may render it developable. After development, followed by fixing and washing to remove the undeveloped crystals, the gelatin is transparent. With a microscope the paths of charged particles that penetrated the emulsion are visible as trails of minute dark silver grains. The 3D paths of particles, outlined by silver, literally exist in space.

The latent image

For many years the nature of silver halide sensitivity has been one of the most challenging problems of solid-state physics and physical chemistry. The useful effect is this: when a silver halide crystal absorbs energy from photons or moving charged particles incident on it, it may be conditioned by this experience so that, under the action of a chemical reducing agent, conversion of the halide to metallic silver will proceed more rapidly than in an unirradiated crystal. This capacity to be rendered developable by a small amount of energy is for us the important attribute of silver halide crystals. The physical condition in the crystal that makes it developable is called latent image.

It is well established that the latent image consists of a small quantity of elemental silver (known as specks, germs, etc…) collected at one or more points in the crystal known as latent image sites. The amount of silver in the latent image has been measured in several experiments, the result is that about 3 atoms is the mean amount of silver in a crystal of 0.1μm volume in emulsion that has received just a threshold exposure; whereas 30 atoms constitutes a medium exposure, and 100 atoms is a heavy exposure. Svedberg found that the number of latent-image sites per crystal was distributed according to Poisson's law when one considers crystals only of a single size. This means that, unless the average number of latent image sites is large, there will be a finite probability that some crystals will possess no site where a stable latent image can form.

The silver that collects in latent image specks as a result of exposure to light is called photolytic silver. It is possible to broaden this meaning somewhat to include also the silver reduced by the passage of charged particles trough the crystal. If the exposure of a crystal is prolonged, photolytic silver may continue to accumulate on that already deposited, and the process can go on to the point that much of the silver in the crystal is reduced; it is known as the print-out effect.

It has been demonstrated that the latent image is actually silver, X-ray powder diffraction patterns of silver halide that have been exposed to light show evidence of metallic silver, while unexposed halide does not. When the silver halide is dissolved in the fixing solution (usually sodium thiosulfate solution) only a silver lattice remains of the exposed crystal. Much of modern thought of the photographic process stems from ideas developed by Gurney and Mott who proposed a theory of silver halide sensitivity in 1938. For the first time quantum mechanics and then the available solid-state theory were applied to this problem. As their most important contribution Gurney and Mott adduced the idea that both electronic and ionic conduction play a part in the production of the latent image, more precisely they consider two processes: photoconductivity and ionic conductivity.

Ionic conductivity

The high ionic conductivity [4] in silver halide crystals is one of the properties which distinguishes them from most other ionic crystals. This conductivity is important to all considerations on the photolysis of silver halides; as will be discussed below, it can occur both by ions in interstitial positions and by the holes left in the structure when interstitial ions are formed.

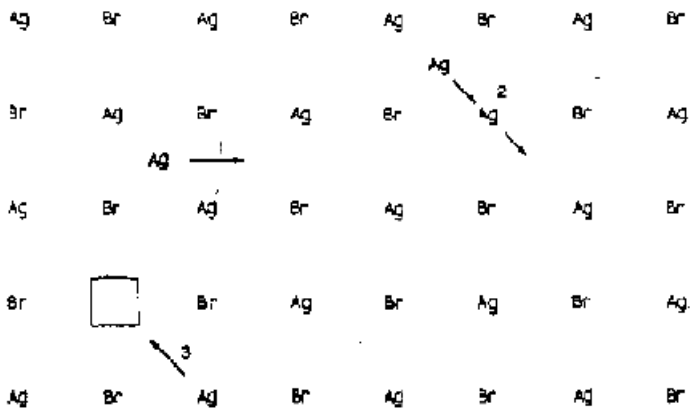

Fig. 1.1 - Mechanism of ionic conductivity in silver halides (bromide). The Ag and Br ions are arranged as in a cubic face of the crystal. In (1) an Ag ion moves from one interstitial position to another, which must be imagined to he situated one half of a lattice distance below or above the plane; in (2) a silver ion in a normal position moves into an interstitial position and is replaced by one coming from an interstitial position; (3) is the replacement by which the holes move.

The interstitial silver ions always formed in silver halide crystals in thermal equilibrium must be imagined to occupy positions in the centre of the unit cube of the structure. Some distortions of the structure occurs and thus a formation of energy is involved. The bromide ions are to large to be able to occupy interstitial positions. The silver ions are mobile, although requiring a certain activation energy.

The hole left in the structure when an interstitial ion is formed has been shown to be itself mobile, the mechanism is a replacement; a neighboring ion jumps into the hole, leaving a hole at the place whence it came (mechanism 3 in figure 1.1). The activation energy of this process is of the same order of magnitude as that for the movement of interstitial ions. Holes and interstitial ions, therefore, contribute similar amounts of the overall electrolytic conductivity. The concentration of both in a crystal may be affected by the presence of impurities , such as bivalent ions, which according to their charge are balanced by surplus silver ions or holes.

It has been estimated that at room temperature it takes 10^{-3} to 10^{-6} seconds to form a thermal equilibrium concentration of interstitial ions in silver bromide and between 10^{-2} to 10^{-1} second for silver chloride.

The values for the concentration of ions and holes in the small crystals which exist in a photographic emulsion are likely to differ considerably from those in the bulk material. Grimley and Mott (1947) have investigated theoretically the conditions existing at the interface between silver bromide and an electrolyte or metallic silver respectively. The calculations show that adsorption in the normal meaning of the term of bromide or silver ions to a silver halide surface is unlikely to occur. The crystal is negatively charged because near its surface there exists a surplus of vacant silver lattice points, and in the electrolyte surrounding it there is a surplus of silver ions. As a result, the ionic conductivity of the crystal near the surface may be several orders of magnitude higher than that in the bulk. The whole of an emulsion grain must be considered as being "near the surface" in this sense. Similarly, near the silver bromide-silver interface, there is a stechiometric surplus of vacant silver lattice points. Thus a thin layer of silver halide on metallic silver will have a considerably higher ionic conductivity than a large crystal.

Photoconductivity

A silver halide crystal kept in the dark at sufficiently low temperature is an electric insulator. Absorption of light by the crystal produces a conductivity of electronic nature. Each quantum of light absorbed is capable of producing an electron which can be drawn across the crystal to the anode if an electric field of sufficient strength is applied. Electrons carrying photo-current are considered to be removed from the halogen ions in the crystal lattice and raised into the conduction levels. In the conduction levels electron moves with thermal energy and its diffusion coefficient is of the order of 1 cm^2/s. A crystal of silver halide containing colloidal metal particles or particles of silver sulphide exhibits the effect of trapping of electrons to a much greater degree than a pure crystal. This means that the conduction levels of silver or silver sulphide are below those of the silver halides, so that electrons passing from the silver halide into a silver speck cannot be free again.

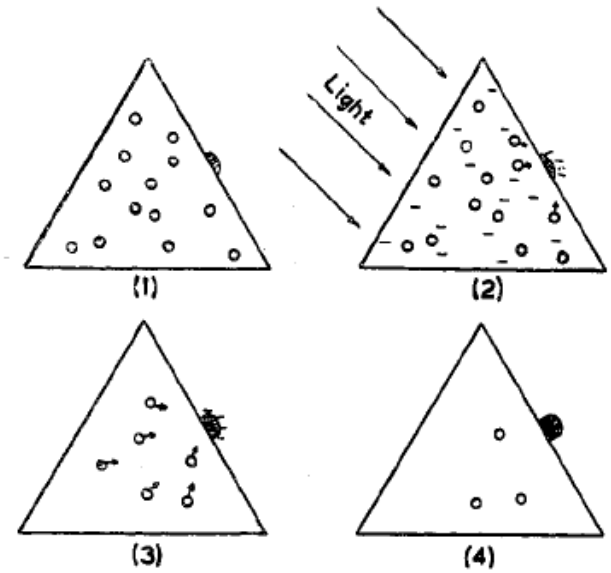

Fig.1.2 – Diagram of latent image formation according to Gurney and Mott. The triangle represents a silver halide grain, O=interstitial ions, -=photo-electrons; shaded areas=sensitivity specks; solid area=latent image.

Latent image formation

Gurney and Mott proposed that photons are absorbed in silver halide to produce electrons in conduction band and positive holes. The electrons move freely until they encounter a local potential energy minimum where they can be trapped. Colloidal silver and sensitivity specks, believed by Sheppard to be silver sulfide, were conceived to be such traps. The traps after capturing electrons, being then negatively charged, would attract interstitial silver ions to the trap sites, and particles of silver can be formed. The migration of silver to the surface latent images sites can proceed with low activation energy and it is supposed to take place.

This description is devoted to the effect of light on photographic emulsions, which is characterized by the fact that a single quantum of light has sufficient energy to make a grain developable. The photographic process, however, is not confined to light, and it is applied to the recording of energy quanta as of X rays and gamma rays or charged particles.

Fading

The latent image of a particle track gradually fades after exposure; so that if the emulsion is left unprocessed the developed grain density will be smaller the longer is the elapsed time between exposure and processing. This action is more rapid in emulsions of small grain size, and for emulsions kept at high temperature and/or humidity. This effect is used to eradicate old tracks from the emulsion. The stability of the latent image apparently depends at least partly on the sensitizing agent used in the manufacture of the emulsion; gold is known to produce quite a stable image. The presence of oxidizing agents such as hydrogen peroxide or chromic acid greatly accelerates fading. Because of the fading that takes place emulsions should be developed soon after exposure and in the interim they should be kept cold and dry. The fading is expressed as a coefficient:

$$F = \frac{N_0 - N}{N_0}$$

the quantity N_0 is the initial grain density while N is the grain density at a later time.

Albouy and Faraggi have carried out extensive studies of latent image fading with the following results: at constant humidity the rate of fading increases exponentially with the absolute temperature and at constant temperature the fading increase exponentially with the quantity of water retained by the gelatin, at constant temperature and humidity the fading increases with increasing oxygen content of the gas in contact with the emulsion. All experimental results confirmed also that the rate of fading varies inversely with the size of the latent image speck.

It was found that the fading near the surface is most pronounced, but this effect falls off rapidly with dept so that at 40 to 60 μm below the surface, the surface effect has vanished. In addition, a uniform fading that varies with the time, temperature, humidity, and degree of development, takes place throughout the emulsion volume. The surface effect is attributed to oxygen from the atmosphere, but the volume effect seems to have a different origin.

Ionization and track structure

The aim of nuclear research emulsion is to detect tracks of ionizing charged particles. Their detection depends on the fact that directly or indirectly they transfer energy to the medium they are traversing via ionization or excitation of the constituent atoms [5]. The Bethe-Bloch formula for the mean rate of energy loss of a charged particle is given by

$$\frac{dE}{dx} = \frac{4\pi N_0 z^2 \alpha^2}{mv^2} \frac{Z}{A} \left\{ \ln\left[\frac{2mv^2}{I\left(1-\beta^2\right)} \right] - \beta^2 \right\}$$

where m is the electron mass, z and v are the charge (in units of e) and velocity of the particle, $\beta = \frac{v}{c}$, N_0 is Avogadro's number, Z and A are the atomic number and mass number of the atoms in the medium, and x is the thickness, which is measured in g cm^{-2} or Kg m^{-2}, corresponding to the amount of matter transversed. The quantity I is an effective ionization potential, averaged over all electrons, with approximate magnitude I=10ZeV.

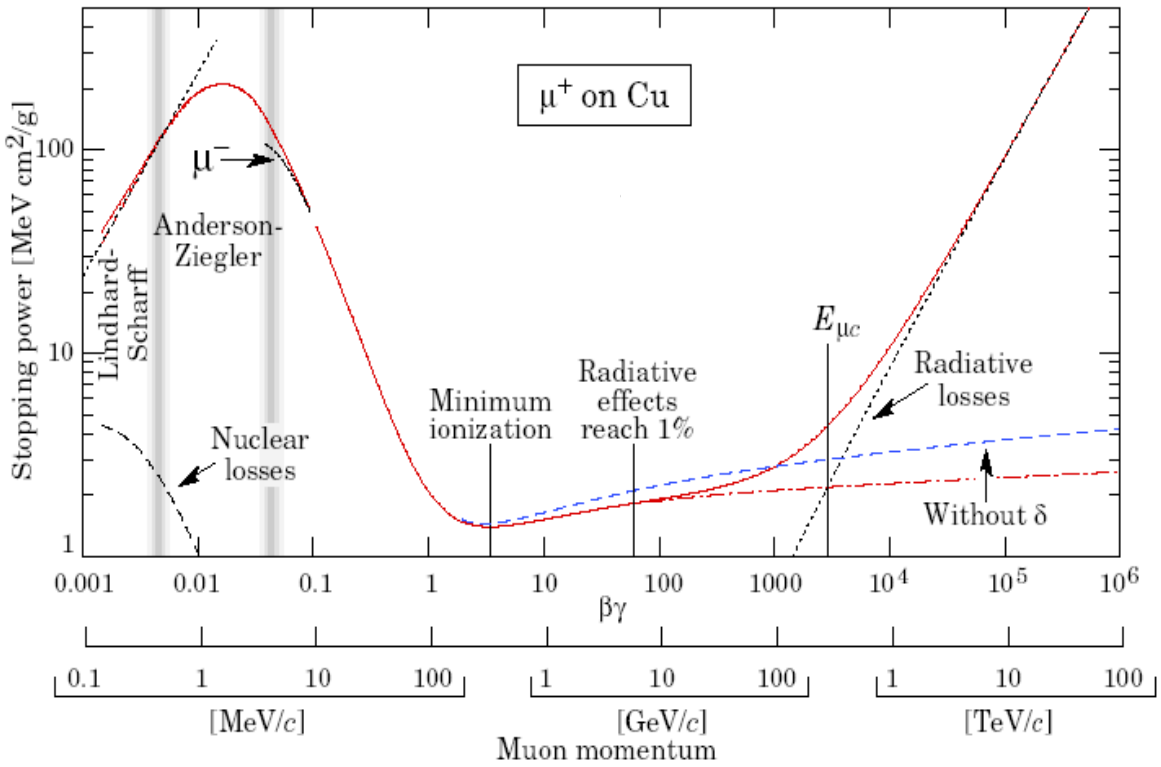

Fig.1.3 – Energy loss by a charged particle.

Equation shows that dE/dx is independent of the mass M of the particle, it varies as $1/v^2$ at non-relativistic velocities and, after passage through a minimum for $E \approx 3Mc^2$, increases logarithmically with $\gamma = E/mc^2 = \left(1-\beta^2\right)^{-1/2}$. The dependence of dE/dx on the medium is very weak, since $\frac{Z}{A} \approx 0.5$ in all the heaviest elements. Numerically $\left(dE/dx\right)_{\min} \approx 1-1.5 MeV$ cm^2 g^{-1} (or $0.1-0.15 MeV$ m^2 kg^{-1}).

Figure 1.3 shows the relativistic rise in ionization loss as a function of $p/mc = \left(\gamma^2-1\right)^{1/2}$ for relativistic particles; for $\gamma \approx 10^3$ it reaches 1.5 times the minimum value. The relativistic rise is partly associated with the fact that the transverse electric field of the particle is proportional to γ, so that ever more distant collision become important as the energy increases. Eventually, when the impact parameter becomes comparable to interatomic distances, polarization effects in the medium (associated with the dielectric constant) halt any further increase.

The bulk of energy loss results in the formation of ion pairs in the medium. The electrons knocked out in this process have a distribution in energy E' roughly of the form $dE'/(E')^2$; those of higher energy, called δ rays, can themselves produce fresh ions traversing the medium (secondary ionization). The resultant total number of ion pairs is 3-4 times the number of primary ionization, and it is proportional to the energy loss of the incident particle in the medium. Our equation gives the average value of energy loss dE in a layer dx, but there will be fluctuations about the mean, dominated by the relatively small number of primary collisions with large E'. The so-called Landau distribution about the mean value is therefore asymmetric, with a tail extending to values much greater than the average. Nevertheless, by sampling the number of ion pairs produced and removing the tail the mean ionization can be measured within a few percent. In this way γ can be estimated from the relativistic rise and, if the momentum is known, this can provide a useful method for estimating the rest mass and differentiating between pions, kaons and protons.

Energy loss in emulsion

The energy loss in unit path occurred to a point charge penetrating matter is usually estimated using Bethe-Bloch formula[6], it is derived from the differential energy transfer cross section, the energy loss per centimeter J is:

$$J = n\int_{w_0}^{w_{\max}} w\frac{d\sigma}{dw}dw + n\int_{w_{\min}}^{w_0} w\frac{d\sigma}{dw}dw = J_1 + J_2$$

where n is the electron density in the stopping medium, w_0 is the energy sufficient to consider free the electrons in the stopping medium involved in the collision.
In case of close collision the result is and it is related to secondary ionization:

$$J_1 = \frac{2\pi n z^2 r_0^2 mc^2}{\beta^2}\left[\ln\frac{w_{\max}}{w_0} - \beta^2\right]$$

The second part (J_2) is related to the energy transferred to the crystal in the process of latent images formation, the calculation should consider all the possible electronic transitions inside the molecules so it is important to study the detailed structure of the material. In this case in the result we have the quantity I, for a range of high velocities it depends only on the atomic number Z of the stopping material. It is defined in terms of the oscillator strengths f_α as follows: $\ln I = \sum f_\alpha \ln W_\alpha$. The transition probability from the initial state in which an electron exists to an excited state of relative energy W_α is governed by the oscillator strength $f_\alpha = \left(2mW\alpha/\hbar^2\right)\left|x_\alpha\right|^2$. The matrix element $\left|x_\alpha\right|$ is calculated for the electron coordinate x between the two states in question and the set of final states extends into the continuum, these calculations are difficult and have not been done exactly.

For a composite material such emulsion, I is defined by:

$$n \ln I = \sum N_i Z_i \ln I_i$$

where N_i is the density of atoms of atomic number Z_i and mean ionization potential I_i in the composite material. Except at low velocities the stopping effect of the various atoms is nearly additive. In this way a mean ionization potential $I = 331 \pm 6$ eV was found.

For protons of energy above 40 MeV the computed rate of energy loss is consistent with these experimental data; at somewhat lower velocities, where the detailed structure of the stopping atoms introduce great theoretical complications, the empirical energy-loss behavior is best described by a smooth deviation from the formula.

Restricted energy loss

In the previous section the total energy-loss rate has been divided in two parts: J_1 that is related to close collisions and J_2 that is related to the latent image formation. In emulsion close collisions produce δ rays and they don't contribute to the track and also the energy dissipated in the gel has little effect on the grain density of the tracks. Only energy remaining in silver bromide atoms can be used to produce latent image and grains.

So it is needed to calculate the energy-loss rate available to produce primary grains and it is called restricted energy–loss, there are empirical data (Table 1.2) and the formula is the following:

$$i' = \frac{2\pi r_0^2 mc^2 (n/\rho)}{\beta^2}\left(\ln\left(\frac{2mc^2}{I^2}\beta^2 y^2 w'\right) - \beta^2 - 2C(\beta)\right)$$

where n/ρ is the number of electron per gram of Ag Br, I≅ 450 eV and the relativistic factor $C(\beta)$ has been calculated by Sternheimer and Walsk .

Energy (MeV)	i' (MeV g^{-1} cm^2)	$C(\beta)$MeV
2	56	--
5	27.3	0.077
10	15.8	0.104
20	9.13	0.095
100	2.65	0.037
1000	0.824	0.002
5000	0.781	0.171
10^4	0.814	0.431
2×10^4	0.848	0.792

Table 1.2

From the above formula we have that the primary ionization and so the primary track density is expected to be the same for particles having the same speed in emulsion, no exceptions to this results has been found since now.

δ rays

In case of close collisions when an electron receives an energy exceeding w_0 (for example 2 KeV), it could be projected out of the trajectory of the primary particle and it is called δ ray[1]. The differential cross section for transfer of energy in the interval dw to a stationary unbound electron is:

$$\left(\frac{d\sigma}{dw}\right)dw = \frac{2\pi z^2 r_0^2 mc^2}{\beta^2}\left(1 - \frac{\beta^2 w}{w_{\max}}\right)\frac{dw}{w^2} \quad \text{cm}^2$$

The particle velocity is βc, m is the electron mass and $r_0 = e^2/mc^2$. The energy of such knock on electrons extends up to the maximum value

$$w_{\max} = \frac{2mc^2\beta^2\gamma^2}{1 + 2\left(\frac{m}{\mu}\right)\gamma + \left(\frac{m}{\mu}\right)^2}$$

The lower limit of w that defines a recognizable delta ray in emulsion depends on many things. These include the range energy relation for low-velocity electrons, the grain size of the emulsion, the scattering of these slow electrons, the sensitivity of the emulsion and the density of background electron tracks. The density of delta tracks increases with the square of particle

charges, but in counting them it must be considered that the core of the tracks broadens as the particle charge increases, and the conventions may require adjustment for tracks of very heavy nuclei. For light nuclei the delta rays density is $n_\delta = z^2 v$ when the velocity is high enough for nucleus to be stripped of electrons. The total number of delta rays on a track between the point where the particle velocity is βc and the point where it comes to rest is:

$$N_\delta = \int_0^R n_\delta dR$$

There is an apparent narrowing of a multiply charged ion track as it slows down in emulsion, this effect is known to be a delta ray phenomenon. The maximum range of delta rays increases with the particle velocity, a wide track will be observed when the velocity is high enough so that the delta rays extends beyond the primary particle trajectory, and when they are also dense enough to give an appearance of continuity. Obviously, the emulsion grain size and sensitivity, as well as the amount of physical development, affect the appearance of the track.

Theory of the primary grain density

Barkas [1] developed a theory to describe the primary track grain density, that theory is related to all the phenomena after the latent image formation. He wanted to obtain some relations between the amount of energy lost by a charged particle traversing nuclear emulsion and its track. The restricted average energy loss per unit path of a moving particle is:

$$J' = ne \int_0^{w'} w \frac{d\sigma}{dw} dw$$

where w' is the maximum energy that the electrons can absorb from the moving particle before escaping from AgBr crystals and produce δ rays.
It is possible to evaluate the probability $E(w)$ that the energy will be used to make a crystal developable only measuring the emulsion sensitivity to photons of different energies.
Then we can evaluate the effective rate of energy loss as:

$$J'' = ne \int_0^{w'} w \frac{d\sigma}{dw} E(w) dw$$

It turned out that the energy usage is very inefficient; a charged particle in emulsion loses about 1KeV per developed grain, while photons require only 10 eV per grain. Barkas, Brown, Fowler and Perkins claimed that the energy dissipation of a charged particle in a grain is a stochastic process. In a simple model we assume that the probability to have a developable grain depends on the local sensitivity s, the effective rate of energy loss J'' and the path dy. In this scenario we define a probability Ψ that a crystal of diameter D remains undevelopable after being penetrated by a charge particle and we define that

$$\Psi = e^{-sJ''y}$$

The probability that the crystal has been completely traversed without being developable is

$$G = e^{-sJ''\delta}$$

where δ is the track segment in the crystal.

In this scenario we assume that there is a mean free path $\frac{1}{sJ''}$ for developability; we are neglecting the fact that the developability also depends on the cumulative effect of previous charged particles traversing the same crystal and we are also considering s as constant. In fact we know that surface sensitivity centers are more accessible to the reducing action of the developer and the migration distances of electrons and silver are not know.

Barkas introduced some free parameters to offer to his theory the possibility of an experimental evaluation and fine-tuning. If it is to be taken into account a radial variation of sensitivity we will have the following probability that a crystal would not be rendered developable:

$$G = e^{-J''s\delta F\left[(D-\delta)/b,\,\delta/b\right]}$$

Where b is a characteristic length describing how rapidly the sensitivity varies along the radius and the function f is expected to increase when $(D-\delta)/b$ increases, to take into account cumulative effects, it has been introduced a second characteristic length, a, which has the meaning that the effect of a charged particle passage will have little effect on points more remote than a distance a. Then to allow for all these probabilities we have such expression:

$$G = 1 - \sum_{i=1}^{\infty}\sum_{j=0}^{\infty}\sum_{k=0}^{\infty} A_{ijk}\left(D/b\right)^{j}\left(\delta/a\right)^{k}\left(\delta sJ''\right)^{i}$$

If the total cross-section Ω for one crystal developability can be calculated as:

$$\Omega = (\pi/2)\int_{0}^{D}(1-G)\delta d\delta$$

the primary grain density in a track will be:

$$g_p = N\int_{0}^{\infty}\Omega F(D)dD = \frac{\pi N}{2}\int_{0}^{\infty}F(D)dD\int_{0}^{D}(1-G)\delta d\delta$$

All the coefficients introduced should be measured by experiments and they are different in any emulsion type, only the value J'' can be fixed by the investigator.

From experimental results we also found out that g_p is a function of J'' and that all the track formation process is largely affected by fluctuations. Each single crystal sensitization is an independent event and its probability is a function of δ, the number of developed grains per unit path has a poissonian law.

Structure of the developed track

From the restricted energy loss equation we evaluate that the energy used to render developable a single AgBr crystal is $J_0 \cong 34KeV/100\mu m$. In Figure 1.2 [6] we have J/J_0 as a function of γ for single charged particles. If $J/J_0 >> 2.5$ it is better to consider that $J = K\frac{Z^2}{\beta^2}$.

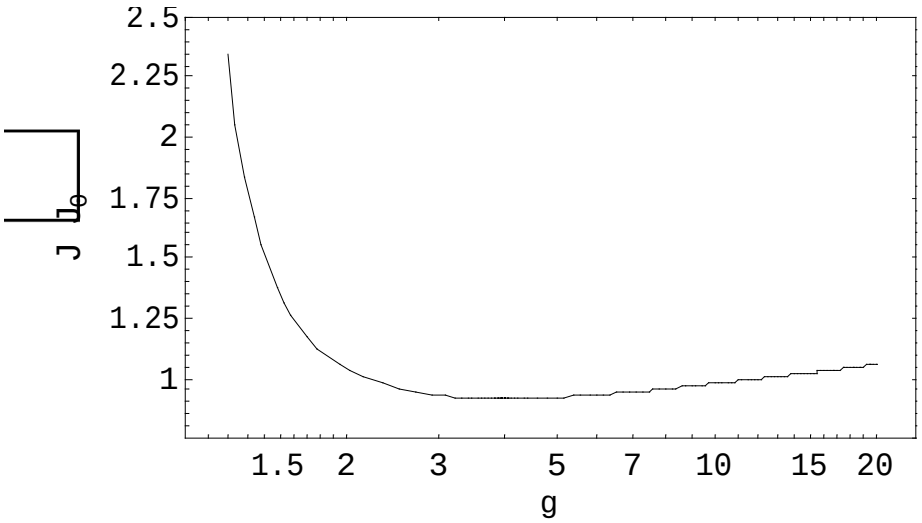

Fig.1.2

The ionization curve should be calibrated on each emulsion type; usually the calibration is realized used electron having γ≈ 3. It is very difficult to measure the primary grain density directly in emulsion because of fading and distortions; there are also problems because the development is not uniform as a function of depth in emulsion.

Grain distribution along tracks is not uniform and there are agglomerates and holes along the trajectory. Gaps' distribution has the following law:

$$N(l) = N_0 e^{-\frac{l}{\lambda}}$$

where $N(l)$ is the number of gaps having a length bigger than l and N_0 is the total amount of gaps in one track; λ is proportional to the ionization I. In this way it is possible to know I only counting gaps. These measurements are difficult in case of very short gaps ($l < 0.5\mu m$), in this case it is possible to count only gaps longer than some fixed values as α_1 and α_2 and we will have that:

$$\lambda = \frac{\alpha_1 - \alpha_2}{\ln(N_1 - N_2)}$$

δ rays coming from close collision do not take part in the track formation but they exist along the developed track and they look like small and curly emerging from the primary one. Their number can be used to evaluate extremely big energy loss in emulsion and also the primary particle direction. In fact they are usually emitted in the forward direction and then suddenly scattered everywhere. When $\beta \to 1$ we know that $N_\delta \to AZ^2$ and so the measure is quite easy. The exact density depends on emulsion sensitivity and grain dimensions but usually it is measured N_δ <1 δ ray/100 μm.

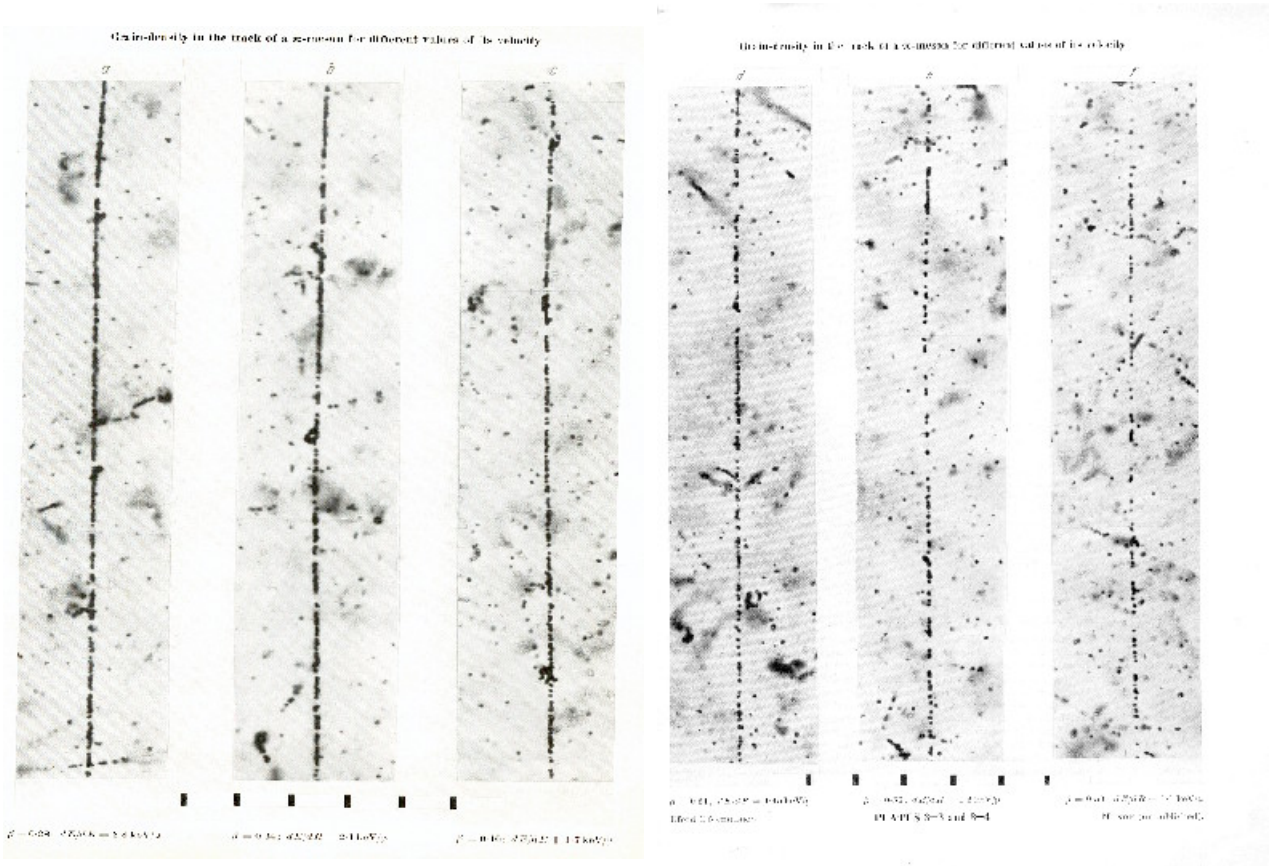

Restricted energy loss

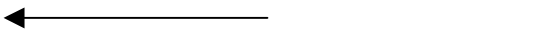

β

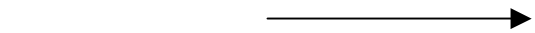

Neutrino Oscillation

Neutrino existence was postulated in 1931 by W. Pauli [7][8] to explain the apparent energy non-conservation in nuclear weak decays, 28 years after this bold theoretical proposal was verified experimentally in a reactor experiment performed by C. Cowan and F. Reines [9]. Pauli based his prediction on the fact that energy and momentum did not appear to be conserved in certain radioactive decays. He suggested that this missing energy might be carried off, unseen, by a neutral particle which was very difficult to detect.

In 1934 Enrico Fermi developed a comprehensive theory of radioactive decays, including Pauli's hypothetical particle and he called it neutrino. With inclusion of the neutrino, Fermi's theory accurately explains many experimentally observed results.

The neutrino was shown to be left-handed in an ingenious experiment by Goldhaber, Grodzins, and Sunyar in 1957[10]. The distinct nature of ν_e and ν_μ was demonstrated in 1962 in a pioneering accelerator neutrino experiment at BNL by Danby[11]. The following years saw a remarkable progress in neutrino experiments, especially those utilizing accelerators as their sources. Increases in available accelerator energies and intensities, advances in neutrino beam technology and more sophisticated and more massive neutrino detectors were all used to do ever more precise neutrino experiments. Together with experiments utilizing electrons and muons, the worldwide neutrino program played a key role in measuring the nucleon structure functions. And together with a variety of other efforts (especially $e^+ e^-$ annihilations and deep inelastic electron scattering) the neutrino experiments played a key role in establishing the validity of the Standard Model (SM), through the discovery of neutral currents, measurements of the NC/CC ratio, and measurements of the neutrino lepton scattering cross sections.

The main thrust in the future will probably be twofold: better understanding of the nature of the neutrino and use of the neutrino in astrophysics and cosmology as an alternative window on the universe, complementing the information obtained from studies of the electromagnetic spectrum.

The first experiment to detect [12](electron) neutrinos produced by the Sun's burning (using a liquid Chlorine target deep underground) reports that less than half the expected neutrinos are observed (1968). This is the origin of the long-standing solar neutrino problem. The possibility that the missing electron neutrinos may have transformed into another type (undetectable to this experiment) is soon suggested, but unreliability of the solar model on which the expected neutrino rates are based is initially considered a more likely explanation.

The tau particle is discovered at SLAC (1978), the Stanford Linear Accelerator Center. It is soon recognized to be a heavier version of the electron and muon, and its decay exhibits the same apparent imbalance of energy and momentum that led Pauli to predict the existence of the neutrino in 1931. The existence of a third neutrino associated with the tau is hence inferred and experimentally proved by DONUT collaboration in 1999[13].

Neutrino oscillation hypothesis

Phenomenology

We believe that neutrinos are among the fundamental constituents in nature. In addition, the space around us is permeated with neutrinos that are relics of the Big Bang. But our knowledge of the neutrino's properties lags far behind our knowledge of other elementary constituents, for example, the charged leptons.

We do not know whether neutrinos have a mass; our current information gives us only upper limits ranging from a few eV for ν_e to some 20 MeV for ν_τ. We can contrast that with a fractional mass error of about 3×10^{-7} for the electron and muon and about 2×10^{-4} for the tau.

We do not know if neutrinos are stable or decay, either into neutrinos of other flavors or into some new, as yet undiscovered, particles. In contrast, we know that electron is stable, and we know the μ lifetime with a fractional error of 2×10^{-5} and the τ lifetime at the level of 0.5%.

Finally, we do not know if the neutrinos have electromagnetic structure, like for example, a magnetic moment. The electron moment is known with a precision of about one part in 10; the magnetic moment of the muon to one part in 10.

The study of neutrino oscillations offers us what is potentially a most sensitive investigation or measurement of neutrino masses (neutrino mass squared differences to be precise). Observation of a non-zero neutrino mass, which would follow directly from observation of neutrino oscillations, would be a clear example of breakdown of the SM and thus an indication of physics beyond it. Many of the popular extensions of the SM do indeed predict non-zero neutrino masses and existence of neutrino oscillations. Furthermore, neutrino oscillations are not only an attractive theoretical concept, but also a phenomenon hinted at by several experimental observations. These observations are:

- An apparent need for dark matter. One example of this need is the observed deficit of sufficient matter to account for the gravitational forces needed to explain the rotation velocity of stars in spiral galaxies. Neutrinos could account for at least a part of this deficit if they had a finite mass .
- The solar neutrino problem: observation of fewer sun-originated neutrinos on earth than expected from the known solar luminosity .
- The atmospheric neutrino anomaly , a measured $\nu_\mu/\nu e$ ratio for neutrinos from cosmic ray interactions in our atmosphere that is significantly smaller than predicted.

The second and third effects could be explained by neutrino oscillations: νe oscillations into another flavor in the case of the solar neutrino deficit and ν_μ oscillating into νe or (more likely) into ν_τ in the case of the atmospheric neutrino anomaly.

Pontecorvo's hypothesis

Neutrino oscillations were first considered by Pontecorvo in 1957 [14] he assumed that there exists an analogy between lepton charge and strangeness and that not only the strangeness but only the lepton charge is not conserved by the weak interaction. In accordance with this hypothesis it was natural to assume (in analogy with the $K^0, \overline{K^0}$ system) that the neutrino state vector represents a superposition of state vectors of two Majorana neutrinos with small but different masses. In this case the oscillation should take place in the neutrino beams and can be established by the shortage of initial type neutrinos.

The usual weak interaction Hamiltonian is:

$$H_W = H_W^c + H_W^0 \qquad H_W^c = \frac{G}{\sqrt{2}} j_\alpha \overline{j_\alpha}$$

Here

$$j_\alpha = (\nu_{eL}\gamma_\alpha e_L) + (\overline{\nu}_{\mu L}\gamma_\alpha \mu_L) + j_\alpha^h$$

is the weak charged current, $\Psi_L = \frac{1}{2}(1+\gamma_5)\Psi$ is the left-handed component of Ψ, $G = 10^{-5}/M^2$ is the weak interaction constant. The second term of the Hamiltonian is the neutral current contribution.

In case of leptonic charge non-conservation it is possible to write the following Hamiltonian

$$H = m_{\overline{ee}}\,\overline{\nu}^c_{eR}\nu_{eL} + m_{\overline{\mu\mu}}\,\overline{\nu}^c_{\mu R}\nu_{\mu L} + m_{\overline{\mu e}}\left(\overline{\nu}^c_{\mu R}\nu_{eL} + \overline{\nu}^c_{eR}\nu_{\mu L}\right) + h.c.$$

where the parameters m_{xy} have the dimensions of a mass.

The Hamiltonian can be written more compactly as:

$$H = \overline{\nu}^c_R M \nu_L + \overline{\nu}_L M^+ \nu^c_R$$

where

$$\nu_L = \begin{bmatrix} \nu_{eL} \\ \nu_{\mu L} \end{bmatrix} \qquad \nu^c_R = \begin{bmatrix} \nu^c_{eR} \\ \nu^c_{\mu R} \end{bmatrix} \qquad M = \begin{bmatrix} m_{\overline{ee}} & m_{\overline{\mu e}} \\ m_{\overline{\mu e}} & m_{\overline{\mu\mu}} \end{bmatrix}$$

The M values are real and if we consider neutrinos as the following Majorana particles like

$$\chi = \begin{bmatrix} \nu_{eL} + \nu_{eR}^{c} \\ \nu_{\mu L} + \nu_{\mu R}^{c} \end{bmatrix} = \begin{bmatrix} \chi_e \\ \chi_\mu \end{bmatrix}$$

and we have $\chi^c = C\overline{\chi} = \chi$. The M matrix can be diagonalized as:

$$M_0 = \begin{bmatrix} m_1 & 0 \\ 0 & m_2 \end{bmatrix}$$

and the Hamiltonian becomes:

$$H = \sum_{\sigma=1,2} m_\sigma \overline{\phi}_\sigma \phi_\sigma \qquad\qquad \phi = M^T \chi$$

Thus in the usual weak interaction there appear orthogonal superimpositions of fields of Majorana neutrinos, the masses of which m_1 and m_2 are not equal to zero.

Formalism of neutrino oscillation

The underlying principle behind neutrino oscillations [15] is that if neutrinos have mass, then a generalized neutrino state can be expressed either as a superposition of different mass eigenstates or of different flavor eigenstates. Other well-known examples of this principle in particle physics are the system (strong interaction and weak interaction eigenstates) and the quark system (weak interaction and flavor eigenstates connected by the CKM matrix).

From the study of e^+e^- annihilations at the Z^0 peak [16], we know that there are only three neutrino flavor eigenstates. Accordingly, the most likely situation is that we have three masses eigenstates and that the connecting unitary matrix is a 3×3 matrix. For the three-flavor case, the weak eigenstates $|\nu_\alpha\rangle = \nu_e, \nu_\mu, \nu_\tau$ and the mass eigenstates $|\nu_i\rangle = \nu_1, \nu_2, \nu_3$ are related by

$$\begin{bmatrix} \nu_e \\ \nu_\mu \\ \nu_\tau \end{bmatrix} = U \begin{bmatrix} \nu_1 \\ \nu_2 \\ \nu_3 \end{bmatrix}$$

where U is a unitary matrix that can be parameterized as (in analogy with the CKM matrix):

$$U = \begin{bmatrix} C_{12}C_{13} & s_{12}C_{13} & s_{13} \\ -s_{12}C_{23} - C_{12}s_{23}s_{13} & C_{12}C_{23} - s_{12}s_{23}s_{13} & s_{23}C_{13} \\ s_{12}s_{23} - C_{12}C_{23}s_{13} & -C_{12}s_{23} - s_{12}C_{23}s_{13} & C_{23}C_{13} \end{bmatrix}$$

where $C_{ij} = \cos\theta_{ij}$ and $s_{ij} = sen\theta_{ij}$, and for simplicity, we have taken the phase δ = 0. The probability that a state which is pure ν_α at t = 0 is transformed into another flavor β at a time t later (or distance L further) is:

$$P_{\alpha\beta} = \delta_{\alpha\beta} - 4\sum_{j>1} U_{\alpha i} U_{\beta i} U_{\alpha j} U_{\beta j} \sin^2\left(\frac{\Delta m_{ij}^2 L}{2E}\right)$$

where E is neutrino energy and:

$$\Delta m_{ij}^2 = m^2(\nu_i) - m^2(\nu_j)$$

Thus (assuming CP invariance) we have five independent parameters: three angles and two squared masses differences (the third Δm_{ij}^2 must be a combination of the first two). All of the neutrino oscillation data must then be capable of being described in terms of these five parameters.

Clearly, the above expression is complicated and the relationship of experimental results to the five basic parameters is somewhat obscure. Partly due to a desire for simplicity and partly because of the possibility that the leptonic mixing matrix U has a similar structure to the CKM matrix (almost diagonal), it has become customary to represent the results of a single experiment in terms of oscillation between two flavors and involving only two mass eigenstates, hence only one Δm_{ij}^2.

These two basis representations are then related by

$$\begin{bmatrix} \nu_\alpha \\ \nu_\beta \end{bmatrix} = \begin{bmatrix} \cos\theta & \sin\theta \\ -\sin\theta & \cos\theta \end{bmatrix} \cdot \begin{bmatrix} \nu_1 \\ \nu_2 \end{bmatrix}$$

Clearly, such a representation will be a good approximation if the pattern of the U matrix is similar to the CKM matrix.

We can now consider a state which is a pure $|\nu_\alpha\rangle$ at t = 0. Decomposing it into mass eigenstates, we have:

$$|\nu_\alpha\rangle = \cos\theta|\nu_1\rangle + sen\theta|\nu_2\rangle$$

At subsequent times t, we have:

$$|\nu(t)\rangle = \cos\theta e^{-iE_1 t}|\nu_1\rangle + \sin\theta e^{-iE_2 t}|\nu_2\rangle$$

Treating neutrinos as stable particles and assuming that $E^2 >> m^2$, we obtain

$$\left|\nu(t)\right\rangle = e^{-ipt}\left[\cos\theta e^{-\frac{1}{2}i\frac{m_1^2}{p}t}\left|\nu_1\right\rangle + \sin\theta e^{-\frac{1}{2}i\frac{m_2^2}{p}t}\left|\nu_2\right\rangle\right]$$

We now transform back to the flavor basis, using

$$\left|\nu_1\right\rangle = \cos\theta\left|\nu_\alpha\right\rangle - \sin\theta\left|\nu_\beta\right\rangle$$
$$\left|\nu_2\right\rangle = \sin\theta\left|\nu_\alpha\right\rangle + \cos\theta\left|\nu_\beta\right\rangle$$

and ignoring the initial phase factor since eventually we shall be interested in the square of the coefficient of $\left|\nu_\beta\right\rangle$. We obtain:

$$\left|\nu(t)\right\rangle = \left[\cos^2\theta e^{-\frac{1}{2}i\frac{m_1^2}{p}t} + \sin^2\theta e^{-\frac{1}{2}i\frac{m_2^2}{p}t}\right]\cdot\left|\nu_\alpha\right\rangle - \left[e^{-\frac{1}{2}i\frac{m_2^2}{p}t} - e^{-\frac{1}{2}i\frac{m_1^2}{p}t}\right]\cdot\sin\theta\cos\theta\left|\nu_\beta\right\rangle$$

We now take the magnitude squared of the coefficient of $\left|\nu_\beta\right\rangle$ and use trigonometric identities to simplify the equation. This magnitude squared is then the probability P ($\alpha \to \beta$), the transition probability of a neutrino of flavor α into a neutrino of flavor β. If L is expressed in Km (m) and E in GeV (MeV) then the expression reduces to

$$P(\alpha \to \beta) = \sin^2 2\theta \sin^2\left(1.27\Delta m^2 \frac{L}{E}\right)$$

where $\Delta m^2 = m_1^2 - m_2^2$ and is expressed in eV^2. This expression is obviously much simpler than the one for the three-flavor case, and the results of an experiment analyzed in this formalism can be easily displayed in a two-dimensional plot since only two parameters, θ and Δm^2, are involved.

Neutrino oscillation experiments

As can be seen from the last equation, results of any neutrino oscillation experiment can be displayed graphically on a two dimensional plot. It is customary to use log scale representation, but sometimes $\sin^2 2\theta$ is expressed on a linear scale. An experiment claiming a positive result delineates a contour in this space (1σ, 90% C.L., etc.) within which the true answer must lie if

the experiment is correct. A negative result can be represented by a curve delineating the region (again at 1σ, 90% C.L., etc.) excluded by that particular experiment.

It is clear that if the experiments want to probe a region of small $\sin^2 2\theta$, it needs good statistics since the effect will be small. Since the neutrino flux, and so the event rate, falls off with source-detector distance L like $\Phi_\nu \propto (1/L)^2$ it is needed to be relatively close to the source to have a large event rate. In addition the second factor $\left(1.27.\Delta m^2 \cdot \frac{L}{E}\right)$ has to be of the order of unit. Hence, it is needed $\Delta m^2 \approx E/L$, and thus for large E/L, such an experiment will be limited to probing large values of Δm^2. This basically defines a short baseline experiment, where the source detector distance is relatively small and where the region probed extends to small values of $\sin^2 2\theta$ but are limited to large values of Δm^2.

On the opposite end of the spectrum there are long baseline experiments that try to focus on investigation of low values of Δm^2. Again, to keep the argument of the second factor close to unity, L/E has to be large, so the detector has to be far away; in this case the region covered in $\sin^2 2\theta$ is smaller.

It is the value of the ratio L/E that provides the factor determining the experiment category.

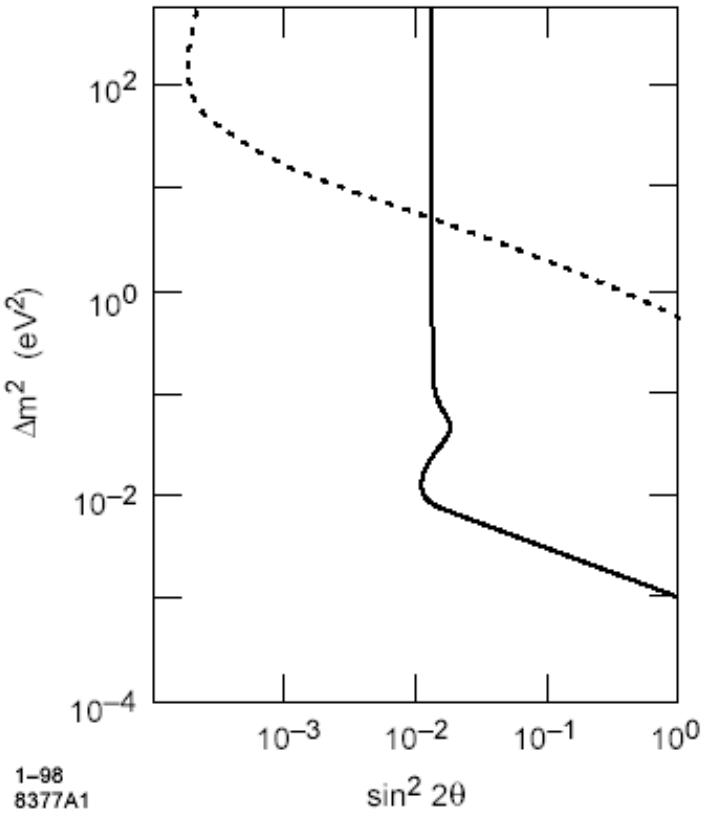

Fig. 2.1 – A rough illustration of the region in oscillation parameter space that might be covered by a long baseline experiment (solid line) and a short baseline experiment (dashed line).

Thus, long baseline experiments are able to probe low values of Δm^2 but their reach in $\sin^2 2\theta$ is more limited. Solar neutrino studies are clearly long baseline; the initial reactor and accelerator oscillation searches would be classified as short baseline experiments. The regions covered by each kind of experiment are shown graphically in Fig. 2.1.

An alternative classification is between appearance and disappearance experiments. Considering a search for the possible oscillation $\nu_\alpha \rightarrow \nu_\beta$, the latter kind of experiment would measure the ν_α interaction rate at one or more locations and compare it with the expected signal, based on the knowledge of the neutrino flux at (or near) the source. The use of two detectors, one near and one far from the source, can reduce systematic errors in this kind of an experiment. They cannot see very small signals because their observation would involve subtraction of two large numbers from each other; they also cannot tell the mode of oscillation, whether we see $\nu_\alpha \rightarrow \nu_\beta$ or $\nu_\alpha \rightarrow \nu_\gamma$, since only the ν_α interaction rate is measured. Study of solar neutrinos is clearly via disappearance experiments. Appearance experiments try to detect the potentially created new flavor. Their sensitivity for small signals is much better and is generally limited by the knowledge of the amount of ν_β in the initial ν_α beam and the ability of the detector to distinguish clearly ν_β from ν_α. Searches for ν_τ, identified by τ production and decay in emulsion with essentially no background in a predominantly ν_μ beam are examples of appearance experiments.

Sensitivities

In this section we discuss how the reach of a given experiment depends on the experimental parameters L, E, and N (number of events). We distinguish between two qualitatively different situations: a background-free experiment (e.g. search for $\nu\tau$ in emulsion), and an experiment relying on a statistical subtraction (e.g., a disappearance experiment or a measurement of the NC/CC ratio). The reach can be parameterized by the lowest value of Δm^2 accessible and by the lowest value of $\sin^2 2\theta$ that can be explored.

The number of signal events N_β, is given by

$$N_\beta = N_\alpha \sin^2 2\theta \sin^2\left(1.27 \cdot \Delta m^2 \cdot \frac{L}{E}\right)$$

where N_α is the expected number of events of the original flavor in the absence of oscillations at a given location L.

$$N_\alpha \propto N_\alpha^0 \left(\frac{1}{L}\right)^2$$

with N_α^0 being the number of ν_α interactions at the source (L = 0).

We may write $N_\alpha^0 = I \cdot f(E)$ where I is the total proton intensity on target, and $f(E)$ is a function describing energy dependence of the neutrino flux which is determined by the initial hadronic production spectrum, details of the focusing system, length of the decay volume, and energy dependence of the neutrino cross section (which is proportional to E in the GeV region).

To investigate sensitivity at low Δm^2 ($\Delta m^2 << 1$ eV^2), we can write:

$$N_\beta = N_\alpha \sin^2 2\theta \cdot \left(1.27 \cdot \Delta m^2 \cdot \frac{L}{E}\right)^2 \propto N_\alpha^0 \cdot \left(\frac{1.27 \cdot \Delta m^2}{E}\right)^2$$

where N_β is the number of β flavor events detected necessary to establish presence of a signal. For the truly background-free case, $N_\beta = 1$ (or 2 or 3 for very small background case). Thus the sensitivity for background-free case is independent of L. For the statistical case, the figure of merit for determination of sensitivity is the quantity δ defined by

$$\delta = N_\beta \Big/ \sqrt{N_\alpha}$$

that is the number of standard deviations away from zero, namely from no effect. For low Δm^2 we have

$$\delta \propto N_\alpha^0 . \left(\frac{1.27.\Delta m^2}{E}\right)^2 / \sqrt{N_\alpha} = N_\alpha^0 . \left(\frac{1.27.\Delta m^2}{E}\right)^2 / \sqrt{N_\alpha^0} \cdot \frac{1}{L} = \sqrt{N_\alpha^0} \left(\frac{\Delta m^2}{E}\right)^2 L$$

Thus, the sensitivity in Δm^2 in this case goes as $\left(N_\alpha^0\right)^{-1/4} \left(\frac{E}{\sqrt{L}}\right)$. The above arguments illustrate the importance of choosing as small a value of E/L as feasible for good low Δm^2 sensitivity; because of fourth root dependence on , it is laborious and expensive to gain more sensitivity by increasing the running time.

We turn now to the question of sensitivity in $\sin^2 2\theta$. Maximum sensitivity is generally taken as one that will occur at values of Δm^2 high enough so that we shall have

$$\sin^2 \left(1.27 \cdot \Delta m^2 \cdot \frac{L}{E}\right) = \frac{1}{2}$$

where the average is over the energy spectrum and we have

$$N_\beta = \frac{1}{2} N_\alpha \sin^2 2\theta \propto N_\alpha^0 \left(\frac{1}{L}\right)^2 \sin^2 2\theta$$

For the background-free case the sensitivity in $\sin^2 2\theta$ will vary inversely with N_α^0 and as L^2. For statistical analyses

$$\delta \propto N_\alpha^0 \left(\frac{1}{L}\right)^2 \sin^2 2\theta \,/\, \frac{1}{L}\cdot\sqrt{N_\alpha^0} = \frac{1}{L}\cdot\sqrt{N_\alpha^0}\sin^2 2\theta$$

The sensitivity will be proportional to $1/\sqrt{N_\alpha^0}$ and L. Thus, clearly a mistake in the proper choice of E/L is less costly in the reach for $\sin^2 2\theta$ than for Δm^2. Knowing now the dependence of the intercepts of our sensitivity contour, it remains to ask about the shape of the contour in the intermediate region. Taking the logarithm of our probability equation for low Δm^2 we have

$$\log N_\beta = \log N_\alpha + \log\left(\sin^2 2\theta\right) + 2\log\left(1.27\cdot\frac{L}{E}\right) + 2\log\left(\Delta m^2\right)$$

Thus the slope of the sensitivity curve on a log-log plot will be 1/2. The general shape of a typical sensitivity plot is shown in Fig. 2.2. The turnaround point corresponds roughly to

$$1.27\cdot\Delta m^2\cdot\frac{L}{E} = \frac{\pi}{2}$$

and the sharpness of the wiggles near that region increases for a relatively narrow beam energy spectrum and is washed out for a broad spectrum.

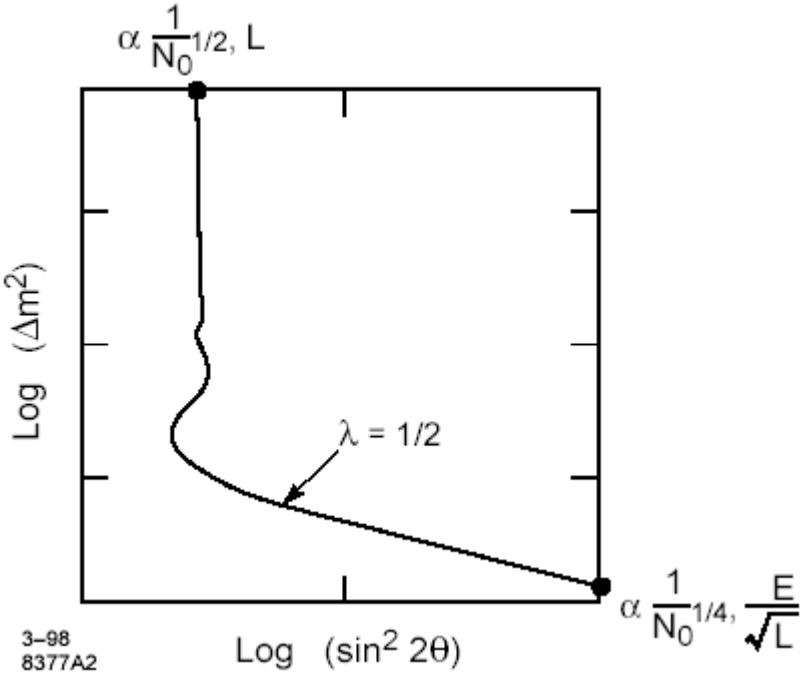

Fig. 2.2 A typical shape of a sensitivity plot for an oscillation experiment.

Experimental results

Direct neutrino mass search

The investigation of the kinematics of weak decays is based on measurements of the charged decays products; using energy and momentum conservation, the missing neutrino mass can be reconstructed from the kinematics of the charged particles. The part of the phase space which is most sensitive to the neutrino mass is the one which corresponds to the emission of a non-relativistic massive neutrino. Therefore decays releasing charged particles with a small free kinetic energy are preferred.

The electron neutrino mass is determined by the investigation of the electron energy spectrum (β spectrum) of a nuclear β decay. In a β^- decay

$$(Z, A) \rightarrow (Z+1, A)^+ + e^- + \bar{\nu}_e$$

the available energy is shared between the electron and the antineutrino, because the recoiling nucleus practically receives no kinetic energy because his mass is heavier. The phase-space region of non-relativistic neutrinos, where the highest sensitivity to the neutrino mass is achieved, corresponds to the very upper end of the β spectrum. To maximize this part, a β emitter with a very low endpoint energy E_0 is required, this requirement is fulfilled by ^{187}Re and tritium, which have the two lowest endpoint energies of E_0=2.5 KeV and E_0=18.6 KeV, respectively. Although tritium has higher endpoint energy its use has several advantages:

- due to the super allowed decay, the transition matrix element does not depend on the electron energy
- tritium has the simplest atomic shell minimizing the necessary corrections due to the electronic final states or inelastic scattering in the source.

In the early '90 tritium β decay experiments yielded controversially discussed results because the values for the observable $m^2(\nu_e)$ populated the unphysical negative $m^2(\nu_e)$ region. In 1991 and 1994 two new experiments, Mainz and Troitsk [17], started using a new type of electrostatic spectrometer; in this way they could have better energy resolution and luminosity.

The Mainz experiment uses a film of molecular tritium quench-condensed onto a graphite substrate, it has a diameter of 17 mm and a typical thickness of 40 nm. The main systematic uncertainties of this experiment are originating from the physics and the properties of the tritium film: the inelastic scattering of β electrons with the source, the excitation of neighbor molecules due to the decay and the self-charging of the tritium film by radioactivity. The better result obtained for neutrino mass is the following:

$$m^2(\nu_e) = -1.6 \pm 2.5 \pm 2.1 \text{ eV}^2$$

Considering its uncertainties, this value corresponds to an upper limit on the electron [17]

neutrino mass of

$$m(\nu_e) \leq 2.2 \text{ eV}$$

During spring 2002 the Mainz group has installed a new electrode system to check new ideas for the KATRIN experiment to avoid background rate by a factor 3. The experiment is nowadays in preparation.

The muon neutrino mass has been investigated in the two-body decay of a pion at rest:

$$\pi^+ \rightarrow \mu^+ + \nu_\mu \quad \text{or} \quad \pi^- \rightarrow \mu^- + \bar{\nu}_\mu$$

Energy and momentum conservation result in a sharp muon momentum from which the mass of the muon neutrino would follow as:

$$m^2(\nu_\varpi) = m^2(\pi) + m^2(\mu) - 2m(\pi)\sqrt{m^2(\mu) + p^2(\mu)}$$

This equation only holds if the muon neutrino is a well defined mass eigenstates, which does not apply in the case of neutrino mixing. Hence, if the muon momentum for pion decay at rest could be measured with sufficient precision three different values $p_i^2(\mu)$ would be detected with relative fraction $\left|U_{\varpi i}^2\right|$ corresponding to the measurements of the corresponding squared mass values contributing to the muon neutrino. Up to now no direct neutrino masses measurements has discriminated different neutrino masses or has established a signal for any non-zero neutrino mass. Therefore on the left-hand side of the equation a mean-squared average of mass eigenstates of the muon neutrino is defined as:

$$m^2(\nu_\mu) = \sum_i \left|U_{\mu i}^2\right| \cdot m^2(\nu_i)$$

and from this the best upper limit to muon neutrino mass is [18]:

$$m(\nu_\mu) < 190 \text{ KeV} \qquad (90\% \text{ C.L.})$$

The most sensitive information on tau neutrino mass comes from the investigation of τ pairs produced at electron positron colliders decaying into multipions. Due to the large mass of the τ, decays into 5 and 6 pions give the highest sensitivity because they restrict the available phase space of the tau neutrino. However, the corresponding branching ratio are rather small.
The quantity looked at is the invariant mass of the multiple pions M_π, in the rest frame of the decaying lepton, M_π^2 is expressed as:

$$M_{\pi}^{2} = \left(\sum_{j} E_{j}(\pi), \sum_{j} \vec{p}_{j}(\pi) \right)^{2} = \left(m(\tau) - E(\nu_{\tau}), -\vec{p}(\nu_{\tau}) \right)^{2} \leq \left(m(\tau) - m(\nu_{\tau}) \right)^{2}$$

The most sensitive investigation comes from the ALEPH experiment at LEP [19]:

$$m(\nu_{\tau}) < 18.2 \text{ MeV} \qquad (95\% \text{ C.L.:})$$

A further improvement based on data from B-factories can be expected with an estimated sensitivity limit of 3 MeV.

Neutrino less double-β decay

Double beta decay (DBD) involves three isotopes, where single beta decay from (A.Z) to (A, Z+1) is either energetically forbidden or at least strongly inhibited by a large change of parity and angular momentum. Disregarding other less popular processes, DBD can occur in two channels:

- $(A, Z) \rightarrow (A, Z+2) + 2e^{-} + 2\bar{\nu}_{e}$
- $(A, Z) \rightarrow (A, Z+2) + 2e^{-}$

The standard electroweak model allows the first channel but forbids the second one because of leptonic number non-conservation. Searches for neutrino-less DBD were at the beginning considered only a very powerful tool to search for violation of the lepton number but now the represent a way to search for a finite neutrino mass and/or for the presence of right-handed currents in the weak interaction amplitude.

CUORE experiment and its preliminary version CUORICINO would have a resolution 1-6 KeV in the region of neutrino less DBD. If the background could be kept at low levels they can get also a sensitivity of 0.60 eV using a compact structure of $Te0_2$ crystals kept at a temperature of ≈ 10 mK.

The Solar Neutrinos problem

The Sun is essentially a fusion reactor effectively transforming four protons into a He^4 nucleus trough a fusion process that reduces to

$$4p \rightarrow He^{4} + 2e^{+} + 2\nu_{e}$$

with an energy release per fusion $E(pp) \approx 27$ MeV.

Thus the number of neutrinos emitted can be readily obtained from the total thermal power of the Sun that is in turn directly related to the measurable solar constant 1.3 kW/m^2 on the earth surface. The emitted neutrino spectrum will depend on the details of the energy producing solar cycle. Precise knowledge of the spectrum is important in the interpretation of the experimental data on solar neutrino interactions on the earth. The spectrum prescribed by the current Standard Solar Model is shown in Fig. 2.3.

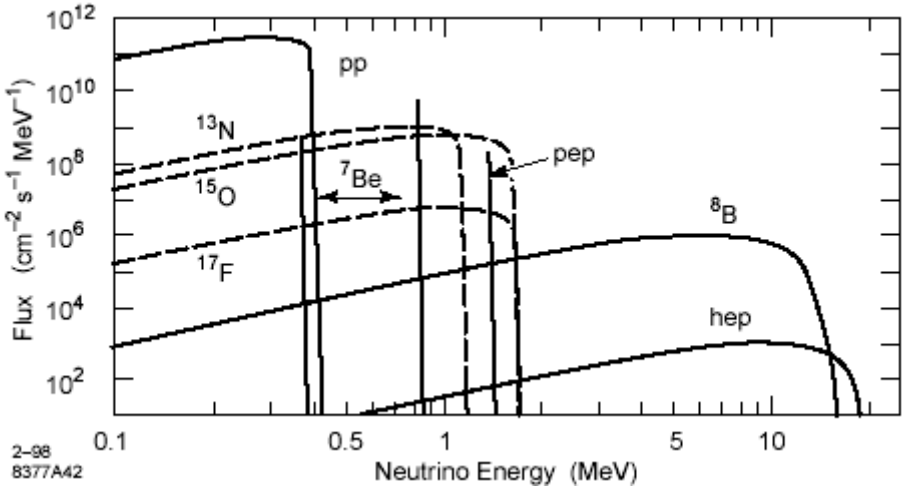

Fig. 2.3 – Energy spectra of solar neutrinos. The pp chain is indicated by the solid curve; the less important CNO cycle by dashed curves.

The first pioneering work of Davis and his collaboration team was to prove that neutrinos were really coming from the Sun; the result was that they detected less neutrino than expected. This gave birth to the Solar neutrino problem and many speculations afterwards.

Solar neutrinos can be detected by two reactions:

- inverse beta decay
- scattering of electrons

Inverse beta decay is a process in which a neutrino is absorbed by a target nucleus, giving as products a new nucleus plus one electron, at the energies of interest only electron neutrinos are active, owing to family lepton number conservation:

$$\nu_e + (A, Z) \rightarrow e^- + (A.Z+1)$$

The cross section is synthetically described by the Fermi's Golden rule and presently only two measurements have been performed on ^{71}Ga, using an artificial neutrino source, and the historical experiment of Reines with antineutrinos on deuterium, the order of magnitude is the following:

$$\sigma_0 \approx 8.8\times10^{-46}\,cm^2 \quad (^{71}\mathrm{Ga})$$
$$\sigma_0 \approx 1.7\times10^{-46}\,cm^2 \quad (^{37}\mathrm{Cl})$$

Electron scattering is the process of diffusion of a neutrino by an electron, since incoming and out going particles are the same the threshold is zero and any kind of neutrino can scatter on electrons triggering this process via Z_0 exchange.
A special case, which is anyhow extremely important, is the neutrino disintegration of deuterium, it can proceed via two reactions:

- $\nu_e + d \rightarrow p + p + e^-$ CC reaction
- $\nu_x + d \rightarrow p + n + \nu_x$ NC reaction

The study of both those reactions allows counting how many electron neutrinos and how many neutrino of different flavors reach the target. Here is a review of the most important solar neutrino experiments:

Homestake

The Homestake [20] experiment (South Carolina, USA, a mine under 1480 m of rock, corresponding to about 4200 m water equivalent) started in 1970 and lasted up 1996. It was a radiochemical experiment since nuclei produced by neutrino interactions were radioactive. The target is exposed to solar neutrinos for a time long enough to reach equilibrium among production an decay. After long time neutrino-inducted nuclei have been extracted from the target bulk and inserted in counters where their decay back to the original nucleus can be detected. In this phase measurement time is much longer than four/five half-lives during which the unstable nuclei decay; the tail of the measurement has been used to determine counter background.
The experiment was intended to detect solar neutrinos with energies greater than 814 KeV, the threshold imposed by the choice of ^{37}Cl as target via the reaction

$$\nu_e + {}^{37}Cl \rightarrow {}^{37}Ar + e^-$$

Pontecorvo has suggested this target because of the following reasons:

- isotopic abundance is rather high and there is a chemical compound C_2Cl_4 that is cheap and available in huge amounts.
- Energy threshold allows the detection of the more relevant of the two ^{7}Be lines, of the p-e-p line, and of ^{8}B beta plus decay. A small contribution comes from CNO cycle.

The expected signal is reported in the following table 2.1 (SNU units)

^{7}Be	Pep	^{8}B	CNO	Total
1.1	0.2	6.1	0.4	7.8 SNU

Table 2.1

Results of the experiment are represented in the so-called Davis plot. The overall result is:

$$R\left(\frac{data}{theory}\right) = 0.33 \pm 0.06$$

The conclusion is that neutrinos produces by the Sun have been detected with a strongly reduced rate. Thus because of some failures in the Solar Model and also because a new neutrino property showing up: neutrino flavor oscillation.
The neutrino experimental oscillation length is

$$L(m) = \frac{2.48 E_{\nu}(MeV)}{\Delta m^2 (eV)^2}$$

so the parameters set explored by solar neutrino experiment s is the following:

E=10 MeV, L = 1.5×10^{11} m $\rightarrow \Delta m^2 = 10^{-10}$ eV^2

Kamiokande & SuperKamiokande

The Kamiokande experiment, located in Kamioka mine (Japan) at the depth of 1000 m, started in 1983 as a detector intended to study the nucleon decay channel:

$$p \rightarrow e^+ + \pi^0$$

It was a 3 kton water Cherenkov detector; light direction allowed to reconstruct the original particle direction and its amount was a measure of the particle energy. In the case of solar neutrino, electrons were produced trough the elastic scattering :

$$\nu_e + e^- \rightarrow \nu_e + e^-$$

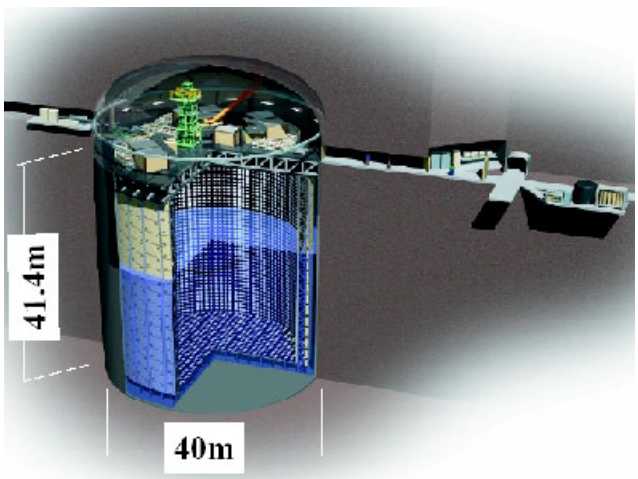

Fig. 2.4 –Sketch of Kamiokande detector

A set of 1000 20-inch photo multipliers placed uniformly on the inner surface water-tank walls; by the information of time and charge from PMT's, it was possible to obtain the information of vertex point, particle id, direction, and momentum.

The first phase allowed to put a limit on proton's life: $\tau_p \geq 10^{32}\, years$ for nucleon decay channel $p \to e^+ + \pi^0$, during further investigations it was found out that it could be possible to detect low energy electrons and in 1986 the detector has been improved to collect with high efficiency data of events in which the energy threshold was of 9 MeV.

The most important feature of the solar neutrino measurements is the confirmation that neutrino come from the Sun, this is due to the possibility to reconstruct particle directions. In conclusion Kamiokande results confirmed also the neutrino deficit:

$$R\left(data/theory\right) = 0.49 \pm 0.06$$

During the last operation period of Kamiokande a new bigger detector has been built in the same site SuperKamiokande, it is a bigger water Cherenkov detector with a 50kton mass and more than 10000 PMTs. In this case there has been a huge background reduction due to external radioactivity and internal radon background.
The final result based on 2000 events is the following [21]:

$$R\left(data/theory\right) = 0.451 \pm 0.005$$

Gallium –based solar neutrino experiments

The experiment described previously detected neutrinos coming from ^{8}B chain that is only marginal in nuclear reactions in the Sun. New experiments able to detect pp neutrinos were studied and they should be able to detect low energy signals E< 420 keV.
In the late '80s two groups, the SAGE collaboration in Baksan and the European Gallex worked on this problem using inverse beta decay on ^{71}Ga. It was a good candidate for radio-chemical experiments because the energy threshold is 233 keV and the induced ^{71}Ge decays back to ^{71}Ga with a half-life of $\tau_{1/2} = 11.4 days$.

The Gallex/GNO [22] experiment was located in Italy at Gran Sasso Underground Laboratory, under 1400 m of rock (about 4000 m of water equivalent) that guarantees a muon flux reduction of a factor $\cong 10^6$ and it has been stopped in 2003. There was a 100 ton tank filled with $GaCl_3$ in HCl solution. The run consisted of three phases: exposure, extraction and counting, and each lasted 6 months. After more than 10 years of data taking results are shown in Fig. 2.5 and they confirmed the discrepancy with the Solar Standard model predictions; it is well explained by neutrino flavor oscillations with parameters in the low mixing angle region.

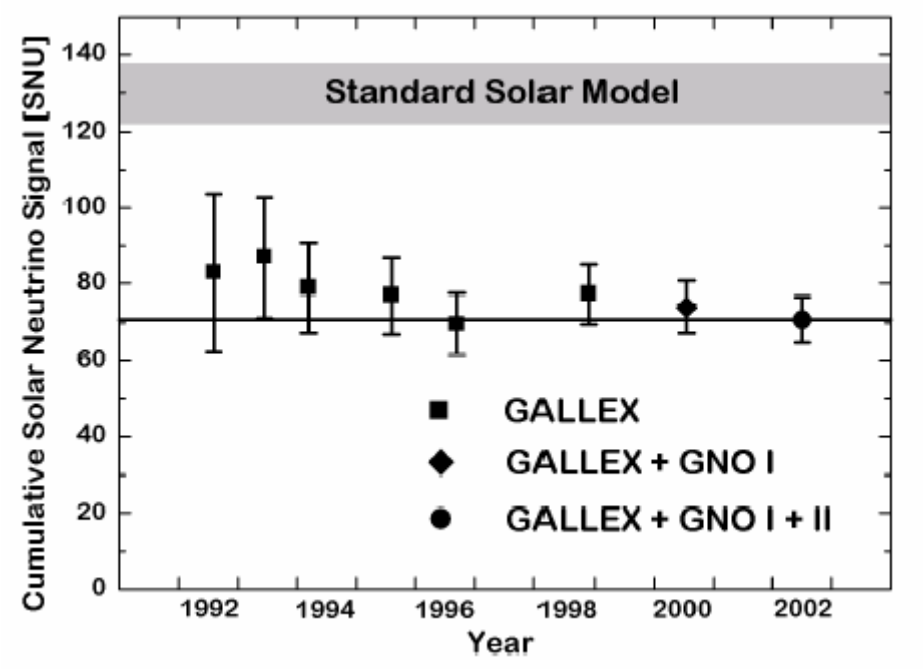

Fig. 2.5 – Cumulative results of the Gallex and GNO experiments[23].

SNO experiment

The Sudbury Neutrino Observatory is a real time heavy water Cherenkov detector located in the Inco Ltd., Creighton mine near Sudbury, Ontario, Canada [24]. The center of the detector is at a depth of 2092 m, or 6010 meters of water equivalent. At this depth, approximately 65 muons enter the detector per day. The neutrino target is 1000 ton of 99.92% isotopically pure D_2O contained inside a 12 m diameter acrylic vessel. An array of 9456 20 cm PMTs, which is mounted on an 18 m diameter stainless steel geodesic structure, is used to detect Cherenkov radiation in the target. A non-imaging light concentrator is mounted on each PMT to increase the effective photo cathode coverage by the complete array to approximately 54% of 4π.

To minimize the effects of radioactive backgrounds, materials with low intrinsic radioactivity were selected for the construction of the detector. The acrylic vessel and the geodesic sphere are immersed in ultra-pure H_2O to provide shielding against radioactive backgrounds from the geodesic structure and the cavity rock. An additional 91 PMTs are mounted looking outwards on the geodesic sphere and 23 PMTs are suspended facing inwards in the outer H_2O volume to act as cosmic veto counters.

The SNO experiment detects solar neutrinos through the CC and NC interactions on the deuteron, and by elastic scattering (ES) on electrons. The NC channel has equal sensitivity to all active neutrinos, while the ES channel is sensitive primarily to electron neutrinos. Hence, the NC measurement can determine the total active solar neutrino flux even if electron neutrinos transform to another active flavor [18]. In the first phase of the experiment with pure D_2O, NC

interactions were observed by detecting the 6.25-MeV γ-ray following capture of the neutron by the deuteron. For the second phase of data taking, (0.196±0.002)% by weight of purified NaCl was added to the D_2O in May 2001 to increase the capture and the detection efficiencies of the NC neutron. The thermal neutron capture cross section of ^{35}Cl is 44 b, which is significantly higher than that of the deuteron at 0.5 mb. When a neutron captures on ^{35}Cl, the total energy released is 8.6MeV. The combination of the increased cross section and the higher energy released results in a larger neutron detection efficiency at the same analysis threshold.

Neutron capture on ^{35}Cl typically produces multiple γ-rays (□2.5 per capture), while the CC and ES reactions produce single electrons. Each γ-ray predominantly interacts through Compton scattering, producing an energetic electron. The Cherenkov light from neutron capture events, compared to that from CC and ES events, is more isotropic as the light is typically from several electrons rather than one. This greater isotropy, together with the strong directionality of ES events, allows good statistical separation of the event types. A precise measurement of the total active solar neutrino flux can be made through the NC channel without assumptions about the underlying neutrino energy spectrum. This is relevant because the neutrino energy spectrum can be distorted from the generated ^{8}B spectrum via oscillation effects.

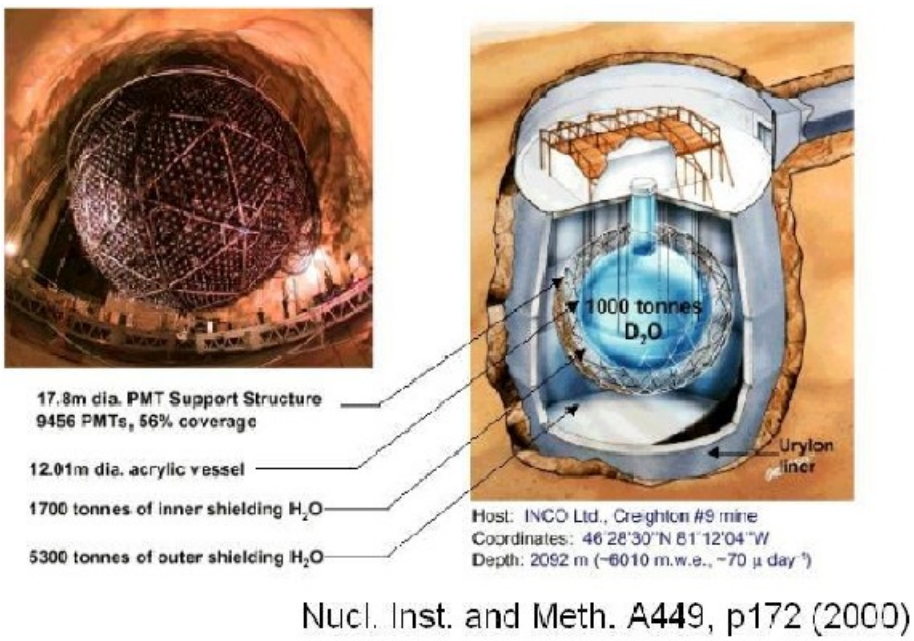

Fig.2.5 – SNO detector

The SNO data in Fig.2.6 and Fig. 2.7, when combined with other solar neutrino measurements and reactor antineutrino results from the KamLAND experiment [25], show that neutrino oscillations are the dominant cause of flavor transformation and significantly restrict the allowed range of the relevant neutrino mixing parameters. In terms of neutrino mass and mixing parameters Δm^2 and $\tan^2\theta$, solar neutrino data favor the so-called Large Mixing Angle (LMA) region. Maximal mixing is ruled out with a high-degree of confidence.

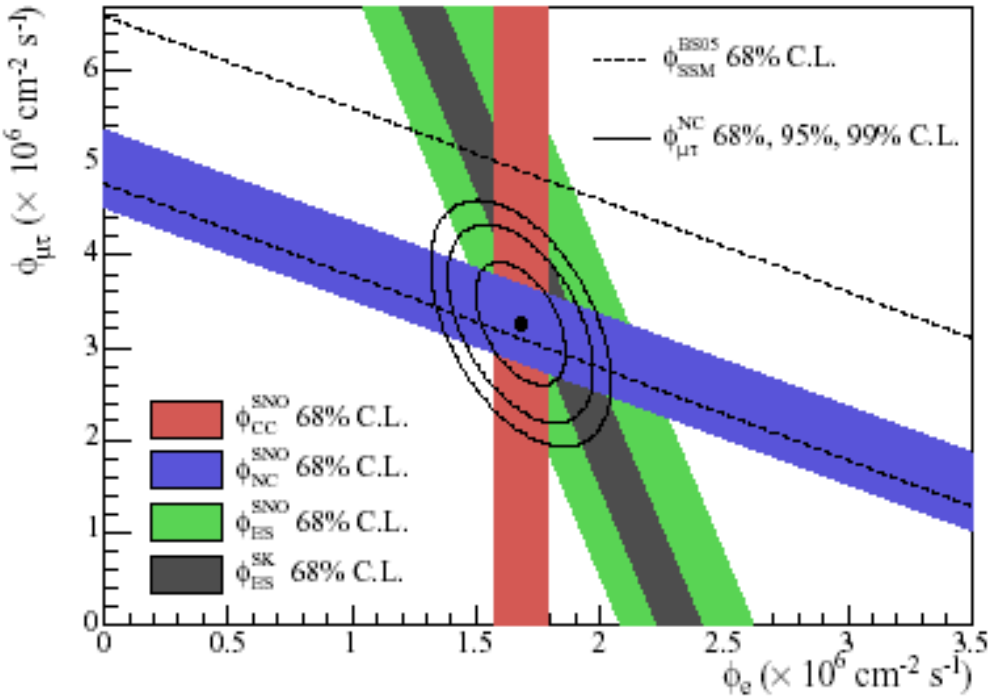

Fig. 2.6 -Flux of $\mu + \tau$ neutrinos versus flux of electron neutrinos. CC, NC and ES flux measurements are indicated by the filled bands. The total ^{8}B solar neutrino flux predicted by the Standard Solar Model is shown as dashed lines, and that measured with the NC channel is shown as the solid band parallel to the model prediction. The narrow band parallel to the SNO ES result corresponds to the Super-Kamiokande result. The intercepts of these bands with the axes represent the $\pm 1\sigma$ uncertainties. The non-zero value of $\varphi_{\mu\tau}$ provides strong evidence for neutrino flavor transformation. The point represents φ_e from the CC flux and $\varphi_{\mu\tau}$ from the NC-CC difference with 68%, 95%, and 99% C.L. contours included.

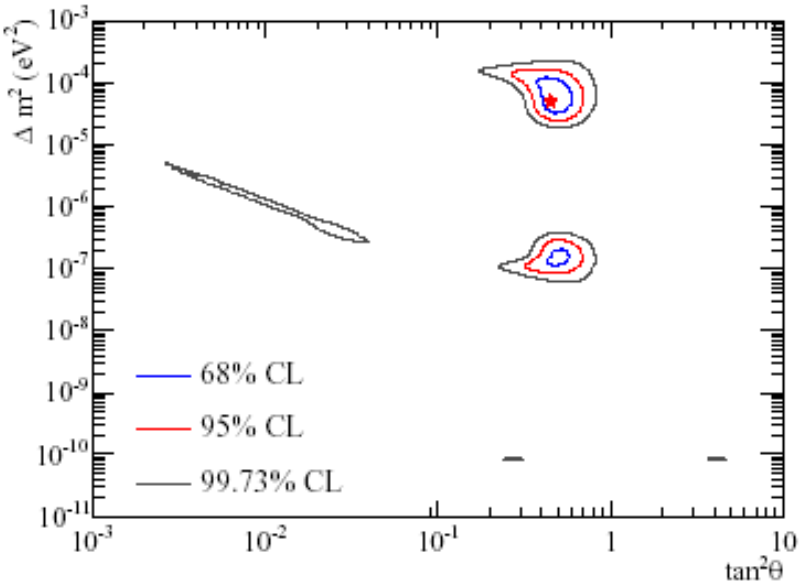

Fig.2.7 – SNO only neutrino oscillation analysis, including pure D_2O phase day and night spectra, and salt extracted CC spectra, NC and, ES fluxes, day and night.

Probing and completing the solar neutrino solution ($\nu_e \rightarrow \nu_\mu/\nu_\tau$) at nuclear reactors

Assuming validity of CPT, it is possible to investigate the oscillation solutions to the solar neutrino problem also using antineutrinos. KamLAND detector (located in Kamioka mine) has been planned to measure antineutrino flux from nuclear power plants in Japan, fluxes and distances are checked against previous reactor experiments; it turns out that KamLAND is sensitive just to the Δm^2 range of the LMA solution to solar neutrino deficit. Eight reactors are grouped at a distance of 175 ± 35 km from the detector; their fluxes can provide up to 300 events /kton/year by the reaction (threshold E=1.8 MeV)

$$\nu_e + p \rightarrow e^+ + n$$

The KamLAND detector consists of 1 kton active pure liquid scintillator contained in 6.5 m radius transparent balloon surrounded by 1.5 kton of passive mineral oil shielding. The inner detector is covered by 1879 PMTs providing 34% photo-cathode coverage resulting in a good energy resolution of $6.2\%/\sqrt{E(MeV)}$. The KamLAND scintillator is made 80% of dodecane, 20% of pseudocumene and 1.52 g/l PPO. Visible energy for detected events is reconstructed from the number of observed photo-electrons after correction for gain variations, position dependence, balloon ropes shadowing, scintillator and mineral oil transparencies.

The major components of the measured background below 1 MeV are ^{14}C, ^{85}Kr, ^{210}Bi, ^{210}Po and probably ^{39}Ar. Background above 1 MeV is dominated by ^{40}K contained in the balloon supporting ropes, ^{208}Tl γ-rays from rocks, and various muon spallation products such as ^{9}C, ^{10}C, ^{9}Li, and ^{12}B. Background composition was carefully studied in order to evaluate impact on reactor ν_e disappearance results. Background due to muon spallation products is suppressed by 2 ms veto.

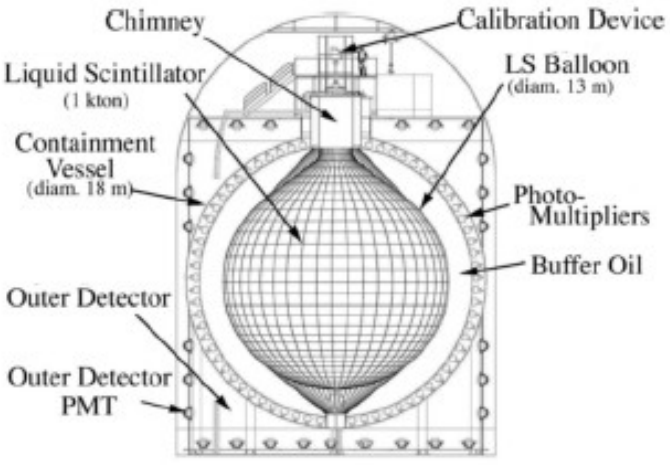

Fig.2.7 – Schematic view of KamLAND detector

Most of the anti-neutrinos observed in KamLAND originate from 53 Japanese nuclear reactors. Anti-neutrinos are detected via inverse β^- decay with 1.8 MeV ν_e energy threshold. The prompt signal comes from the light produced by e^+. The 2.22 MeV γ-ray from neutron capture on hydrogen is delayed by ¡« 200μs. Prompt-delayed events correlation in space and time give clean detection signature that reduces accidental background.

In absence of ν_e oscillations the number of expected events above 2.6 MeV threshold is 365.2± 23.7(*syst*). Number of observed events is 258 that results in probability of ν_e disappearance at 99.998% significance level. The ratio of observed to expected is

$$R = 0.658 \pm 0.044\ (stat) \pm 0.047\ (syst)$$

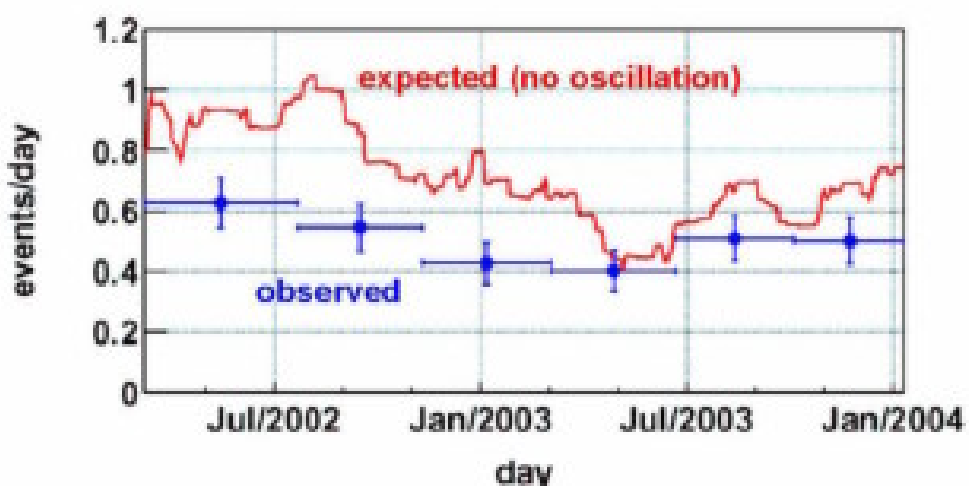

Fig. 2.8 – Expected neutrino event rate for no oscillation and observed event rate.

The observed oscillatory pattern provided precise determination of $\Delta m^2 = 7.9 \times 10^{-5}$ eV^2. Determination of mixing angle requires precise measurement of absolute flux and the large systematic error is limiting the current resolution. If one combines the KamLAND allowed region with the solar neutrino allowed region assuming the CPT invariance, both the mixing angle and Δm^2 are determined, precisely as shown in Fig.2. 9. Obtained values are:

$$\Delta m^2 = 7.9^{+0.5}_{-0.5} \times 10^{-5} eV^2$$

$$tg^2 2\theta = 0.40^{+0.10}_{-0.07}$$

where Δm^2 is mainly determined by KamLAND and mixing angle by solar neutrino experiments.

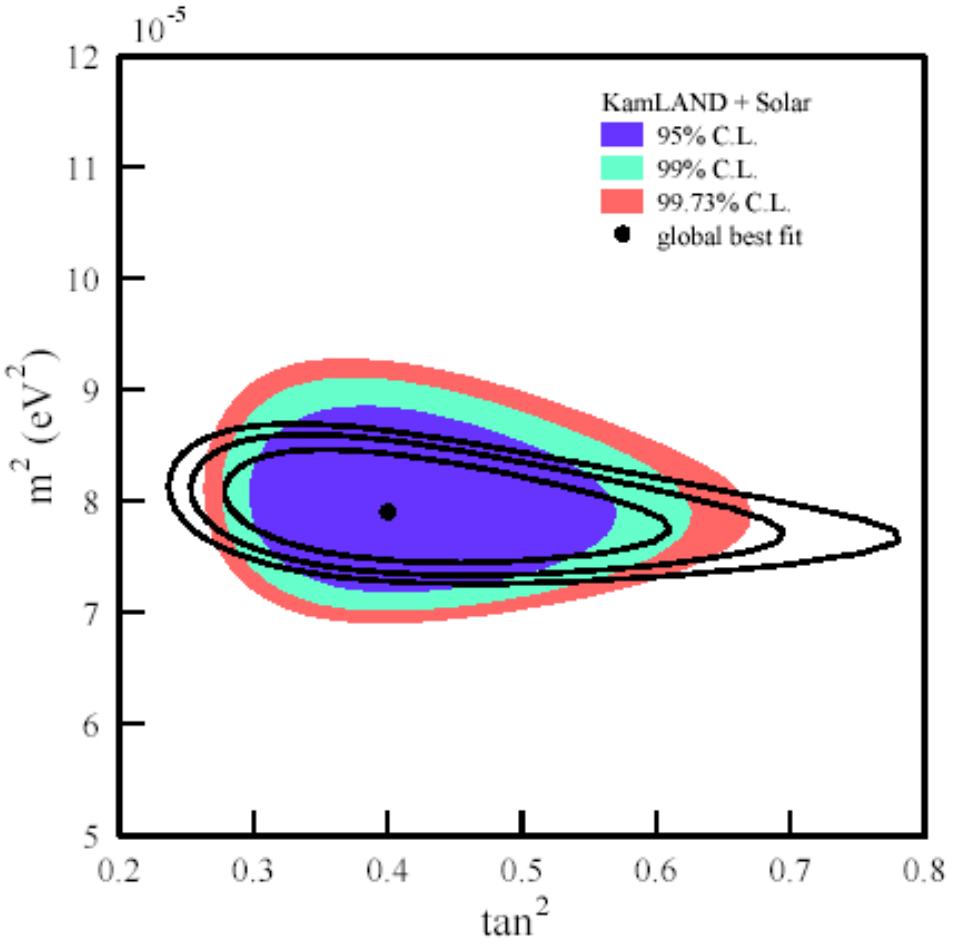

Fig. 2.9 – Allowed region of KamLAND + Solar global analysis. Black curves represents a future sensitivity of the experiment.

The atmospheric neutrino anomaly

Atmospheric neutrinos are produced from the decays of particles resulting from interactions of cosmic rays with Earth's atmosphere, in these interactions there are produced pions and kaons which subsequently decay:

$$\pi, k \rightarrow \mu + \nu_\mu \quad \text{and} \quad \mu \rightarrow e + \nu_\mu + \nu_e$$

Each decay produces two ν_μ and one ν_e and a ratio of the numbers of ν_μ to ν_e of 2 is therefore expected, instead the ratio is found to be 1. These neutrinos can also be studied as a function of their direction with the respect to the vertical, the zenith angle θ. This variable is directly related to L, the distance between their production and observation point. Down going neutrinos will have be produced at a distance of about 15 km from the detector, whereas up going neutrinos will have had to traverse the Earth and will have therefore been produced at a

distance of about 12500 km. This allows the study of oscillation pattern and parameters, they have been found by Super-Kamiokande experiment.

Super-Kamiokande is a 50-kiloton water Cherenkov detector located deep underground in Gifu Prefecture, Japan. Atmospheric neutrinos are observed in Super-K in two ways. At the lowest energies, 100 MeV -10 GeV, they are observed via their charged current interactions with nuclei in the 22.5 kiloton water fiducial mass, these interactions are classified as fully contained (FC) if all of the energy is deposited inside the inner Super-K detector, or as partially contained (PC) if a high energy muon exits the inner detector, depositing energy in the outer veto region. The neutrino energies that produce partially contained events are typically 10 times higher than those that produce fully contained events. The Super-K detector started observation on April, 1996 achieving a 92 kiloton/year exposure to atmospheric neutrinos through July 2001, during the Super-Kamiokande I running period.

Neutrinos can also be detected by their interactions with the rock surrounding the detector. Charged current ν_μ interactions with the rock produce high energy muons which intersect the detector. While these interactions can not be distinguished from the constant rain of cosmic ray muons traveling in the downward direction, muons traveling in an upward direction through the detector must be neutrino induced. Upward-goingmuon events are separated into two categories: those that come to rest in the detector (upward stopping muons) and those that traverse the entire detector volume (upward thoroughgoing muons).

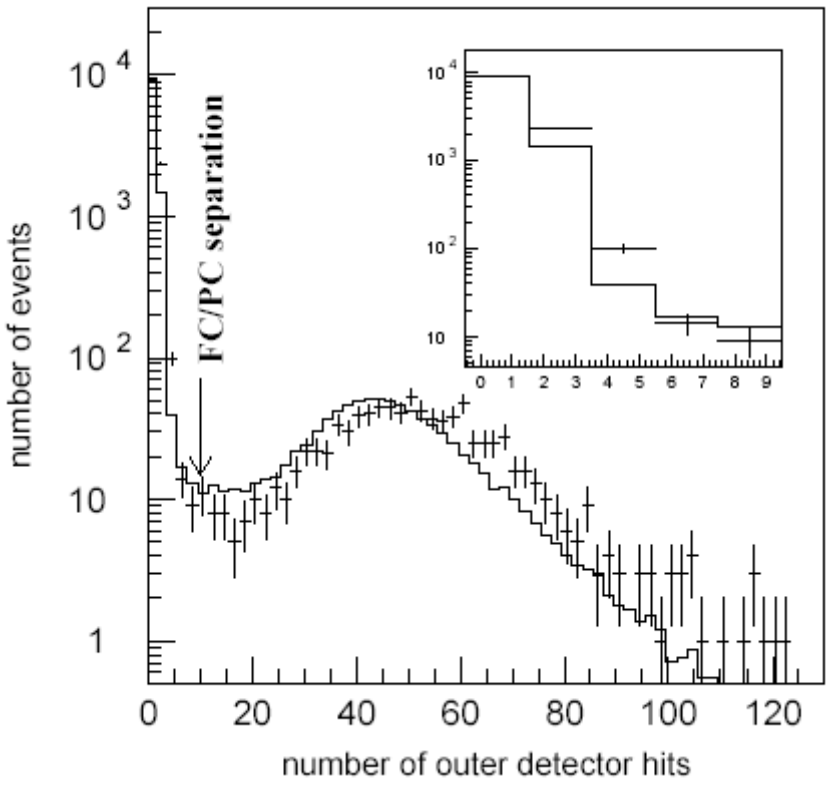

Fig.2.10 - The number of hits in the largest outer detector cluster, which is used to separate FC an PC event samples. The histogram shows the MC prediction with neutrino oscillation.

The energies of the neutrinos which produce stopping muons are roughly the same as for partially contained events, □10 GeV. Upward through going events, however, are significantly more energetic; the parent neutrino energy for these events is about 100 GeV on average. There have been several other measurements of atmospheric neutrinos. Kamiokande , IMB and Soudan 2 observed significantly smaller ν_μ to ν_e flux ratios of □ 1 GeV atmospheric neutrinos, which were interpreted as a signals of oscillation. In order to identify the neutrino flavor in CC interaction it is important to determine the identity of the final state particles, a particle identification algorithm was applied which exploited systematic differences in the shape and the opening angle of Cherenkov rings produced by electrons and muons. Cherenkov rings from electromagnetic cascades exhibit a more diffuse light distribution than those from muons. Figures 2.11 and 2.12 show observed single-ring e-like and μ-like events, respectively. The opening angle of the Cherenkov cone, which depends on $\beta = \frac{v}{c}$, was also used to separate electrons and muons at low momentum. The validity of the method was confirmed by a beam test experiment at KEK . The misidentification probabilities for single-ring muons and electrons were estimated to be 0.7% and 0.8% respectively, using simulated CC quasi-elastic neutrino events.

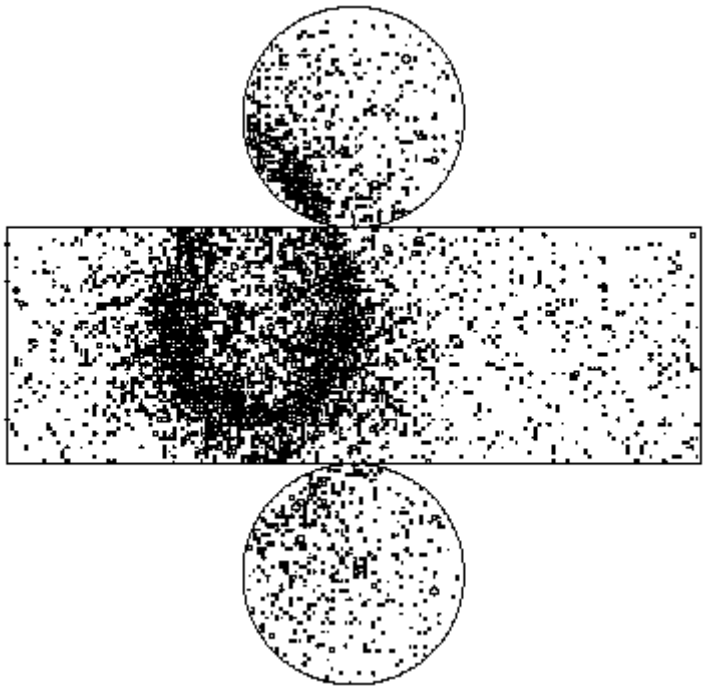

.

Fig. 2.11 - An example event display of a single-ring e-like event. Each small circle represents a hit PMT and the size of the circle represents the number of photons to hit it. In this event the boundary of the Cherenkov light is smeared over many PMTs as the light comes from numerous positrons and electrons in the electromagnetic shower.

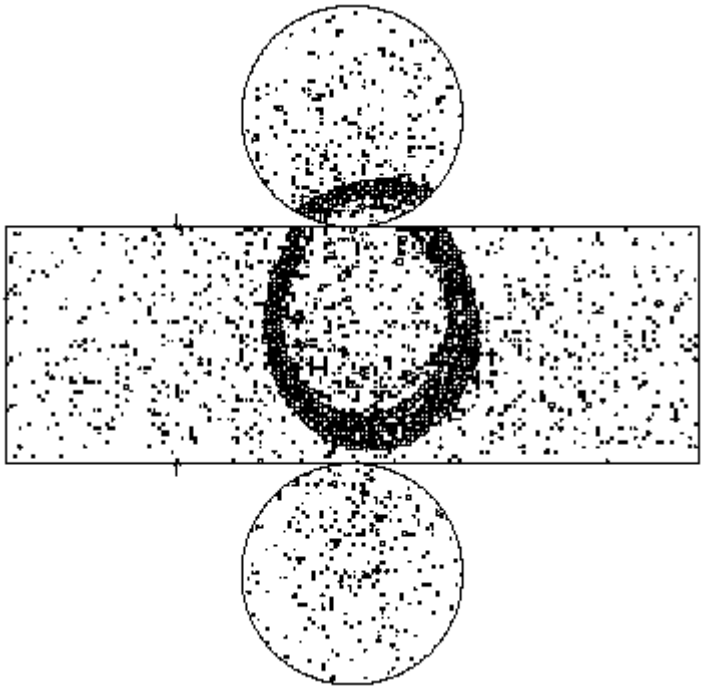

Fig. 2.12 - An example event display of a single-ring μ-like event. In this event the boundary of the Cherenkov light is sharp as the muon travels relatively straight as it comes to a stop. Distant hit PMTs come from scattered light and Cherenkov light from delta-rays.

The observed deficits of muon neutrino interactions are in strong disagreement with the expectation in the absence of neutrino oscillations. Oscillation between electron neutrinos and muon neutrinos cannot explain the data .A variety of exotic alternatives such as neutrino decay were considered, however, none fit the data as well as the $\nu_\mu \rightarrow \nu_\tau$ oscillation scenario. Super-Kamiokande has observed more than 15,000 atmospheric neutrino events during the first data taking period between 1996 and 2001. Atmospheric neutrino events observed have an energy range from about 100 MeV to 10 TeV, and a neutrino flight-length from about 10 km to 13,000 km. These wide energy and flight length ranges together with high statistics made it possible to study neutrino oscillations. Especially, the predicted up-down asymmetry of the atmospheric neutrino flux enabled to accurately estimate the mixing parameter $\sin^2 2\theta$. The observed muon neutrino events showed a clear zenith angle and energy dependent deficit of events, while the electron neutrino events neutrino oscillation parameters were [26]

$$\sin^2 2\theta = 092 \text{ and } \Delta m^2 = 3.4 \square 10^{-3} \text{ eV}^2$$

at 90% C.L.

From atmospheric neutrino to long-baseline accelerator experiments

It remains to determine whether oscillations are indeed the source of the deficit of ν_μ's . Oscillations into ν_e's are excluded by CHOOZ and SuperKamiokande itself since they do not observe corresponding excess of ν_e's. It is advisable to investigate the disappearance of ν_μ's under controlled conditions, namely with beams produced by accelerators. Referring to the oscillation probability equation, it can be seen that in order to probe a $\Delta m^2 \approx 10^{-3} eV^2$ an $L/E \approx 1000 km$ is necessary. Three such projects are in progress: K2K in Japan, the NUMI beam between Fermi Lab and the Soudan Mine and the CNGS beam between CERN and Gran Sasso Laboratory in Europe.

K2K

The main goal of the KEK to Kamioka (K2K) long-baseline neutrino oscillation experiment is to probe neutrino oscillations around $\Delta m^2 \approx 10^{-3} eV^2$ which is suggested by the SK atmospheric neutrino analysis [27]. It will use a low energy beam directed both a near and a far (SuperKamiokande) detector. It is a disappearance experiment and its goal is to confirm the ν_μ deficit. The basic strategy of the neutrino oscillation analysis in K2K is as follows:

- the neutrino flux and spectrum before neutrino oscillations are measured by the near detectors (ND) in KEK, and the neutrino interaction model is also studied by the ND,
- the neutrino flux and spectrum at the far detector are evaluated using the far to near (F/N) ratio, which is estimated with the Monte Carlo and confirmed

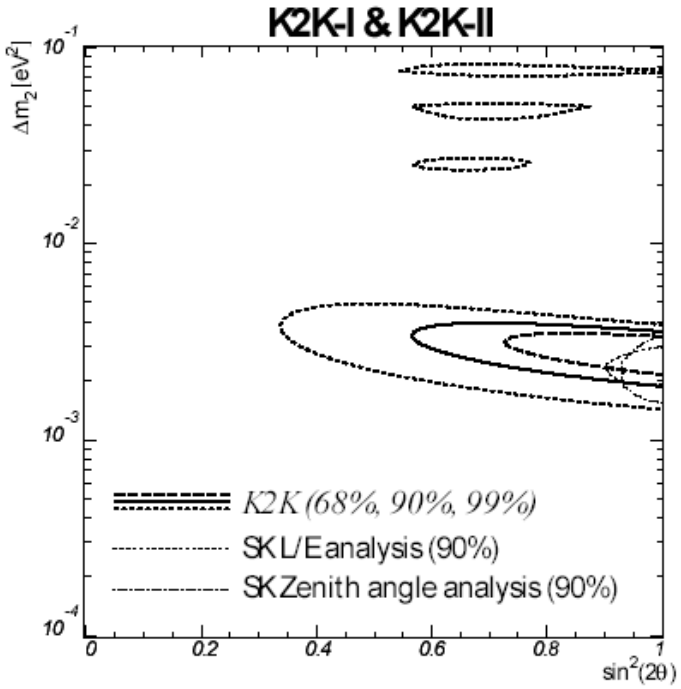

Figure 2.13 - Allowed regions oscillation parameters on K2K oscillation analysis. Thick dashed, solid and dotted lines are 68.4%, 90% and 99% C.L. contours, respectively. Thin dot dashed and dashed lines are 90% C.L. allowed regions obtained by SK zenith angle and L/E analyses.

In long-baseline experiment, the neutrino path length is fixed; this distance is 250km in the case of K2K. The neutrino energy is reconstructed assuming the quasi-elastic (QE) interaction. The K2K result is consistent with the SK atmospheric neutrino oscillation analysis results. The 90% C.L. allowed region crosses the $\sin^2 2\theta = 1.0$ between $1.8 \times 10^{-3} eV^2$ and $3.6 \times 10^{-3} eV^2$. The sensitivity on $.m_2$ of K2K based on 107 event observation is almost similar level with that of the SK atmospheric neutrino oscillation analysis.

MINOS

The MINOS (Main Injector Neutrino Oscillation Search) experiment [28] will use the intense NuMI beam (Neutrinos at the Main Injector). The neutrinos pass through the Earth and are detected at a distance of 735km in the 5.4 kton MINOS Far Detector which is located at a depth of 714m in the Soudan mine, Northern Minnesota. A 1 kton near detector is located at a distance of 1 km. The near detector is similar in design to the far detector. By comparing the observed neutrino energy spectrum in the far detector (which includes the effects of neutrino oscillations) to the unoscillated spectrum in the near detector the oscillation minimum can be resolved yielding a 10% measurement of Δm^2.
For the NuMI/MINOS baseline of 735 km, the Super-Kamiokande results suggest that the first oscillation minimum will occur for neutrino energies in the range 1.0 - 2.5 GeV. Consequently, the low energy beam configuration will be used for the initial physics running.

The MINOS far detector is a 5.4 kton steel scintillator sampling calorimeter consisting of two super-modules (SM) separated by a gap of 1.1m. The basic detector structure consists of octagonal planes of 2.54 cm thick steel followed by planes of1 cm thick scintillator and a 2 cm wide air gap. Each SM is magnetized to an average value of 1.5 T by a 15 kA current loop which runs along the coil hole along the detector central axis and returns below the detector. Each scintillator plane is made up of 192 optically isolated 4 cm wide strips of length up to 8m depending on the position in the plane. The strips in alternating planes are oriented at ±45° to the vertical thereby providing two orthogonal coordinates. The scintillation light is collected using wavelength shifting (WLS) fibers embedded within the scintillator strips. The WLS fibers are coupled to clear optical fibers at both ends of a strip and are read out using 16-pixel multi-anode photomultiplier tubes (PMTs). The experiment has just started to take data in March 2005, first results are expected by next year.

I will discuss about CNGS project and OPERA detector in the following chapter.

Neutrino physics with nuclear emulsions

Nuclear emulsions have a long history in high energy physics. Their unsurpassed spatial granularity and resolution make them particularly suitable for the detection of very short lived particles. In recent years nuclear emulsions have been used in a number of neutrino experiments as a tool for detecting τ leptons: CHORUS at CERN and E531 and DONUT at Fermi lab. All these experiments have a hybrid design: electronic detectors predict the emulsion region where to look for neutrino interactions and emulsion are active targets [29].

While nuclear emulsions used today are very similar to those used fifty years ago, the analysis techniques have changed dramatically: electronic detectors are used to localize events and advances in computers have been exploited to increase scanning speed. Japanese and European Scanning groups have constructed several stations consisting of computer controlled fast microscopes read out with CCD or CMOS cameras. Those systems provide fully automatic charged particles tracks reconstruction and event selection and they have been used to analyze hundreds of thousands of neutrino interactions from the CHORUS and DONUT experiment.

These capabilities for large scale automatic analysis of emulsion data are changing the way that emulsion sheets are used in experiments. The ECC approach, in which thin emulsion sheets interspersed with passive material serve as a target is becoming widely used. The nuclear emulsion sheets are used as very fine granularity high spatial resolution tracking detectors with the particles of interest traversing the sheets perpendicular to the surface. Such a configuration has been employed in an experiment designed to directly observe ν_τ ' s, DONUT at Fermi lab and will be used for the long-baseline $\nu_\mu \rightarrow \nu_\tau$ oscillation search in OPERA at LNGS.

The first attempt to study neutrino interactions and oscillation by hybrid technique has been E531 experiment [30]; it was designed in 1980 to measure the lifetimes of charmed particles produced by the Fermi Lab neutrino beam and has obtained the lifetimes of the D^0, $D^{\pm}$, $F^{\pm}$ and $\Lambda^+_{C.}$ Since the τ lepton has a similar life-time it could also be seen in an emulsion target, they searched for the reaction

$$\nu_\tau + N \rightarrow \tau^- + hadrons$$

where the incident neutrino was originally a muonic one, the event analysis used looked for the τ decay and no background subtraction were required. The experiment was performed with a hybrid emulsion spectrometer as shown in Figure 3.1. The detector was located 560m downstream the neutrino beam, the spectrometer consisted of a 23 l nuclear emulsion target, drift chambers on both sides of a large-aperture analysis magnet, time-of-flight hodoscopes for triggering and charged-particle identification, a lead-glass array, a coarse-grained hadronic calorimeter and two banks of counters behind steel for muon identification. The detector was triggered by two or more charged tracks passing trough the magnet. During the data run the

neutrino beam was produced by 350 GeV protons and the observed energy spectrum for reconstructed ν_μ events was peaked at 25-30 GeV. The interactions were found by following secondary tracks back into the emulsion or by scanning the volume around the predicted vertices.

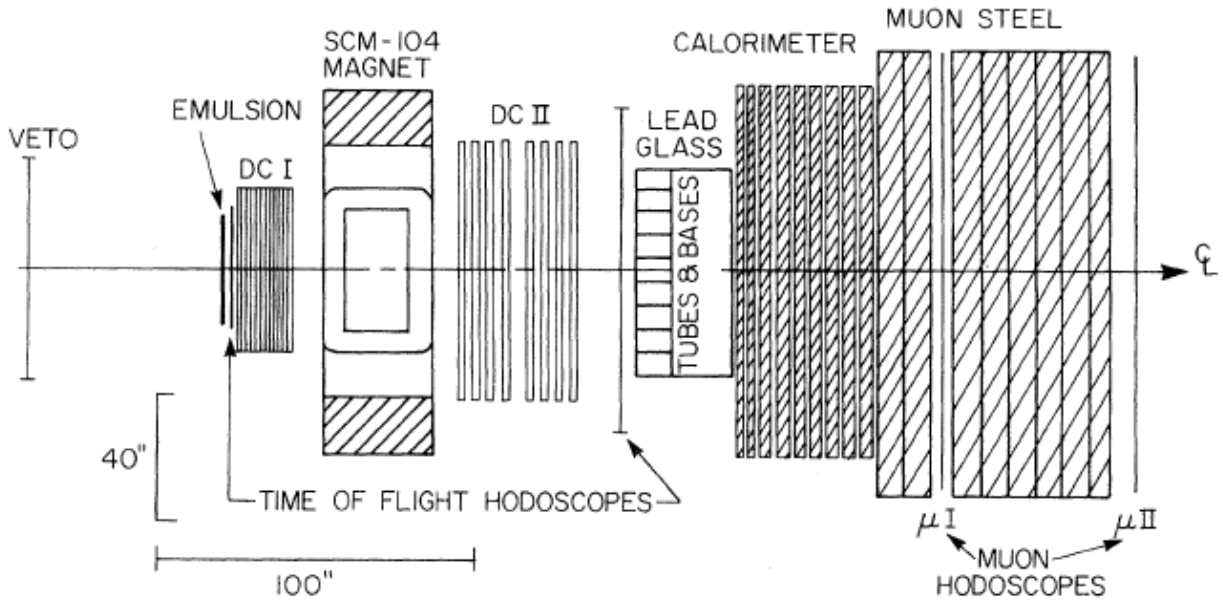

Fig. 3.1 – Plan view of E531 detector.

They found in total 3886 neutrino and antineutrino interactions in the fiducial emulsion volume, charged particles decays were found mainly by following all the charged tracks from the neutrino interaction vertex and by following back tracks from the spectrometer into the emulsion. The final sample consisted of 104 charged particles decay candidates, because of possible background due to scattering a single prong topology, kink, was not considered a τ decay candidate if the secondary track has a momentum perpendicular to the parent direction, p_T , less than 125 MeV/c. After cuts on low momentum tracks no τ decay candidates remained.
The final limits to neutrino mass differences and mixing angles are shown in Figure 3.2.
The most important result coming from E531 experiment was the D^0 life-time measurement.
They final charm candidate sample published in 1986 consisted of 58 decays and it was the larger charm statistic in a single experiment by that time. All of them had visible decay topology due to emulsion fine granularity. Most of these interactions were found by the follow back technique: drift chamber tracks were followed back to their origin, in addition they performed a volume scanning for at least 300 μm downstream of the primary neutrino interaction. <the ratio of interactions found to those searched for from the spectrometer predictions was on average 82%, most of the inefficiency is a result of interactions occurring outside the fiducial volume of the emulsion. The D^0 lifetime was calculated by the use of the maximum-likelihood estimation method and the final result was $4.3^{+0.7+0.1}_{-0.5-0.2} \times 10^{-13} s$.

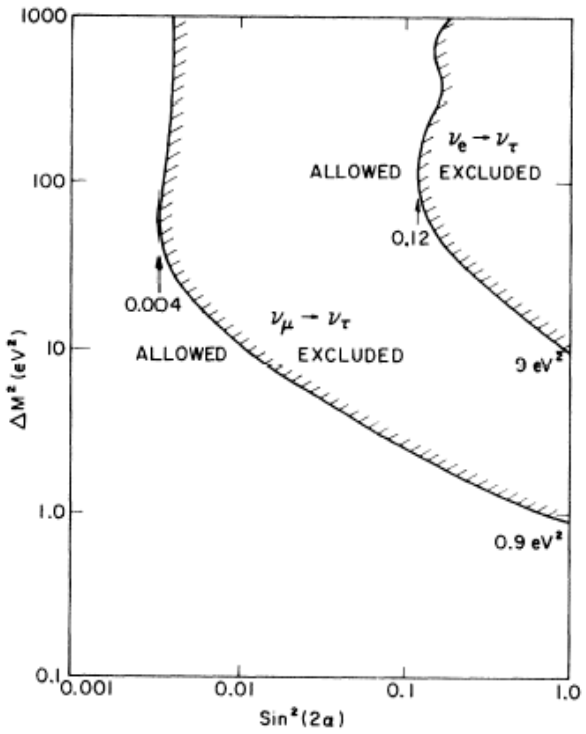

Fig. 3.2 - Δm^2 vs. . $\sin^2(2\alpha)$ plane.

CHORUS experiment

CHORUS (CERN-WA95) was an experiment designed to search for $\nu_\mu \rightarrow \nu_\tau$ oscillation through the observation of ν_τ charged current interactions, followed by the decay of the τ lepton [31]. The search was sensitive to very small mixings if the mass difference is of the order of a few eV or larger. The experiment was performed in the CERN Wide Band Neutrino Beam, which contains mainly ν_μ with a contamination of ν_τ well below the level of sensitivity that can be reached by this experiment. Neutrino interactions occurred in a target of nuclear emulsions, whose spatial resolution (below one micrometer) allowed a three dimensional visual reconstruction of the τ lepton and its decay products; so the experiment was sensitive to most of the τ decay channels and also very important in charm physics. A schematic picture of the CHORUS apparatus is shown in Fig 3.3; the hybrid set-up was composed of an emulsion target, a scintillating fiber tracker system, trigger hodoscopes, a magnetic spectrometers, a lead-scintillator calorimeter and a muon spectrometer. Nuclear emulsions acted as a the target and simultaneously as detector of the interaction vertex and the decay point of the τ lepton; the total mass of the target was 770 Kg. The emulsions were subdivided in 4 stacks of 36 plates, oriented perpendicularly to the beam and with a surface of 1.44 × 1.44 m^2. each plate was made

of a 90 μm transparent plastic film with 350 μm emulsion sheets on both sides. The nuclear emulsion target is equipped with a high resolution tracker made out of planes of emulsions and planes of scintillating fibers. Each stack was followed by three special interface emulsion sheets.

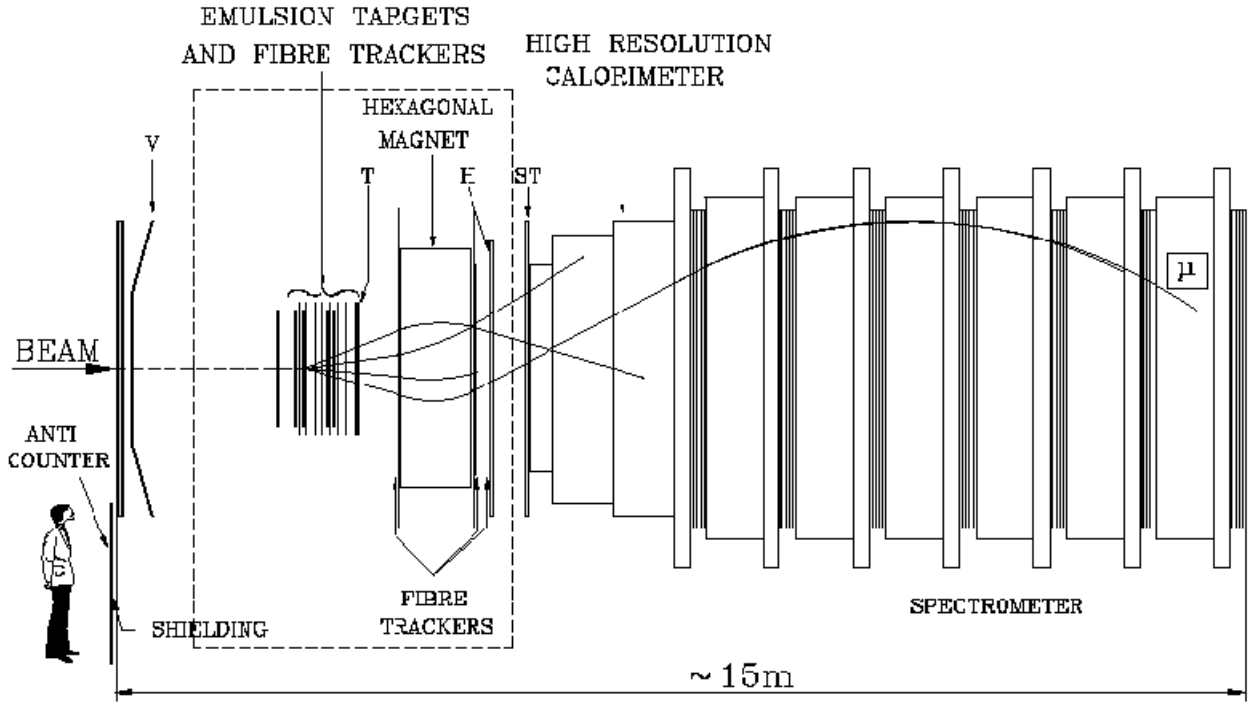

Fig. 3.3 – General layout of the detector.

Eight planes of trackers of scintillating fibers interleaved between emulsion stacks reconstructed the trajectories of the charged particles with a position resolution of 150 μm and an angular resolution of 2 mrad. Downstream of the target region there was a magnetic spectrometer that performed the charge and momentum reconstruction of charged particles, a calorimeter and an air-core hexagonal magnet.

The events kept for the analysis in the emulsion were those for which the scintillating fiber trackers allowed track reconstruction and determination of the interaction vertex position [32]. The event must contain at least one negative track, as a possible decay product of a τ. They studied also events having only one reconstructed track and in that case it was assumed that the interaction vertex was located in the middle of the emulsion stack. All the events have been selected as:

- 1 μ : they had one negative track reconstructed by the muon spectrometer or by range measurements. CC interactions selection efficiency was 80% and depends on the scintillating fiber signal computation. The full sub-sample consisted of 713000 interactions.

- 0 μ: in this case there was no muon track reconstructed at the interaction vertex and the sub-sample consisted of 335000 events. Some of this events were originated by secondary interactions or γ conversions so it was applied a cut on events having a total energy smaller than 1 GeV.

Emulsion scanning strategy in Salerno Laboratory

CHORUS emulsion target has been shared among several scanning laboratories in Japan and Europe, the Salerno laboratory joined the emulsion scanning and data analysis and developed its own automatic scanning system. That system is called SySal (System of Salerno) [33] and is the back-bone of the European Scanning system presently fully developed and used in OPERA experiment.

That system consists of a Nikon microscope (Nk-35-L, 50X or 22X magnification) equipped with a CCD camera and a frame grabber working at 30 fps, emulsion are mounted on a motorized wide stage controlled by host PC.

All images acquired by the camera are processed by the frame grabber and stored in a digital format (256 grey levels), the system performs a fast tomography of the emulsion and is able to perform on-line track recognition by superimposition of consecutive emulsion layers; each track is recognized requiring the alignment of darker spots, clusters, in different layers (Fig. 3.4). To speed up tracking algorithms each image is divided into 25-100 virtual cells and the search for aligned clusters is restricted only to the nearest cells in consecutive layers. The system is able to reconstruct more than one track at every angle in the same field of view and also to perform track intersection analysis to locate neutrino interactions[34]. The mean speed reached during CHORUS emulsions scanning was 1 s/event.

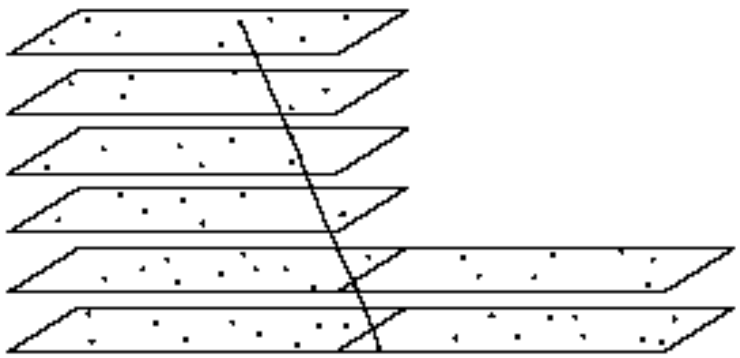

Fig. 3.4 – Track reconstruction among different emulsion layers.

The first task accomplished was the neutrino interaction location by scan-back technique, each event reconstructed by electronic detector has a list of related tracks with different identifiers

and properties. The negative charged muon has been used to find the interaction point: we selected its position on the interface sheet and followed it back till its disappearance in target sheets. SySal system was able to reconstruct also other tracks in the same field of view and perform intersections between them to locate neutrino interactions. The track finding efficiency was very high, around 98%, and the high emulsion spatial resolution allowed us to perform vertex location in a very detailed way. We also performed a volume scanning around the vertex position to search charged and neutral particles decays; this was the so called CHORUS phase II and was mainly related to study charm physics and to increase the statistics since the Collaboration did not found any ν_μ interaction candidate.

Salerno lab took part also to CHORUS phase II and developed the Total Scan technique [35]. I have been personally involved in this study and I had the opportunity to refine dedicated algorithms to study data quality and perform charm decay search. The Total Scan has been performed around located and manually confirmed neutrino interaction points, we scanned an area of 1.3 mm^2 along 8 consecutive emulsion plates, thus to have a proper fiducial volume to search for charmed particles decay. Each volume has been aligned on selected high momentum tracks and then a dedicated software performed off-line tracks and vertex reconstruction. Vertex reconstruction was as detailed to located several charm decays by topological and kinematical cuts. The final charm sample consisted of 71 neutral and 60 charged candidates that have been included in the general CHORUS statistics.

CHORUS main results

The emulsion scanning procedure used in all other scanning labs has been developed in Nagoya University and it is fully automated using computer controlled microscopes equipped with CCD cameras and fast processors. The processor, which is called track selector [36], is capable of identifying tracks inside the emulsions, measuring their parameters on line.

The location of the plate containing the interaction vertex is based on the following back of the selected negative tracks. A track which is found in the interface emulsion sheets is followed upstream in the target emulsion stack, using track segments reconstructed in the most upstream 100 μm of each plate, until it disappears. The corresponding plate is defined as the vertex plate, since it should contain the primary neutrino vertex or the secondary (decay) vertex, or both, from which the track originates. The Net Scan system is used to perform a detailed analysis of the emulsion volume around the vertex position, recording, for each event, all track segments within a given angular acceptance. the scanning volume is 1.5 mm wide in each transverse direction and 6.3 mm along the beam direction, corresponding to eight emulsion plates. The six plates downstream of the vertex act as decay space and are used to detect the tracks of the decay daughters.

From analysis of the complete set of data collected by CHORUS in the years 1994-1997 the Collaboration did not found oscillation signal and the neutrino mixing is excluded down to

$$\sin^2 2\alpha = 6.8 \times 10^{-4} \text{ for large } \Delta m^2 \text{ (90\% C.L.).}$$

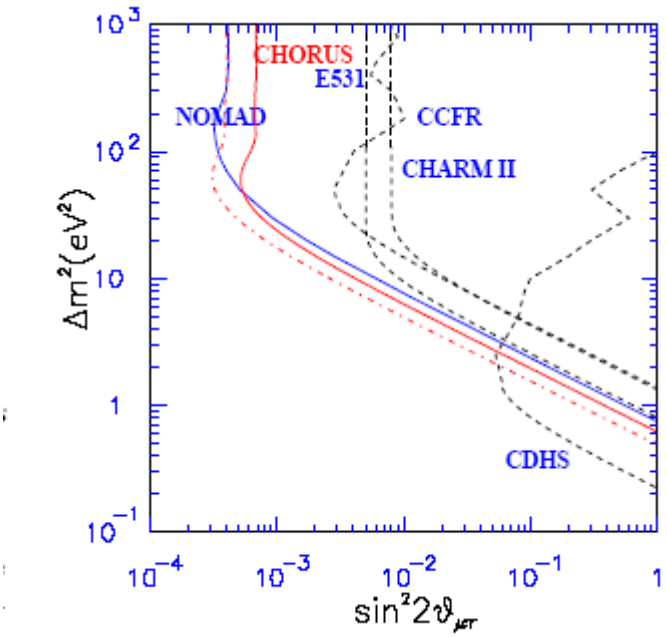

Fig. 3.5 - Present limit on $\nu_\mu \rightarrow \nu_\tau$ oscillation compared to the results of previous experiments (dashed lines).

In total about 100 000 charged-current neutrino interactions were located in the nuclear emulsion target and fully reconstructed. From this sample of events which was based on the data acquired by new automatic scanning systems, 1048 charged-current interactions with a D^0 in the final state were selected by a pattern recognition program and confirmed as neutral-particle decays through visual inspection; this is the larger charm statistic in nuclear emulsion neutrino experiments and allowed a lot of interesting results. The ratio of decay branching fractions of the D^0 into four charged particles to two charged particles was measured to be [37]

$$B(D^0 \rightarrow V4)/B(D^0 \rightarrow V2) = 0.207 \pm 0.016 \pm 0.004.$$

The inclusive measurement of the observed production rate of the D^0 with a decay into four charged prongs in combination with external measurements of this topological branching ratio was used to determine the total D^0 production rate by neutrinos without additional assumption on the branching fractions. The value of this rate relative to the charged-current cross-section was found to be $\sigma(D^0)/\sigma(CC) = 0.0269 \pm 0.0018 \pm 0.0013$. In addition, the same normalization method was used to deduce the inclusive topological decay rate into final states with neutral particles only. A value of $0.218 \pm 0.049 \pm 0.036$ was found for this branching fraction. From an observed number of three charged six-prong events the branching ratio into six charged particles was determined to be $(1.2^{+1.3}_{-0.9} \pm 0.2) \times 10^{-3}$. A measurement of the energy dependence of the D^0 production by neutrinos relative to the total charged-current cross-section was also published . This measurement was used to deduce for the effective charm-quark mass a value of (1.42 ± 0.08) GeV/c^2.

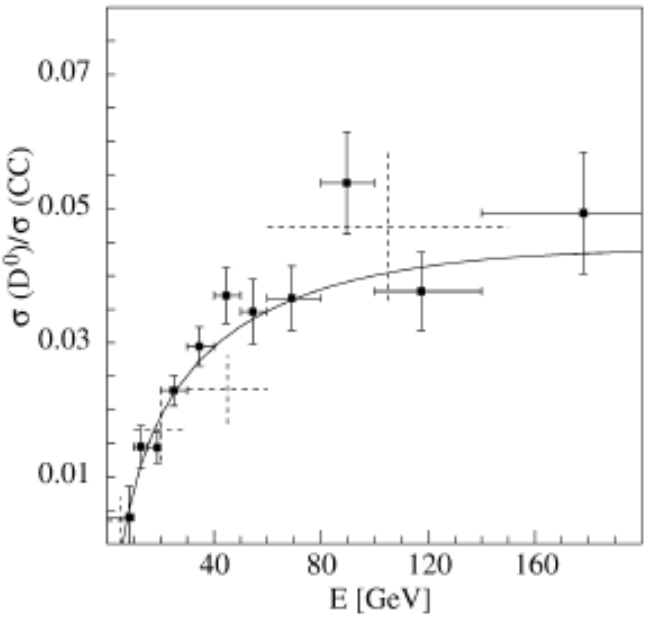

Fig. 3.6 - Energy dependence of the cross-section ratio. The data points drawn as full lines show the measurements reported here, the dashed lines the E531 results. The curve through the data points shows the result of the model calculation.

A measurement of Λ^+_c production in neutrino nucleon charged-current interactions was also realized [38]. In a sub-sample of about 50000 interactions located in the emulsion target of the CHORUS detector, criteria based on the flight length allowed a statistical separation among the different charm species thus enabling a sample particularly rich in Λ^+_c to be defined.

There have been also searches for associated charm production in neutrino charged-current interactions based on the visual observation of charmed-particle decays: one event with a double charm-decay topology has been found and a corresponding background of 0.04 events has been evaluated . This result is unique and peculiar of nuclear emulsion experiments.

A systematic search for super-fragments [39] (charmed nuclei) has been performed in 22200 neutrino-emulsion interactions by automatic off-line image analysis. The absence of candidates provides an upper limit for the super-fragment production rate of 1.9×10^{-4} (90% C.L.) relative to neutrino charged-current interactions at an average neutrino energy of 27 GeV. In the same analysis 28 hyper-fragment decays were found. For the first time, a production rate of hyper-fragments in neutrino–emulsion interactions was obtained. The value of the hyper-fragment production rate relative to the neutrino charged-current cross-section was found to be

$$2.0 \pm 0.4(\text{stat}) \pm 0.3(\text{syst}) \times 10^{-3}.$$

A measurement of antineutrino induced charm production is performed by using the presence of a 5% $\overline{\nu_\mu}$ component in the beam [40]. The measurement takes advantage of the capability to observe the decay topology in the emulsion. The analysis is based on a sample of charged-current interactions with at least one identified positive muon. By requiring a positive

muon charge as determined by the CHORUS muon spectrometer, 32 $\overline{\nu_\mu}$ induced charm events were observed with an estimated background of 3.2 events. At an average antineutrino energy in the neutrino beam of 18 GeV, the charm production rate induced by antineutrinos is measured to be ($\overline{\nu_\mu}$ + N $\rightarrow \mu^+$ + c +X)/($\overline{\nu_\mu}$ + N$\rightarrow \mu^+$ + X) = (5.0$\pm$ 0.7)%.

The charm production rate as a function of the antineutrino energy is found to be in good agreement with previous results derived from non-emulsion experiments.

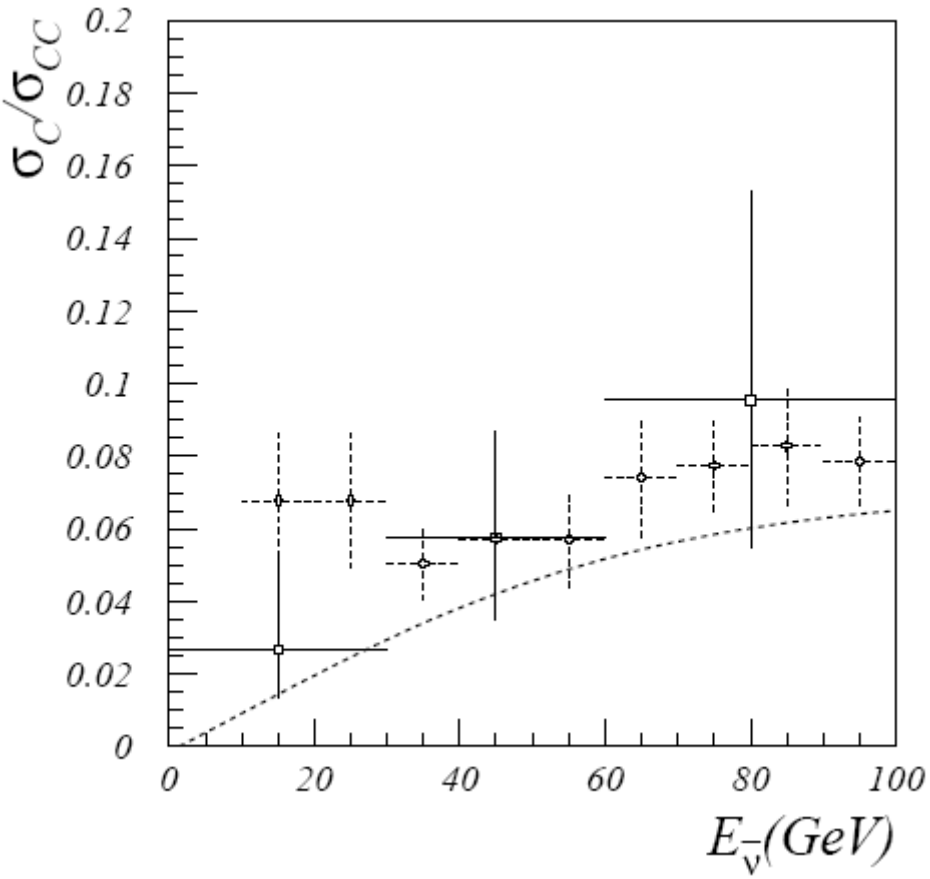

Fig. 3.7 - Charm production rate in $\overline{\nu_\mu}$ CC interactions as a function of the antineutrino energy: measured in CHORUS (empty box) and derived from di-lepton data (dashed lines). The line shows the theoretical prediction obtained from a leading-order calculation with m_c = 1,31 GeV/c^2.

DONUT experiment: first direct observation of the τ neutrino

The τ neutrino was postulated in 1975 after the discovery of the τ lepton by M. L. Perl as the third generation neutrino in the Standard Model of electroweak interactions.

The DONUT experiment established the existence of the τ neutrino in July 2000 by its charged current interaction; the same manner as the two other neutrino flavors has been detected.

The DONUT detector (Direct Observation of NU-Tau) was built to observe the charged current interactions of ν_τ and its charge conjugate. These interactions are identified by the detection of the τ lepton as the only lepton created at the primary vertex. τ lepton has a lifetime of 2.9×10^{-13} s. The detectors were constructed and installed in the Fermi lab PW beam line in 1996. The neutrino data were taken from April 1997 until September 1997. The first phase of the analysis was completed by July 2000 and the observation of four events satisfying the requirements of τ production in emulsion was published.

The emulsion was the heart of the experiment. The electronic detector was also used in the analysis of the tau neutrino magnetic moment where the emulsion was used passively. This experiment had shown that the integrated penetrating charged particle track density through the emulsion had to be limited to less than $5 \square 10^5$ tracks per cm^2. The two significant backgrounds from the dump were muons and neutrons. The high-energy muons, with momentum greater than 20 GeV/c, were not absorbed but detected horizontally by sweeping magnets. At DONUT beam energy the τ typically decays within 2 mm from the vertex into a single charged particle and neutrinos:

$$\nu_\tau + N \rightarrow \tau^- + X$$
$$\tau^- \rightarrow \left(\mu^- or \quad e^- \right) \nu_\mu \nu_\tau$$
$$\tau^- \rightarrow h^- \nu_\tau$$

The characteristic signature of a τ neutrino event is the observation of a primary interaction track with a bend point or kink, identifying this track as a τ lepton.

Nuclear emulsions were used as high resolution tracking devices in this experiment. The resolution achieved with emulsions is better than 1 μm. The emulsion target was followed by a spectrometer that was used to determine the charge, energy and particle identification of the decay products. A schematic of the experiment is shown in Figure 3.8.

The neutrino beam used by the experiment was produced by 800 GeV protons from the Fermi Lab Tevatron interacting in a one-meter long tungsten beam dump. The principal source (85%) of τ neutrinos and τ anti- neutrinos is the leptonic decay of the charmed meson D_s, into τ and ν_τ. All charged particles produced in the dump were swept away from the emulsion target region by magnets or were absorbed by concrete, iron and lead shielding.

The DONUT detector consisted of a scintillation counter veto wall, emulsion target, trigger hodoscopes, analyzing magnet, drift chambers, calorimeter and muon identifier. They used two different types of emulsion targets. The first type called ECC, was composed of 1 mm thick stainless steel plates interleaved with emulsion plates. These plates were composed of 100 mm

thick emulsion layers on either side of a 200 μm or 800 mm thick plastic base. A target module consisted of 50 steel/emulsion layer pairs to obtain a thickness of 0.16 interaction lengths. The bulk type was composed exclusively of emulsion plates with 350 mm thick emulsion layers on either side of a 90 mm thick plastic base. These modules were 0.13 interaction lengths thick. The transverse size of all emulsion and steel sheets was 50 cm x 50 cm; between emulsion modules, 44 planes of scintillating fibers provided precision tracking, and were read out by an image intensifier system.

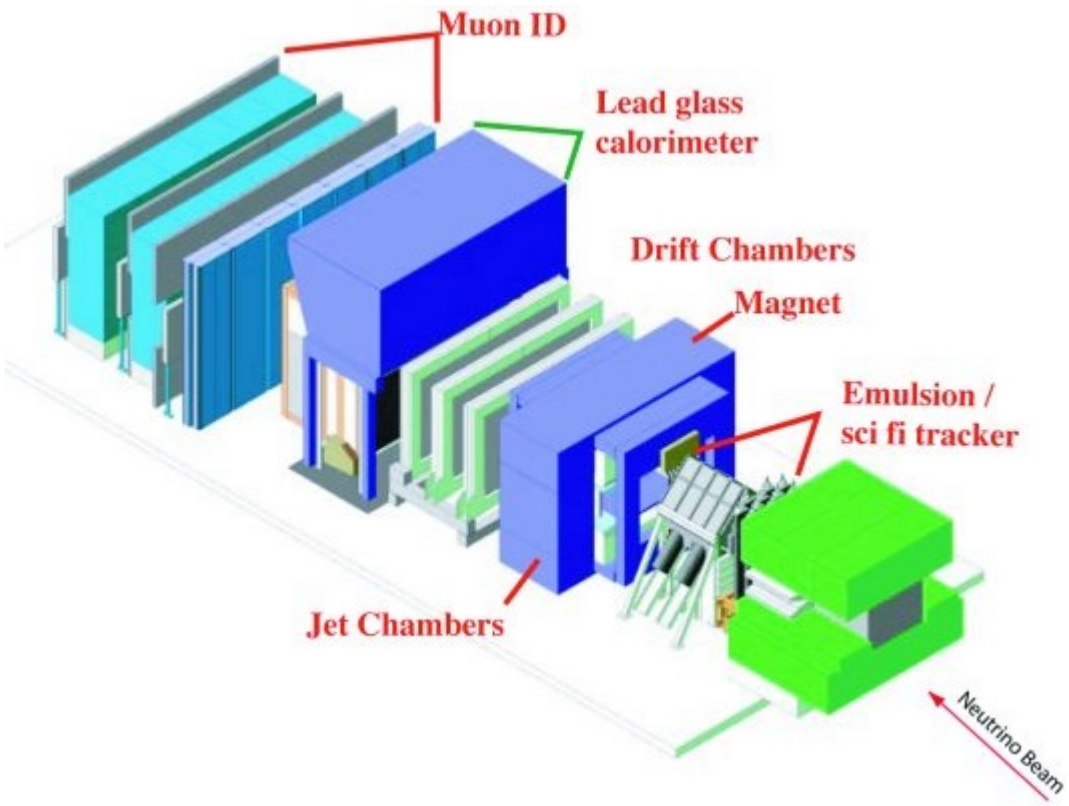

Fig. 3.8 – Schematic view of the DONUT detector.

Neutrino interactions in the emulsion target were selected by trigger hodoscopes in the target region. For each accepted event all electronic detector components were read out. The information from the spectrometer and calorimeter was used to select possible candidate events. All charged particle tracks from these candidate events were projected back to the exit point of the emulsion target using the scintillating fiber tracking system. The reconstructed tracks were then used to reconstruct a vertex with a typical precision of 1 mm in the transverse coordinate and 7 mm in the beam direction. This event selection was used to limit the size of the search volume in the emulsion target. During the run, 4.0×10^{6} triggers were recorded from 3.54×10^{17} protons incident on the tungsten target. After further cuts on the event geometry and energy a total of 898 events were classified as neutrino interaction candidates. Of the 898 candidates, 698 had a vertex predicted within the emulsion fiducial volume. Additional requirements on the

event topology and vertex precision reduced the sample to 499 events. These 499 events were scanned using a fully automated emulsion scanning stations, which followed all tracks from the vertex through the different emulsion sheets. The result of this scanning is a 3D digitized image of the interaction with a precision better than 1 μm. A valid vertex was located for 262 of the 499 events.

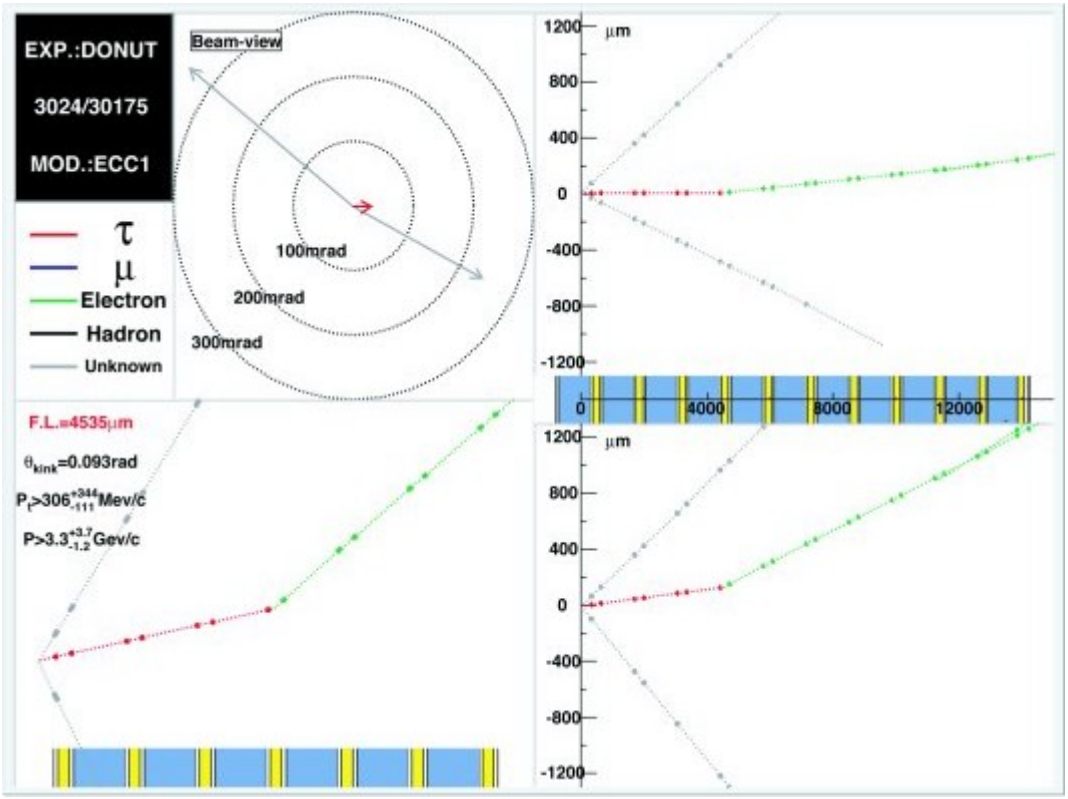

Fig 3.9 - One of the five observed τ neutrino charged current interactions. The kink signature of the τ decay is clearly visible. The target is represented at the bottom: steel=blue, emulsions=yellow. In this example the τ decays into an electron.

A method of fully automated scanning has been developed over the past 20 years by the group of prof. K. Niwa and his colleagues in Nagoya, Japan. This technique was used in the CHORUS experiment, and most recently allowed the direct observation of the ν_τ in DONUT. Emulsion plates containing located events were rescanned within an adjusted scanning volume centered on the event. After further alignment 203 events satisfied the criterion of track resolutions better then 0.6 μm. In these 203 events a detailed decay search was performed, looking for the event topology of a τ neutrino interaction - a kink in one of the primary tracks.

The selection criteria for ν_τ events were established by Monte Carlo simulation. After the application of these selection criteria to the sample of 203 events, five events remained. This experimental result is consistent with the number of expected t events in the sample, 4.2 events. The total number of background events is estimated to be 0.34 ± 0.05. Therefore the probability that all five events are a result of a background fluctuation is 4×10^{-4}.

Figure 3.9 shows one of the five events, the first direct observation of charged current τ neutrino interactions. These events confirm the existence of ν_τ as a partner of the τ lepton in the Standard Model of electroweak interactions.

OPERA experiment

OPERA is a long-baseline experiment for the direct observation of ν_τ appearance from $\nu_\mu \rightarrow \nu_\tau$ oscillations in the CNGS beam from the CERN SPS to the Gran Sasso Laboratory. OPERA aims at high sensitivity in the parameter region indicated by the deficit of atmospheric muon neutrinos and by its zenith angle dependence as observed by the Super-Kamiokande experiment [41]. The experiment exploits nuclear emulsions as very high resolution tracking devices for the direct detection of the decay of the τ produced in the target ν_τ CC interaction. The design is based on the ECC detector, a modular structure made of sandwich of passive material interspaced with emulsion layers. By assembling a large quantity of such modules, it is possible to conceive and realize a ~ 2000 ton fine-grained vertex detector optimized for the study of ν_τ appearance.

OPERA detector construction in Gran Sasso underground laboratory….

The feasibility of OPERA is linked to the production of emulsion films on an industrial scale and to the impressive progress in the field of computer controlled microscopes read out by fast CCD and CMOS cameras with automatic pattern recognition and track reconstruction.

At present, OPERA is under construction; emulsion films are in production, the underground detector at Gran Sasso will be ready by the middle of 2006, when the CNGS beam will be ready.

In order to realize ν_τ appearance experiment, the beam energy of the CNGS beam is above the tau lepton production threshold (~3.5*GeV)*. The expected number of neutrino interactions in a 1 kton detector per year is ~ 2500$\nu_{CC\mu}$ and ~ 15$\nu_{CC\tau}$ in the case of the SK best fit neutrino oscillation parameters; Table 3.1 shows some basic parameters of the CNGS beam.

$< E >_\nu$	17 GeV
$\nu_\mu^{cc} / pot / kton - GS$	5.44×10^{-17}
Proton on target (pot) in shared mode per year	4.5×10^{19}
ν_τ^{prompt}	Negligible
$\left(\nu_e + \bar{\nu}_e\right) / \nu_\mu$	0.85%

Table 3.1

ECC is a stack of one-millimeter thick lead plates and thin nuclear emulsion films. The size of the ECC brick is 10*cm* × 12.5*cm* perpendicular to the beam and the thickness is about 7.5cm. Each brick contains 56 lead plates and 57 emulsion films. Each brick is attached to a doublet of special emulsion sheet independently packed named Changeable Sheet (CS). The CS doublet will be used in order to tag the right brick where the neutrino interaction occurs, in the following chapters I will discuss in more details the CS use and scanning in OPERA.

The thickness of one brick is 10 X_0, which is enough to identify electrons, measure their energies and measure the momentum of charged particles by multiple scattering.

The total number of bricks (206336) will be produced by an automatic machine called BAM (Brick Assembly Machine) being designed by external firms following specifications listed in a technical document.

The OPERA detector is composed by 2 Super Modules (SM in the following) each of them formed by a target section followed by a muon spectrometer. In front of the SM1 there is a Veto plane made of Resistive Plate Chamber, whose role is to detect particle entering the detector different from neutrinos. The target section is made of 31 brick Walls interleaved with 31 Target Tracker planes. Each Wall consists of 3328 bricks removable by the side using an automatic system called Brick Manipulator System (BMS). The whole target section on each SM contains 103168 Bricks equivalent to about 900 tons. This is the target on the detector where neutrino interactions are detected. A TT plane consists of 4 horizontal + 4 vertical modules to measure x-y coordinate. Each module contains 256 plastic scintillator strips read out at both

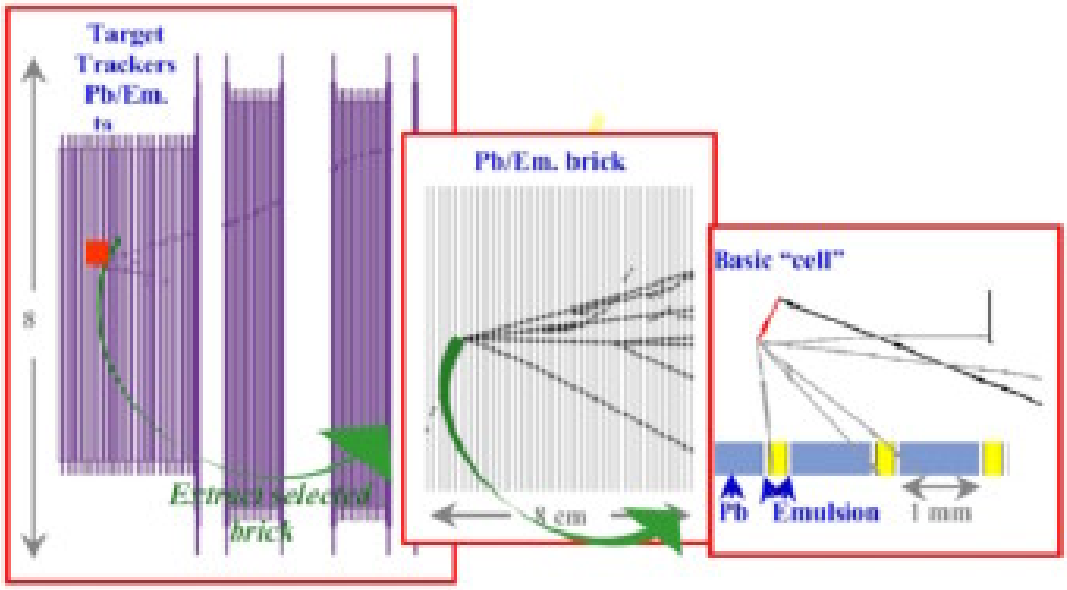

Fig. 3.10 – The structure of the OPERA target and some details of the "basic cell".

ends using optical fibers. Each target tracker plane will indicate in real time the neutrino interaction, pointing to the corresponding brick to be removed and analyzed. The Muon Spectrometer consists of a 10x10 m section dipole magnet formed by 11+11 iron planes interleaved by 11+11 RPC planes. In front, in the gap and behind the magnet there are 3 couples of Precision Tracker (PT) planes made of 16 modules (each plane) of streamer tubes. The role of the PT is to measure the angle of the passing trough muons. In order to improve the angular resolution on the measurement of the incoming particle, in front of the magnet is positioned an additional couple of RPC planes with inclined read out strips with respect to the horizontal and vertical ones these planes are called XPC. The role of the muon spectrometer is to measure the sign and momentum of the muon produced by the neutrino interactions in the target section. Once the neutrino interacts in the target section, the TT planes will indicate the brick where the interaction has happened. The "triggered brick" will be removed by the BMS and send to the brick analysis procedure and it will not be replaced by a fresh one.

In 5 years data tacking there will be removed about 15% of the bricks in the OPERA detector. The triggered bricks will be exposed to cosmic ray for 1 day in order to accumulate passing trough tracks needed for emulsion sheet alignment, then they will be dismounted and all the emulsion sheets will be developed in a dark room.

Several Scanning Station are now under construction (Japan and Italy) to analyze the OPERA bricks and validate the neutrino interaction. A precision measurement will be then performed on each validated brick.

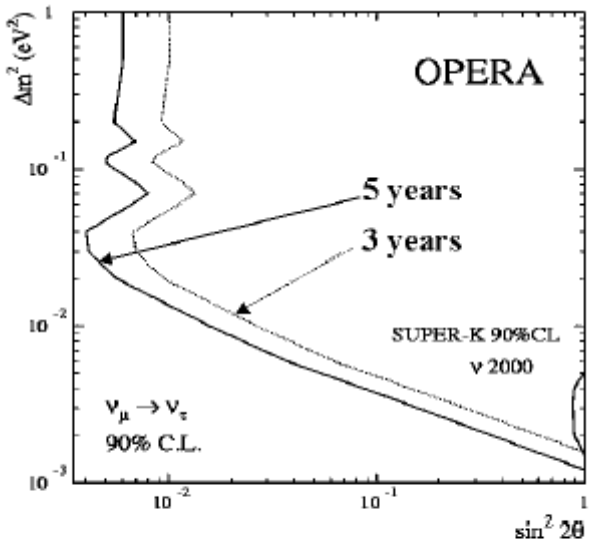

Fig. 3.11 – Sensitivity of the OPERA experiment (90% C.L.).

Using advanced emulsion scanning technologies, recorded tracks in the extracted bricks will be read-out automatically within a day. Interaction vertex location in the brick, decay hunting and decay analysis will be performed as like the case of DONUT experiment. For the candidate events, extra-bricks located downstream of the vertex will be extracted and the corresponding particles will be investigated further in order to check the existence of secondary leptons from the interaction. Tight cuts on the momentum and decay-P_t will be applied to the decay candidate picked up topologically in order to suppress the backgrounds to of order 0.1 events. The expected number of golden $\nu_{CC\tau}$ events is 11 in the case of 5 years running and the best-fit SK parameters. The total background is estimated to be 0.7 events. Fig. 3.11 shows the exclusion plot in the case of no signal, the sensitivity (90% CL.) covers the SK expected region.

Present status

The whole detector is now under construction in Gran Sasso Laboratory and all sub-detectors have been successfully tested and are now ready to be commissioned.

Emulsion film, the key detector element of OPERA, is now under production at Fuji Photo film Co., Ltd in Japan. The production is performed by machines of commercial photographic films in order to get the required large amount of emulsion films, 150000m^2.

A cooperative R&D between Nagoya University and Fuji Photo Film has implemented refreshing capability; by this procedure, unwanted tracks recorded during the film production can be erased before its use. After the production in the factory, refreshing is applied in the facility located underground of the TONO mine. Then the films are vacuum-packed, closed into boxes and transported to the Gran Sasso underground laboratory by ship. The film production will continue until the end of 2005 and the refreshing at TONO mine will continue until the beginning of 2006.

In Hall C of Gran Sasso underground laboratory, detector construction is in progress. The target supporting structure including muon magnet has been constructed successfully. 25 target

tracker plane and relative walls support structure for ECC brick have been installed. In parallel, second super module construction has been started.

The next milestone is the start-up of the ECC brick construction by BAM. This will be started in the beginning of 2006 after a long R&D phase involving the selected firm and Italian and Japanese collaborators; in the next chapter I will discuss all the related items. According to the current planning, the CNGS beam will be on OPERA target in July 2006.

	Signal ($\Delta m^2=1.9x10^{-3}eV^2$)	Signal ($\Delta m^2=2.4\ x10^{-3}eV^2$)	Signal ($\Delta m^2=3.0x10^{-3}eV^2$)	BackGround
OPERA 1.8 kton	6.6	10.5	16.4	0.7

Table 3.2 –OPERA expected oscillation signal.

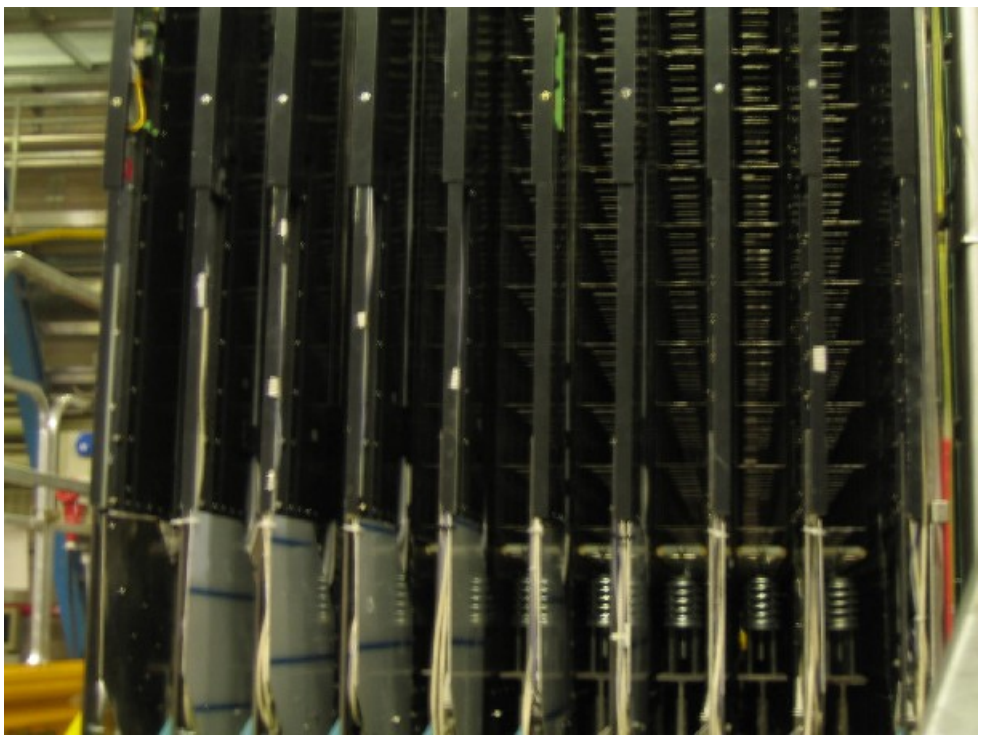

Fig. 3.12 - Target region already assembled (TT planes interleaved by ECC wall support).

R&D on Opera ECC

Opera ECC are called bricks (because they are arranged in walls) and they are the basic and vital component of the entire detector; they will be the neutrino target and, at the same time, they will record as well as possible all the interactions that we will study in the next years to search for ν_τ appearance, interaction and τ decay. The whole detector will consists of more than 206000 bricks, that means 12 millions of emulsion and lead thin foils; it has been clear from the beginning that the construction of all of them should have been accomplished by an automatic procedure, this project is the so called BAM (Brick Assembly Machine). The BAM project started at the very beginning of the OPERA project with an intense collaboration between European and Japanese emulsion and automation experts; the final design of this machine has been finally fixed in the last few months after a large number of fruitful tests. Salerno Emulsion group has been deeply involved in this R&D activity through the work of Prof. G. Romano and Dr. C. Sirignano and all the BAM related studies and tests carried on in the last three years will be reported in this chapter.

Emulsions and lead sheets are supposed to be in contact for years inside Opera bricks, so it is necessary to guarantee no damage on the emulsions due to lead radioactivity or chemical reactions between lead, emulsion films, other brick components and the Gran Sasso experimental environment. Therefore there have been planned dedicated tests for each of these items regarding emulsion and lead manipulation during the brick construction and their long-term compatibility. The brick design changed a lot from the baseline option according to experimental results and it has been reached a promising compromise after long discussions within the collaboration and the external firm selected to build up the BAM.

Brick base-line option

ECC packing must preserve the lead planarity to allow measuring particles direction within few milliradiants accuracy and the alignment of all emulsion films within few microns accuracy [41]. In order to guarantee brick long-term mechanical stability and to preserve the alignment for five years it has been asked to have vacuum packing, the brick-stack would have been kept together by the so-called origami packing[1] (Fig. 4.1). The packaging material foreseen was an aluminum-coated paper closed under vacuum by thermo-sealing. The paper quality should have been selected in order to avoid chemical contamination that could affect the emulsion sensitivity. Due to the aluminum layer and the thermo-sealing, the inner pressure and humidity should be kept stable. In previous emulsion experiments[2] it has been successfully used the vacuum and origami packing so at the beginning the collaboration was confident on the base-line option feasibility.

The new challenge posted by Opera is to guarantee the long-term (5-10 years) emulsion-lead direct contact compatibility without any problem due to lead radioactivity and/or unwanted chemical reactions. Opera emulsions have been produced by commercial photographic film machines by Fuji- Film Co. in Japan, the entire pouring and coating process has been established after an extensive R&D project between the company and Nagoya University. In order to prevent the occurrence of black or gray patterns on the emulsion surface due to silver chemically deposited during the development procedure it has been decided to put

[1] The aluminum foil should have been folded as accurately as ancient Japanese art of paper folding.

[2] For an account of mentioned experiments see chapter 3.

a 1μm protective gelatin coating on the sensitive layers. The removal of these stains is a time-consuming procedure and it is not suitable in the case of a daily handling of thousands of emulsion films, as in the case of Opera. In addition the presence of this protective coating allows direct contact with the lead plates; without this protection it should have been compulsory to insert thin insulator sheets in order to avoid chemical reactions between the lead plates and the silver halides contained in the emulsion.

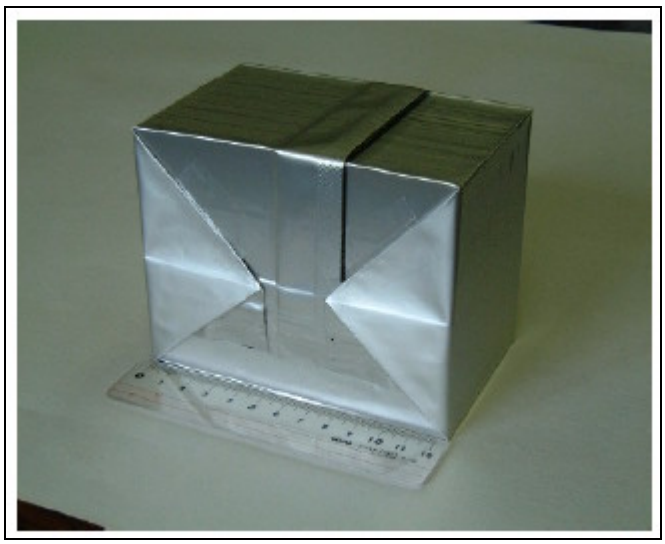

Fig. 4.1 – Opera ECC, origami packing

Lead is a well suited passive material for the Opera ECC bricks due to its high density and short radiation length; it enhances the neutrino interaction rate and allows the momentum determination by multiple scattering as well as the electron identification and energy measurements. However, lead has the drawback of being radioactive and creates background tracks in the emulsion films. The collaboration performed an extensive search for low radioactivity lead in samples from companies in different countries; three producers were found able to satisfy the following requirements: 10 alpha tracks/cm^2/day and 50 electron tracks/ cm^2/day. In this limit the density of fake tracks created by the mismatching of unrelated low energy segments can be estimated to be $\sim$ 1/mm^2 even after seven years, without considering fading effects. This value has been accepted by the collaboration that stated to use low radioactivity lead coming from Boliden mine in Sweden. The total number of lead plates needed for Opera is about 12 millions and it can be produced by automatic commercial machines, after usual procedure of laminating the lead, slicing the rolls, cutting the plates and cleaning. Because the pure low radioactivity lead is very soft and not easy to handle by machine without being deformed it has been necessary to foresee a kind of hard lead that is possible to have adding 0.7% of Calcium. This solution has been proposed by the Goslar firm (Germany) that has been chosen to produce Opera lead foils.

In the base-line option the three characters playing brick-tale are consequently emulsion, lead and aluminum-coated paper; their chemical and mechanical long-term compatibility has been extensively tested during the last three years. All tests have been simultaneously performed in Europe and in Japan to crosscheck data and get stronger conclusions. I joined European team that was composed by CERN people mainly interested in the automatic BAM machine design and Salerno people mainly interested in emulsion behavior. It has been used

the CERN Emulsion lab facility for emulsion packing, handling and development and Salerno microscopes for measurements.

Lead - emulsion compatibility

Emulsion-lead compatibility tests have been performed in several steps in order to evaluate degradation and/or chemical contamination effects on emulsion films as a function of time. The Opera exposure will last five years and ageing effects have been evaluated putting lead and emulsion in contact at high temperatures (30° C - 40° C); from theoretical evaluations 60 days at 35°C corresponds to five years ageing at 20°C (Opera realistic conditions).

Goslar Company shipped to CERN several samples of lead and they have been tested time-by-time.

Test # 1 (28 July 2003 - 18 September 2003)

In July 2003 Goslar shipped several samples of Boliden lead + 0.7% Ca, Fuji Opera Emulsion films were available at CERN since June 2003 and so the BAM group at CERN planned some dedicated tests. It has been decided to prepare some small piles made of Lead and emulsions (Fig. 4.2) and some single reference emulsions. The pile structure has been carefully studied in order to get as much data as possible from the test. The structure Lead-Emulsion-Lead-Emulsion-Emulsion-Lead combined the Opera basic cell and a reference cell having two emulsions in contact, in this way it would have been possible also to evaluate on the same emulsion the difference between the side in direct contact with lead and the one in contact with the safest material. It has been interesting to study the contamination effect also on one reference emulsion because, even if the Fuji production is uniform, it is possible to have slight differences between emulsions due to storing conditions or small handling accidents.

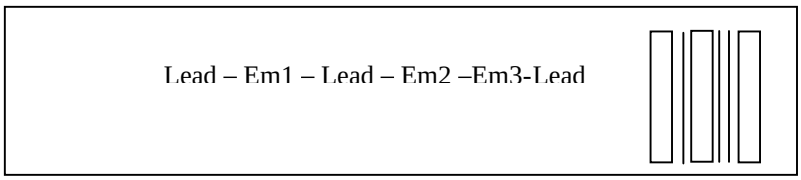

Fig. 4.2 – Test pile schema.

Some piles have been stored at 20°C and some others have been stored at 35°C in an oven to perform an accelerate ageing test, emulsion melting temperature is around 40°C so it has been decided not to run accelerate tests at maximum speed; values expected from theoretical calculations are reported in Table 4.1 (assuming 60% R.H while packed):

20°C	35°C	40°C
1 day	30 days	80 days
25 days	2 years	5.5 years
50 days	4 years	11 years
60 days	5 years	13 years

Table 4.1

In order to avoid chemical contamination on lead plates due to rolling and punching oils some lead plates have been washed by an UltraSonic bath before packing. Some piles have

been packed using vacuum and thermo-sealed aluminium-coated paper bags and some others have been realized by means of 100 Kg mechanical pressures and wrapped in adhesive tape. The second packing option was rather different from the base-line option but was strongly recommended by external firms in charge of BAM project; infact they worried about the long term stability and mechanical robustness of the vacuum packed 8 Kg Opera ECC. Mechanical piles were different from the vacuum packed previously described; they were standard ECC made of 6 emulsion films and 5 lead plates, flatness was obtained by 1 mm thick plastic foils put at the beginning and at the end of the pile. Emulsions have been developed in September 2003 and results were not so encouraging: almost all films were grey and some of them completely black; that was because it occurred a serious contamination that caused a huge fog increase on emulsions. All grains randomly present in emulsion and not belonging to a high energy track are usually called fog, their density can be measured in grains/$(10\mu m)^3$ and the normal value found in Opera films is smaller than 6. Fog measurements have been performed by eyes on all test plates and results are shown in Tables 4.2a and 4.2b.

57 days vacuum	Pb + Ca 0.07 %		Pb + Ca 0.07 % (US washed)	
	20°C	35°C	20°C	35°C
Emulsion 1	35 $\pm$ 4	Black >100	31 $\pm$ 4	Black >100
Emulsion 2 (Top side)	35 $\pm$ 4	Black >100	37 $\pm$ 4	Black >100
Emulsion 2 (Bottom side)	31 $\pm$ 4	Black >100	34 $\pm$ 4	Black >100
Emulsion 3 (Top side)	31 $\pm$ 4	Black >100	33 $\pm$ 4	Black >100
Emulsion 3 (Bottom side)	34 $\pm$ 4	Black >100	40 $\pm$ 4	Black >100

Table 4.2a

Emulsions stored alone in a vacuum bag were the references and they had a fog density of (10.0 ± 0.5) g / $(10\mu m)^3$. Measurements reported in Table 4.2a clearly showed that there have been huge contamination effects due to lead. The fog increase was present every time on both emulsion sides and consequently appeared to be a volume effect due to a very light poisoning gas able to go trough 44 μm emulsions layers and the plastic base.

It has been possible to measure fog densities only for piles stored at 20°C, after high temperature storage emulsion film were completely black and impossible to measure, so it is reported a symbolic value of fog density >100.

There have been performed fog measurements also on mechanically packed piles and the final result was that all emulsion films were in the same condition as the reference ones; conclusion was that a packaging without vacuum has been less dangerous.

57 days mechanical	20° C	35°C
Emulsion 1	9.0 ± 0.5	11.0 ± 0.5
Emulsion 2	10.0 ± 0.5	9.0 ± 0.5
Emulsion 3	8.5 ± 0.5	11.5 ± 0.5
Emulsion 4	9.0 ± 0.5	10.5 ± 0.5
Emulsion 5	9.5 ± 0.5	9.0± 0.5
Emulsion 6	9.0 ± 0.5	10.0 ± 0.5

Table 4.2b

All those data have been reported to the OPERA collaboration [42] and compared with compatibility tests performed in Japan. Both European and Japanese results were the same and they pointed out a clear chemical contamination effect on emulsion in contact with lead that turned out to be not suitable for Opera experiment ECC in case of vacuum packaging.

Automatic fog count

Fog measurements are the best technique to test emulsion conditions; they are usually performed by eye and by manual driven optical microscopes, these methods are highly time consuming and do not allow high statistic. Furthermore manual fog measurements strongly depend on the scanners' personal criteria and could be affected by different systematic errors time by time. Since it was strictly needed reliability and repeatability on each measurement, Salerno group decided to realize some algorithms to measure fog density by means of automatic scanning. This software dramatically speed up all the analyses and became a very powerful tool to understand Opera emulsions features. By automatic measurements it has been also possible to study emulsion sensitivity and grain density distributions along the depth because we have been able to precisely assign 3D coordinates to each grain and reconstruct horizontal tracks.

The hardware components presently used have been inherited from CHORUS experiment scanning activity; they are a Nikon microscope (Nk-35-L, 50X magnification) equipped with a CCD camera and a Genesis frame grabber working at 30 fps; emulsions are mounted on a motorized wide stage controlled by host PC. Preliminary tests have been performed using the SySal software (see Chapter 3); it acquired emulsion images using a 0.5 μm pitch and they have been subsequently processed by the frame grabber and stored in a digital format (256 gray levels). The basic idea was to identify clusters in each layer trying to avoid the shadow effect and assigning to each grain 3D coordinates having the best affordable spatial resolution. For example, in Fig. 4.2 it is possible to see two emulsions with rather different fog densities and related plots. Those two emulsions came from the same Fuji production; the darker one has been stored in vacuum between two lead plates at 20°C for 57 days, the other one has been stored alone in an envelope at 20°C for 57 days. Both automatic and manual measurements showed that the fog density in one case is 5 times bigger.

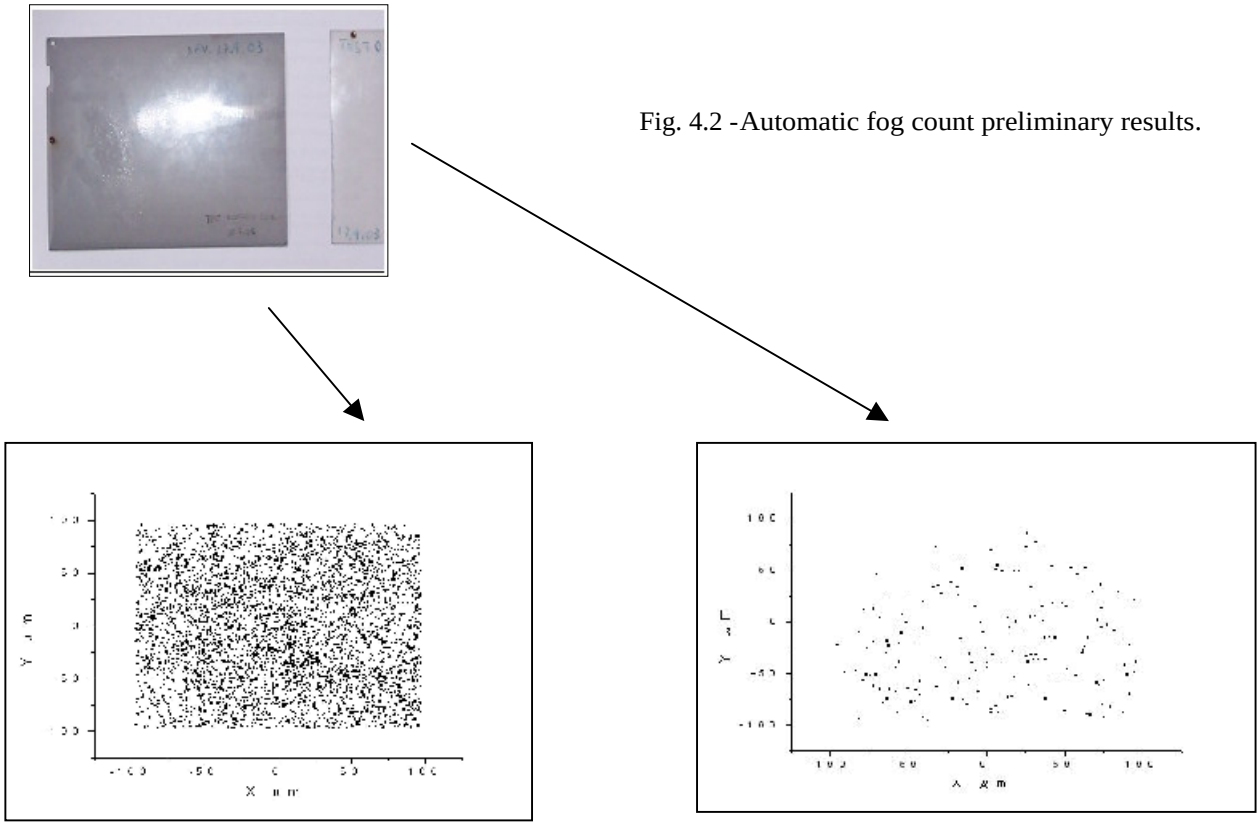

Fig. 4.2 -Automatic fog count preliminary results.

From preliminary data it came out that in order to gain high resolution it was compulsory to develop a new clustering procedure to correct the "focal depth aberration" and to get completely rid of the shadow effect. Considering the clustered data profile it has been measured a spherical curvature having a 7μm getter (Fig. 4.3) and the focal depth of the objectives that was around 3 μm.

A specific property of OPERA emulsion films has been used to correct these two hardware problems. OPERA emulsion is poured in two steps by Fuji machines, during the first step they pour a 21μm active (gel+AgBr) layer, then they add a 1μm inert (only gel) layer and

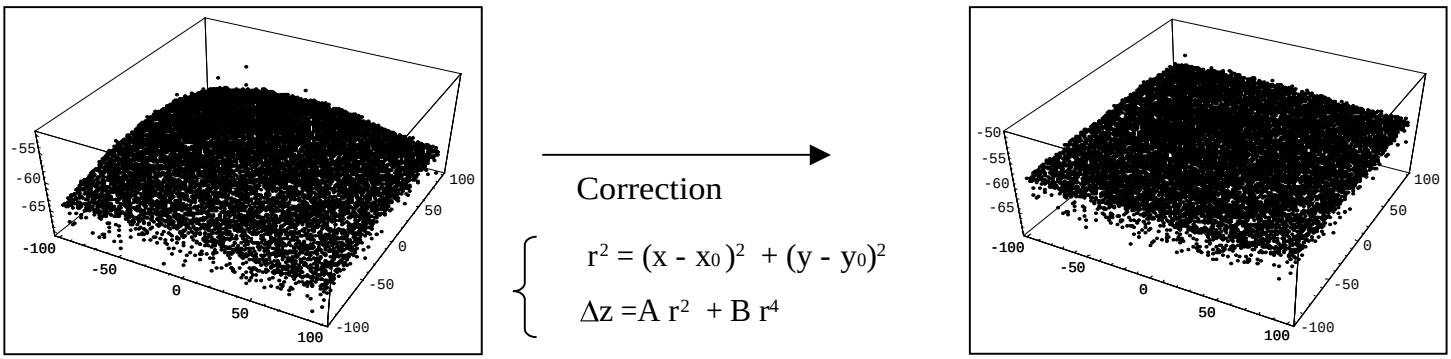

Fig. 4.3 – Grains profile before and after the optical aberration correction.

finally they pour a second 21μm active layer. Referring to this composition it has been developed a specific routine to correct the spherical aberration in such a way to have the

minimum grain number in the central inactive layer. After several trials it turned out that it should be applied a polynomial correction (fourth grade) to every cluster z coordinate as a function of their distance from the field of view center. After this preliminary correction grains 3D coordinates has been defined computing "minimum grey levels" and comparing them with the average. Special care has been devoted to identify correctly the depth of each grain, it is interpolated between three consecutive layers near the minimum by means of a parabolic fit.

A typical output is the histogram shown in Fig. 4.4: depth assignment is refined and so it is possible to identify the insensible gelatin layer, obviously such kind of measurements would have been impossible to be done by manual counts.

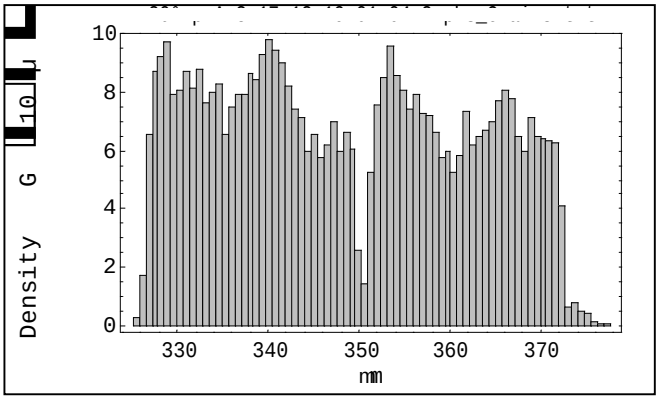

Fig. 4.4 – Grains distribution vs. depth in emulsion.

This software has also a graphical interface that allows the user to check directly on emulsion images the clustering quality and, if it is needed, to change some parameters and thresholds. It is also possible to verify the spherical aberration correction and change it in order to have more precise measurements. The clustering time has been reduced to few seconds so it is now possible to identify grain during the data taking and store them in binary files as well as emulsion images. Obviously the software is not able to distinguish fog grains from low energy electrons and all the measurements will be intended as the sum of these two contributions.

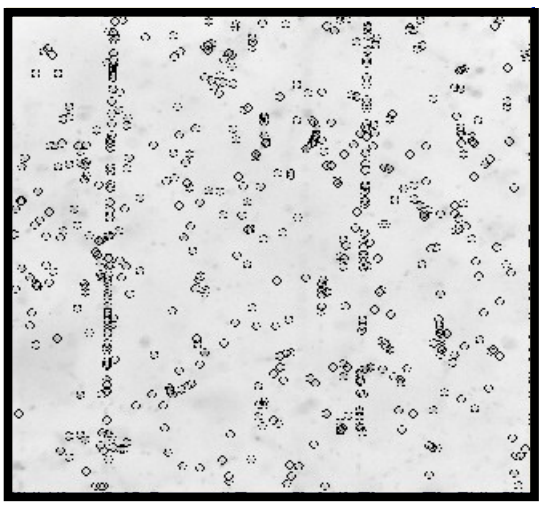

Fig. 4.3 – Off-line display of all reconstructed grains in one microscope view (200 $\times$ 200 μm^2).

After clustering and grain recognition the software is able to reconstruct horizontal tracks, it has been optimized to reject background grains belonging to different emulsion layers, thus to identify correctly the tracks depth. The software takes aligned grains in the top and bottom part of each view and tries to connect them within few micron allowances. Whenever a connection has been established some more grains are searched in the middle of the view. The intrinsic emulsion spatial resolution is smaller than 1μm so it is applied a very severe cut on grains displacement from the fitted trajectory on both longitudinal and transverse coordinates. As it is shown in Fig. 4.4 the accuracy achieved is very good and it has been possible to evaluate the emulsion sensitivity as a function of depth.

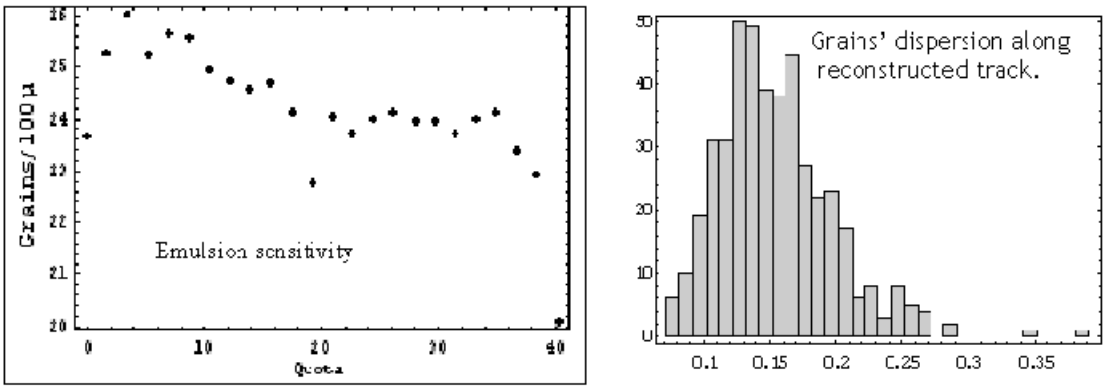

Fig. 4.4 – Horizontal tracks reconstructed in emulsion.

This measurement needs a large statistic (more than 1000 tracks) and it is impossible by manual measurements; only using this dedicated software Salerno group has been able to evaluate this OPERA film feature. It has been usually observed a sensitivity decrease in the upper layer, in Chapter 4 there will be described some tests about the developing procedure made to gain a more uniform sensitivity along emulsion depth.

Test # 2 (22 September 2003 – 18 October 2003)

Considering all the results coming from Test #1 it was decided to investigate deeply the lead effect on emulsions using different types of lead and studying the poisoning effect as a function of time. There have been realized small piles (Lead - Em1 - Lead - Em2 - Em3 - Em4 -Lead) using several kind of lead: Goslar PbCa, pure lead available at CERN, Goslar PbCa painted and Goslar PbCa US washed. Some piles have been stored at 20°C and some of them have been stored at 35°C; some of them have been packed in vacuum and others by mechanical pressure and adhesive tape. After developing and measuring fog densities on all these emulsions there was detected no clear lead effect. Every emulsion has the same colour of a reference emulsion stored alone. The only visible effect was that painted lead lost its varnish. Automatic measurements performed in Salerno confirmed that emulsions put in contact with lead at 20°C or 35°C did not have an higher fog density than the reference one that was 10 g / $(10\mu m)^3$ for vacuum piles and 6 g / $(10\mu m)^3$ for mechanical piles.

	PbCa		PbCa painted		PbCa US washed		Pure Lead CERN	
	20°C	35°C	20°C	35°C	20°C	35°C	20°C	35°C
Vacuum	12.0 ± 0.5	13.0 ± 0.5	13.0 ± 0.5	11.0 ± 0.5	10.0 ± 0.5	11.0 ± 0.5	11.0 ± 0.5	10.0 ± 0.5
	11.0 ± 0.5	12.0 ± 0.5	12.0 ± 0.5	11.0 ± 0.5	10.0 ± 0.5	10.0 ± 0.5	11.0 ± 0.5	12.0 ± 0.5
	11.5 ± 0.5	11.0 ± 0.5	10.5 ± 0.5	10.5 ± 0.5	10.0 ± 0.5	9.5 ± 0.5	10.0 ± 0.5	12.0 ± 0.5
Mechanical	8.0 ± 0.5	8.0 ± 0.5	7.0 ± 0.5	9.0 ± 0.5	7.0 ± 0.5	7.0 ± 0.5	8.0 ± 0.5	8.4 ± 0.5
	8.2 ± 0.5	8.5 ± 0.5	7.0 ± 0.5	9.2 ± 0.5	8.0 ± 0.5	7.5 ± 0.5	8.5 ± 0.5	8.0 ± 0.5
	8.3 ± 0.5	8.0 ± 0.5	7.4 ± 0.5	9.5 ± 0.5	7.0 ± 0.5	7.1 ± 0.5	8.6 ± 0.5	9.0 ± 0.5

Table 4.3

Those tests have been performed also on short periods (1 and 2 weeks) and the result was that all emulsions were compatible with the reference emulsion. Some emulsions had a severe fog increase on the surface in contact between emulsion and plastic, as it is possible to see in Fig. 4.5. It has been discussed about this point with our Japanese colleagues and they pointed out that some emulsion production batches could have been badly stored. It has been observed also that CERN pure lead is deformed and that painted lead lots is varnish.

Conclusions were that:

- painted lead would not be used any more.
- compatibility test must be longer than 3 weeks to detect any severe poisoning effects.
- there could be some discrepancies among different emulsion productions.

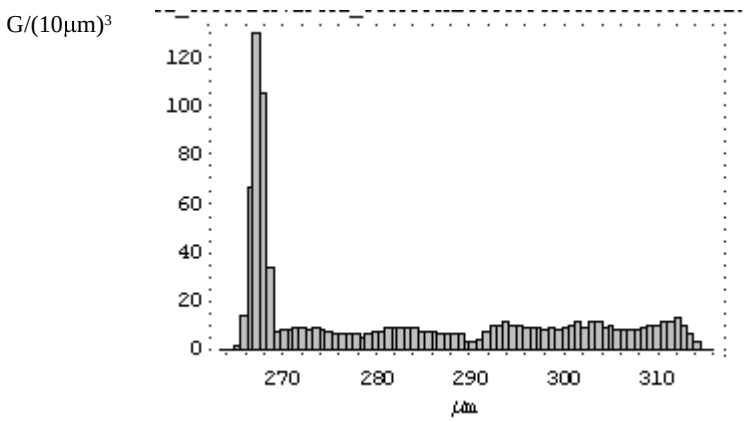

Fig. 4.5 – Fog increase on the plastic-base contact surface.

Test #3 (13 October 2003 – 23 November 2003)

In order to check a surface chemical contamination Goslar has been asked for some lead samples that have been washed to remove lamination and punching dirty residuals. Goslar shipped the following samples to CERN:

1. Lead + Calcium rolled and punched with the same oil
2. Lead + Calcium rolled and punched with the same oil and cleaned with distilled water and ultrasonic.
3. Lead + Calcium rolled with the usual oil and punched with Survos Rapid D.
4. Lead + Calcium rolled with the usual oil and punched with Survos Rapid D, cleaned with distilled water and ultrasonic.

As usual some piles were prepared (Lead – Em1 – Lead – Em2 – Em3 – Em4 -Lead) using new lead plates and they have been stored at 20°C and 35°C.

Results were the following (Reference: 7 g/ $(10\mu m)^3$):

	Type 1		Type 2		Type 3		Type 4	
	20°C	35°C	20°C	35°C	20°C	35°C	20°C	35°C
Vacuum	31.0 ± 0.5	41.0 ± 0.5	28.0 ± 0.5	51.0 ± 0.5	27.0 ± 0.5	36.0 ± 0.5	28.0 ± 0.5	35.0 ± 0.5
	33.0 ± 0.5	26.0 ± 0.5	27.0 ± 0.5	36.0 ± 0.5	26.0 ± 0.5	27.0 ± 0.5	21.0 ± 0.5	31.0 ± 0.5
	21.5 ± 0.5	37.0 ± 0.5	21.5 ± 0.5	30.5 ± 0.5	19.0 ± 0.5	19.5 ± 0.5	24.0 ± 0.5	26.0 ± 0.5
	34.5 ± 0.5	35.0 ± 0.5	26.5 ± 0.5	37.5 ± 0.5	25.0 ± 0.5	31.5 ± 0.5	35.0 ± 0.5	34.0 ± 0.5
Mechanical		7.0 ± 0.5		6.0 ± 0.5		8.0 ± 0.5		6.4 ± 0.5
		7.5 ± 0.5		7.0 ± 0.5		7.5 ± 0.5		7.0 ± 0.5
		6.0 ± 0.5		5.0 ± 0.5		7.1 ± 0.5		7.0 ± 0.5
		8.0 ± 0.5		7.0 ± 0.5		7.5 ± 0.5		8.0 ± 0.5

Table 4.4

A severe poisoning effect was observed for all 4 lead types and vacuum packaging while the same effects was absent in mechanical packaging. Lead surface showed a large amount of oxidation residuals in the case of washed plates. CERN surface treatments division suspected that those residuals came from a bad drying procedure and started to study a better washing-drying procedure to passivate the lead surface.

Test #4, December - January '04 (4 weeks)

CERN experts performed several surface treatment tests to try Lead passivation using washed and etched samples to perform surface residual pollution measurements; the lead samples used were degreased by a solution of NGL detergent (15g/l, T=60°C; 20 hours), rinsed by demineralised water and dried by compressed air. Some samples have been degreased, etched by a 50% H_2SO_4 solution for 10 s and then rinsed and dried [43].

After those treatments they performed surface analysis by an electronic microscope using the XPS technique; the samples is irradiated and the photo-emitted electrons are collected and divided by binding energies in such a way to identify the atoms from which they come from.

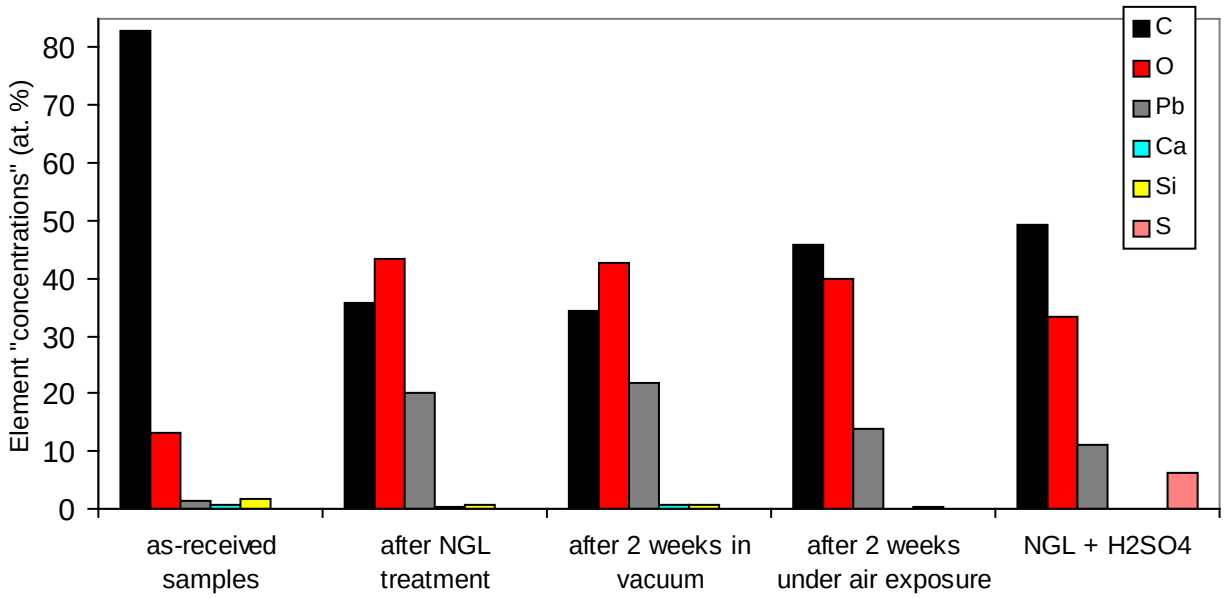

Fig. 4.6 - XPS results.

In Fig. 4.6 there are reported XPS measurements showing that the NGL detergent solution allows having the smaller surface contamination.

After those test Goslar shipped some new lead samples to test:

1. Pure CERN lead
2. Goslar Lead + Ca not washed
3. Goslar Lead + Ca washed at CERN by NGL in order to remove Ca from the surface

Performing the usual packing and storing procedure there have come out results reported in Table 4.6 (Reference: 9 grains / (10 μm)^3).

	20°C		35°C	
	Vacuum	Mechanical	Vacuum	Mechanical
Pure Pb	9	8	9	8.5
PbCa	12	8	>50	8.5
PbCa NGL washed	11.5	8	40	8.5

Table 4.6

From these data it has been possible to understand that the poisoning effect was mainly related to Ca and that the surface contamination was less dangerous to the emulsions. Furthermore it has been observed one more time that the vacuum packaging enhanced the effect and will not be suitable for Opera ECC.

The Ca poisoning effect can be explained by the following considerations: emulsion films contain water and PbCa is not an alloy but Ca is present as an interstitial defect and so it can easily move in the lattice toward the lead surface.

Once that Ca gets in contact with water it took place the following chemical reaction

$$Ca + 2H_2O \rightarrow Ca(OH)_2 + H_2$$

while in the case of pure lead the reaction is:

$$Pb + H_2O + 1/2O_2 \rightarrow Pb(OH)_2$$

Hydrogen can reduce Ag ions and produce latent images of several fog grains; in addition it can easily go trough one whole emulsion and produce the volume poisoning effect that has been observed several times. $Pb(OH)_2$ does not react with emulsion gel or AgBr.

It is reasonable to figure out that in case of vacuum packaging the chemical reactions is accelerated because it is possible to extract much more water from emulsion while in case of mechanical packaging hydrogen can escape from the ECC because it is not gas- tight.

This hypothesis has been supported also by our Japanese colleagues and the OPERA collaboration decided to search from new types of lead alloys and to change the brick packing base-line to the mechanical one in May 2004. This decision has been strongly supported by three experimental evidences described in the following sections:

- long term compatibility between emulsion and PbCa mechanically packed
- alignment measurement accuracy on mechanical packaging

- brick gas-tightness

In the mean time there have been also tested some new lead samples coming from Goslar firm.

Long term test (26/11/2003→26/4/2004)

From November 2003 it has been decided to perform a long term compatibility test using the following components:

- PbCa and one year old emulsions
- lead not washed
- mechanical pile (27 lead + 28 emulsion)
- thin PE to avoid glue-emulsion direct contact

After 5 months the grain density was 5.2 ± 0.4 g / $(10\ \mu m)^3$ and there were no traces of α or β dangerous activities. Emulsion were in good shape and they were not stickled to lead foils or damaged by PE wrapping and aluminium tape protection. The grain distribution was stable along the depth and there were not any contamination.

Alignment accuracy on mechanical bricks (Frascati procedure)

In October 2003 Frascati engineers realized a full ECC by a mechanical procedure using the following components:

- emulsions + Goslar PbCa delivered at CERN in July 2003.
- brick assembled in October 2003 (Frascati procedure)
- brick exposed to PS pions beam429 tracks/cm^2 π 8 GeV/c (110; 0)mrad

Frascati packing procedure consists of several steps: emulsions and lead are first piled up and wrapped with an adhesive tape, later a carbon spring is added to the first and last emulsion and fixed to the ECC by a glass fiber tape by a custom machine able to provide constant tension and speed in order to give uniform pressure on the pile.

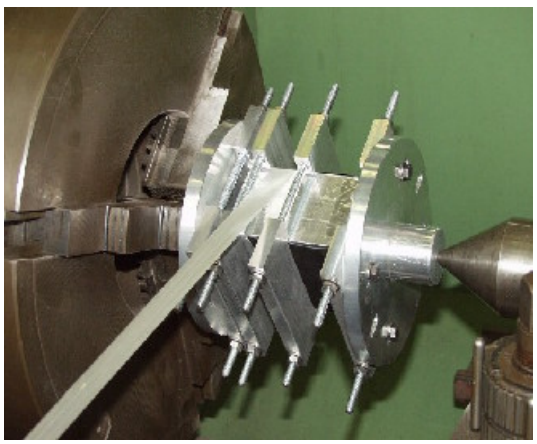

Fiber glass tape after adding carbon fiber springs

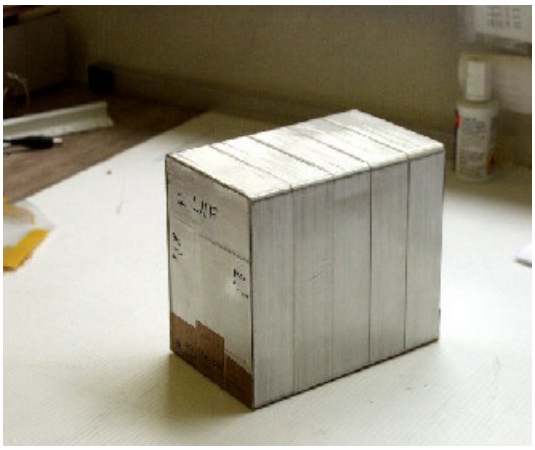

Final Package

In order to check volume alignment and mechanical stability of the pile these ECC were assembled at CERN, exposed to a reference beam of pions and finally scanned with Opera microscope in Salerno lab. There have been scanned 5 zones on each plate and then computed the alignment parameters and the tracks slopes along the full brick. The alignment has been performed by Salerno AΩ Reconstruction software by means of affine transformations:

$$X_2 = A \cdot X_1 + T = \begin{bmatrix} axx & axy & 0 \\ ayx & ayy & 0 \\ 0 & 0 & 1 \end{bmatrix} \cdot \begin{bmatrix} x_1 \\ y_1 \\ z_1 \end{bmatrix} + \begin{bmatrix} dx \\ dy \\ dz \end{bmatrix}$$

(where X_1 and X_2 are the tracks coordinates before and after the affine transformation. Dilatations and shear ($|axy| \neq |ayx|$) are taken into account).

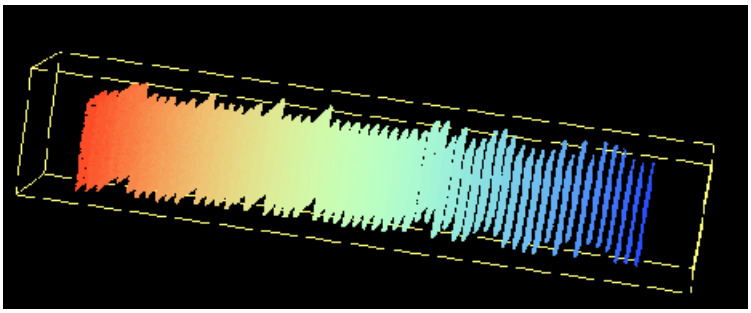

Fig. 4.7 – Aligned brick profile.

Salerno software has been the first one to successfully align a whole brick; the procedure has been successful both in central and corner zones having a 0.7μm accuracy; no critical misalignments between sheets was reported checking relative shifts and relative rotation angles; no critical transverse deformation was reported comparing central zone alignment transformation with large-scale alignment transformation. No discrepancy was observed on beam slopes between pairs of following sheets in corner zones; some recoverable beam slopes dependency on zones positions in sheet was detected.

C Sx=(83.9±1.4) Sy=(12.8±0.7)

1 Sx=(77.3±1.1) Sy=(9.35±0.9)

2 Sx=(84.1±1.6) Sy=(9.60±0.9)

3 Sx=(79.3±1.5) Sy=(13.2 ±1.5)

4 Sx=(88.4 ±1.5) Sy=(10.1 ±0.9)

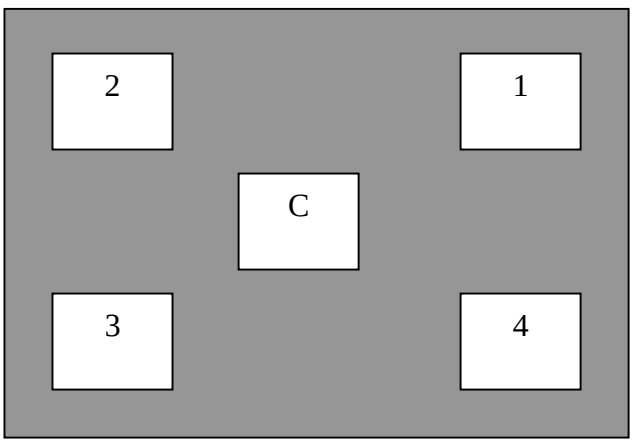

This test showed that the mechanical packing was suitable for precise emulsion measurements and so it could be used for OPERA ECC.

Brick gas-tightness tests

The last test required to choose between vacuum and mechanical option was to prove the pile gas-tightness. To perform this test it has been settled down a specific facility at CERN, EP division prepared a turbo molecular pump providing an effective pumping speed of 250 l/s connected to a chamber. A residual gas analyzer could follow the partial pressure evolution. After the bricks insertion (Figure 4.8) the vacuum system could be pumped down and when the pressure reached 10^{-5} Torr any gas can be injected. First tests have been performed injecting H_2 to check its severe poisoning effect on emulsion films. It has been injected 100 Torr H_2 and some small piles have been removed from the test chamber after 20 hours.

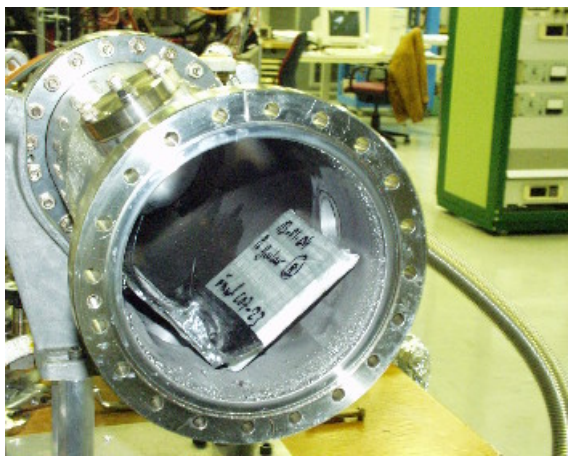

Fig. 4.8 - Insertion of the bricks in the vacuum chamber.

As expected emulsions showed a very high fog density along the whole volume and the fog increase with respect of the reference emulsion was a factor 8.

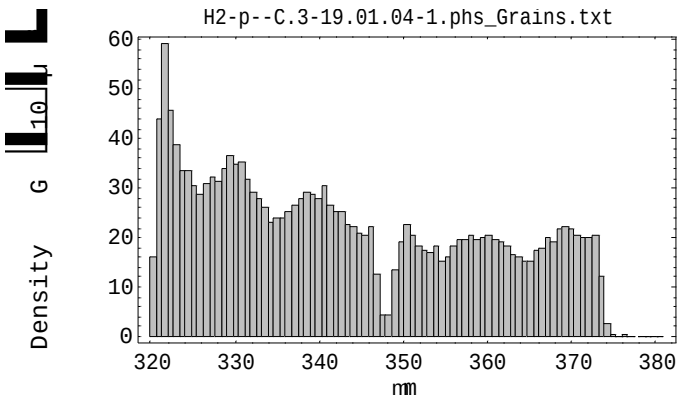

Fig. 4.9 – Fog distribution after H_2 test.

This test was not realistic because the LNGS atmosphere will not be completely composed of hydrogen but confirmed worries about hydrogen contamination in case of PbCa.

During the experiment bricks could be polluted by the gas coming out from OPERA RPC, so that gas should be tested (38 % Ar, 60 % TetraFluorEthylen, 2% Iso-Butan) and also a reference atmosphere (10 % H_2 + N_2). In case of RPC gas the gas exposure lasted 1 week and there was no fog increase on emulsions. In the case of hydrogen + nitrogen atmosphere the exposure lasted 1 day and results are shown in Table 4.7, there were vacuum, mechanical and mechanical plus additive PE bag piles.

	1 day
Vacuum	5.3 ± 0.2
Mechanical	5.3 ± 0.2
Mechanical + PE protection	5.7 ± 0.3

Table 4.7

Those data showed that a mechanical pile could be as tight as a vacuum one because the aluminum tape used for wrapping is strong enough and can shield water and any realistic gas vapor. After this check the collaboration validated the mechanical packaging option and the external firm in charge of BAM project started to produce robot prototypes and to explore suitable and robust ECC packing solutions.

New lead alloys

Meanwhile the Goslar firm was studying a new Lead alloy suitable for our emulsions. Since February 2004 they shipped at CERN samples of PbCu, pure Pb and PbAg. They decided to try these options because those are alloys and so there would have been no metallic surface migration along the lattice and also because all of those elements do not strongly interact with water as Calcium does. There have been made several small piles (Lead-Em1-Em2-Em3-Lead) stored at 35° C for 77 days (9/2/2004 $\rightarrow$ 26/4/2004) under vacuum, thus to get results in shorter time. Related data are shown in Table 4.9 (Reference (6.8 ± 0.7) g/$(10\mu m)^3$).

	PbCa	PbAg	Pb	PbCu
Emulsion 1	80 ± 5	5.8 ± 0.4	6.1 ± 0.6	7.6 ± 0.7**
Emulsion 2	78 ± 5	5.9 ± 0.3	6.3 ± 0.4	7.5 ± 0.4
Emulsion 3	82 ± 5	5.8 ± 0.4	6.2 ± 0.3	8.1 ± 0.8**

** These emulsion were seriously damaged on the surface in contact with lead

Table 4.9

From these data it turned out that those new alloys were chemically compatible with Opera emulsion and one more time there was a bad result only using vacuum packed Calcium lead.

In case of PbCu it has been found a huge alpha tracks density on the surface in contact with emulsion. This effect could be explained as a radioactive material contamination of lead samples and Goslar firm conformed this hypothesis.

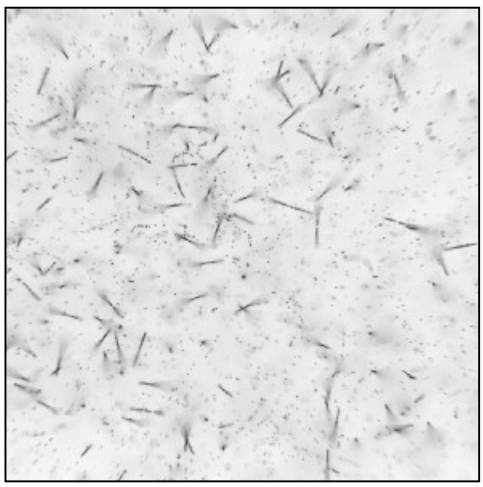

Fig. 4.9 – Alpha tracks coming from PbCu surface.

Even if this new lead samples were chemically safe and showed a clean surface they are very soft and easy to be deformed and scratched. This feature was not completely suitable from the mechanical point of view and also did not guarantee emulsion planarity, as it is required for emulsion precision angular and position measurements.

Ternary lead alloys

Goslar shipped at CERN some more lead samples of PbCu, PbAgAl and PbAgSn. Those ternary alloys should have been much more strong and rigid because of their lattice structure. Unluckily they had a very dirty surface and even the NGL surface cleaning could easily damage their surface. There have been realized some small piles (Lead-Em1-Em2-Em3-Lead) under mechanical pressure and under vacuum and we stored them at 35° C for 96 days (9/8/2004 → 15/11/2004). Data are shown in Table 4.10 (Reference (4.8 ± 0.7) g/(10μm)^3).

	PbAgAl	PbAgSn	PbCu
Emulsion 1	4.5 ± 0.3	4.1 ± 0.1	4.0 ± 0.1
Emulsion 2	4.2 ± 0.2	4.2 ± 0.3	4.1 ± 0.1
Emulsion 3	4.3 ± 0.2	4.3 ± 0.1	3.9 ± 0.3

Table 4.10

Ternary lead was chemically compatible with emulsion but it was not suitable for mass production within planarity specs and both Goslar and BAM firms rejected this solution because that lead foils were to soft to be handled by robots.

PbSb (6/9/2004 $\rightarrow$ 9/10/2004)

Goslar suggested to test PbSb; this solution is well known and widely used in commercial mass production. In September 2004 they shipped two samples of PbSb (1% and 2.5 % Sb). There have been realized some small piles (Lead-Em1-Em2-Em3-Lead) under vacuum and mechanically, stored at 35° C for 33 days (6/9/2004 $\rightarrow$ 9/10/2004). Fog measurements results are shown in Table 4.11 (Reference (7.2 ± 0.7) g/(10μm)^3).

	PbSb1% Vacuum	PbSb 1% Mechanical	PbSb 2.5% Vacuum	PbSb 2.5% Mechanical
Emulsion 1	7.4 ± 0.5	6.1 ± 0.4	6.1 ± 0.6	7.6 ± 0.7
Emulsion 2	6.9 ± 0.5	5.9 ± 0.7	6.3 ± 0.4	7.5 ± 0.4
Emulsion 3	7.0 ± 0.6	6.5 ± 0.4	6.2 ± 0.3	8.1 ± 0.8

Table 4.11

From those data PbSb was chemically compatible with emulsion but on the contact surface between lead and emulsion there were several alpha tracks and their density (tracks/mm^2) was the following:

	PbSb 1% Vacuum	PbSb 1% Mechanical	PbSb 2.5% Vacuum	PbSb 2.5% Mechanical
Emulsion 1	23.1 ± 0.3	23.4 ± 0.3	23.5 ± 0.3	23.1 ± 0.3
Emulsion 2	3.0 ± 0.3	3.0 ± 0.3	3.1 ± 0.3	3.3 ± 0.3
Emulsion 3	24.0 ± 0.3	23.5 ± 0.3	23.0 ± 0.3	23.2 ± 0.8

Table 4.12

These alpha tracks were ≈ 25 μm long and ≈ 2.5 μm thick; since they had all the same length it was reasonable to think they have been originated on the lead surface and that all the lead plates had suffered a surface contamination by some radioactive material during the lamination process at Goslar site. Considering their 25 μm length, alpha particles energy was around 5.4 MeV; this energy is compatible with the decay of Po^{210}, that is a radioisotope of Pb^{210}.

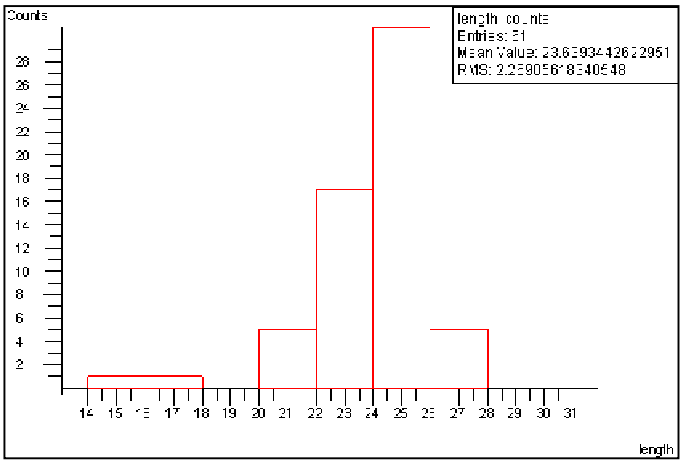

Fig. 4.11 – Alpha tracks length in emulsion.

The measured radioactivity of these lead foils has been estimated of the order of 70 alpha/cm²/day, this value was seven times bigger than the one quoted in OPERA proposal and measured for Boliden lead, the collaboration strongly complained with Goslar firm about the surface contamination and asked to test some new samples of PbSb and some samples of PbCa as well for relative radioactive measurements comparisons.

PbSb vs. PbCa (26/10/2004 → 3/11/2004 & long term test)

Goslar claimed that the surface contamination has been originated by some welding procedures around lead lamination line. Some new lead samples have been delivered and used to make some small piles (Lead-Emulsion-Lead) with PbCa, PbSb 1% and PbSb 2.5%, they have been stored under vacuum at 35° C for 8 days, after the development there were the following results about alpha tracks density (Reference (4.1 ± 0.5) Tks/mm²):

PbCa	PbSb 1%	PbSb 2.5 %
4.2 ± 0.5	4.2 ± 0.5	4.2 ± 0.5

The alpha tracks densitiy measured on all the samples was 55 alpha/cm²/day and it still looked like a surface contamination; from those data it had been also clear that the radioactivite was not due to the Sb but to the intrinsec properties of bulk lead used. It turned out that those samples were not made by Boliden lead, parallel measurements performed by electronic

detectors and CR 39 detectors confirmed those results and pointed out that the bulk radioactivity of the lead was approximately 80 Bq/Kg, four times bigger than the activity requested by the OPERA collaboration and measured in the Boliden lead. Electronic detectors also confirmed that the alpha energy range was ≈ 25 μm and that there was a surface enhancement of the radioactivity. Goslar firm provided some more samples of PbSb washed by NGL and ultrasonic baths till September 2005 but they all showed an alpha particle flux stronger than 50/cm^2/day.
To confirm the statement that the radioactivity originated from bulk lead, that was rather different from the Boliden one, on November 2004 there have been prepared some bricks using PbCa and mechanical packaging. After one year storage at 35°C (November 2005) it has been found no chemical contamination and an alpha flux of 6/alpha/cm^2/day, furthermore the alpha tracks spectrum was continuous (Fig. 4.12) and PbCa radioactivity has been measured by electronic counters to be 30 Bq/Kg (as Boliden lead specs).

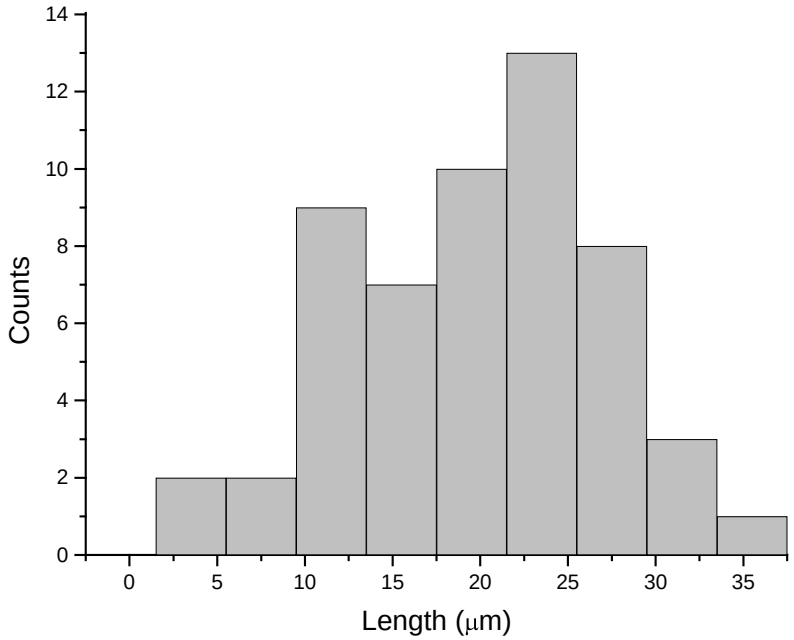

Fig 4.12 – PbCa alpha tracks continuous spectrum.

After this long term compatibility test the Collaboration clearly stated that all Goslar lead samples received after September 2004 were not compatible with the OPERA specifications because the bulk lead radioactivity was > 30 Bq/Kg. Meanwhile during the last three years the Boliden mine that has been supposed to be used for our experiment has been closed and it seems really difficult to find 2 Kton of Ultra Low Radioactivity Lead in few months and for reasonable prices. In order to find a reasonable solution the Collaboration organized a Lead task force and, at present time, in Salerno we are trying to estimate the scanning efficiency of Opera automatic microscopes as a function of the number of alpha and electron tracks/view; considering the constraints coming from physic measurements and analysis performances the

collaboration will try to cope with radioactivity problem. The considerable number of alpha tracks/view in emulsion will arise the following scanning problems:

- dead areas on scanning views, it has been estimated a 5 % fiducial volume loss due to tracks dimensions.
- focusing problems coming from black areas on the view
- increase of instrumental background because of multiple mips 'reconstruction

Limits set on lead radioactivity in the proposal were10 alpha/cm^2/day and 50 electrons/cm^2/day, that means (after 5 years) 22 alpha/view and 100 electrons/view; those numbers were based on the hypothesis of Boliden lead. Opera lead will be much more radioactive than Boliden one (factor 2-3). In order to evaluate European Scanning System efficiency as a function of alpha/view we need a realistic emulsion sample. In March 2005 Bologna group made a vacuum-packed stack (27 plates refreshed at GS in underground, PbSb lead delivered at CERN in March 2005) to check rare Pb muonic decay. The stack has been stored in Hall B of LNGS underground laboratory using a lead shielding at 17°C for 8 month; I brought it to Salerno lab and after 24 hours cosmic rays exposure (without shielding in Salerno lab) I developed 8 emulsion films. This emulsion sample is the only one we have to evaluate scanning efficiencies; all the emulsion have a Fog Density of (6.5 ± 0.4 g/(10 μm)^3) and (30 ± 1) alpha tracks/view, corresponding to ≈ 100 alpha /cm^2/day lead radioactivity. The alpha range is (25 ± 1)μm and there is a strong surface effect; it is possible to see several alphas and electrons coming from the same point on the emulsion surface, this is a clear signature of alpha decays on lead surface. It as been used a freshly installed microscope for plate scanning, tracking efficiency has been previously checked to be in the range 90-94% on reference plates. We scanned 5 consecutive plates of alpha-filled plates, it has been selected a sample of good quality volume tracks aligned on 4 consecutive plates and then we looked for them on the 5th plate. The tracking efficiency obtained was not better than 82%. The emulsion quality is definitely not identical to the quality of reference plates.
In particular:

- taking clusters with the same gray level threshold as for the reference plates (900) we got 50% track finding efficiency
- taking clusters with a much lower threshold (750-800) and reducing the number of emulsion active layers (because emulsion are thinner than the reference ones) we achieved 77% track finding efficiency as our best result and finally 82% if we apply a geometrical fiducial cut.
- further decreasing the clustering threshold did not improve the efficiency.

The sample manually checked includes 146 tracks, 34 of which are not found on the 5th plate, in details we found that:

a) In 12 cases (8.2% of 146) the track did not exist at least one emulsion side.
b) In 18 cases (12.3% of 146) the tracks exist and are systematically missed by the ESS but there was no alpha-track nearby.
c) In 4 cases (2.7% of 146) the track has been missed and an alpha-track was nearby (Fig. 4.13).

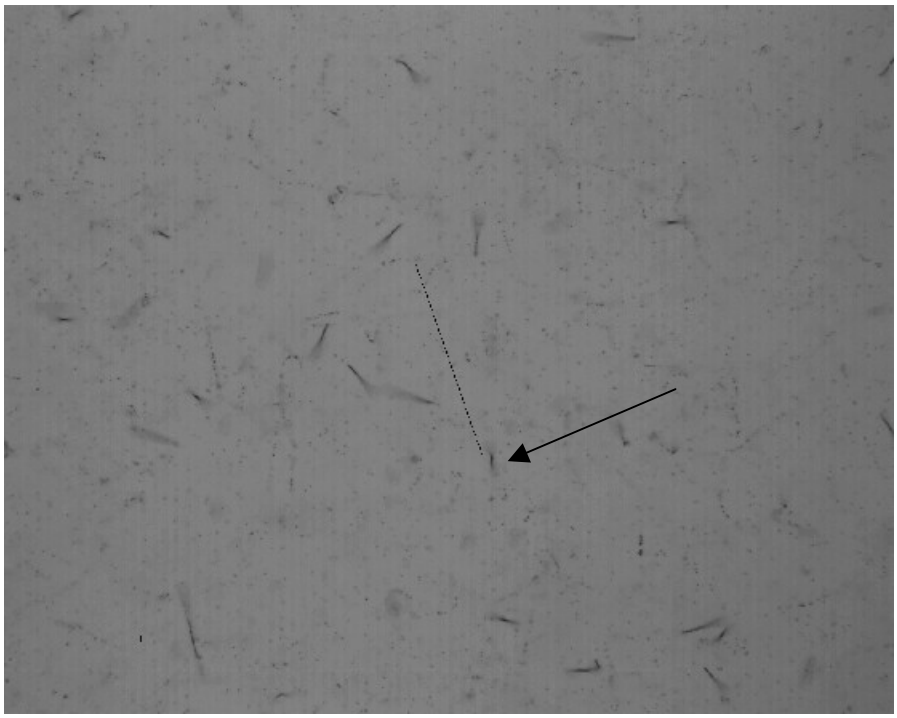

Fig. 4.13 – The straight line is a track and the arrow points the black alpha path.

The fact that we had to lower the threshold shows that contrast was not optimum, this could have been an indirect effect of the presence of alpha-tracks. Indirect effects of alphas such as decrease of contrast, worse focusing, surface detection, and distortion of the light equalization curve are possible and should be investigated deeply.
It is also clear that alpha-tracks pose problems when they are very near to some grains of the mip track, or when they have a position and/or direction that is similar (in 2D) to the real track. Furthermore in order to understand completely these items we are planning to scan some more emulsion samples exposed to different alpha and beta particles flux.
Our Japanese colleagues, in order to complete the analysis and compare scanning performances in case of severe radioactivity, will provide those samples to Salerno laboratory. The Lead task force is now interacting with Goslar firm experts in order to find suitable procedures to passivate the lead surface; at present the best solution appears to be a surface thin (20 μm) lamination with Ultra Low Radioactivity Lead, this upper layer could be effective to stop alpha decay products.

Spider – bricks

In April 2004 the Collaboration decided to change the brick base-line option from vacuum to mechanical packing; the external firm in charge of BAM construction suggested to realize the pile by the so called spider packing; that solution has been approved and the firm is now building all the robots required to prepare Opera bricks [43]. The basic idea is that an 800 μm aluminum thin foil, the spider, will provide the pile mechanical stability.

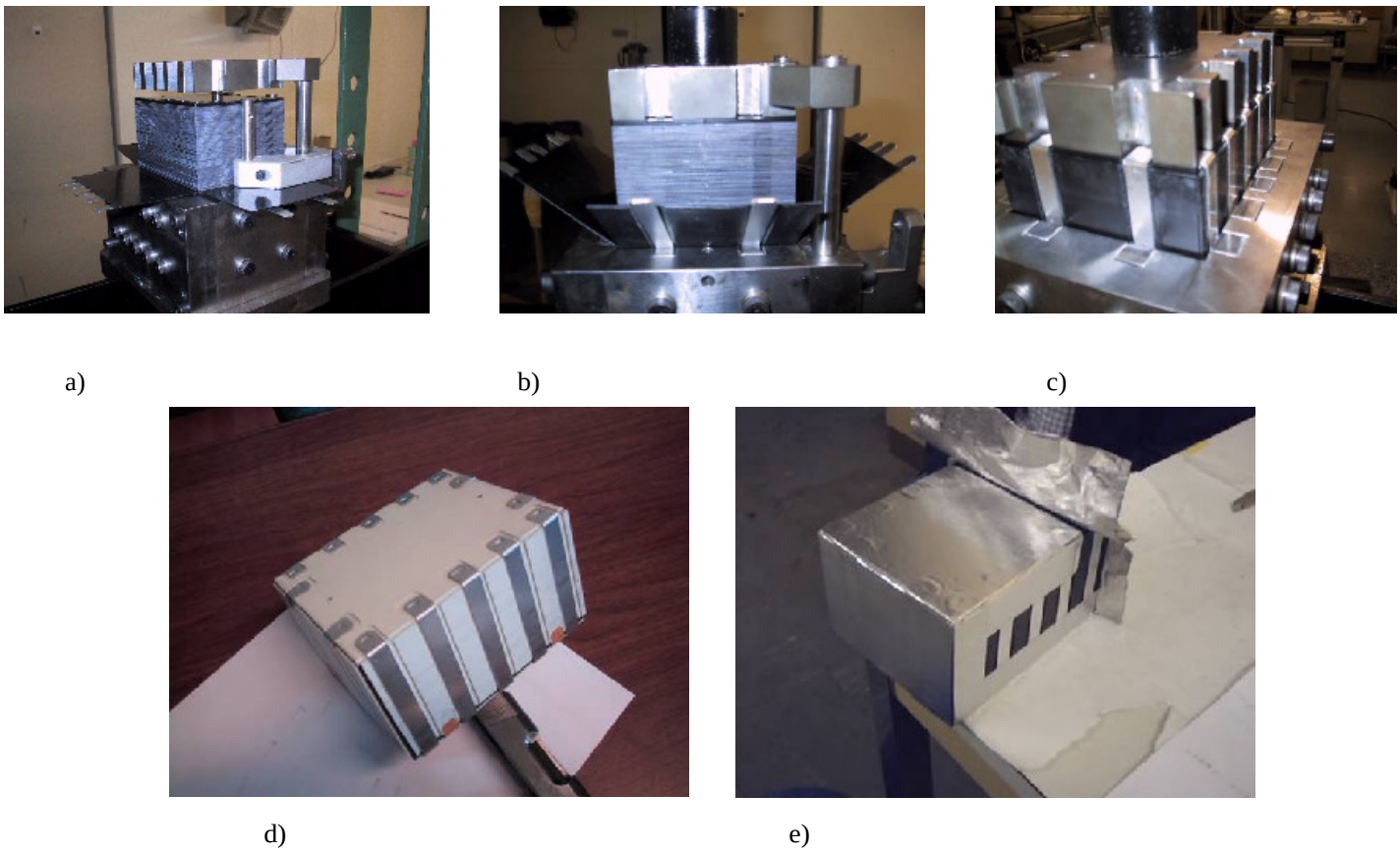

a) b) c)

d) e)

Fig. 4.14 – Spider packing procedure.

The spider will be placed under the emulsion-lead pile (Fig. 4.13a), folded on the sides by mechanical pressure (Fig. 4.13b) and closed on the upper emulsion film (Fig. 4.13c). Plastic side protection and cover will keep the rigidity and avoid the direct contact between emulsions and aluminum (Fig. 4.13d); the light shielding will be provided by wrapping and adhesive aluminum tape around the pile (Fig 4.13e).

Emulsion/ plastic compatibility

In case of spider option the plastic cover and the side protection will be in direct contact with emulsion films and so the chemical compatibility must be tested. The BAM firm suggested several kinds of plastics, since brick components will be molded and their thickness will be less than 1 mm it has been required to use plastic having a high rigidity. The first option was Delrin; this polymer is widely used in mechanics applications because it is very robust and also very easy to be molded and machined. The procedure adopted to test emulsion/plastic compatibility was the same used for lead; there have been realized some small piles under vacuum (Delrin-

Emulsion 1- Emulsion 2 –Emulsion 3 – Delrin) and then stored in an oven at 35°C. Results were the following (Reference (8.5 ± 0.2) g/$(10\mu m)^3$ (Table 4.13)

Storage period	Emulsion 1	Emulsion 2	Emulsion 3
2 months	20 ± 1	15 ± 1	21 ± 1
4 months	35 ± 2	24 ± 2	36 ± 2
6 months	>50	>50	>50

Table 4.13

From these data it was unambiguous that Delrin can damage emulsion films, Fuji experts confirmed that result and explained that the poisoning chemical component is HCHO (form-aldeid); HCHO can easily release hydrogen and produce a severe Ag reduction inside the whole emulsion volume.

Delrin was established to be dangerous also in case of mechanical packing; after the long-term compatibility test with PbCa (see also page 79) the emulsion in contact with the plastic cover became completely black and emulsion edges (in direct contact with the plastic side protection) were also black.

After these tests Delrin has been rejected and several new plastic samples have been tested.

During my stay at Nagoya University Particle Physics Laboratory I performed several tests on emulsion/plastic compatibility and I shared and compared my experiences and results with Opera Japanese collaborators.

BAM firm shipped to CERN and Nagoya University the following plastic samples (Table 4.14).

Eraclene MP90 (HDPE)	Flexible
Flexirene MR50 (LLDPE)	Flexible
Moplen	Rigid
Nylon PA + Elastomeri	Rigid
Nylon PA + Glass	Rigid
Polypropylene Omopolimer	Flexible
Politene MM20	Flexible

Table 4.14

I prepared some test vacuum piles at CERN stored at 35°C and I developed all the emulsion samples after 2 months storage; after checking fog density distributions it turned out that only some plastics could be used for OPERA bricks.

Data are shown in Table 4.15 and in the related FD plots it is possible to see the volume and/or surface contamination effects.

Eraclene MP90 (HDPE)	Compatible
Flexirene MR50 (LLDPE)	Not Compatible
Moplen	Compatible
Nylon PA + Elastomeri	Not Compatible
Nylon PA + Glass	Not Compatible
Polypropylene Omopolimer	Compatible
Politene MM20	Compatible

Table 4.15

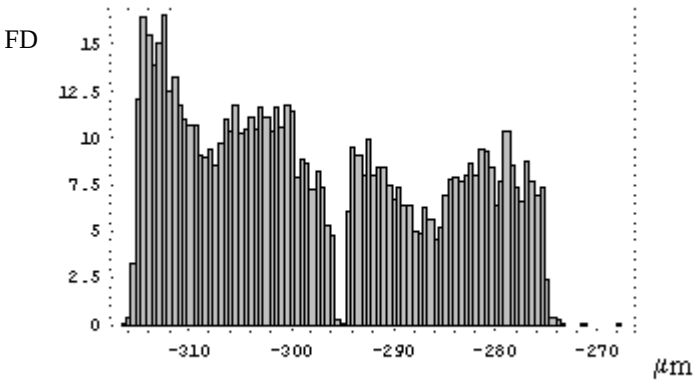

Reference (8.5 $\pm$ 0.2) g/(10μm)^3

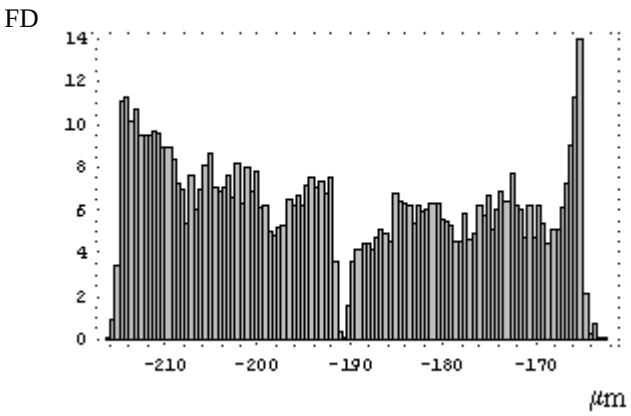

Moplen (7.6 + 0.2) g/(10μm)^3

In this case it is possible to see a small surface contamination effect.

FD

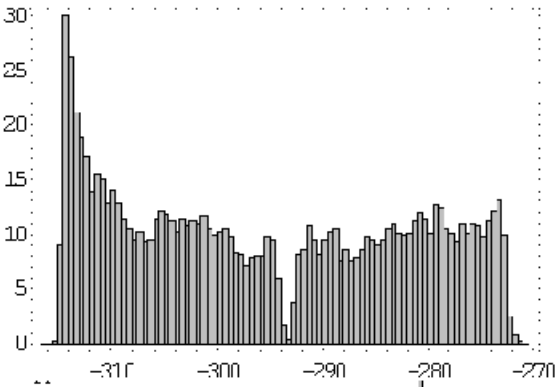

Polypropylene (10.5 ± 0.3) g/(10μm)^3

Meanwhile in Japan they stored emulsions/plastic samples under vacuum at 40°C. Soon after my test at CERN I joined Nagoya group activity and we decided to develop all the emulsion and crosscheck our results. We exposed emulsion films to an electron beam to check their sensitivity; in case of plastic poisoning effects emulsion sensitivity could have been damaged.

Fog densities measurements have been performed in three different emulsion regions:

- emulsion side in direct contact with plastic sample to check surface effects
- emulsion side opposite to the one in contact with the plastic sample to check volume effects
- emulsion region near to the one in contact with plastic samples to check poisoning plastic degassing.

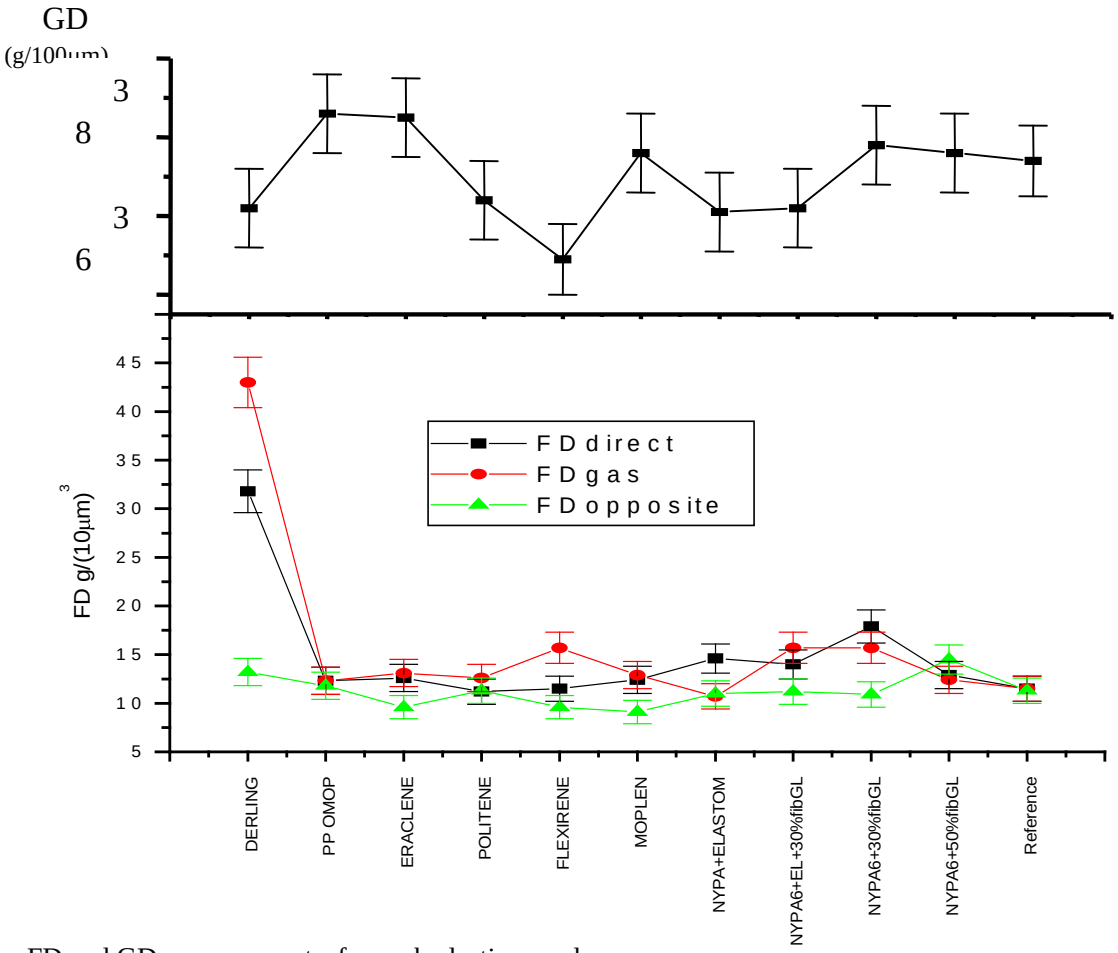

Fig. 4.15 - FD and GD measurements for each plastic sample.

All measurements showed that only Delrin is clearly not compatible with emulsions and that plastic samples belonging to PP and PE families are the safest. Concerning sensitivity measurements we did not observe any relevant damages. Looking at the data we saw that tests done at CERN and in Japan are fully compatible. Since Japanese measurements have been performed by eyes and based on a poor statistic I decided to scan all the plates by automatic microscopes and then to run Salerno software on the clustered data to evaluate FD and GD. Japanese scanning system is rather different from the European one but I successfully converted the output data format and it has been possible to run the usual algorithm on the data and to obtain interesting results. Comparing FD measurements on all emulsion samples (Fig. 4.16) and applying a 2 sigma cut it has been possible to select Moplen (PP HD) as the safest plastic.

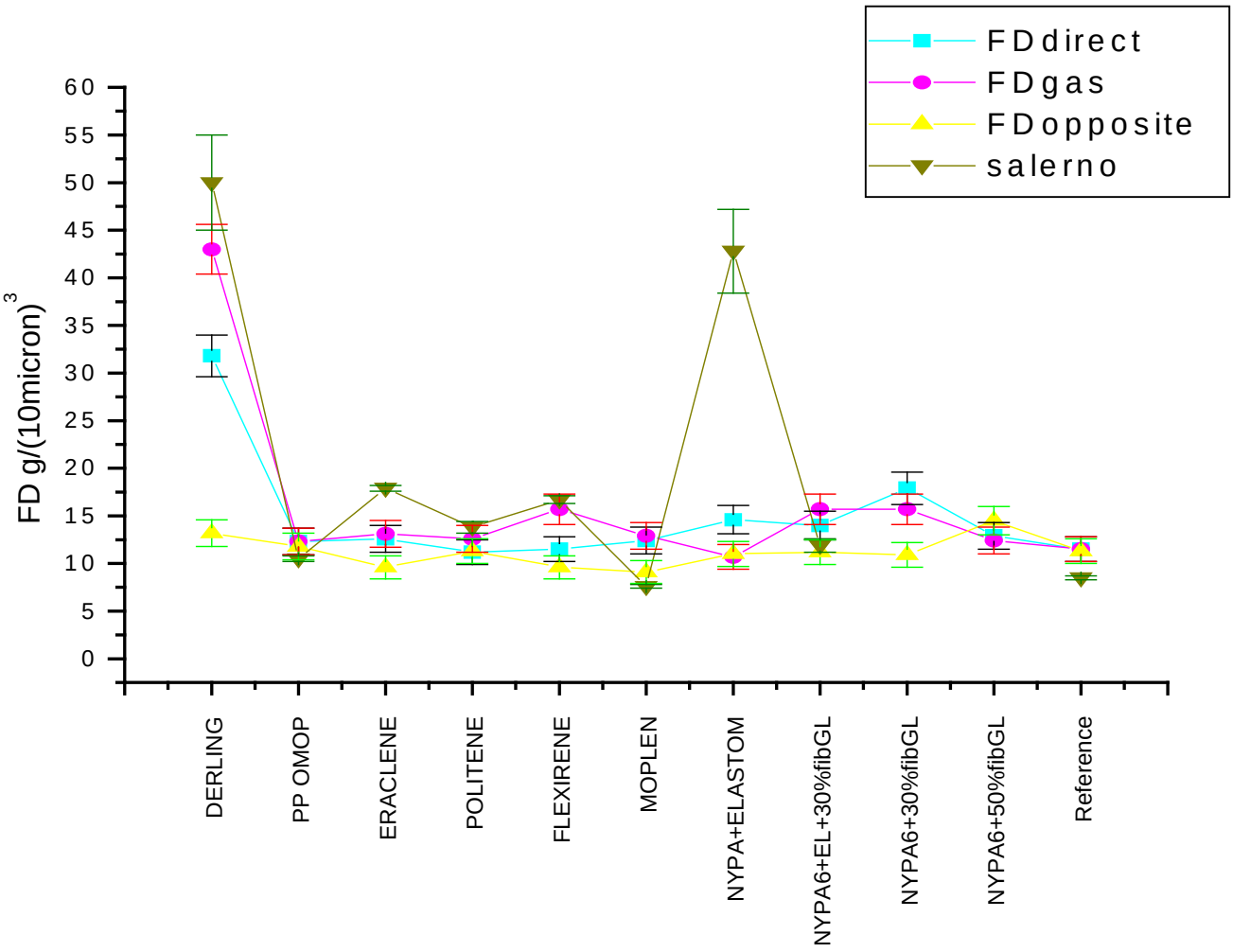

Fig. 4.16 – Comparisons between Japanese and European tests.

PP HD has been accepted by BAM firm for side protection mass production; unluckily this plastic turned out to be to soft for brick cover mass production and I tested some more samples, basically made of PP+ hardeners, at CERN (Table 4.16).

Sample	Days @ 35°C	FD g/(10μm)^3	Reference film FD g/(10μm)^3
ABS	85	(7.0 ± 0.4)	(4.7 ± 0.4)
ABS +30% PC	13	(6.5 ± 0.4)	(4.6 ± 0.4)
PP 100%	28	(2.5 ± 0.4)	(2.6 ± 0.4)
PP+Mg oxide	28	(2.6 ± 0.4)	(2.6 ± 0.4)
PS+flexirene	13	(6.6 ± 0.4)	(4.6 ± 0.4)
PS/SBR	85	(7.6 ± 0.4)	(4.7 ± 0.4)

Table 4.16

Mechanical tests and FD measurements showed that the plastic cover could be made of PP+ Mg oxide. At the present time the BAM firm is building the molds to start the mass production of all the plastic components.

Test measurements on spider – bricks

In order to locate and study neutrino interactions it is required an internal brick alignment ~50 μm and a planarity ~5 mrad, these items should be checked on spider-bricks. Two anthropomorphic robots that will pick up emulsions and lead foils by vacuum suckers will accomplish the piling procedure. First of all it was needed to check the vacuum suckers working pressure; it is important to prevent distortions due to wrong manipulations or surface stress.
In March 2005 the BAM firm realized 10 vacuum packed piles (Lead-Em-Em-Em-Lead); emulsion have been handled with different suckers depressions ranging from 0.4 to 0.8 Bar. Fog has been measured on each plate in the contact area (2 × 3 cm^2) between vacuum suckers and emulsions. Each robot handles emulsion films by means of four vacuum suckers having 1 cm diameter and placed at the corners, in the middle there are also two springs that could avoid big distortions because they keep emulsions as much straight as possible.

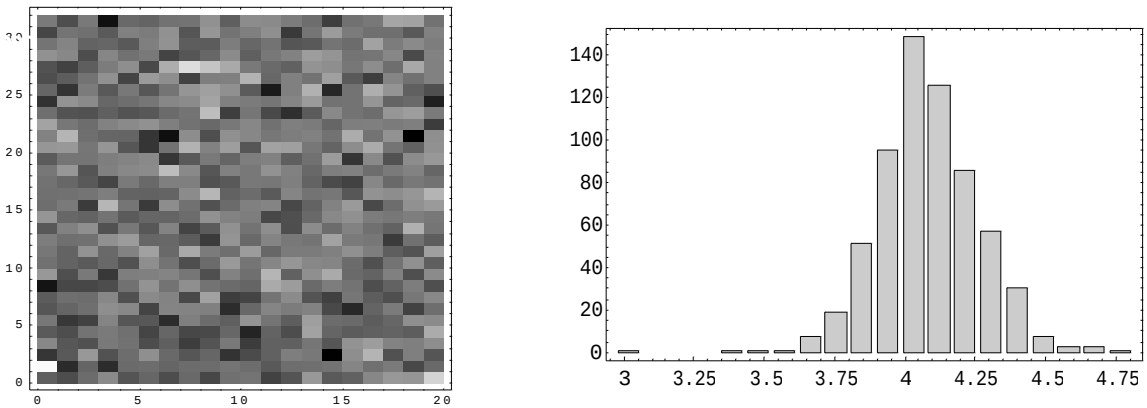

Fig. 4.17 - Contact area FD Gray Level plot & fog density distribution

In Fig. 4.17 it is possible to see a 2D plot showing the FD values among the whole contact area; the values distribution is Gaussian and the mean value is 4 g/(10)μm^3, this result is the same observed in a reference emulsion. This measurement has been performed on all the plates and no surface scratches or damages have been found.
After this test the firm decided to use a 0.6 bar depression for vacuum suckers and realized a full pile that has been exposed to cosmic rays for 24 hours and then developed and scanned by ESS in Salerno laboratory. We checked five areas on each emulsion: a central one as reference and four zones 0.5 mm far from the edges in order to check suckers and spider effects (Fig. 4.18).

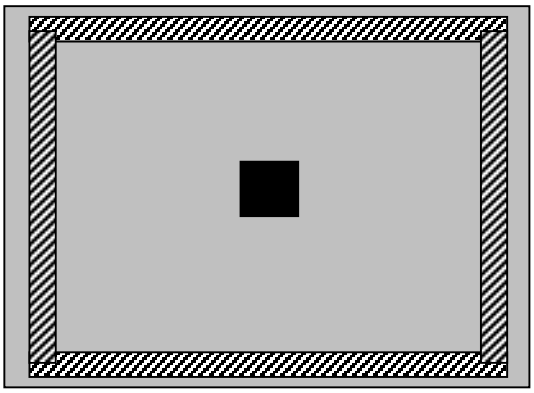

RIGHT & LEFT: scanned areas 1.3 × 8.9 cm^2
CENTER: scanned area 4 cm^2
BOTTOM & TOP: scanned areas 11.6 × 0.92 cm^2

Fig. 4.18 – Scanning areas.

Test piles were composed by three emulsions and three lead foils, emulsion data have been aligned and cosmic ray tracks have been fully reconstructed. The track density was compatible with theoretical expectations (4 tracks/mm^2) and the sample was large enough to study pile planarity along X and Y coordinates. In case of one pile we scanned the whole surface and the number of volume aligned tracks was constant on the emulsion surface; we found no alignment problems due to vacuum suckers additional pressure (Fig. 4.19).

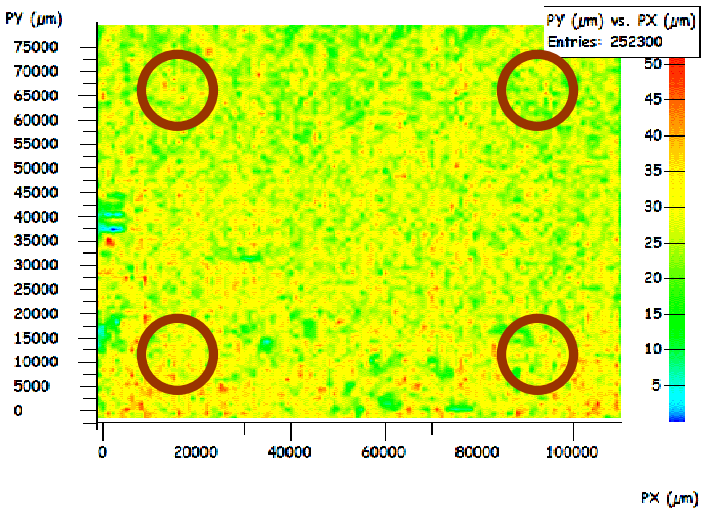

Fig. 4.19 – 2D distributions of volume tracks, red circles show vacuum suckers contact areas

.

In order to check the pile planarity we evaluated the alignment residuals along X and Y stripes scanned, the profile shapes (Fig. 4.20) did not show systematic effects (bending, rotations, tilt) so big that cannot be corrected by alignment software and the affine transformation parameters are the same in the central area and along the edges. It turned out that the alignment residuals are not bigger than 5 mrad, this result is compatible with Opera specs and allows MCS momentum measurements.

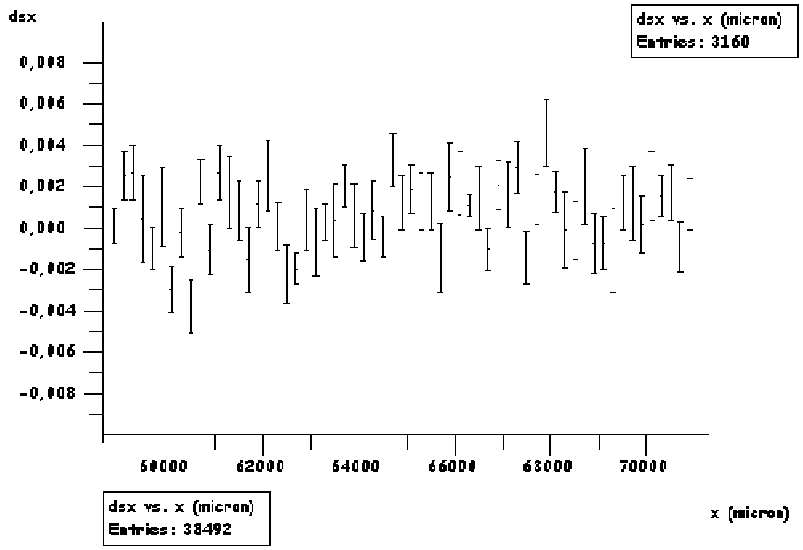

Fig 4.20 a) – Alignment residuals profile in the reference central area.

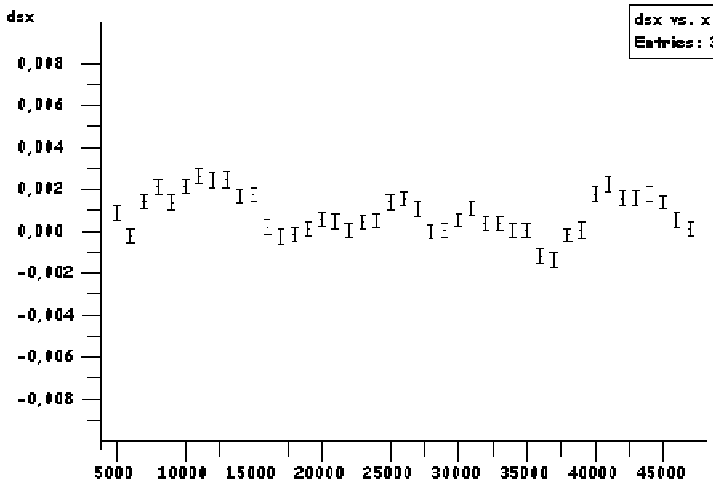

Fig 4.20 b) – Alignment residuals profile along the left side.

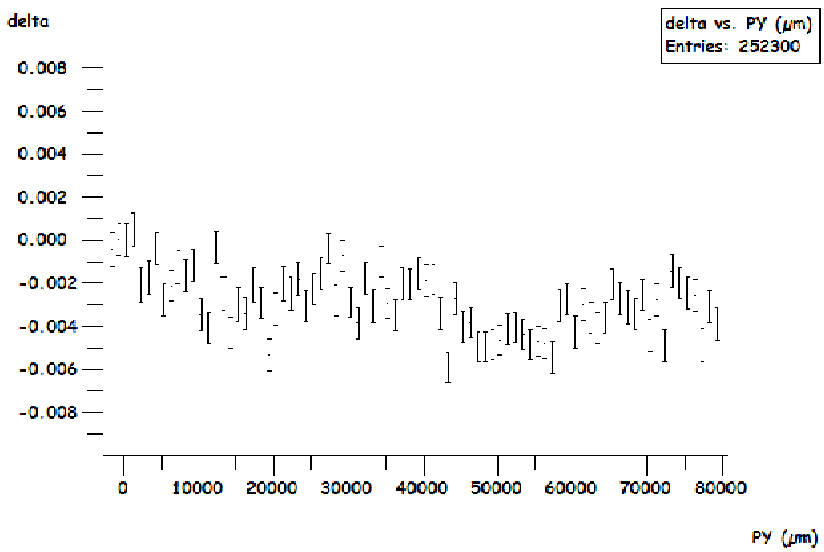

Fig 4.20 c) – Alignment residuals profile along the left side

.

Once that vacuum suckers have been successfully commissioned, in April '05 there have been developed at CERN 4 Spider-Bricks automatically piled and exposed to a reference pion beam and to cosmic rays (2 days & 4 days) to test alignment precision in both cases. The aim of this test was to check possible distortions due to spider action and automatic pile pressing and closing devices. Several closing pressures have been tested (3-5-7-10 bar) and emulsions have been scanned in four Italian scanning laboratories.
Bricks were composed of 15 good quality films and all the remnants were mechanical quality film not suitable for scanning purposes (Fig 4.21).

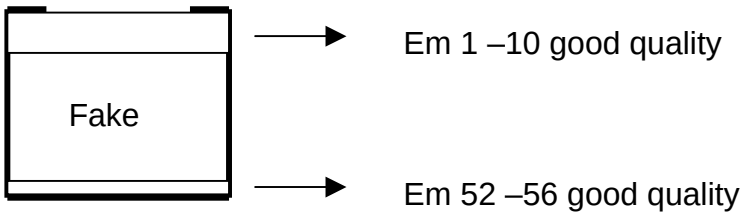

Fig. 4.21 – Brick composition.

The exposure to a reference pion beam has been performed with three angles (Fig. 4.22) in order to gain better alignment resolutions, in order to get the same resolution with cosmic tracks we needed long exposure. In case of reference tracks we checked the alignment just looking at reconstructed tracks slopes, in case of cosmics we have been able to study pile planarity looking at alignment residuals on different plates; in case of distortions due to spider pressing and closing device we would have seen worse alignment parameters between plates 1-2.

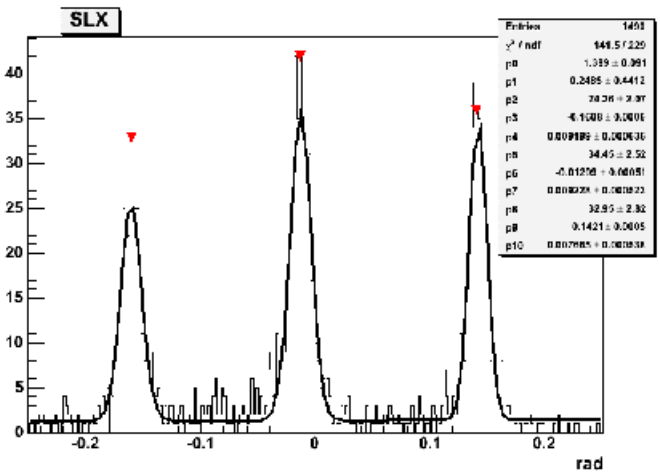

Fig. 4.22 – Reference beam spectrum.

In all scanning laboratories it was possible to perform the alignment with residuals smaller than 5 mrad and no deformations were found in the areas near to the spider legs.

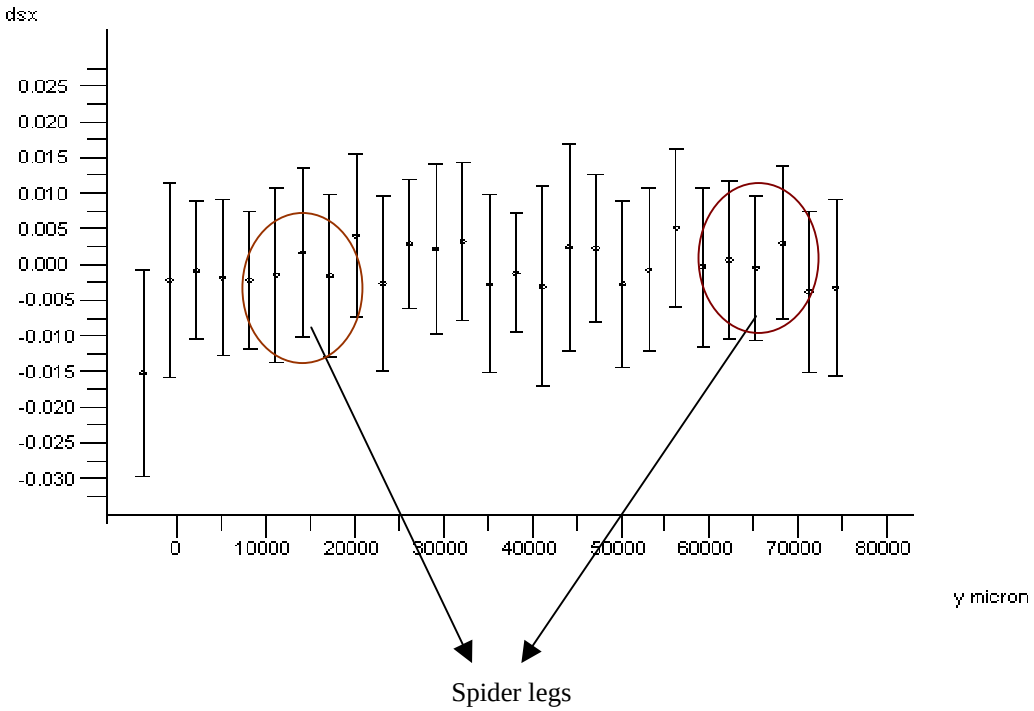

Fig. 4.22 – Side edge alignment profile.

It has been also possible to check alignment precision among different plates using reference tracks and cosmics. In both cases no degradation was found on plate 1-2 and alignment residuals were within 5 mrad.

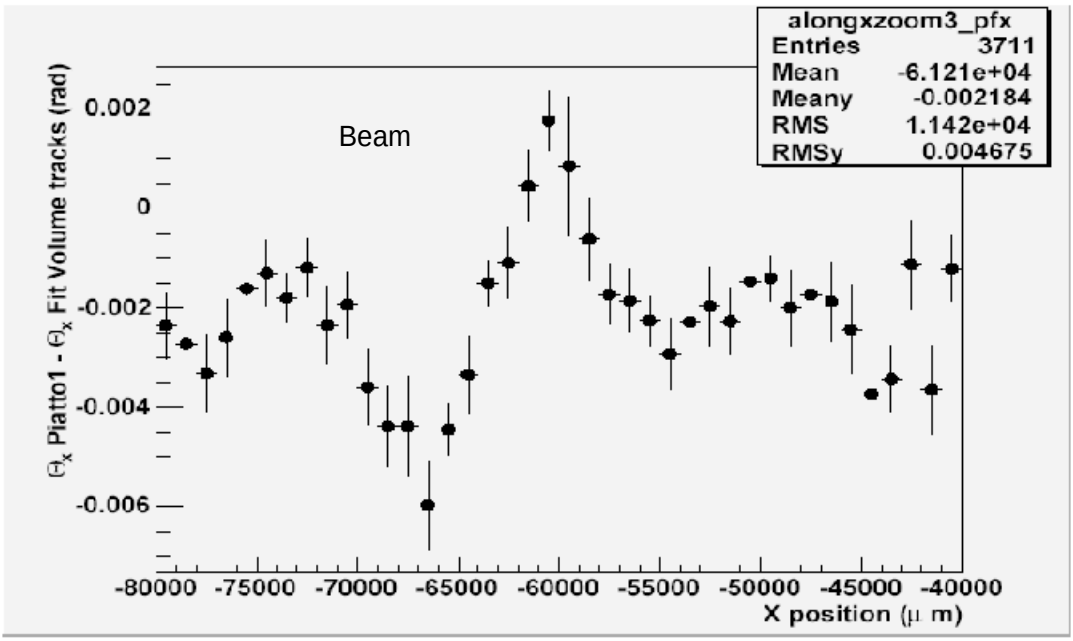

Fig. 4.23- Alignment residuals on plate 1-2 using beam tracks.

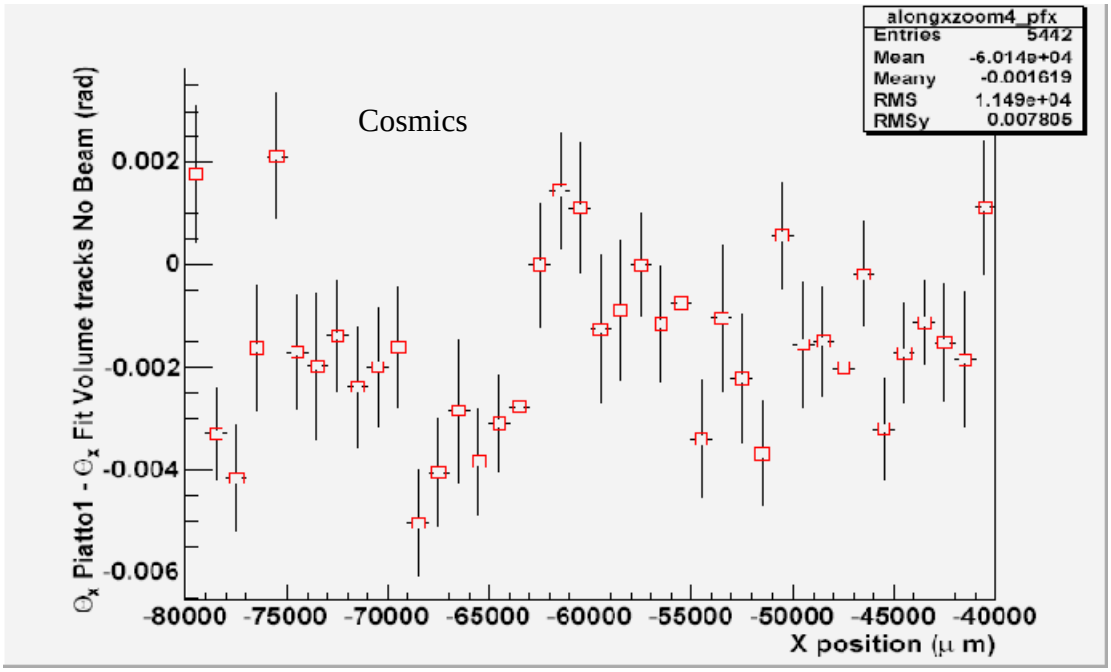

Fig. 4.24- Alignment residuals on plate 1-2 using only cosmic rays tracks.

This test has been successfully performed in all scanning laboratories and results were fully compatible; it showed that spider-brick mechanical solution is able to fulfil Opera requests in terms of planarity and piling accuracy.
This option is really different from the base-line but it turned out to be the safest to guarantee long term compatibility between lead and emulsion films, furthermore this solution has been successfully automatized and will guarantee the production of all Opera bricks in less than one year from now.

OPERA emulsions refreshing, development and handling

The Opera detector will consist of 12 millions of nuclear emulsion thin films, that is the largest amount of emulsion ever used in high-energy physics; they will be produced by the Fuji Co. in Japan for Opera experiment purposes. During the production at Fuji factory emulsion accumulate several background tracks that should be erased before their shipment to Europe. The erasing procedure, called refreshing, has been designed and realized by Nagoya University group in a custom facility situated under the Tono mine in Japan. Then emulsion are shipped by ship to LNGS and stored in a shielded area in underground. Nowadays more then 6 millions of refreshed films are already stored in LNGS. They will be used in the next few months to assemble bricks in the LNGS underground laboratory by the BAM machine. On the downstream side of each brick there will be attached two additional films packed independently under vacuum as changeable sheets (CS); they will be used as an additional prove of the tracks reconstructed by electronic detectors before opening the related ECC. Due to background tracks accumulated during the transportation and refreshing residuals the erasing and packing procedure of CS will be realized at LNGS in underground; the facility is now under commissioning by Nagoya group collaborators.

During the neutrino beam exposure electronic detectors will record charged particles produced in neutrino interactions and the event bricks will be identified and extracted by BMS machine. Every day around 50 bricks will be extracted and their changeable sheets will be developed underground; CS films will be scanned and if the predicted tracks will be found the ECC will be brought on the ground and developed. Development will take place from Monday to Friday; consequently the daily development capability should be of 65 bricks (130 CS films in the cavern, about 3,700 films on the surface). The development facility in underground is already under commissioning and test developments have been successfully carried on. The development lab on the surface is presently under construction; since the number of films that must be processed per day is really huge it has been needed an automatization of the full developing procedure; furthermore the procedure has been defined, tested and optimized in order to guarantee large scale quality and stability. Japanese and European groups have carried on the R&D activity regarding OPERA films developing procedure in parallel and there have been also the significant collaboration of Fuji Co. experts. European groups have the responsibility to built up the development labs, realize the development automatic plant and define the chemical procedure; in particular Roma group and Salerno group are in charge of emulsion development related items.

Before ECC films development it is needed a labeling and gridding procedure; the labeling will guarantee the identity of each film trough the imprinting of ECC and sequential sheet number, the gridding will put on each film a basic reference frame for plate intercalibration and alignment. These procedures will be simultaneously accomplished by custom light exposures by means of an optical device fully designed and realized by Salerno group.

In conclusion emulsion-handling activities related to OPERA films are: refreshing, labeling & gridding and development; they will be fully described in this section trough all the experimental results concerning my activity in the last three years.

Emulsion refreshing at Tono mine

As already described in Chapter 1, the latent image of a particle track gradually fades after the exposure and this effect, when accelerated, can be used to erase old tracks. The latent image can be destroyed by the following oxidation reaction:

$$Ag_4 + O_2 + 2H_2O \rightarrow 4Ag^+ + 4OH^-$$

the speed of the process is regulated by temperature and humidity and the environmental conditions needed for a successful refreshing are $RH \approx 90-99\%$ and $T \approx 20-29°C$. Temperature and humidity must be strictly monitored during the procedure in order to preserve emulsion sensitivity and prevent the increase of fog. The erasing procedure was widely known since the beginning of nuclear research emulsion but the large amount of films that needed to be refreshed for OPERA experiment requested a long R&D procedure and many efforts in order to guarantee stability, reliability and reproducibility.

Nagoya group settled up the refresh activity in the Tono mine [22], designed and produced several refreshing units that can operate in parallel, the final speed reached is 150000 refreshed films/week.

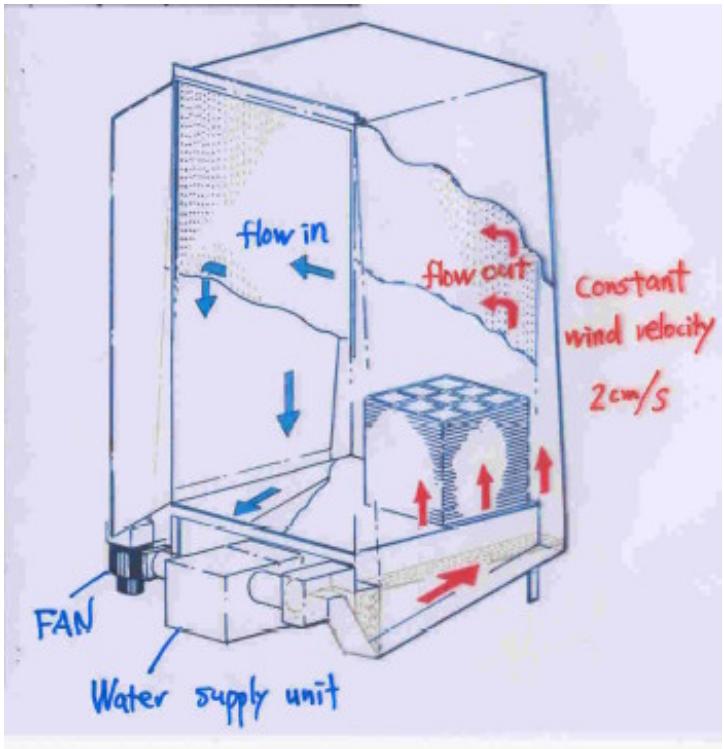

Fig. 5.1 – Refreshing unit schema.

Each refresh unit (Fig. 5.1) is a stainless steel chamber where it is possible to treat 8000 films at once; humidity is provided by a water supply situated on the basement and the air circulation is realized by a fan and several holes in the stainless walls to guarantee a constant circulation speed. Up to 14 chambers are arranged in a refresh room and the temperature is kept constant at 27°C; warm air can circulate trough the chambers and humidification is independently tuned in each unit by its own water supplier. Inside the chamber films lays on plastic trays that have been designed in order to don't disturb the air circulation and avoid the direct contact of films. The full refreshing cycle lasts one week and accomplishes the following phases:

- Pre-humidification: this preliminary step lasts 24 hours; films are stored in the chambers at 27℃ and low humidity (around RH 60%). Air circulation is very fast and there must be a strong regeneration of gas inside the chamber. This procedure is needed because after several tests it turned out that emulsion stored at high temperature can emit a poisoning gas that can produce fog increase and sensitivity reduction.
- Refreshing: this steps lasts 3 days and the conditions needed to erase tracks are $RH \approx 85-99\%$ and $T \approx 26-29°C$. In this case the air flow is all inside the chamber and there is no air regeneration, the warm air circulates counterclockwise inside the chamber through stainless ducts and the humidity is obtained by controlled water supply.
- Drying: after refreshing films should be gradually conditioned to 20℃ and 50% RH, this procedure is accomplished by a 3 days drying. Films remain inside the chamber but there is no water supply and there is very quick air circulation and regeneration.

After drying films are extracted from the refreshing chambers, packed under vacuum in stacks of 9 ECC basic units and stored in underground till the shipment to Europe.

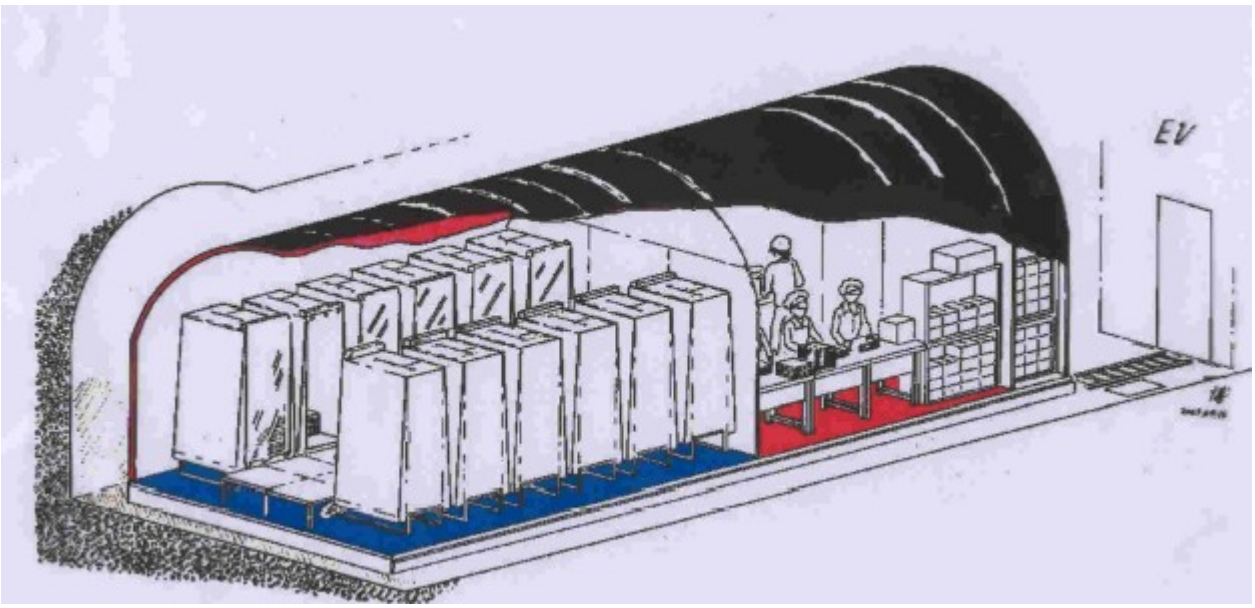

Fig. 5.2 – Refreshing underground facility in Tono mine.

Emulsions quality after refreshing is regularly checked by fog density measurements and exposure to 100 MeV electron beam line. The current estimation of refreshing efficiency is 98% and the film sensitivity is requested to be at least 32 grains/100 μm. Films that does not satisfy these requirements will not be used for OPERA target.

Two fully operational refresh facilities are presently working in Tono (Fig. 5.2) and the refresh procedure is schedule up to summer 2006.

Self-refreshing tests for CS detector at LNGS

CS detector usage has been proposed by the OPERA collaboration in 2002 [23] and the intent was to reduce the overall scanning load and increase the event location efficiency; in particular CS will be crucial to resolve possible ambiguities in TT predictions because CS from more than one brick can be scanned in order to select the proper event brick. In the base-line option CS should be packed independently under vacuum and fixed onto the downstream surface of the brick.

CS films were foreseen to be packed individually at a suitable relative humidity in Japan and shipped to LNGS underground Hall, their mounting would be done within the line of the BAM machine. The experimental knowledge about track erasing at that time envisaged the use of a temperature-humidity tuned self-refreshing technique with a fading life-time that could have been chosen to range from one year down to about one month. In order to reach this goals CS should have been packed with a relative humidity from 80% to 90%, assuming that the Hall C temperature would have been 20℃ or lower during beam exposure. It was foreseen that self-refreshing would have been the only method needed to erase tracks produced during the run and radioactivity of lead plates.

In order to check and tune such new technique several tests have been planned in Europe and in Japan; I joined those activities in LNGS and during my stay at Nagoya University, more relevant results are reported in the following pages.

A stack of 80 not refreshed emulsion[3] was exposed at CERN horizontally to the PS pion beam (8 GeV/c,10^5 tracks/cm^2) on 9th November 2004. The track density was optimized in order to have 2-3 MIP tracks in an effective microscope view of 200 × 200 μm^2 because it was decided to perform automatic tracks recognition and grain counting.

After the beam exposure emulsions were packed at room temperature at different humidity during December 2004 in LNGS Underground Lab and then developed by myself after some hours, 2-3 days and 1 week. Emulsion quality has been checked visually by LNGS microscopes and no relevant damages have been detected.

It was possible to tune humidity in underground dark room and the following stable conditions were reached:

[3] April 2004 Fuji Co. production

- T= 19.5 ° C 90 % R.H.
- T= 19.5 ° C 85 % R.H.
- T= 19.5 ° C 80 % R.H.
- T= 19.5 ° C 50 % R.H. Used for reference emulsions

Opera films have been cut in four pieces and left in the dark room in each of those conditions for 5 hours in order to guarantee a smooth conditioning. Then each piece has been packed in a separate bag and stored in the dark room with stable environmental parameters (20°C and 60% R.H.).

From 18 December 2004 to 23 February 2005 I developed emulsion samples at Salerno Laboratory several weeks after packing and then I measured their sensibility and fog density.

	Reference	80%	85%	90%
1	0.67	0.875	0.875	0.875
2	4	2	4	2
3	7	7	7	3
4	12	14	12	8
5	18	21	18	15
6	26	50	51	22
7	55	69	70	54
8	74	//	//	69

Table 5.1 – Self-refreshing period (days) for each sample.

Results T = 19.5°C 90 % R.H. - 4 days

After 4 days storage at 90% RH it was already possible to see the accelerated fading effect; GD density was – in fact – well below the standard value (≈ 30 g/100 μm) (Fig. 5.3) and also the erasing was higher in the outer surface (Fig. 5.4). Also the number of reconstructed tracks slightly felt down near the surface, that results showed that fading was faster on the surface and that the refreshing procedure was not complete.

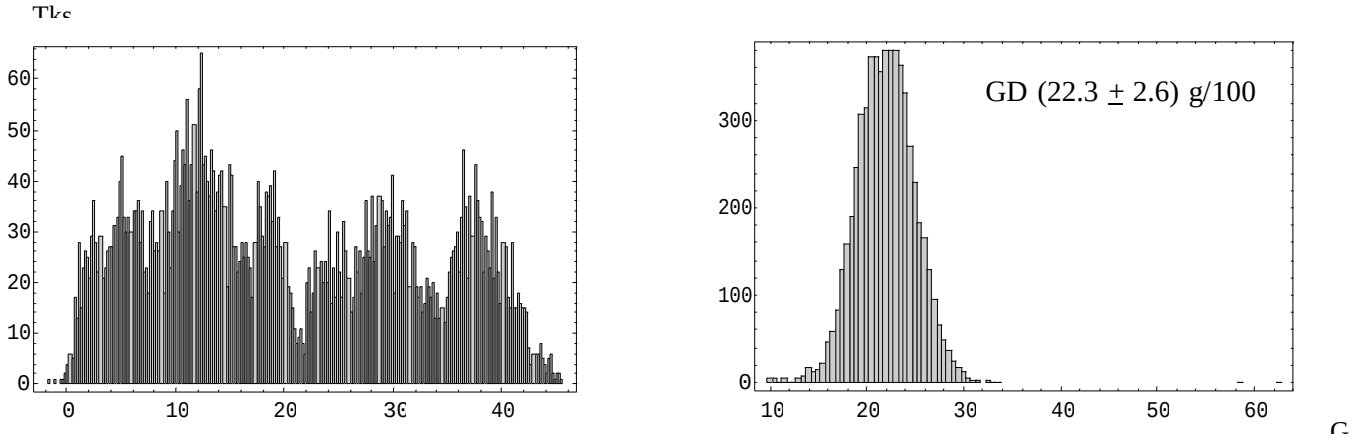

Fig. 5.3 – On the left side there is the track distribution along emulsion depth; on the right there is the overall GD distribution over a sample of more than 10000 horizontal tracks.

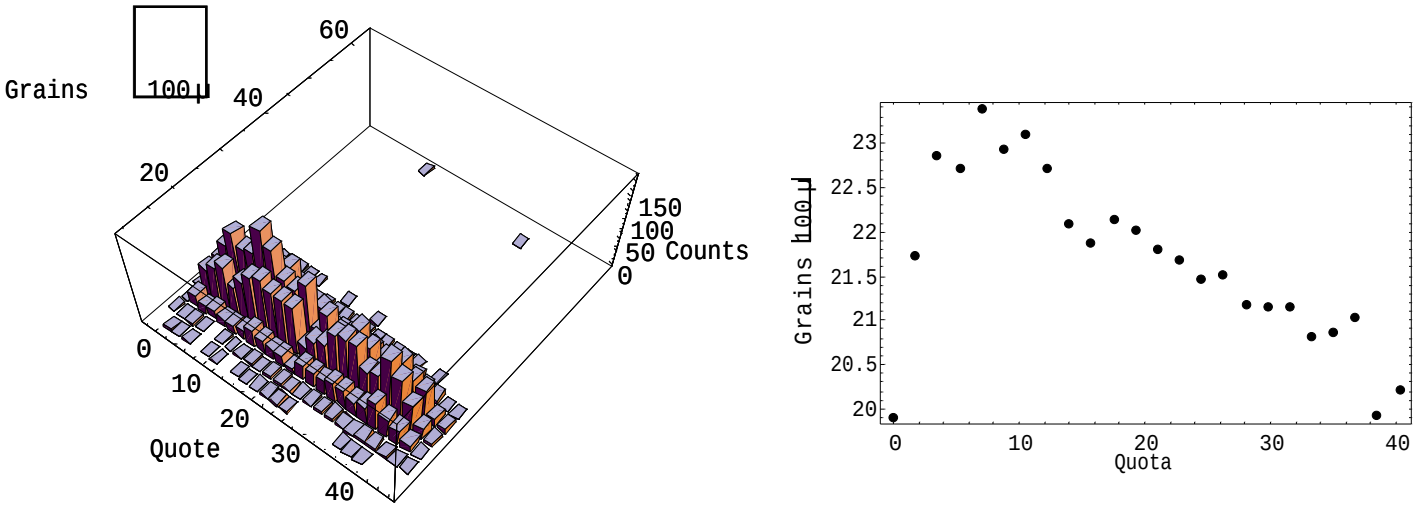

Fig. 5.4 – On the left side there is 3D tracks GD distribution along emulsion depth; on the right there is the GD profile along the depth.

Results T = 19.5°C 85 % R.H. - 21 days

After 21 days storage at 85 % RH it has been clearly detected the self-refreshing effect; GD density was very low (Fig. 5.5) and the erasing rate was constant along the depth (Fig. 5.6). The number of reconstructed tracks did not fall down near the surface, that results showed that after 3 week storage the refreshing procedure is almost completed; the drawback was a large amount of fog.

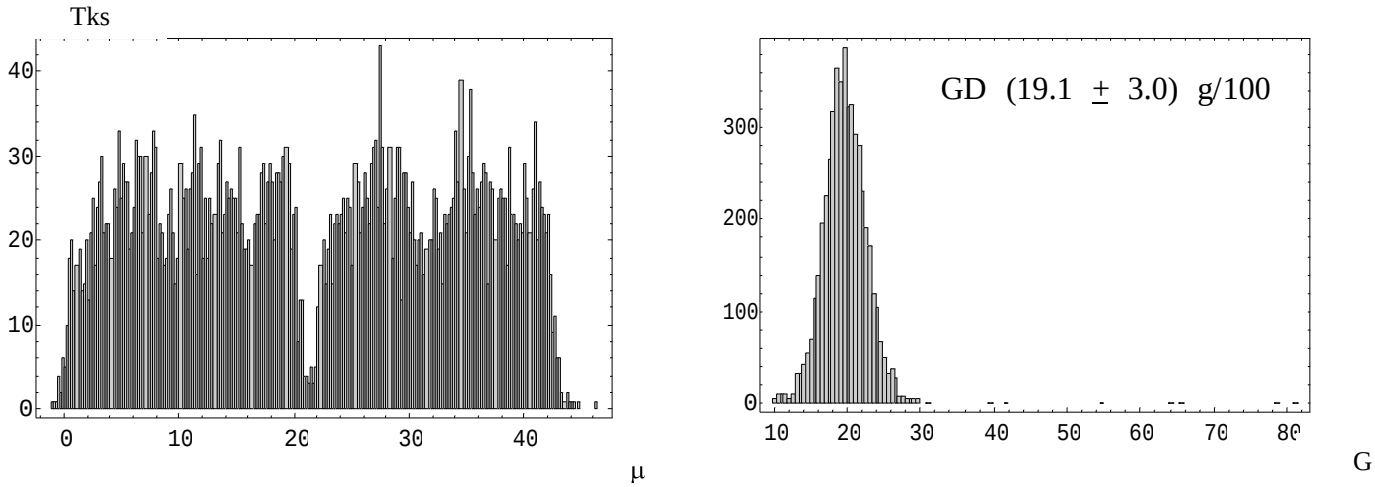

Fig. 5.5 – On the left side there is the track distribution along emulsion depth; on the right there is the overall GD distribution over a sample of more than 10000 horizontal tracks.

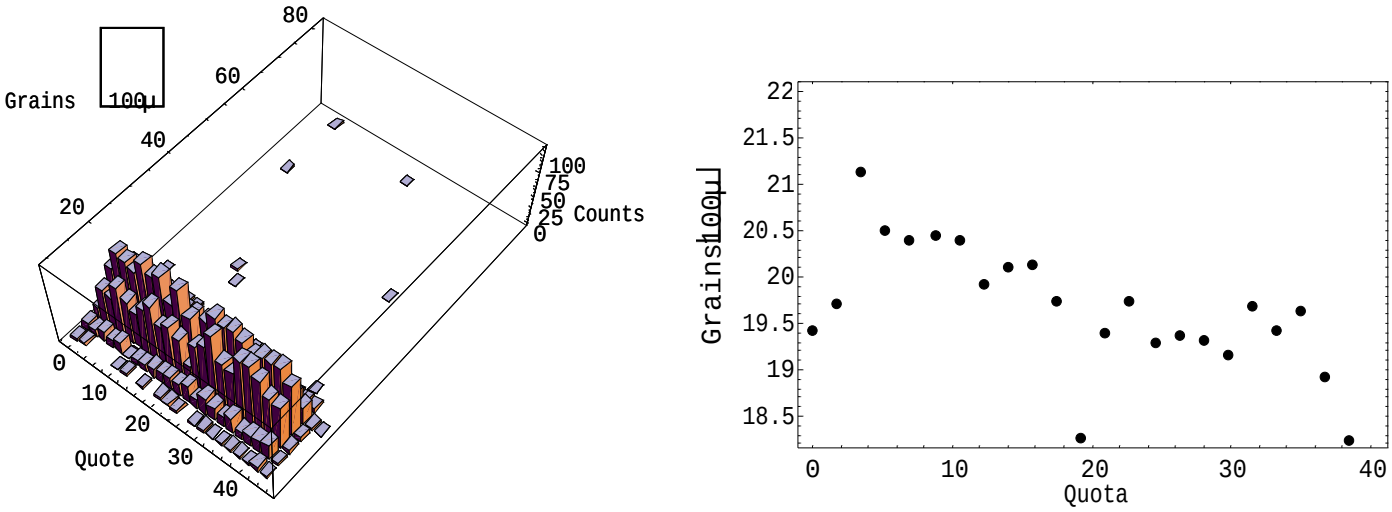

Fig. 5.6 – On the left side there is 3D tracks GD distribution along emulsion depth; on the right there is the GD profile along the depth.

Results T = 19.5°C 80 % R.H. - 8 days

After 8 days storage at 80% RH it has been clearly detected the fading effect; GD density was low (Fig. 5.7) and the erasing rate was not constant along the depth (Fig. 5.8). The number of reconstructed tracks slightly felt down near the surface, those results showed that after 1 week storage the refreshing procedure is still limited to the outer emulsion active layer. Furthermore it has been possible to compare short term storage fading effect among different humidities andthe tracks erasing speed in case of 80% RH is around one half then the one at 90% RHstorage.

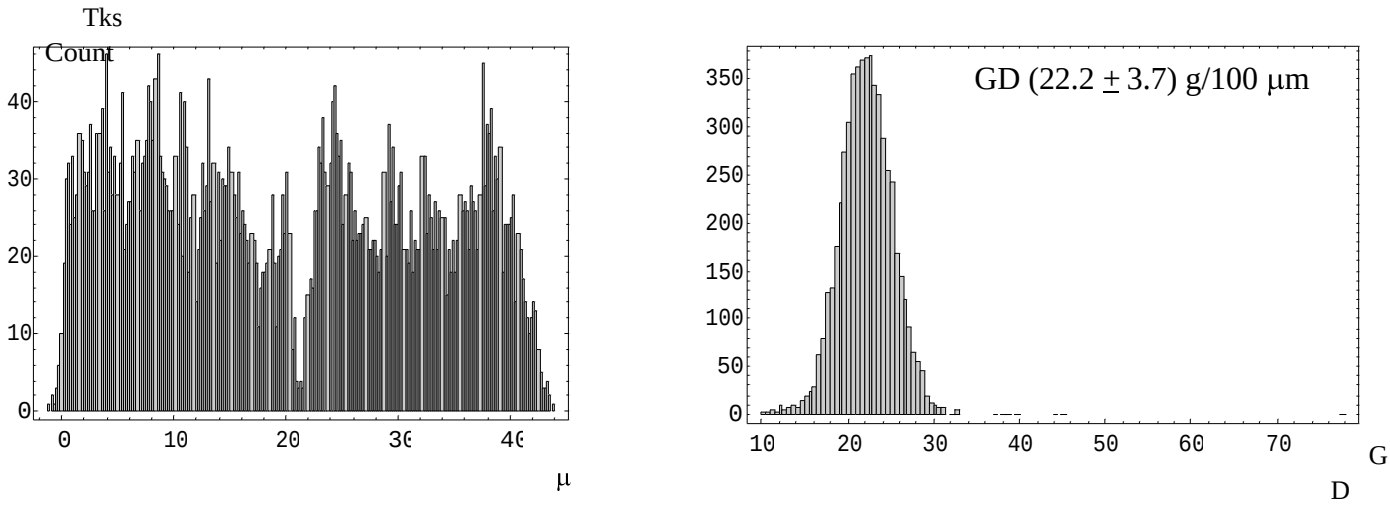

Fig. 5.7 – On the left side there is the track distribution along emulsion depth; on the right there is the overall GD distribution over a sample of more than 10000 horizontal tracks.

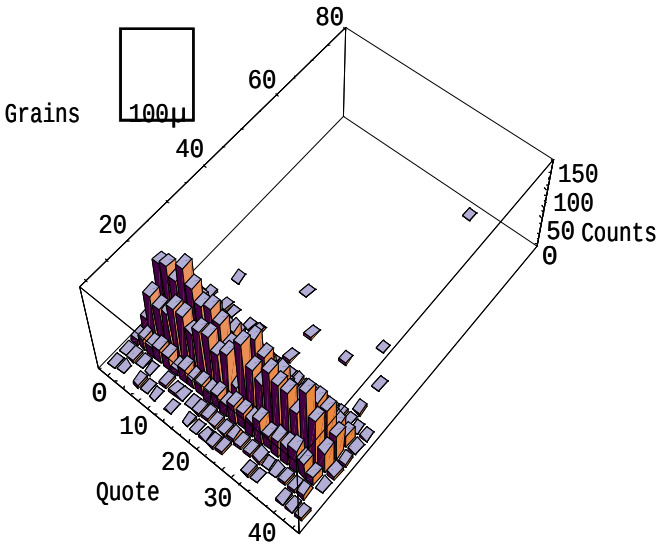

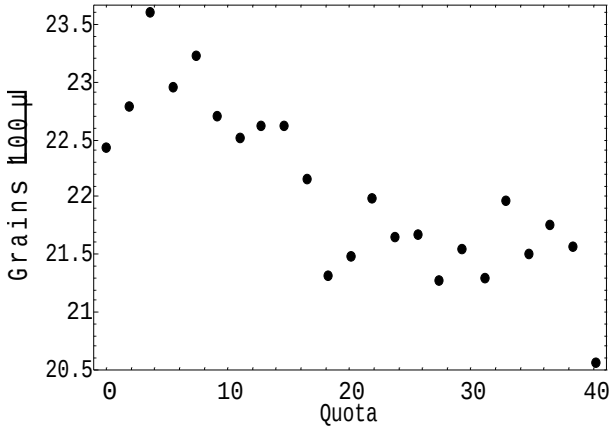

Fig. 5.8 – On the left side there is 3D tracks GD distribution along emulsion depth; on the right there is the GD profile along the depth.

Results T = 19.5°C 50 % R.H. Reference - 26 days

It has been possible to evaluate OPERA emulsions fading ratio measuring a reference sample after 1 month storage at 20°C (beam exposure expected conditions); the effect was constant and the GD has been lowered by a factor 12.5 %. This result is very important to understand the best storage condition for OPERA emulsion meanwhile neutrino interaction and development.

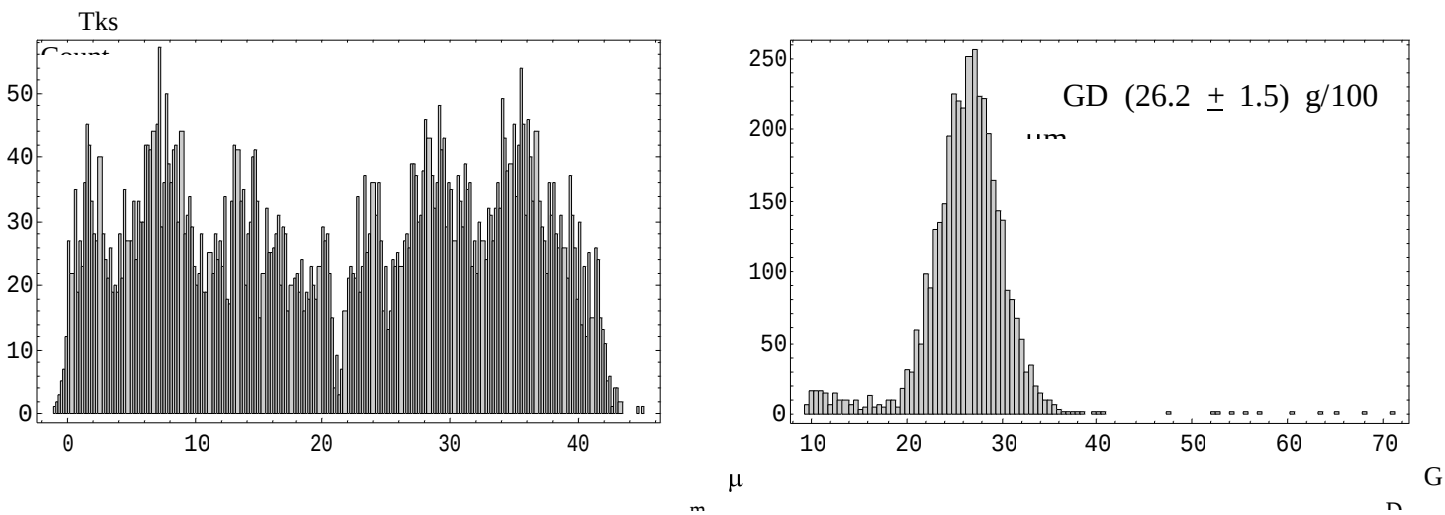

Fig. 5.9 – On the left side there is the track distribution along emulsion depth; on the right there is the overall GD distribution over a sample of more than 10000 horizontal tracks.

In Fig. 5.10 it is reported the final and complete statistic about GD count, the neat result was that the erasing rate was strongly dependent on humidity. In case of 50 % RH only the usual fading phenomena took place, in case of higher humidity the effect was higher and during the first two weeks there was the strongest speed difference among different samples.

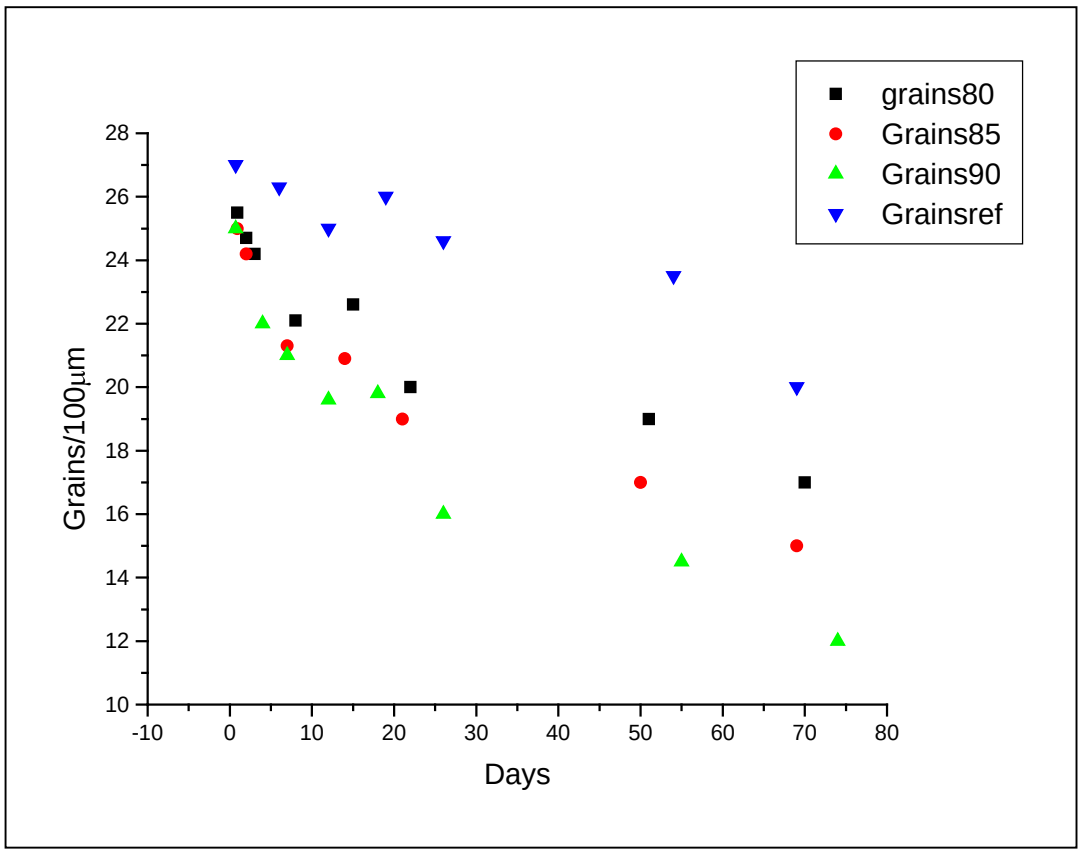

Fig. 5.10 – GD count on all self-refreshing samples developed up February 2005.

In case of high humidity storage the GD after 2 months is lower enough to make tracks not detectable by fast automatic microscopes so, from the point of view of tracks erasing, the self-refreshing has been successfully tested but two side effects that ruled out that procedure have been found. First of all cluster measurements clearly showed a big fog increase after 12 days of storage (Fig. 5.11); the FD values found after 1 month were close to the maximum allowed by microscope scanning and so those storing condition should be avoided during OPERA running. Furthermore it has been found a strong sensitivity decrease in samples stored at high humidity for 2 months; to test this feature I exposed some samples to cosmic rays for 1 week and I measured their GD (Fig. 5.12). All the tracks found, old sample and freshly exposed cosmics, had a GD lower than 20 g/µm; the only explanation to this huge damage on emulsion sensitivity was a chemical poisoning due to a dangerous gas emitted by the emulsion themselves.

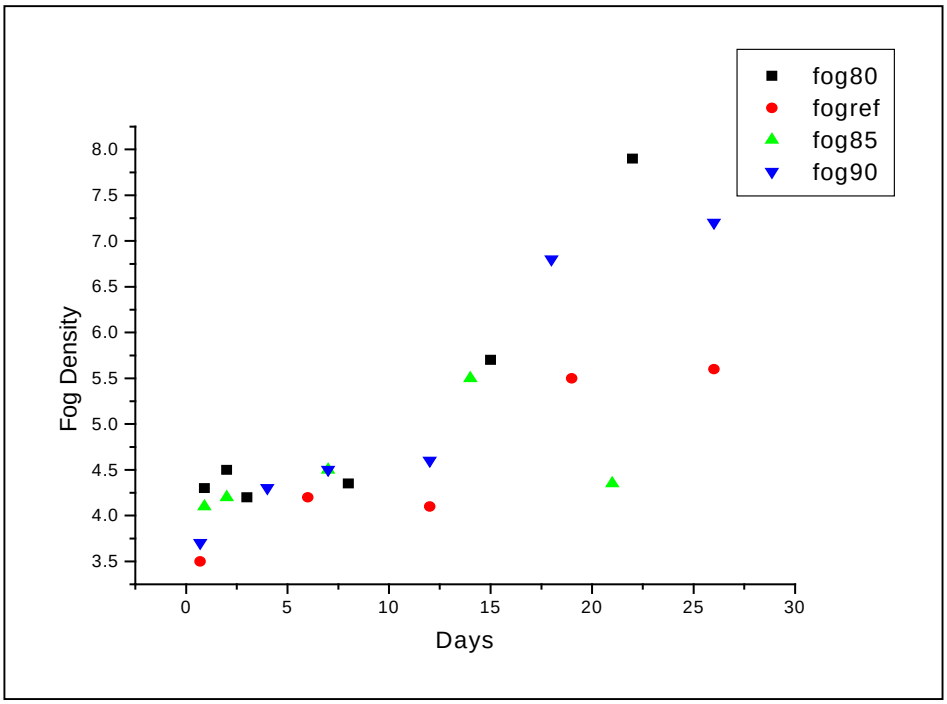

Fig. 5.11 – FD count on all self-refreshing samples developed up to January 2005.

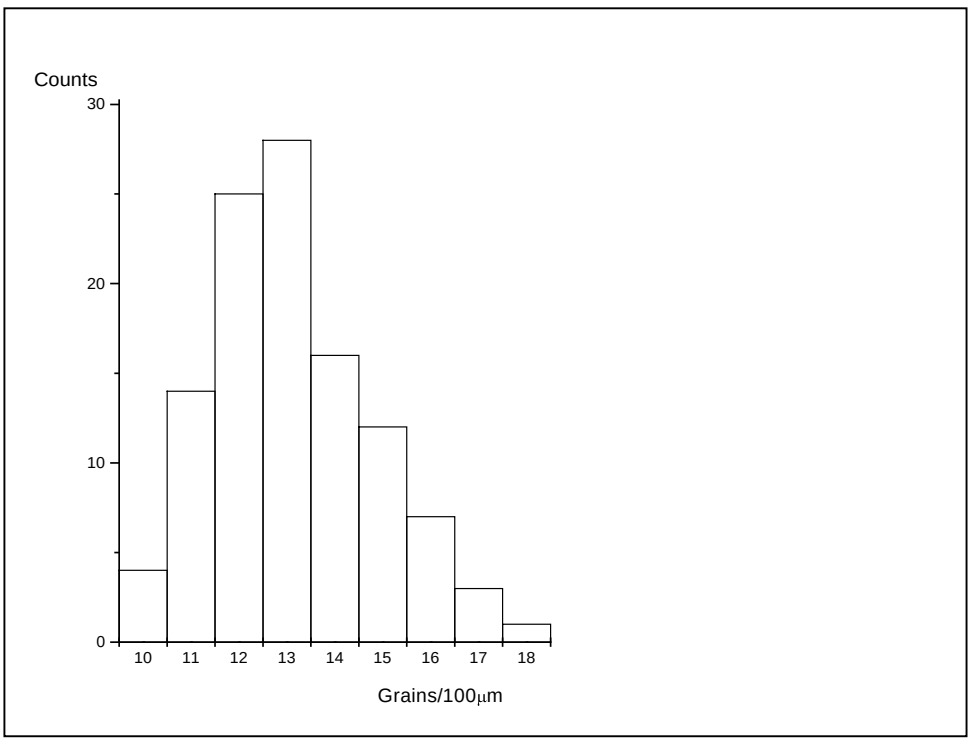

Fig. 5.12 – GD measured on a sample exposed to cosmic rays for 24 hours.

This point has been discussed with Japanese colleagues because they already experienced such chemical damages during refreshing at Tono mine and they confirmed the hypothesis that the poisoning gas has been emitted by emulsion themselves. As previously described (see page 95), the first step during refreshing is a fast air circulation to expurgate poisoning gas; since the samples used in the LNGS test were not refreshed the chemical contamination could have lowered emulsion sensitivity. During my stay at Nagoya University I planned to expose to a 2 GeV/c pion beam at KEK LNGS samples and also some samples refreshed at Tono mine to compare their sensitivity. The exposure took place on June 2005 and results are shown in Fig. 5.13.

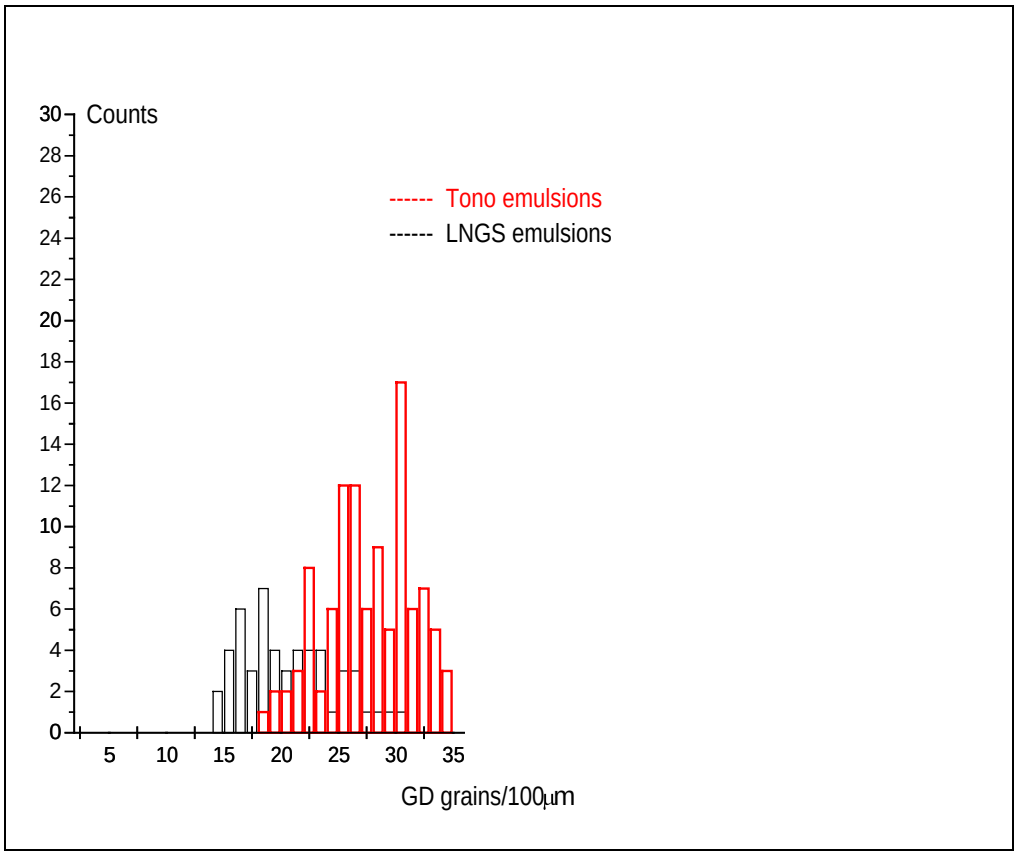

Fig. 5.13 – GD measured on emulsions exposed to KEK pion beam on June 2005.

In case of Tono refreshed samples the sensitivity was high enough, in case of LNGS samples I found one more time a very low GD that confirmed our hypothesis of chemical contamination and ruled out the possibility to use self-refreshing for CS packing. Infact it would have been deserved to pack at high humidity emulsions that have been previously refreshed in Japan; in case of double refreshing the fog density would explode and CS films would be completely useless. Together with Japanese experts I visited the Fuji Co. and we had the possibility to discuss with chemists and engineers that designed OPERA films; they confirmed our worries

and proposed to pack CS films at 50 % RH and 20℃, such conditions can preserve emulsion sensitivity for 10 years at least and do not imply fog density increase.

CS handling in LNGS underground lab

In this scenario the collaboration had to revise completely the CS handling base-line option; it has been taken the decision to ship to LNGS fresh emulsions and to refresh and to pack them on-site. Refreshing efficiency is presently 98% and so the number of residual tracks on each CS is not negligible (about 8000), those tracks cannot be erased because they have been produced by unavoidable heavy ionizing particles accumulated during film pouring, rolling and cutting at Fuji plants. Physical tracks still present on a single film surface would imply a heavy CS scanning load (several hours) and can produce fake misalignment between CS and brick first plate. Both cases will arise several problems in the neutrino interaction location procedure and will reduce to zero the CS detector utility; infact random coincidence could affect the brick selection and increase the scanning load. In order to recover CS convenience the collaboration decided to use two emulsions packed under vacuum instead of a single CS; by means of the coincidence between two sheets it is possible to reduce fake alignments and decrease the scanning load on bricks. In order to benefit of the coincidence between two plates it will be deserved a tight mechanical alignment between CS doublet and between CS doublets and bricks. It has been estimated by MC simulations that it is required an alignment precision better than 50 μm inside CS doublet and better than 1 mm between CS doublet and brick; in this option the number of random coincidence could be reduced to less than 2 giving a half-time scanning load. In order to get those precisions it has been designed a plastic box that will host emulsion very tightly and that can be precisely clipped on the brick downstream side. In addition it is planned to expose the extracted brick to four X-rays spots; X-rays will penetrate trough CS doublet and reach the first brick emulsion marking a reference pattern; this pattern will be used for alignment and can provide the deserved precision. Nowadays the CS facility in underground laboratory at LNGS has been completed and two refreshing units have been successfully installed and tested. The CS doublet packing procedure is under commissioning and already installed in underground.

Emulsion development

Photographic development is the process by which the latent image is made visible by the reduction of silver ions to metallic silver; for this reason a chemical agent that reduces completely those crystals containing a latent image center and leaves the remnants unchanged is usually chosen to develop nuclear emulsions. Developing products may be divided into two main groups depending on the source of silver ions for reduction and most developers are a combination of the two. The first group is known as physical developing agents, in this case silver ions are provided from the solution in the form of a soluble complex; these are deposited on the latent image center and then reduced to metallic silver. This procedure produces spherical particles whose precise shape is affected by pH. Chemical developing agents are the second group and are more usually chosen during the nuclear emulsions processing. However, the choice between a physical developer and a chemical one will mainly depend on the grain

structure required in the processed image. In chemical development, silver ions are provided from the silver halide crystals containing the latent image center; the action of a chemical developer produces a mass of filaments bearing little resemblance to the original crystal. If silver halide solvents, such as sulphite, are present in the chemical developer, an opportunity exists for some physical development to occur; in this case, the filaments will be shorter and thicker. Chemical development, like many other chemical reactions, is dependent on temperature: it occurs more rapidly at higher temperatures while below 10°C it virtually stops. It is important, therefore, to keep the processing temperature constant, otherwise it will not be possible to asses the correct development time. Chemical developers are also dependent on pH, and will maintain a given activity within a narrow pH range. In general, the less alkaline the environment is, the less active the developer will be; for this reason the use of an acid stop bath is often recommended at the end of the development to stop immediately the process and control precisely the time.

A more exact understanding of the development processes is obtained by the quantitative methods of electrochemistry. A metal (specifically silver) in contact with a solution of its ions has an attitude to detach electrons, $Ag \rightarrow Ag^{+} + e^{-}$ and this attitude can be measured. The single-electrode potential of the metal with respect of the solution is the usual measure of this attitude (that means that the activity is relative to hydrogen). The concentration and activity coefficient of metal ions in solution affects the tendency of the solid metal to dissociate, and consequently it influences the measured potential. The potential difference E is related to the electrode-solution system parameters by the equation:

$$E = E_0 - \left(\frac{RT}{F}\right)\ln\left[\frac{a_{H^+}\left(a_M\right)^{1/n}}{\left(a_{H_2}\right)^{1/n}\left(a^{n+1}\right)^{1/n}}\right]$$

Where E_0 is the constant standard electrode potential; T is the absolute temperature; R is the gas constant per mole; F is the Faraday constant; a_{H^+} is the activity of the hydrogen ion; a_M is the activity of the metal; n is the degree of ionization; a_{H_2} is the activity of gaseous hydrogen; and a^{n+} is the activity of the metal ion. The activity of pure, solid unstrained metal is defined to be equal to 1, as are the activities of hydrogen gas at 1 atm pressure and 1 mole of hydrogen ions per liter. Equation for pure unstrained metal relative to the normal hydrogen electrode is:

$$E = E_0 - \left(\frac{RT}{nF}\right)\ln\left(a_{M^{n+}}\right)$$

Activities or concentrations of ions different from hydrogen are sometimes measured by the negative logarithm of the ionic activity.

$$pAg = -\ln Ag^{+}$$

When an electrode releases electrons to the surrounding medium, its action is called reduction; when it accepts electrons, its action is called oxidation. When ions in the medium exist in two different states of reduction their relative activities affect the electrode solution potential difference, E:

$$E = E_0 - \frac{RT}{F} \ln \frac{a^{(n-1)^+}}{a^{n^+}}$$

E_0 is the potential that exists when the ions are equally active; $a^{(n-1)^+}$ and a^{n^+} are the relative activities, at low concentrations proportional to the concentrations, of the ions in the ionized states (n-1) and n. In studying oxidation-reduction processes, it is usual to write the previous equation in the form

$$E = E_0 - \frac{RT}{F} \ln \frac{(OX)}{(RED)}$$

E is called the redox potential. Here (OX) and (RED) are approximately the respective concentrations of the oxidized and reduced forms of the reducing compound. Thus, as an example if ferrous chloride is used to develop the latent image of silver, it is the difference of redox potentials in the oxidized and reduced forms of both that determine the resulting potential difference ΔE. Development speed is regulated by the magnitude of ΔE. Several inorganic materials have been tested as developers for nuclear emulsions; they can be classified according their development rate or their reduction potential relative to a hydrogen electrode at fixed pH. The developers generally used for nuclear emulsions are combined chemical and physical developers, sulphite and bromide are solvents of the silver halide. The silver ions in the complex are reduced to metallic silver that precipitates in the gelatin, and plates out on the silver grains. This causes physical development of the grains and fog. Successful development requires that the reaction in the grains containing the desired latent image proceed more rapidly than the development of fog. The fog always limits the track-grain density obtainable merely by development because prolonged action of strong reducing agent develops all the silver halide micro crystals. The rate of development, in common with that of most chemical reactions, varies rapidly with the temperature. In the small interval of temperatures ordinary used for development, the relationship between the logarithm of the development time t and the centigrade temperature T, is roughly linear:

$$\log t = -KT + Y$$

The temperature coefficient K varies in the approximate range 1.55-2.02, depending on the photographic materials and the composition of the developer. The potential of pure reducing agents grows linearly with the pH of the system. The effect of sulphite in the developer, which tends to prevent oxidation of the developing agent by dissolved oxygen from the air, often changes the speed of the development. A second reason why sulphite affects the development rate is that it is a silver bromide solvent and, therefore, while exposing the internal latent image to the developing agent, may also dissolve away an excessive amount of halide. Because of

common ion effect, the presence of a soluble bromide in the developing solution lowers the silver ion concentration, and restrains the development rate. This effect is discriminatory and generally inhibits the growth of fog more than the development of the latent image. It is particularly important to use bromide in processing nuclear track emulsion otherwise fog will develop in the upper emulsion layers. On the other side an excess of KBr produces a deleterious effect because the silver ion concentration can be driven so low that metallic silver goes into solution destroying the latent image.

The conventional photographic processing steps are: presoak, development, stop, fix, wash and dry; in addition several new procedures are made necessary by the great thickness and concentration of the emulsion, and by the requirements that there be uniformity of development and low distortion. Even the conventional operations are rather deeply modified by these conditions.

The purpose of fixation bath is to remove all the residual silver halide, leaving the metallic silver to form the image. If silver halides are left in the emulsion, they would slowly get brown and degrade the image. The fixing agents most widely used are sodium or ammonium thiosulphate, which form thiosulphate complexes with the silver halide. Silver thiosulphate is soluble in water and so may be removed from the emulsion by washing. It is important to use a fixer that has not been exhausted when processing nuclear emulsion; otherwise some silver halide will remain in the emulsion. After fixation, emulsion must be washed very thoroughly. This is to remove all the silver thiosulphate complexes in the emulsion; any residual, if any, will eventually break down, producing silver sulphite which is brown and will obscure the image. During fixing and washing emulsions can encounter big distortions because at that stage they are soft and fragile; drying procedure is also a serious source of distortion but it has been made much more controllable by the use of alcohol-glycerin baths.

R&D on Opera emulsions development

Solution aging tests

The processing procedure that would have been adopted for OPERA films in large scale development has been discussed with Fuji experts and Japanese collaborators and the base-line option is described in Table 5.2. The first step − presoak − is applied to make easier the developer penetration inside the whole emulsion depth; after the usual development, stop and fixation it has been decided to have a long washing procedure to ensure emulsion transparency long term stability. At the end an alcohol+glycerin bath is used in order to have a stable thickness around 44 μm and a fast driwell immersion to avoid the occurrence of drops on emulsion surface. The last two steps have been introduced because fast microscope scanning requires a uniform emulsion thickness and surface planarity.

During July 2003 at CERN there have been performed several technical tests in order to define the dimensions of developing facilities at LNGS. CERN emulsion laboratory is equipped for small developments (1 or 2 bricks per day) so the idea was to understand how large scale developments should have been organized. It was needed to define tanks dimensions, processing time, the amount of chemicals that would be used per day during OPERA and so on. In order to fix the tanks dimensions it was needed to understand how many emulsion films could be processed with the same solution, first of all it has been investigated how many

emulsions could have been developed and fixed with 1l of solution. The Fuji developer has been designed on purpose for OPERA films and it has been declared a limit of 15 – 20 films/liter; fixer limit depends on the amount of silver contained in each emulsion (nominally 1g of silver per film) and by chemical calculations it could have been possible to fix up to 10 films/liter.

Step	Time	Chemical Composition (1 liter)
Presoak	10’	Sodium Sulphate (70 g) Demineralized Water
Development	25’	Fuji Developer (250 ml) Fuji Starter (20 ml) Demineralized water
Stop	10’	Aluminun Sulphate (8.5 g) Acetic Acid (5ml) Demineralized water
Fixation	35’	Sodium Thiosulphate (300 g) Sodium Sulphite (12 g) Acetic Acid (9m) Aluminun Potassium Sulphate (5 g) Water
Washing	2 h	Circulating Water
Alcohol	20’	Ethyl Alcohol (600ml) Glycerine (200ml) Water (200ml)
Driwell	1”	Fuji Driwell (5ml) Water

Table 5.2 – Base-line processing procedure for OPERA films.

In order to check development performances it was needed to compare GD and FD on different emulsion samples and it has been decided to use horizontal tracks measurements. Thus there have been exposed horizontally a stack of 29 emulsions to the CERN 8 GeV pion beam. Those emulsions were developed two by two in 2l tanks developer and fixer solutions.

Some samples were developed or fixed with fresh solutions to cross-check development quality. It has been achieved to develop 30 films with the same Fuji solution and more than 10 films with the same fixer; results are shown in Fig. 5.15 and it is possible to see a slight GD reduction in the last samples. Regarding fixer it turned out that the limit was 6-7 films/liter: when it has been tried to fix more films consecutively the result was that emulsions became darker (brown zones) after few days. FD measurements showed that the safest limit for Fuji developer will be 20 films/liter, no fog density increase will be induced by the use of old fixer.

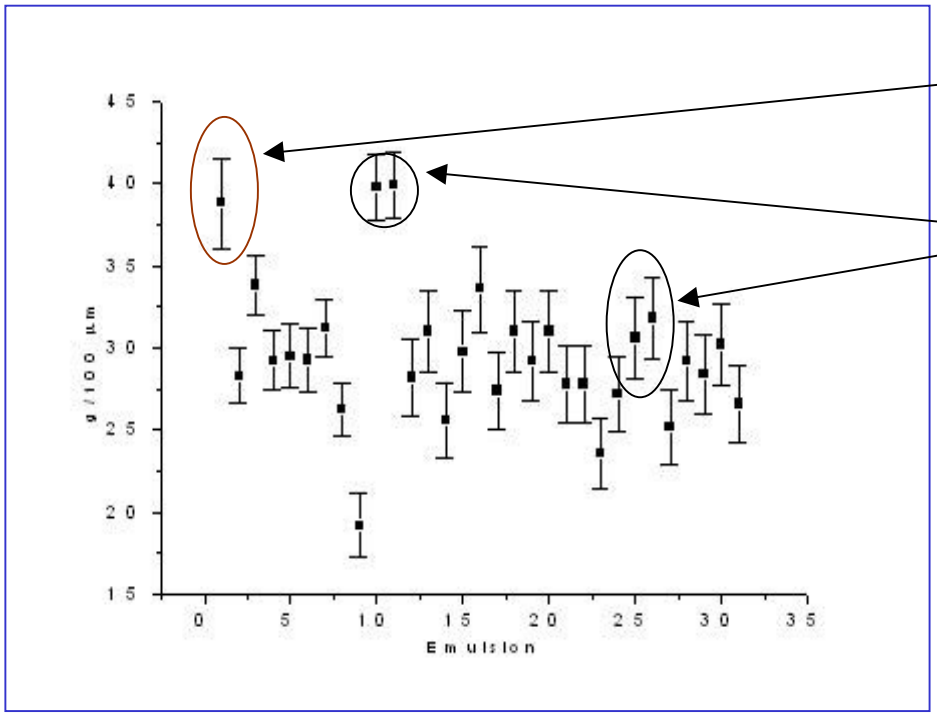

Fig. 5.15 – GD counts on solution ageing tests.

Washing test

Base-line option was to wash emulsions in circulating water for 2 hours; this solution seemed too long for LNGS large scale development, so there were investigated different washing procedures. It has been tried to wash emulsions by putting them into different baths of fresh water, there have been tested several solutions and in the end the result was that 4 baths of 20' would have been enough. In particular it has been found that four baths of fresh water will have the same or also a better effect on emulsions; there have been performed a $KMnO_4$ test (color indicator) to check the amount of residuals Sodium Thiosulphate in the washing water. To figure out the washing process it must be considered that it has to remove fixer residuals from emulsions and also from their stainless steel supports. Considering that emulsion volume is around 1 cm^3 and that there are usually washed 30 of them in an 18l tank full of water, it is possible to evaluate the washing process dilution. Emulsions could keep till two times their volume of fixer (60 cm^3) and their containers also twice so the starting fixer concentration is ≈1% (180 cm^3 / 18 l) and it can be reduced every time using fresh water. Since diffusion time is less than 10' it seems reasonable and also more efficient to change water than to circulate it (typically at a speed of two volumes per hour).

Starter test

Fuji experts suggested to use a starter in the develop bath; this product is a mixture of KBr and Acetic Acid that can control the development speed and quality, it has been performed a small test to check the best conditions in terms of fog density control. Following Japanese suggestions it has been prepared a solution of pure water, KBr and Acetic Acid changing the amount of these components in the range of 1-6 g/l KBr and 1-5 ml/l Acetic Acid. Results showed (Fig. 5.16) that it was essential to measure fog densities to estimate the right quantities. Looking emulsion by eye they seemed darker with less than 3 g/l of KBr. Some analysis of Salerno University chemists suggested to use 2-3 ml /l Acetic Acid and this idea was confirmed by CERN tests. In the end it has been prepared the starter with 4 g/l KBr and 3 ml /l Acetic Acid; development results on emulsions were quite good but emulsions processed whit Fuji starter seemed in a better shape.

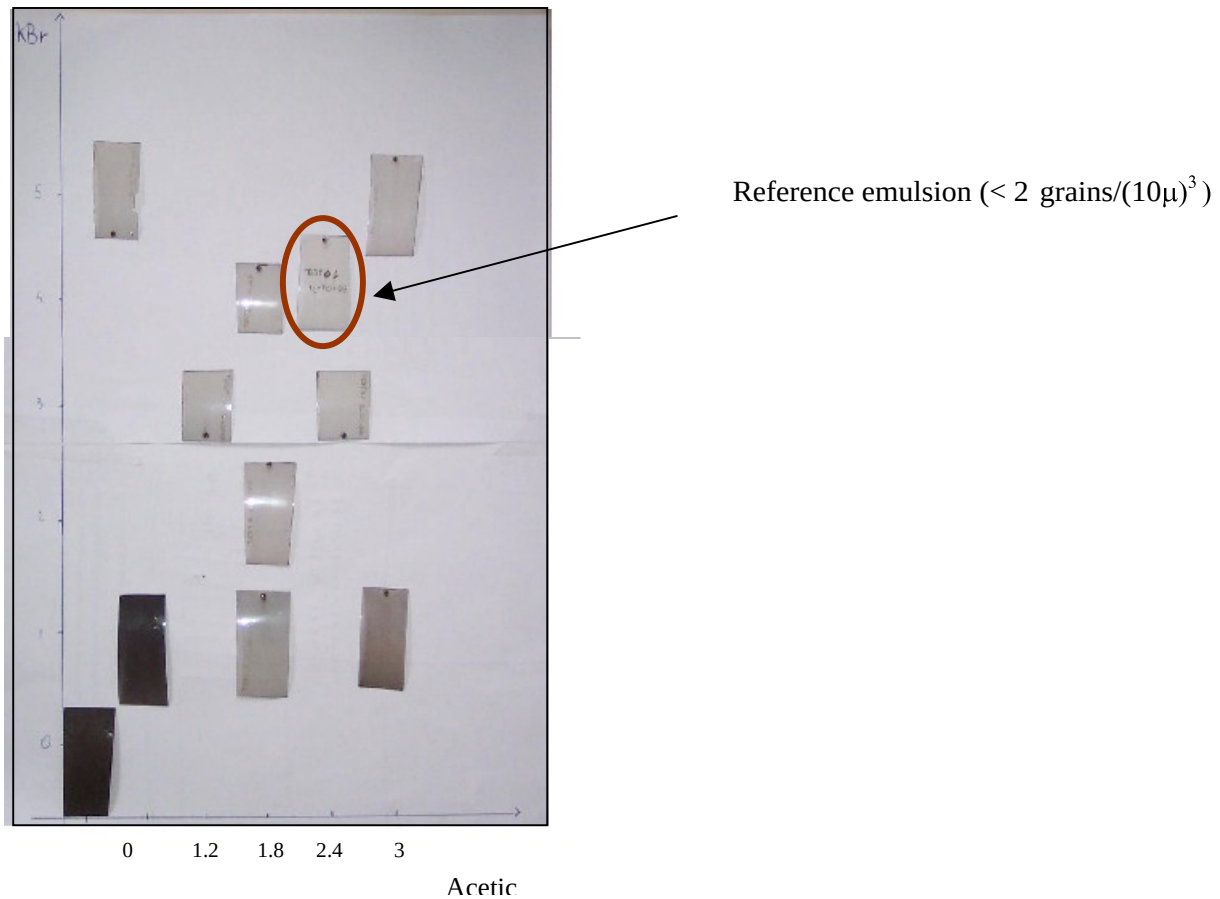

Fig. 5.16 – A picture of emulsion samples developed using different amounts of KBr and Acetic Acid, reference sample has been developed with Fuji starter and FD counts are reported on each film picture; in case of no starter use film was completely black and FD was impossible to be measured.

Presoak test at Nagoya (July 2005)

Discussing with Japanese colleagues in Nagoya it turned out that in case of OPERA thin films the presoak step could be avoided, furthermore I always noticed a slight non-uniformity of emulsion sensitivity as a function of depth and worse conditions on the surface. One possible source of surface problems could be a slight surface fading taking place during the presoak bath, so I tried different presoak conditions on same sample films. The test procedure accomplished the following steps:

- use not refreshed emulsions cut in several pieces
- exposure to 100 MeV electron beam at UVSOR facility
- develop in several conditions (no presoak ,water only presoak, usual procedure)

In order to measure GD and FD I had to use Japanese microscopes that are quite different from the European ones, I stored image files (0.25 micron pitch) and then clustered them by dedicated Nagoya software. Clustered data have been converted in a format similar to the Salerno one and then processed by the usual algorithms. This software chain worked properly and in Fig. 5.17 there are shown some tracks statistics, all parameters such are track length and track fit residuals are good enough to measure GD and FD automatically.

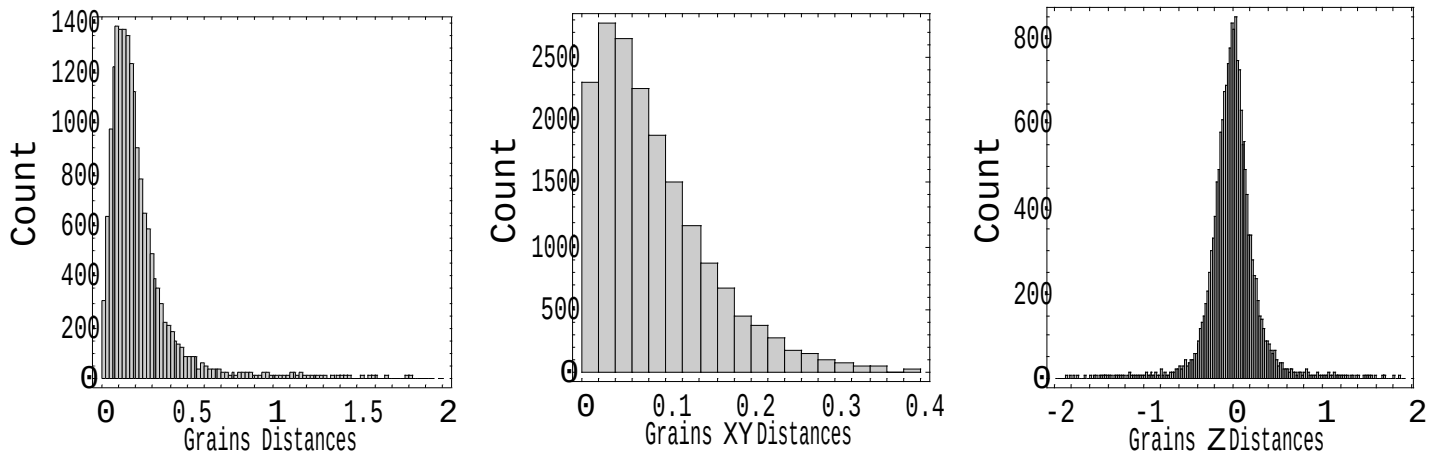

Fig. 5.17 – Some basic track fit parameters measured on Nagoya clustered data.

All samples developed have been measured and results are shown in the following pages, in the end it turned out that presoak can be avoided with no negative effects on emulsion sensitivity or grains size; furthermore a slight GD improvement has been found in case of direct immersion into the develop bath, so the surface fading effect could be avoided. Further test were needed using refreshed films and large scale development, I planned them at CERN.

Reference (10 min presoak + 25 min Fuji developer)

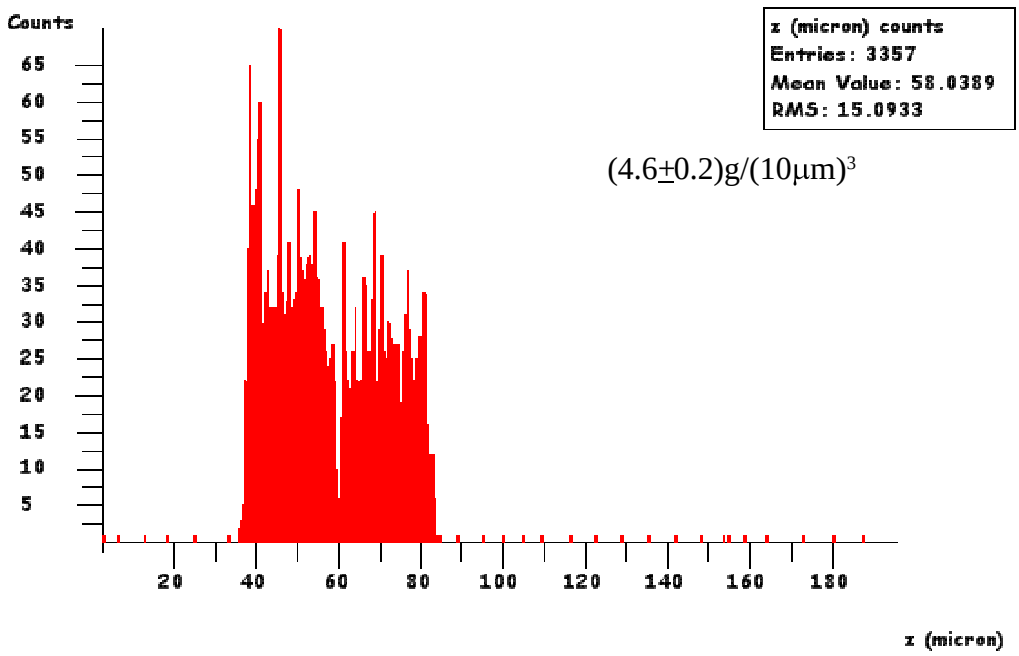

Fig. 5.18 - In the upper graph there is FD count and in the one below there is GD count, in both cases there is a slight sensitivity degradations on upper layers.

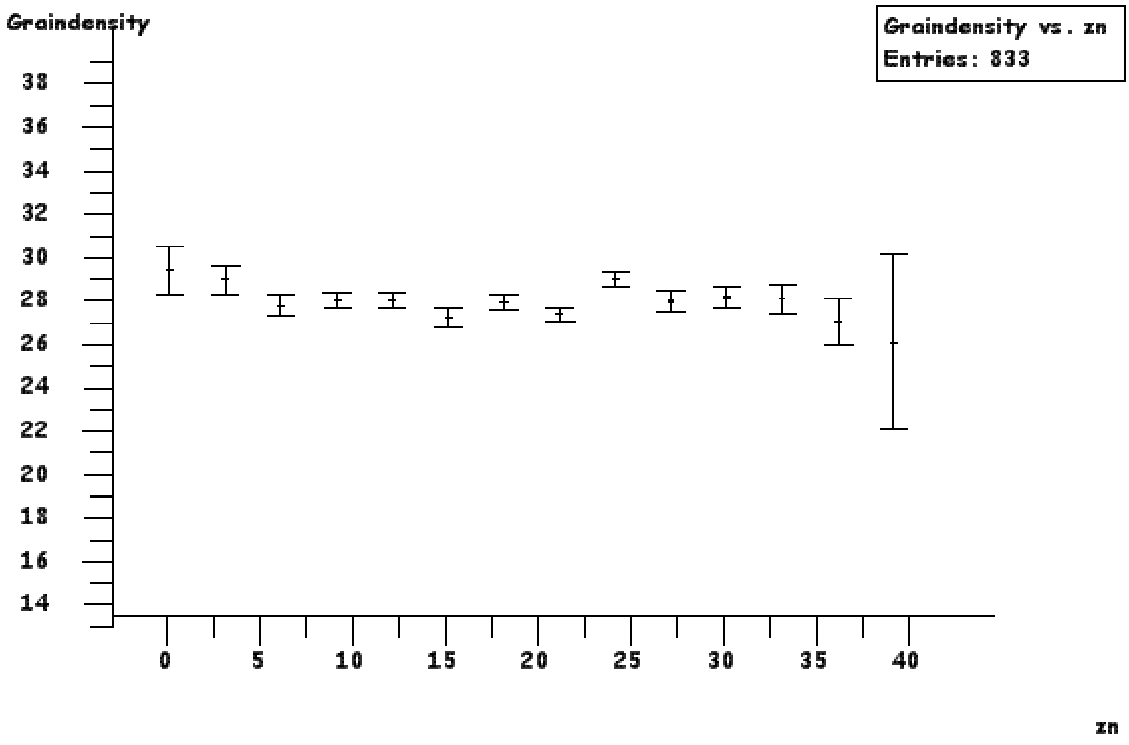

10 min ion exchanged water + 25 min Fuji developer

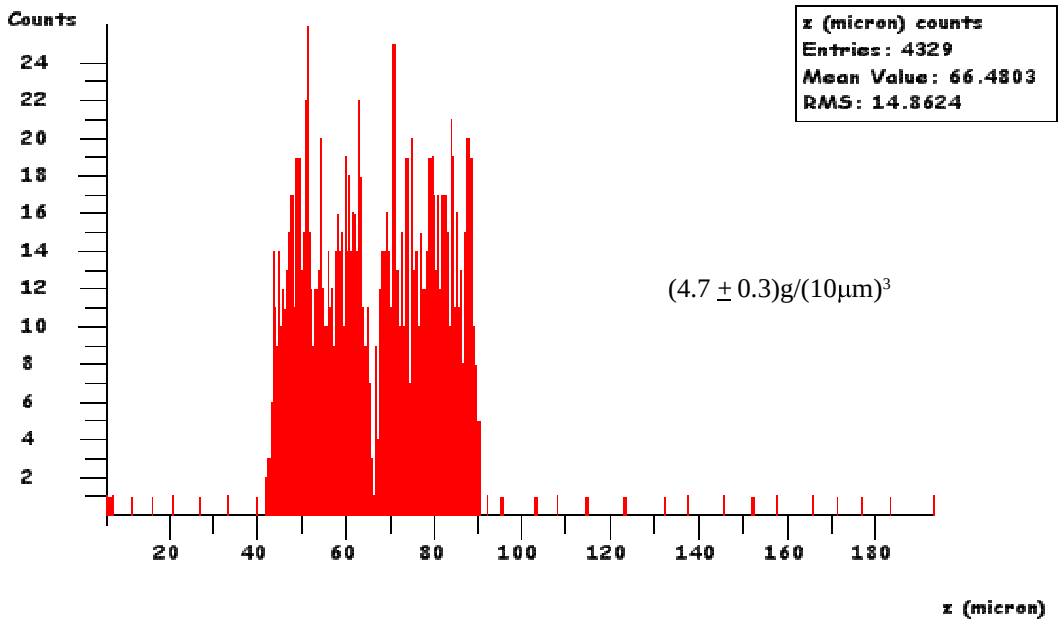

Fig. 5.19 - In both cases there is a constant GD along emulsion depth.

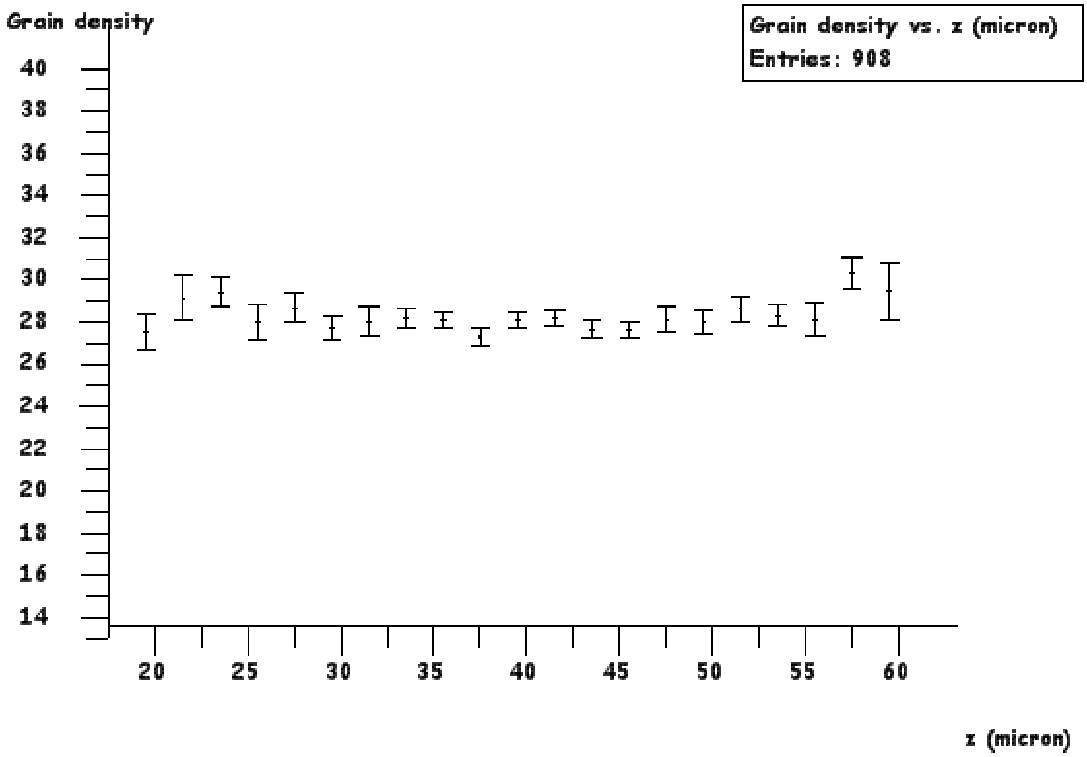

No presoak + 25 min Fuji developer

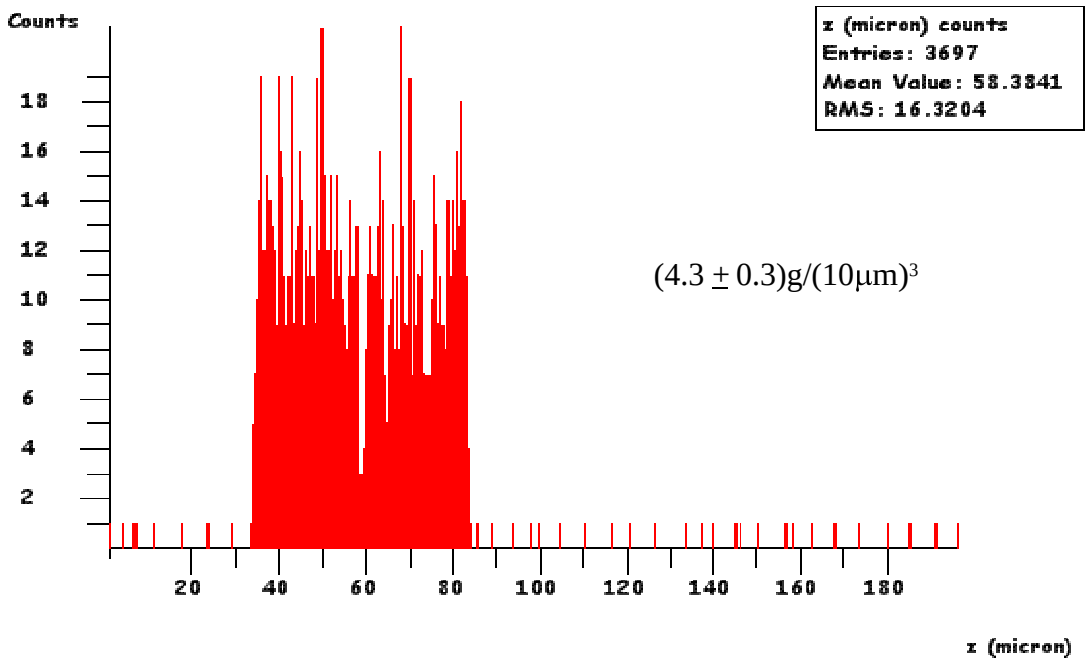

$(4.3 \pm 0.3)g/(10\mu m)^3$

Fig. 5.20 - In both cases there is a slight sensitivity improvement on upper layers.

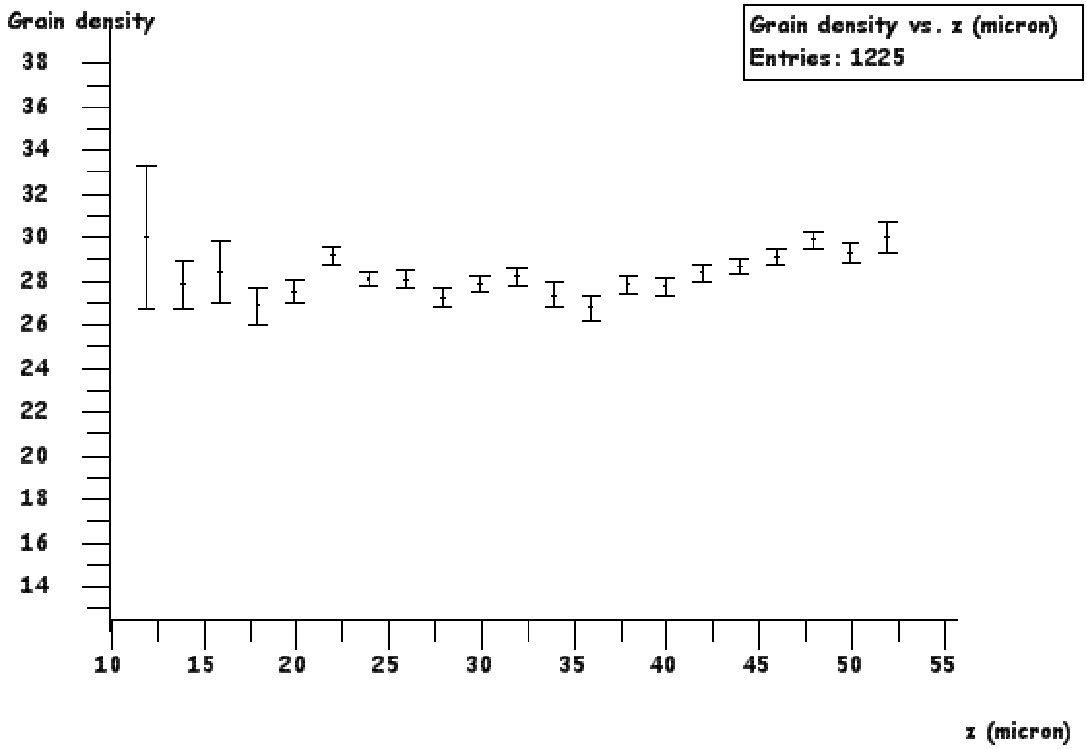

No presoak + 35 min Fuji developer

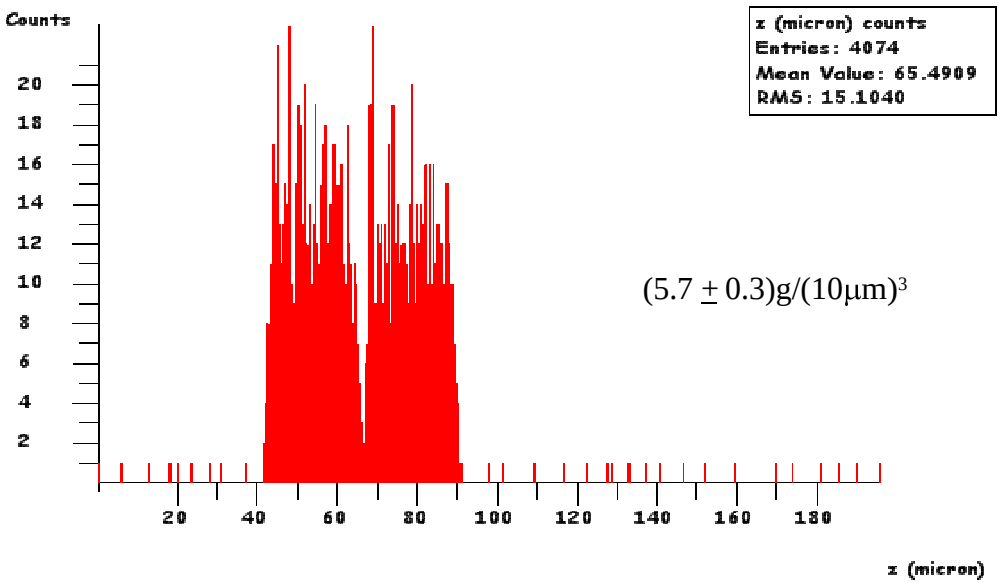

Fig. 5.21 - In both cases there is a slight sensitivity improvement on the whole depth but there is also a significant FD increase due to the longer development time.

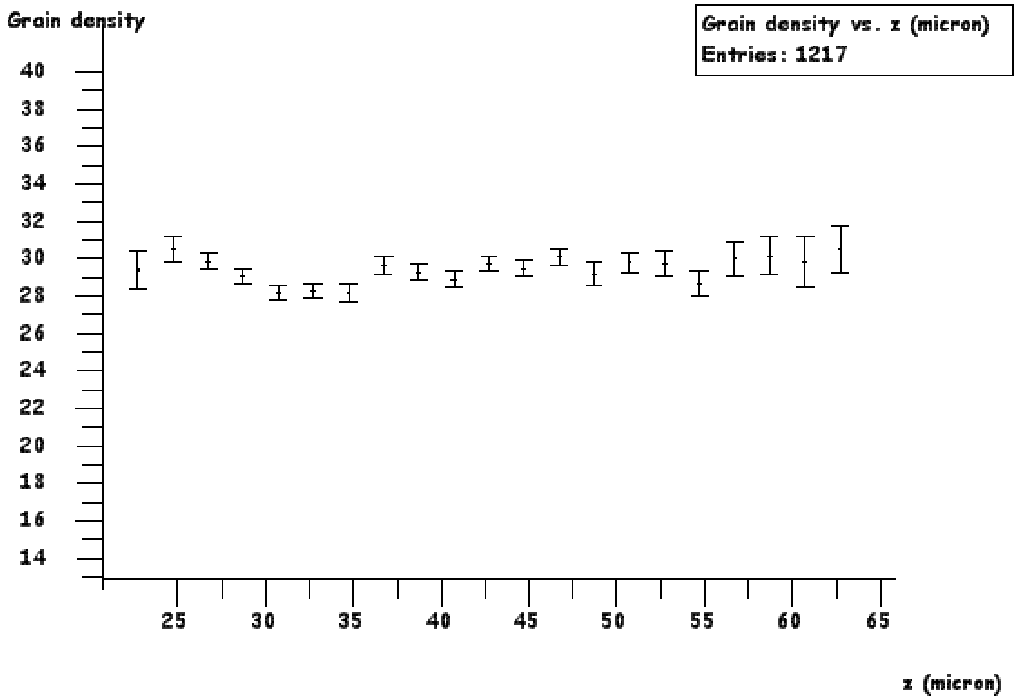

Presoak test at CERN (August 2005)

In order to check large scale development on refreshed emulsion sample I shipped to CERN form Japan some refreshed emulsions already exposed to UVSOR electron beam. I developed them at CERN in different conditions and then I measured them in Salerno. Results are shown in the following plots and showed that the behaviour of refreshed films is not so different from the one observed for not refreshed films. In all the cases the GD was lower than usual because of fading occurred during emulsion transportation from Japan to CERN.

<u>Reference (presoak + 25 min Fuji developer)</u>

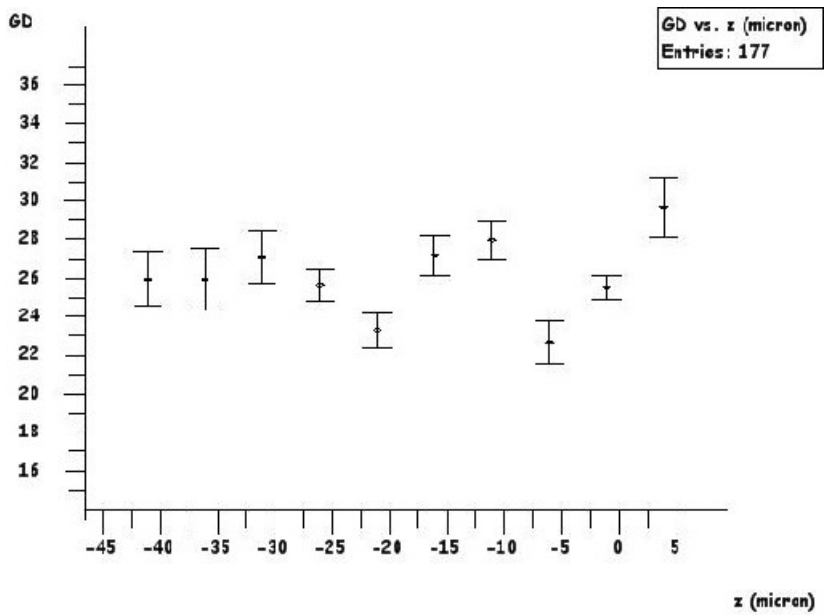

Fig. 5.22 - In both cases there is no GD lowering on the surface.

No presoak + 25 min Fuji developer

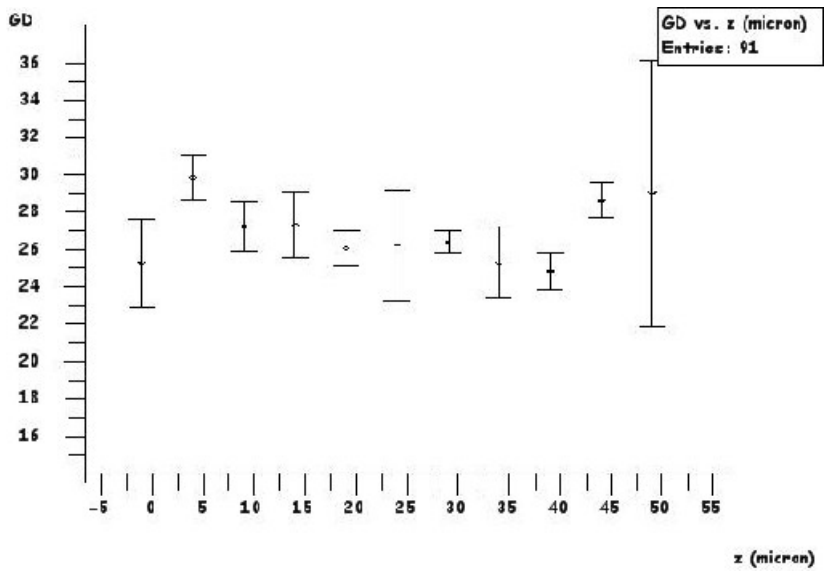

water + 25 min Fuji developer

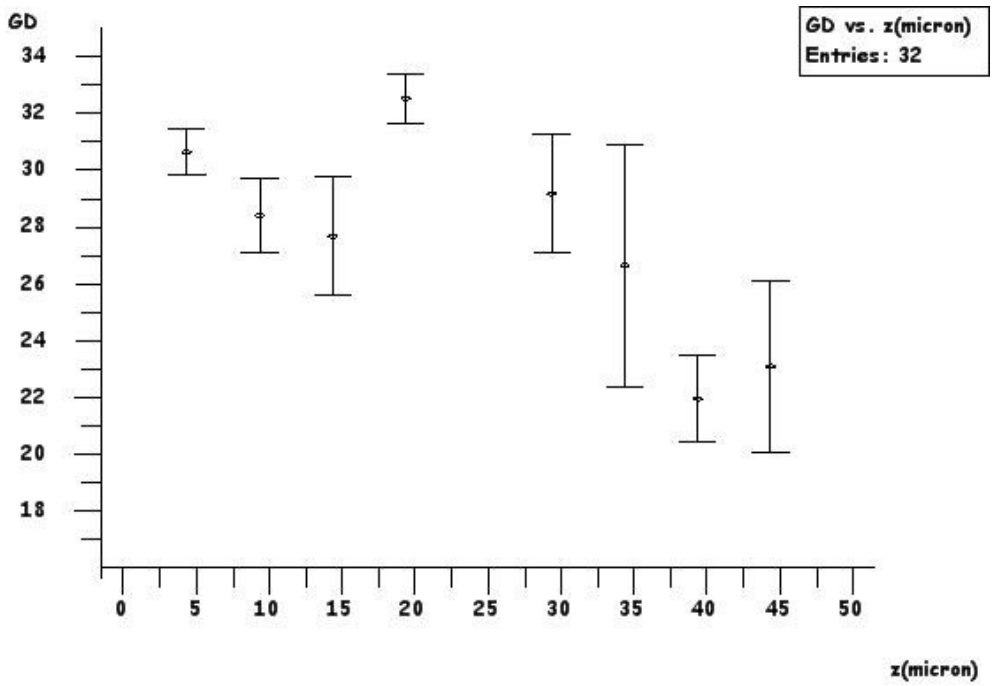

Fig. 5.23 - In this case there is GD lowering on the surface but the statistic is too low to get strong conclusions.

Fixing test at CERN (August 2005)

During the last two years we experienced a serious problem on developed emulsion: some months after processing they started to change color and they turned to yellow, this implied some scanning troubles because the image quality under the microscope became worse in terms of contrast. I discussed this problems with Fuji experts and they suggested to use Fuji fixer instead of the usual sodium thiosulphate solution; Fuji fixer main recipient is ammonium thiosulphate that is very fast to produce silver complexes and remove them from gelatin. The yellow color is caused by residuals of silver that can be reduced by light and alter the gelatin transparency, so a faster and more efficient fixation will solve the problem. Fuji fixer should be diluted in water and it was needed to optimize the dilution for Opera films, then I realized some tests at CERN on refreshed films already exposed to UVSOR electron beam.

Each emulsion has been cut in 6 pieces and there have been prepared 6 different fixers (increasing the Fuji product dilution, from 20% to 60%) in order to develop all samples at the same time and fix them at the same time but in different conditions (Fig. 5.25).

The reference samples have been fixed in a 18 l tank in order to get better conditions and keep the solution always fresh. All the films have been washed for 2 hours in 18 l of circulating water; in this case all yellowing problems due to washing would be avoided.

Fig. 5.25 – Experimental set-up for fixer test, each sample has been fixed in a small amount of solution in order to accelerate solution ageing.

In Fig. 5.26 is shown a picture of all developed samples one day after processing; on X axis are put different fixer dilution and on Y axis there is the equivalent amount of film fixed with one liter; in Fig . 5.27 the same picture has been taken two months later.

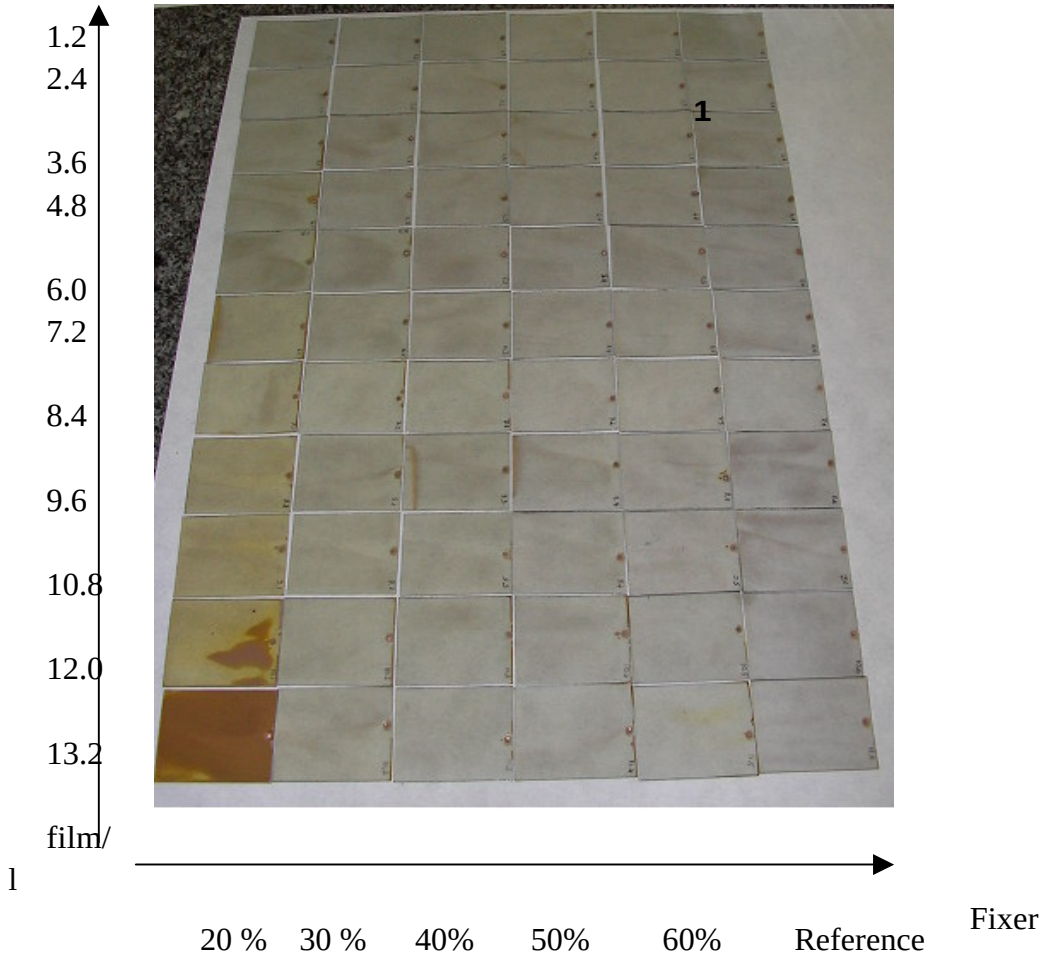
1.2
2.4
3.6
4.8
6.0
7.2
8.4
9.6
10.8
12.0
13.2
film/
l
1
20 %
30 %
40%
50%
60%
Reference
Fixer

Fig. 5.26

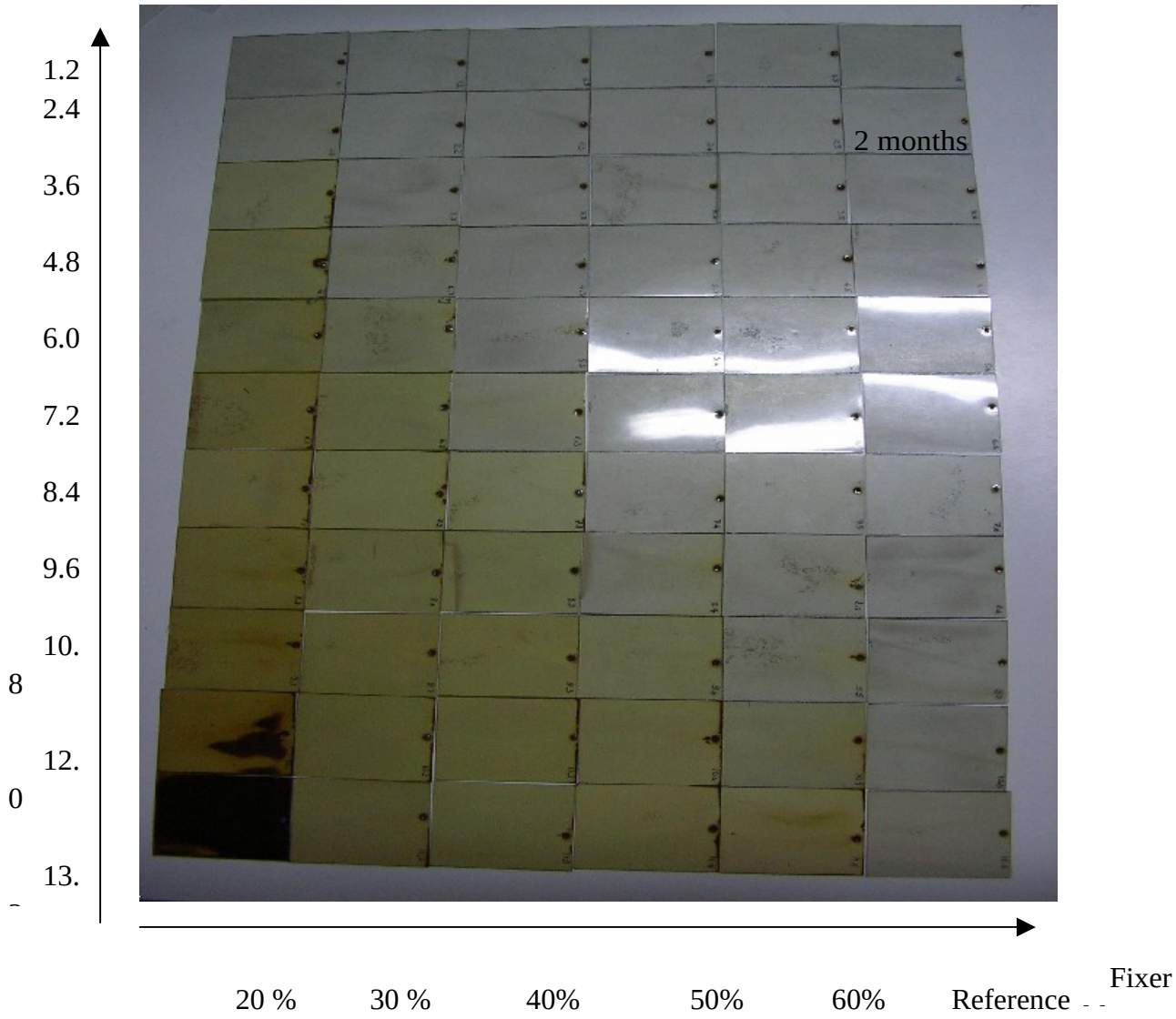

Fig. 5.27

In both pictures it is possible to see a deep saturation in case of 20% dilution, the expected refresh rate for fixer in OPERA will be 5 bricks that is equivalent to 7 films/liter so the suitable dilution should be the one that shows no yellowing after that point. In our case the best dilutions are 50% and 60%.

I measured FD for all those plates and it was (5.7 $\pm$ 0.6) g/(10mm)^3 ; in October 2005 it has been performed BAM test large-scale processing by Fuji fixer and there were no scanning or transparency problems using 50% dilution. In conclusion the standard Fuji fixer, 50% - 60% diluted, will be used for OPERA films; in this option the fixation bath preparation will be simplified and also the related chemical plant will be simpler to design and built up.

Nowadays the specifications for LNGS emulsion laboratory will be the following (Table 5.3):

- 30 l tanks for presoak, develop and stop, that can be used for 10 bricks (20 film/l)
- 45 l tanks for fix, that can be used for 5 bricks (7 films/l)
- 45 l tanks for washing
- 30 l tanks for thickener (glycerin + driwell), that can be used for 10 bricks (20 film/l)
- 10 bricks per developing chain

Solution	Time	Composition	Volume (1 l)
Presoak	10’	Sodium Sulphate Demineralized water	70 g → 1000 ml
Development	25’	Demineralized water Fuji developer Fuji starter	750 ml 250 ml 20 ml
Stop	10’	Acetic Acid Demineralized water	5 ml → 1000 ml
Fixation	35’	Fuji fixer Water	500 ml 500 ml
Wash (4 steps)	4 x 20’	Water	
Glycerine + Driwell	20’	Glycerine (86 %) Fuji driwell Water	235 ml 5 ml 760 ml

Table 5.3 – OPERA films final processing procedure.

The use of fresh water for each process will require a huge water amount, about 12 m^3/day (60 m^3/week); partial recycling of water of last steps into earlier steps could allow a factor 2 reduction and so this solution will be adopted in OPERA; this option will solve the problem of dirty water disposal also. Concerning the thickener bath we have been forced by safety regulations to get rid of alcohol because its high flammability at room temperature; tests

performed showed that no problems will arise and also that it is possible to avoid the last driwell short immersion; it will be enough to mix up driwell in the water+glycerin bath.

For what concerns the presoak it has not yet been decided to skip it because some more large scale test processing are needed to evaluate scanning performances and films long term stability; final decision will be taken in the next few months. Furthermore, it is currently under testing the option of applying a water immersion between stop and fix to preserve the fixer solution and avoid its faster ageing.

The 9 processing steps described in Table 5.3 were applied in several experimental tests by setting up consecutive tanks forming a processing chain. Stainless steel film holders were designed, such that groups of 60 emulsion films could be easily arranged and displaced from one tank to the next. A few processing sequences were performed in a single day along a chain, by introducing a suitable delay (at least 35', the fixation time being the longer step) between two subsequent developments. A conceptual schedule for a full working day is described in Fig. 5.28. To scale-up from test developments to the run-time OPERA case, several chains must be activated in parallel and also a high level of automation is demanded [24]. The coordination and exploitation of several related tasks (such as brick handling and de-packing, film handling before and after processing, handling of chemicals etc.) demands well-conceived logistics, dedicated tooling and trained manpower.

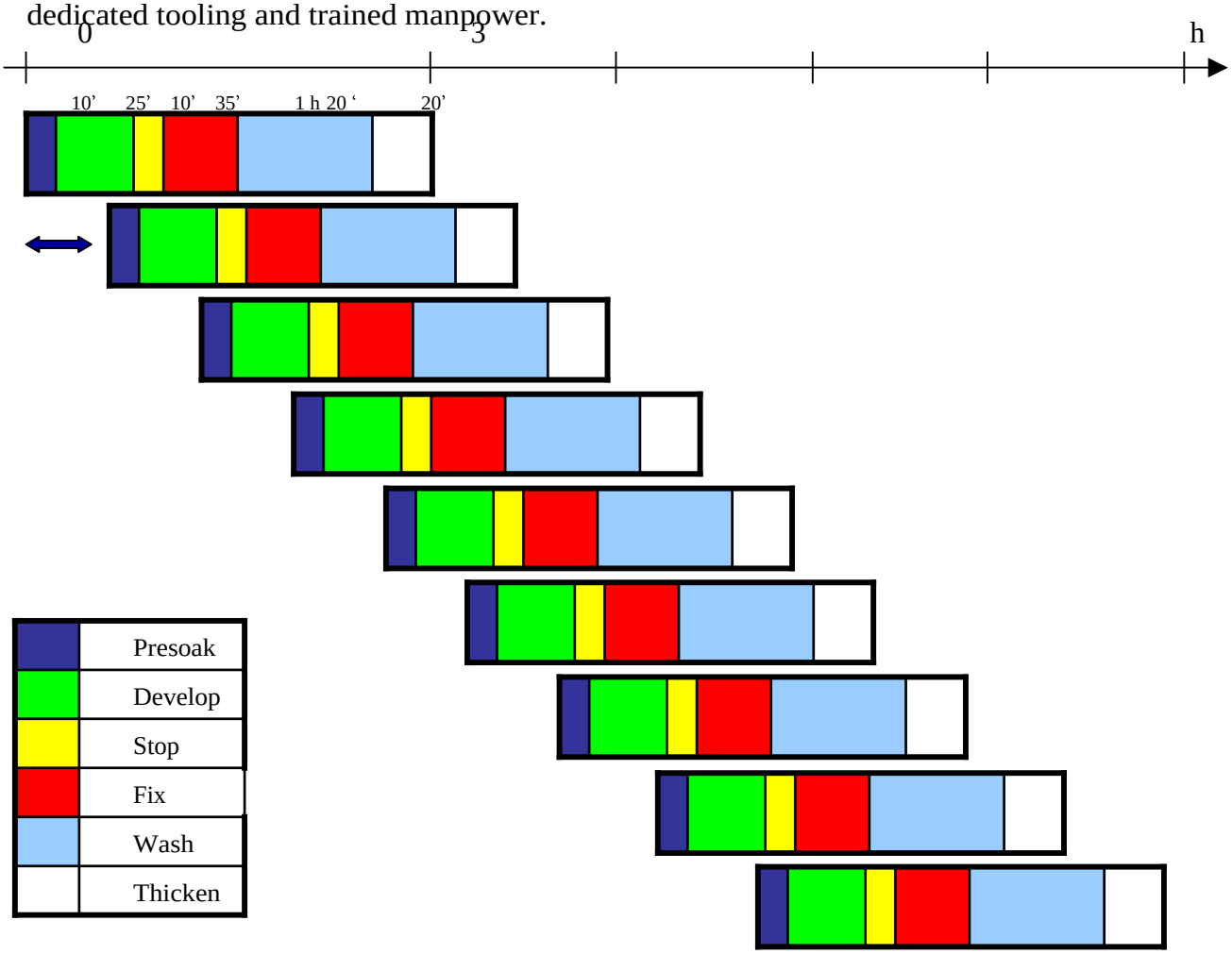

Fig . 5.28 – Conceptual development schedule within one chain and one working day.

The project for an automated development needs control and overall scheduling of subsequent tasks such as: on-time displacement of emulsion film holders from one tank to the next, exhaustion of wasted chemicals, insertion of fresh ones when needed, process monitoring and related feed-back actions. A full scale prototype chain was designed by Roma Group, it was inspired by a similar approach by our colleagues of Nagoya University and by the direct experience of test activity with manually operated development tools. The specific choice of mechanics for automation and related hardware was addressed by experienced technicians of Rome University. Commercial up-to-date technology (UNILINE Roll-On technology) was adopted for the long belt-chains, and high-quality, fully modular elements were selected for the mechanical structure. The arch structure, holding a jaw to pick-up and move the film holders, was designed custom (Fig. 5.29).

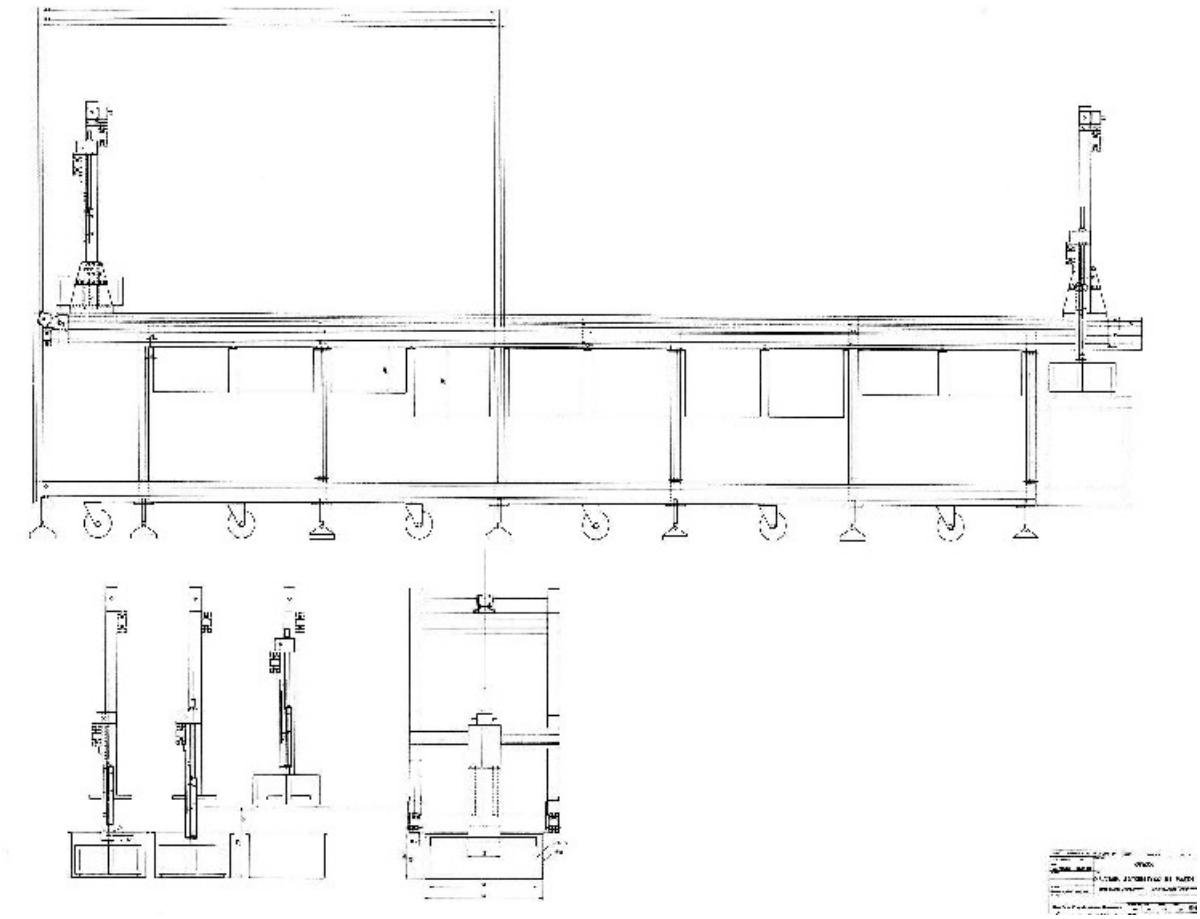

Fig. 5.29 – OPERA style automated develop chain.

The construction and assembly of the prototype has been allocated in a test hall available for OPERA at the LNGS external Laboratory. Custom made high-quality stainless-steel tanks and film holders (Fig. 5.30) were adopted, with fully chemical-proof soldering, and the last generations of similar tools have been successfully exploited in test experiments.

Fig. 5.30 – Last generation of film holders that can host 60 films at once in two independent modules.

The brick handling and development laboratory

A side-view of the OPERA building is shown in Fig. 5.31, it is shown the location of emulsion-handling infrastructures and the shielding structure of the Cosmic-Ray pit. The iron shielding thickness was fixed by on-site cosmic-ray experimental measurements with emulsion films and

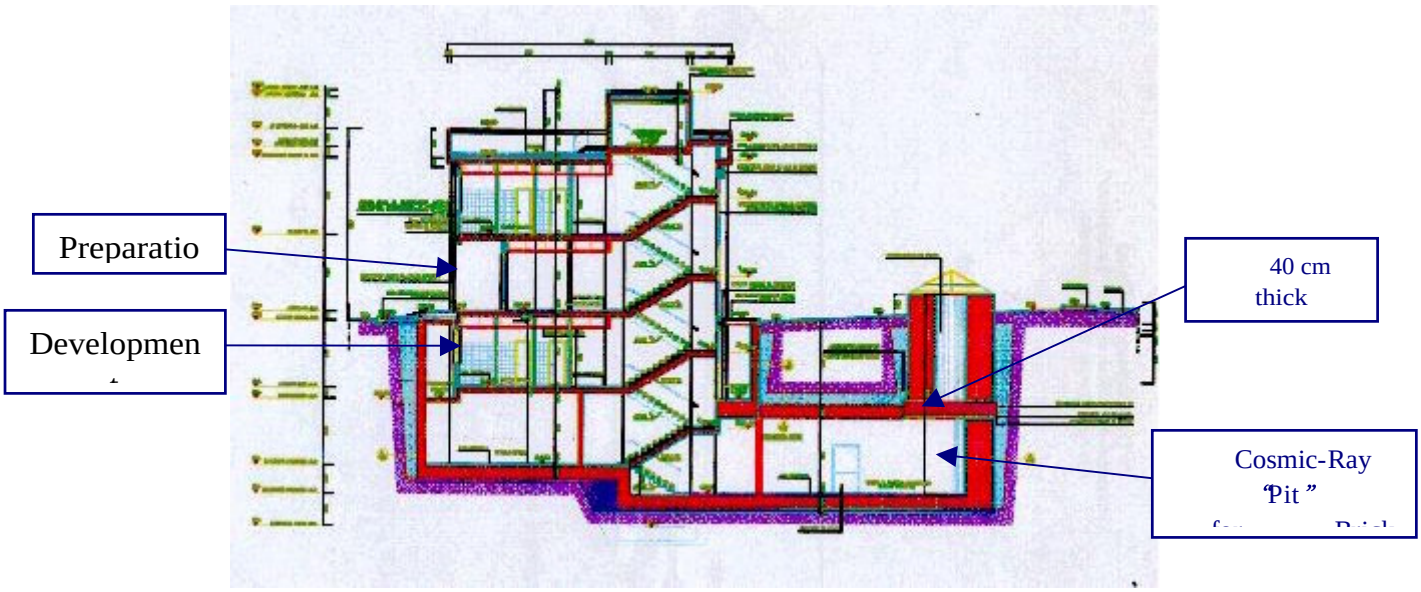

Fig. 5.31 - The building presently under construction.

scintillator counters. Brick unpacking, emulsion film development and handling of processed films will be hosted at the floor below ground that is in communication with the cosmic-ray exposure pit through a corridor and an elevator. In the upper floor, above the development lab, the chemicals will be stored and the chemical solutions will be prepared by an industrial-type plant. In the floor below ground will be settled the automated development plant described in the previous pages. A tentative lay-out of the lab, still under fine tuning, is shown in Fig 5.32.

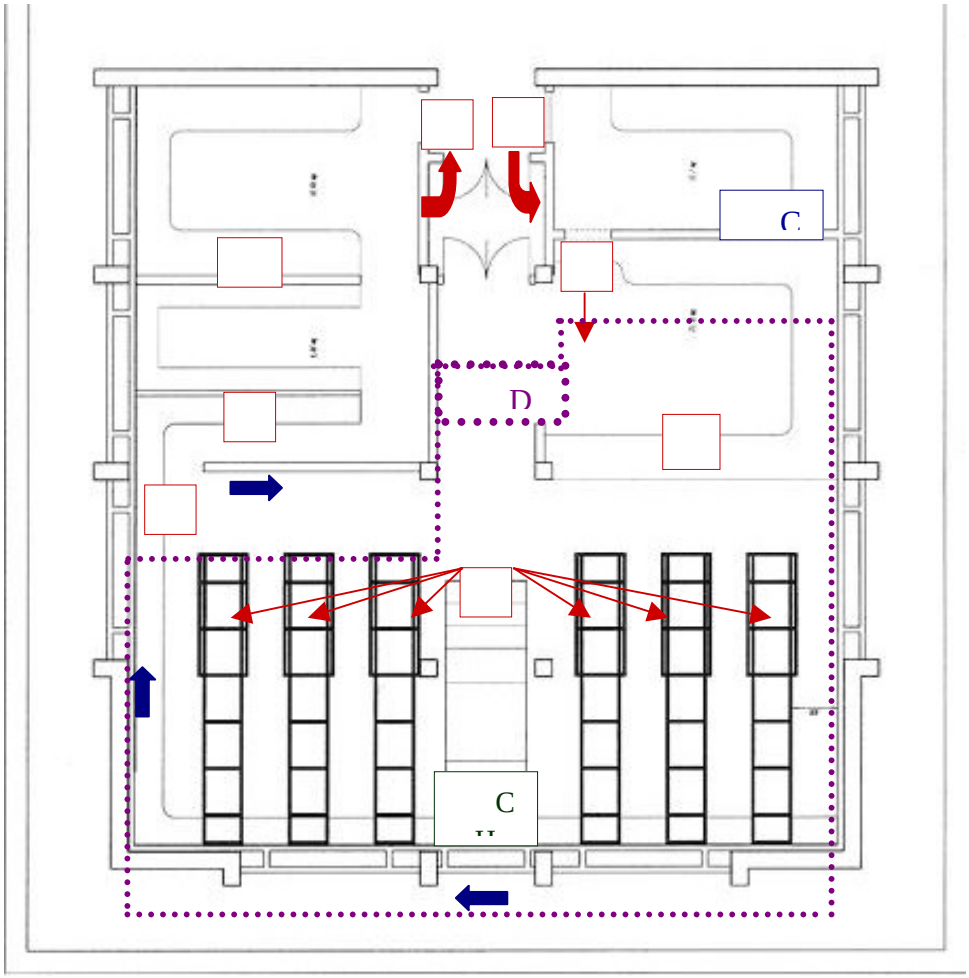

Fig. 5.32 – The area delimited by dots (DR) will be the darkroom, the labels show the brick flow, from cosmic ray pit extraction (1), de-packing and labeling (2-3), to development (4) and film drying (7).

OPERA bricks labeling and gridding

During OPERA data acquisition it will be required to de-pack and develop up to 65 bricks per day; this means that there will be handled around 3800 emulsion films per day. Obviously it will be needed ECC ID and Plate ID on each emulsion film. Furthermore emulsion scanning and measurements require a micron position resolution; this will be realized by means of plate to plate alignment procedures. That is why packed bricks will be exposed to cosmic rays before the development and it will be needed an intrinsic reference systems on each emulsion film.

In past hybrid emulsion experiments there have been used different procedures to realize an intrinsic reference system, ECC ID and Plate ID.

- Emulsion stacks' X- rays exposure
- Light exposure
- Both X-rays and light exposures

Salerno group holds the responsibility of this procedure from the design of the prototype till nowadays and I have been involved in the project from the very beginning. First of all it has been deserved to choose the emulsion marking procedure, each of those techniques could be used in Opera experiment, but positive and negative aspects should be considered. It was needed also to estimate which procedure would have been the less time-consuming and most affordable. From past experiences, as from WA75 experiment, it was clear that X-ray marking could have been time consuming and also difficult to be tested and implemented because of strict safety regulations, then light exposure has been chosen. Our proposal was to realize a reference grid on each emulsion plate by means of a flash and also a binary code for ECC and plate ID; light source could be a matrix of computer driven LEDs and light could be collimated to emulsion plates by optical fibers or optical devices. A similar solution was successfully used by EMU09 collaboration. In that case the triggered Run-Event number was impressed on emulsion tapes by means of a flash lamp and optical fibers enlighten in the right computed sequence (Fig. 5.33).

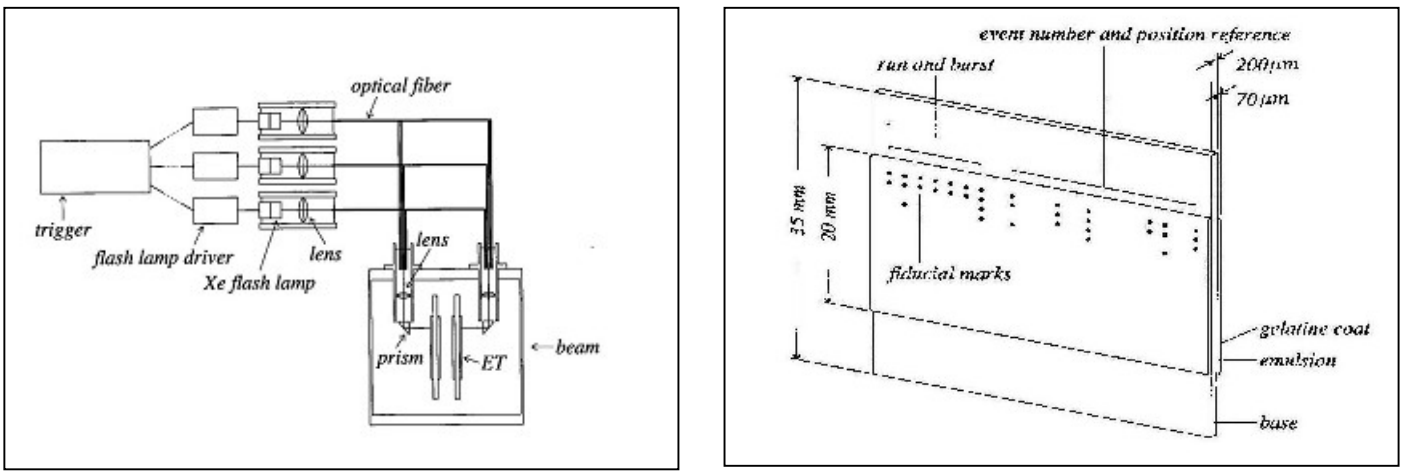

Fig. 5.33 – Experimental set-up used by EMU09 collaboration to print dark dots on emulsion tapes

Since OPERA detector will consist of more than 200000 bricks and 57 plates per brick, in case of binary coding convention there will be needed (18 + 6) digits and each digit will be represented by a dark spot. There will be also 4 dots at the corners on each plate as reference frame (Fig. 5.34). This procedure will be used also for CS films.

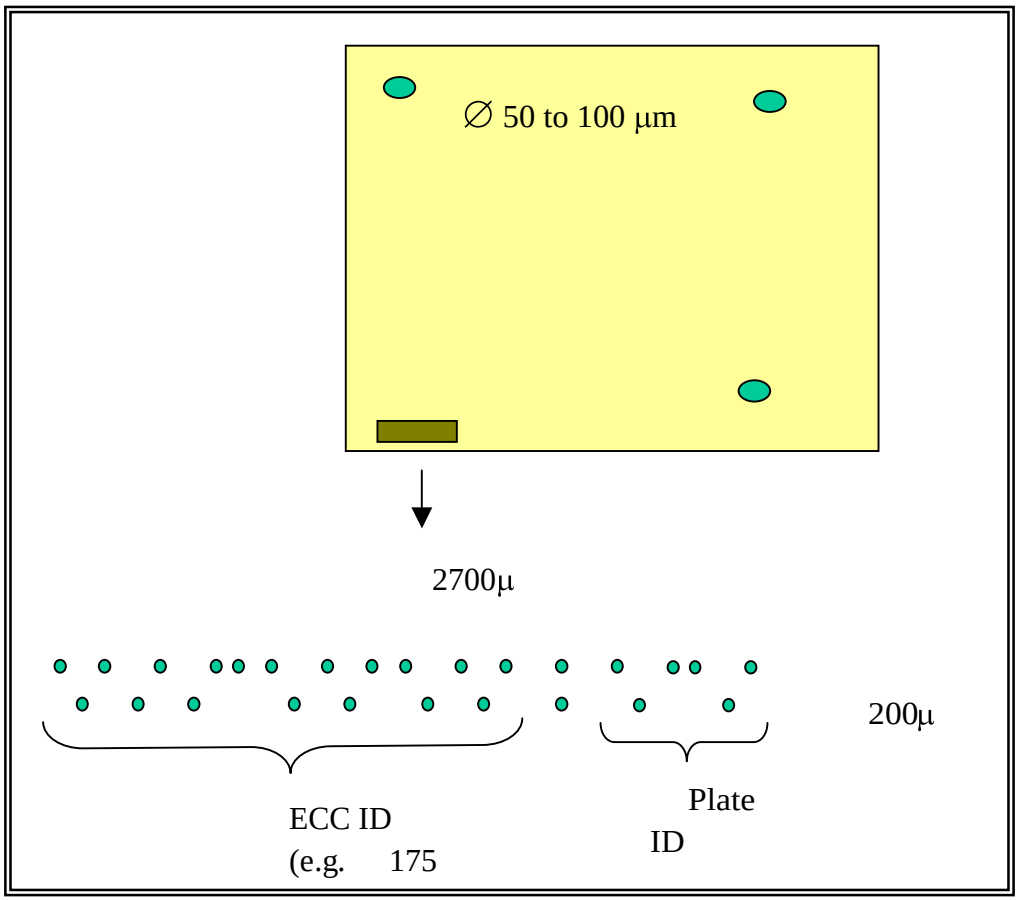

Fig. 5.34 – Proposed label and grid for each film.

An automatic procedure to label each Plate, connected to OPERA central DB would be useful to avoid mistakes; in addition each digit can be represented by a single spot in one of two cells, meaning respectively 0 or 1, then an additional parity check digit helps to increment reliability of the label. This kind of label can be read from automatic scanning software (SySal2000).

It is important to consider that each brick will be identified by a bar code and the OPERA central DB will register the history of each brick, then it will be needed an unique identifier for each brick and so will for each plate. A single identifier is better than the date of development or the position at the moment of extraction from the detector and a progressive binary coded number will be less invading (in terms of fiducial surface) on the emulsion than any other .

Emulsion films are usually affected by distortions, so it is important to have a reference system in order to move around the same plate and to realize plate-to-plate connection with

accurate position resolution. In Chorus experiment were used bigger emulsion plates having severe distortions; it was gained an accurate position calibration using an optical grid; then I made some measurements to investigate if we will need a grid also for Opera emulsions. I acquired 10 times a grid (34 dots) on the same plate; I mounted and unmounted the plate from the stage each time. Then I repeated this procedure on 10 different plates and tested position accuracy. Typical position distribution residuals are shown in Fig. 5.36 ($\sigma \approx 2$ μm). The neat result is that

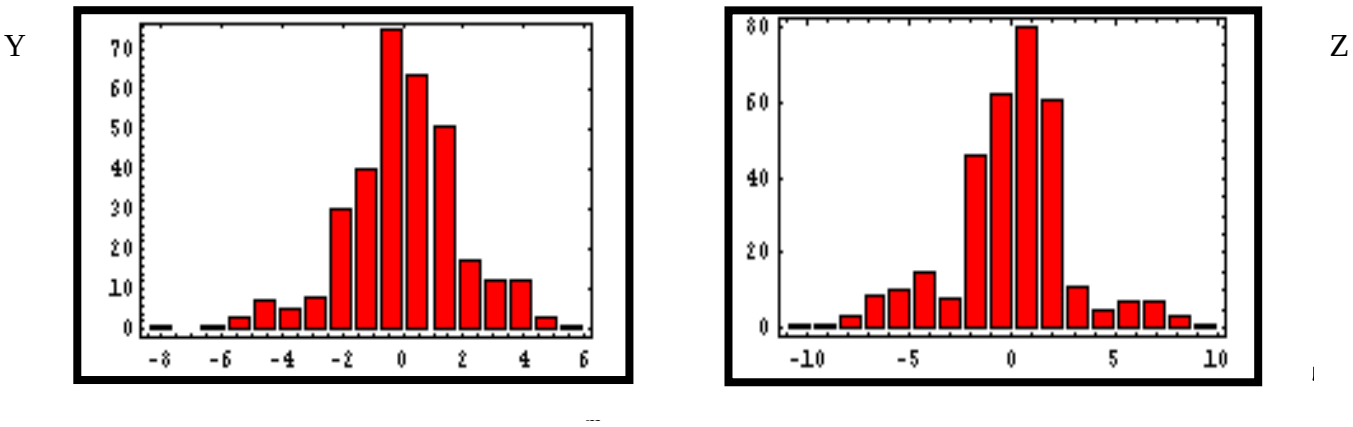

Fig. 5.36 – Affine transformation residuals after several repeated measurements.

a grid is not needed on the whole plate because distortion effects are not so dramatic. Anyway it will be still needed few intrinsic reference points on each plate to know roughly affine transformations parameters and to speed up plate intercalibration procedure. At least 3 dots are needed and they should be impressed some mms far away from emulsion edges to avoid critical points.

Optical fibers solution

The first idea was to use a strong light source impinging on a high resolution LCD, on the display there is a light mask changing at every exposure according to the code that must be transferred on the emulsion film. The light emerging from LCD surface is driven onto film surface by a second optical fiber having micrometric resolution (Fig. 5.37). This set-up has been designed using commercial pieces and profits of the high precision affordable by new generation optical fibers. In this option the image on LCD could be several square mm wide because a lens would have reduced the final spots dimensions on the emulsions; in this way it would have been possible to profit of a high luminosity light source over a big surface in order to reduce the exposure time and speed up the gridding procedure. To test this option we tried first to reproduce on the emulsion a single dot, distances between light source, LCD , lens and emulsion have been tuned to gain a 80 μm diameter spot. There have been tried several exposure times and it turned out that 1s would have been enough to obtain a sharp dot (Fig. 5.38). The dot showed the desired dimensions, even if the shape was not circular, infact there was clearly visible the pattern due to the high resolution conduit used to transfer the light form LCD screen to emulsion surface via a lens.

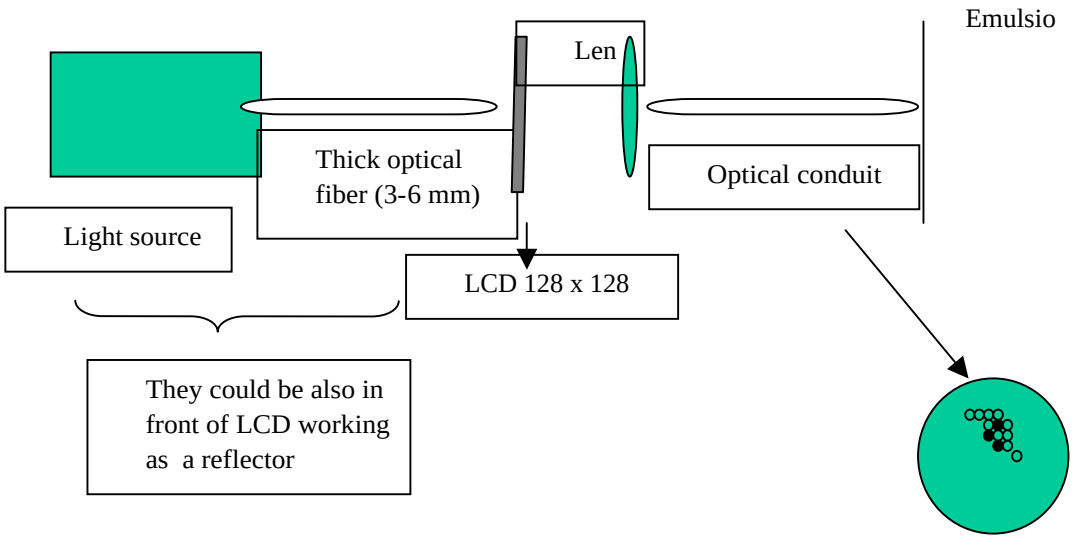

Fig. 5.37 – Optical fibers emulsion marking set-up.

We tried to use this technique to reproduce on emulsion some graphical patterns sent to LCD via serial interface by a host PC but results were not satisfactory; the main problem was that the LCD screen has a own illumination low contrast and we have been forced to use reflected light because it cannot be enlighten from back.

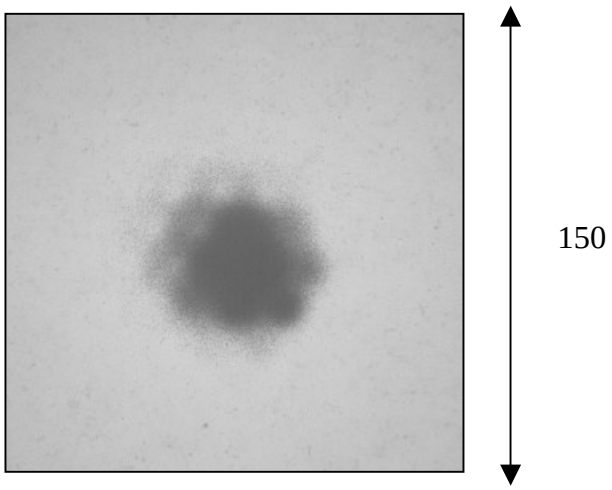

Fig. 5.38 – Spot obtained by optical fibers set-up, it is possible to see the pattern due to high resolution optical conduits.

High luminosity LED matrix solution

The basic idea of the second and final approach was to *"... Take a LEDs picture on the emulsion..."*. Originally, the prototype was an optical device with computer driven LED matrix on the bottom part and a multi-focal objective on top one; the light emerging from the optical tube impinged on a glass surface that acted as emulsion support (Fig. 5.39). The optical device was realized by means of two tubes sliding one into the other and allowed to focus the image on the glass top surface and get different spots dimensions; we used a standard 50x magnification objective from a Canon camera.

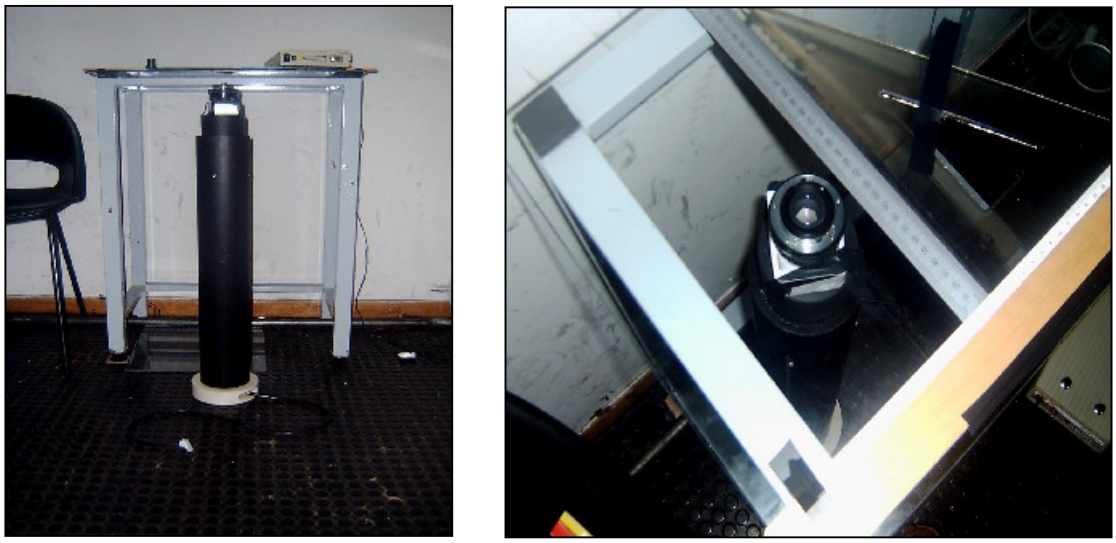

Fig. 5.39 - Optical set-up for emulsion exposure in Salerno dark-room and glass surface.

That prototype LED matrix was assembled by hand and composed by 24 LEDs arranged in four rows; in this option it has been possible to have Brick and Sheet number ranging form 1 to 64. All the LEDs had a 3 mm diameter and an ultrahigh luminosity in the green frequency range; LEDs have been previously tested by custom set-up and they can produce a dark spot on OPERA type emulsions after an exposure lasting less than 1s. This feature was essential because will allow short exposure times and guarantee the gridding and labeling of an entire brick in less than 20 minutes. In addition, near the LED matrix there was a single 4 mm diameter high luminosity LED that will be used to realize one reference grid spot. The light module was controlled by a PC via a custom electronic circuit designed and assembled in Salerno laboratory. The circuit main components were: IC (M5450) acting as LED display driver, IC (NE555) acting as time controller and an array of 100kW resistors and trimmers that have been used to fine tune each LED brightness. The data transfer from host PC to the display driver was accomplished with serial data and clock signals and one IC could control up to 33 output-input channels independently. It has been realized a dedicated software for the data flow and a user interface to set Brick number and Sheet number independently an to perform some simple test

routines. It turned out that working with a separate 5V power supply, a 1 s exposure was enough to have round dark dots (75 μm diameter). In order to measure LEDs brightness one by one it has been a used a photo-resistor and the proper resistivity value for each LED have been fixed by trimmers.

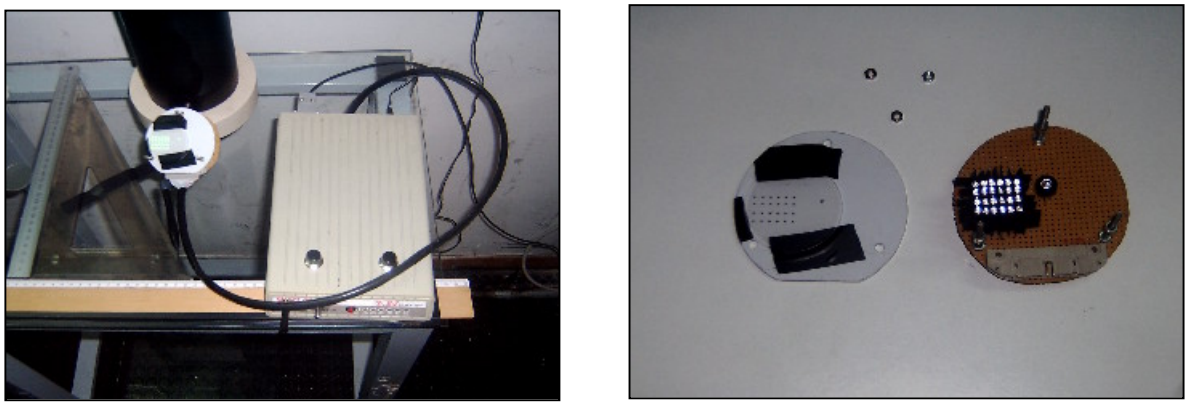

Fig. 5.40 – Light module connected to the electronic circuit and the host PC via parallel cable. Light module components; on the light source there was a diffuser glass and each LED was isolated by black carton paper in order to avoid reflected and refracted light inside the matrix.

After a test exposure having different focus configurations and exposure times we found two suitable conditions (0.5 s and 3.3 s) that gave 75 μm and 150 μm (Fig. 5.41) spots diameters.

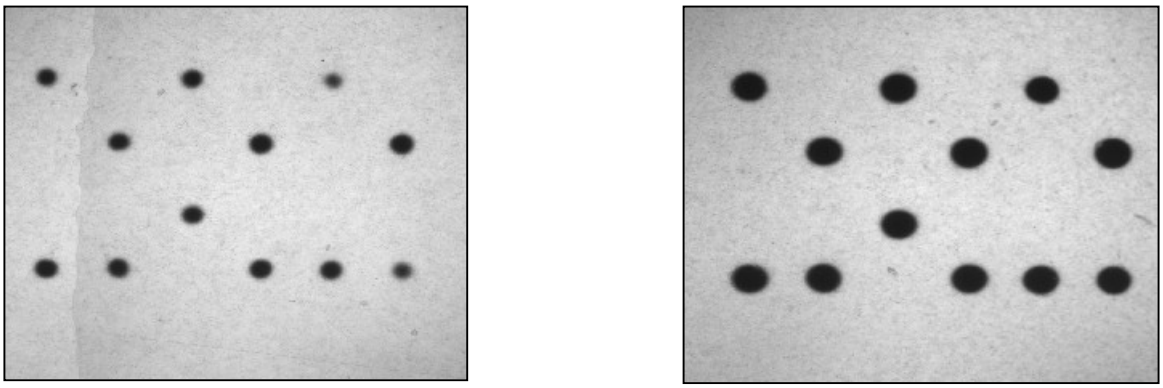

0.5 3.3

Fig. 5.41 - Label on emulsion after different exposure time, the image is really sharp and well focused.

Results gained using this first hand-made prototype were really good and so we started the design and the construction of a complete gridding and labeling device based on computer driven LED matrix approach.

Working prototype

Using the old prototype it was possible to put a label (Sheet Number + ECC ID) on each emulsion film, with the final one it is possible to realize also a four dots reference grid. There are four independent optical systems made of two cylinders screwed one into the other and tunable in order to focus the image on the upper glass surface (Fig. 5.42); on top of each there is an objective and at the bottom part there are the light sources. There is one LED at each corner for the reference grid and also the 24 LEDs matrix for the label in one corner. System mechanical stability is provided by a custom structure made of two aluminum planes; the overall dimensions are 20 cm × 15 cm × 30 cm.

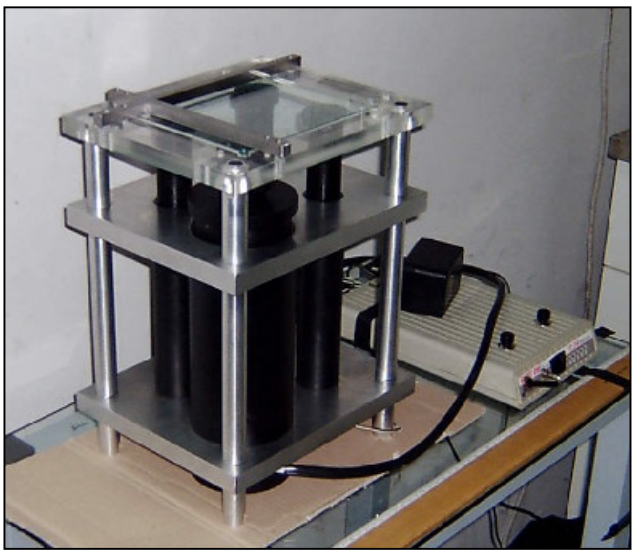

Fig. 5.42 – Picture of the gridding and labeling machine at work.

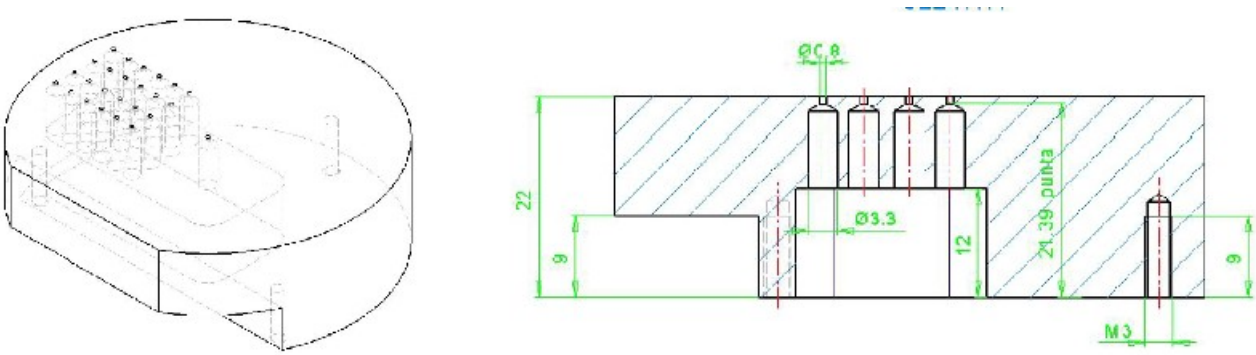

Fig. 5.43 – PVC mask front and side view.

The LED matrix is remotely controlled by the host PC and the custom circuit already described, the user interface has been optimized and it is possible to label one brick setting just the ECC ID; once started, the Sheet Number is automatically incremented after each flash and a LED

display shows the Plate ID to the operator working in the dark-room. In this prototype the exposure time can be settled independently for each LED by PC via the software user interface and there is no need to tune the brightness manually by trimmers for each LED. This apparatus has been built by high precision machines and special care has been devoted in the LED matrix assembly; on top of the lamps there is a PVC black mask (Fig. 5.43) having cylindrical cavities that ensure LED position and direction. The design of this mask was crucial because the light has an intensity that changes a lot according to the emission angle; in order to have uniform LED behaviour it is crucial to have stable and straight positions.

In this prototype there are fixed focus objective 8x magnification for grid spots and a multi-focal lens (2x ÷ 20x) for the label; this choice permitted us to have tuneable spot dimensions according to scanning convenience. The tuning procedure permitted to fix focus for each optical tube and the exposure time for each spot. Results are shown in Fig. 5.44, they were obtained using five different focal configurations and seven increasing exposure times; requesting a constant diameter for all the spots it is possible to fix the exposure time for each LED independently and store them in the software configuration.

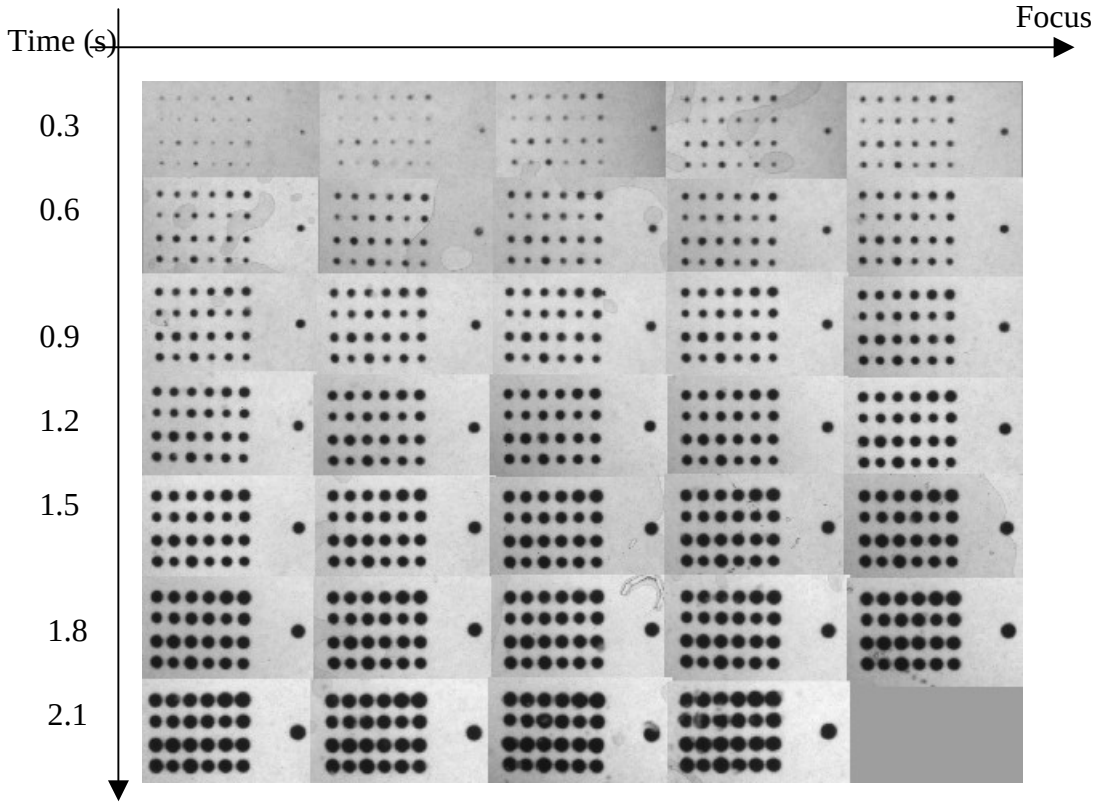

Fig. 5.44 – Exposure time and focusing tuning procedure results.

The solution much more suitable for scanning purposes seemed to be the one having 60μm diamater for label points and 80 μm diamater for fiducials; corresponding to a mean exposure time, among all the LEDs, of 0.5 s (Fig. 5.45).

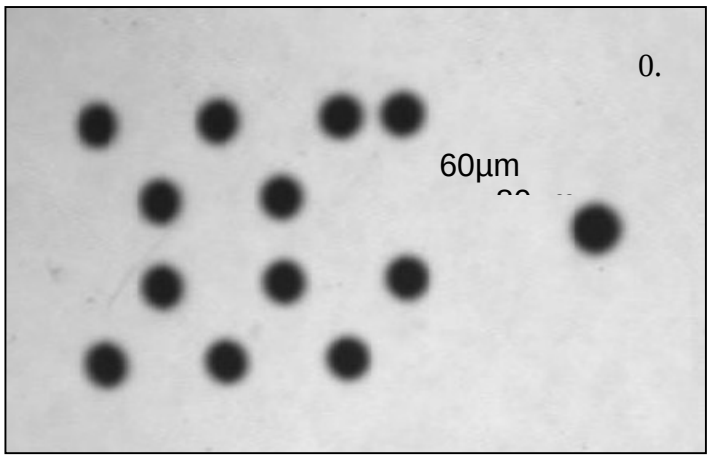

Fig. 5.45 – Full label and fiducial dot, best configuration.

In order to test the accuracy of the reference corner situated on the upper glass one emulsion film has been exposed two times consecutively, as it is possible to see in Figure 5.46 the achieved accuracy is better than 100 µm. I scanned 8 consecutive plates (1cm^2 on each) marked by the old style grid (Chorus) and by the new one. After the alignment I compared the affine transformation parameters found (Table 5.4) and it turned out that the reference grid precision was well inside scanning specifications.

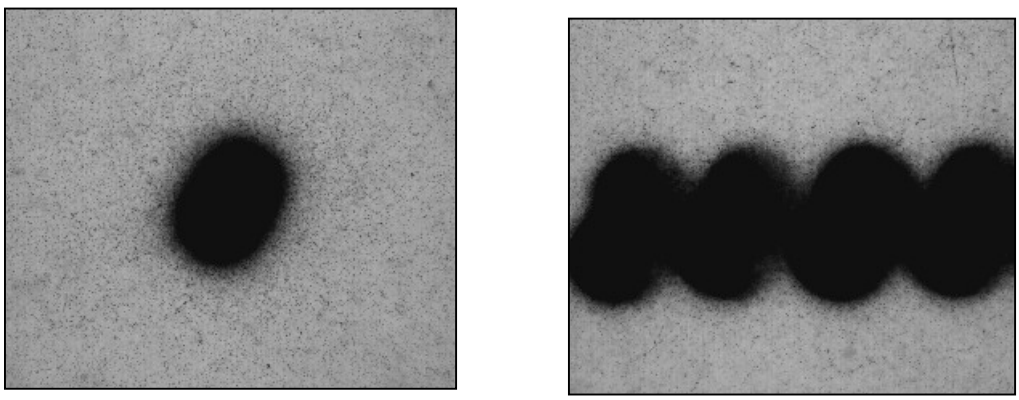

Fig. 5.46 – Pictures of the same emulsion view gridded two times consecutively.

This prototype has been used at CERN test-beam to grid and label more than 20 bricks, those bricks have been scanned among Europe in different labs and no problems were reported.

After several discussions among European colleagues this prototype has been positively validated and the collaboration decided to adopt this technique for OPERA experiment run.

	Dx old style (μm)	Dy old style (μm)	Dx new style (μm)	Dy new style (μm)
1	125	350	16	86
2	-300	230	57	45
3	540	67	34	-75
4	880	-37	-23	54
5	-245	88	34	-11
6	56	663	-6	76
7	103	330	80	88

Table 5.4 – Grid reproducibility computed by emulsion tracks alignment.

A new apparatus that will be used for OPERA is presently under development and construction; several new features will be applied according to discussions and feed-back acquired among people involved in Emulsion Scanning around Europe. It turned out that it will be better to minimize as much as possible the spot diameter in order to reduce dead areas on the emulsion surface. Now the spot diameter has been reduced up to 30 μm in order to put the whole code in one microscope field of view, the 18 digits needed for ECC ID will be splitted in four lines having 9 digits each; for safety reasons there will be a double label. The new machine will use 6x magnification fixed focus lenses mounted on commercial lens holders and spacers (Edmund Optics Technologies Industry), this solution will profit of high precision technology developed by optical companies (Fig. 5.47). It has been asked also to increment the number of fiducial spots in the reference grid and circle them in order to increase their naked-eye visibility. For this purpose the new machine will have 9 optical tubes (6 for fiducials, 2 for the labels and one more for a human readable code) a customized mask permitting to have circled points.

Fig.5.47 – Commercial spacers ad lens holders, on the left there is also the light module for reference circled dots with the custom mask.

During OPERA each scanning laboratory will handle more than 100 films per day and it has been requested to have a decimal plate number that could be read by eye. Commercial LED displays do not have enough luminosity to allow short exposures for human readable code so a

custom seven digit decimal display will be built using the ultra bright LEDs. Several trials have been done in Salerno and results are really good (Fig. 5.48 and 5.49). In this scenario the machine will host more than one hundred LEDs and they will be driven by a host PC connected via fast serial interface to a custom multi-channel I/O board. This board is presently under construction as well as the new mechanical structure that will host optical devices, emulsion glass support and on board electronics.

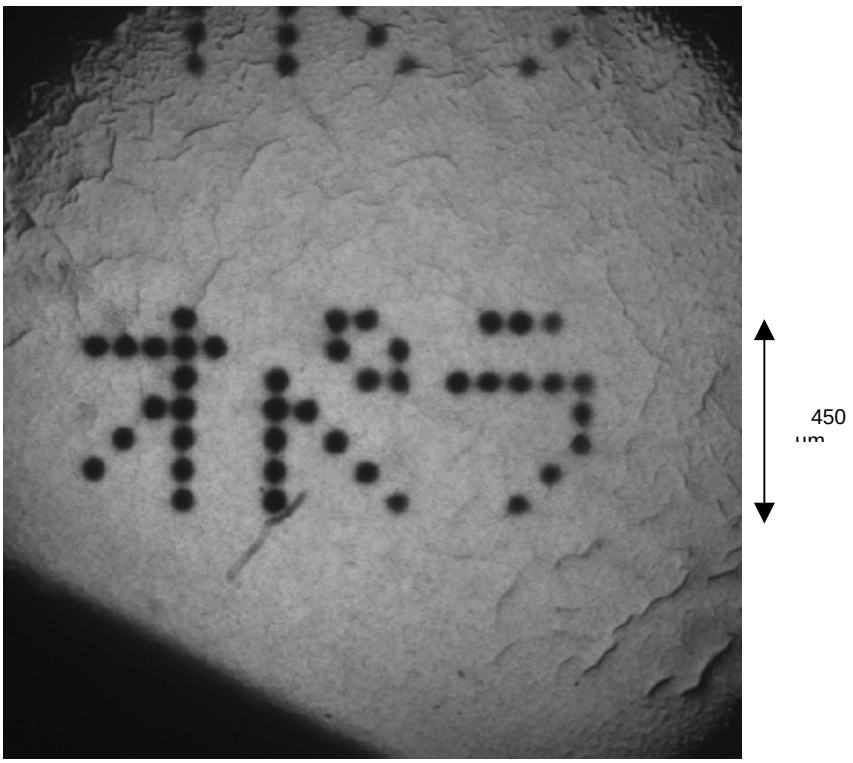

Fig. 5.48 – In this picture it is possible to see the word OPERA written in Japanese katakana realized on emulsion film by computer driven LED display custom matrix.

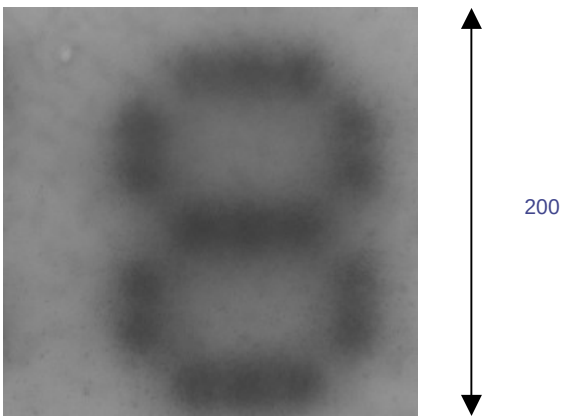

Fig. 5.49 – Decimal code marked on the emulsion by a seven digits LED display.

Emulsion scanning and event reconstruction

The technique of nuclear emulsion found a large scale application in the target of CHORUS experiment (see Chapter 3) in which the automatic scanning of a huge sample of events has first been applied [41]. This technique can be further improved and leads to the much large scale of the OPERA target; in this case emulsions will be used as high precision trackers, unlike in CHORUS where they constituted the target mass. The success of OPERA will be linked to the impressive progress in the field of computer controlled microscope emulsion read out, track and event reconstruction. In order to cope with the expected neutrino interaction rate in OPERA and allow a quasi-online analysis of the events, the emulsion read out have to be more than ten times faster than the previous one; the limited number of signal events expected requires to the system high efficiency, purity and precision. A long and complex R&D phase has been accomplished among European Scanning laboratories to full-fill OPERA requirements. The present European Scanning System has been developed on the basic idea that inspired the SySal scanning software-based system developed by Salerno emulsion group (see Chapter 3).

European Scanning System

The system [48] consists of a microscope (Fig.6.1) equipped with a computer-controlled motorized stage, a dedicated optical system and a CMOS camera mounted on top of the optical tube. Several images of the emulsion are grabbed at equally spaced depth levels for each field of view and processed by a vision processor board. The mechanical stage – MICOS - is equipped with nano-step motors - VEXTA 5-phase - and optical encoders with a resolution of 0.1 μm. The motors are driven by a National Instruments controller and the positioning reproducibility is about 0.3 μm. The optical devices have been developed in collaboration with NIKON-Italia and have been designed to reproduce the performances of standard microscopes used to observe small biological specimens. The illumination system consists of a lamp and a condenser whose positions can be adjusted with micrometric precision. The objective is a 50x CFI Plan Achromatic oil immersion one (WD 0.4mm, NA 0.9). The system is infinity corrected and produces achromatic planar images through the whole thickness of the emulsion. The image is formed on a CMOS camera – Mikrotron MC1310 –, used at 376 fps, sensor resolution is 1280 x 1024 pixels and the resulting field of view is $390 \times 310\ \mu m^2$. Images are grabbed and processed using a Matrox Odyssey frame grabber/vision processor. The system runs under Microsoft Windows 2000/XP on a dual processor (3 GHz) computer.

The scanning procedure accomplishes several tasks in on-line and off-line mode; since the system has a DAQ speed of 20 cm^2/h/side tasks are decoupled and performed in an asynchronous way. The complete sequence of tasks accomplished in on-line mode is:

- Image grabbing
- Clustering
- Grains detection
- 3D tracking on each emulsion side, micro-tracks building

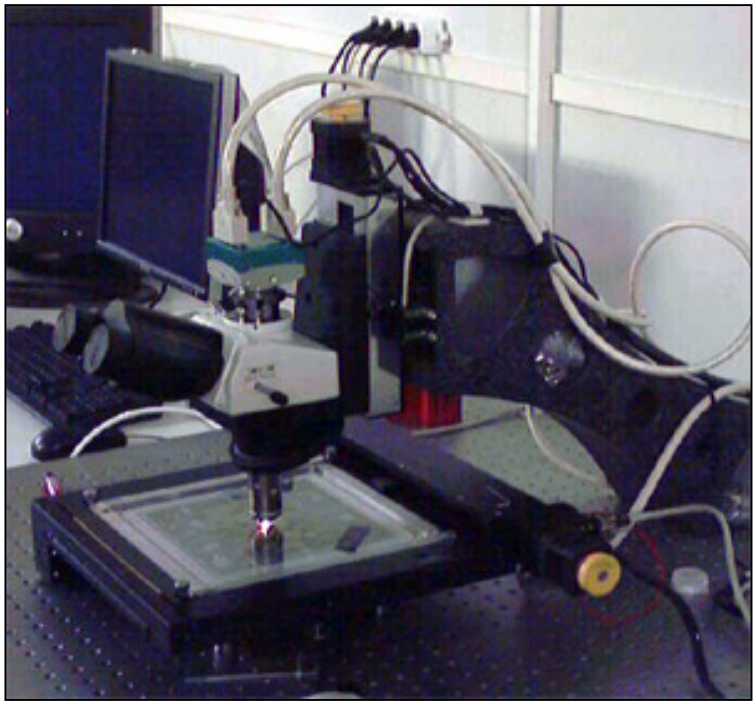

Fig. 6.1 – A picture of European Scanning System at work.

Thus the DAQ extract emulsion micro-track from raw images grabbed by the fast camera; considering the amount of raw data and to speed up the process there are four independent threads that are synchronized at the end of each cycle:

A. moves the optical system along the vertical axis during the grabbing; at the end of the image taking, it resets the Z-axis position and moves the X and Y axes to the next field of view.
B. acquires images via the frame grabber;
C. it is responsible for image processing; processed images are stored in a temporary memory buffer;
D. loads the processed images from the previous field of view and performs cluster and track recognition.

Presently, one cycle lasts 180 ms; after a detailed study of the timing of each operation and a careful design of the system the goal of a scanning speed of 20 cm^2/h/side has been achieved. The basic idea of the tracking algorithm is that a track is a straight sequence of grains lying in different levels. Since OPERA emulsion sensitivity is around 31 grains/100 μm, the number of expected grains constituting a vertical track follow a Poisson's law distribution with an average of about 13 grains; some trigger levels are defined (Fig. 6.2), if none of these levels has a grain along the predicted line, the track search along that line stops immediately. Micro-tracks with fewer than 6 grains (about 1%) are discarded.

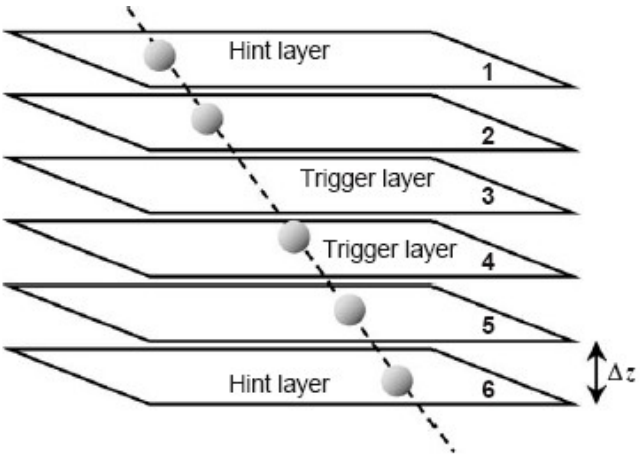

Fig. 6.2 – In this picture it is possible to see the track search algorithm.

At small angles measurement errors along X and Y directions are larger, at large slopes, the misalignment is mainly affected by the term due to the uncertainty in Z. Aligned grains are then selected according to transverse and longitudinal tolerances. The transverse alignment residuals can, therefore, be used as an estimation of the micro-track quality (Fig. 6.3). After micro-track selection, multiple reconstructions are filtered out: if a grain belongs to two or more micro-tracks, only the track with the highest number of grains is saved.

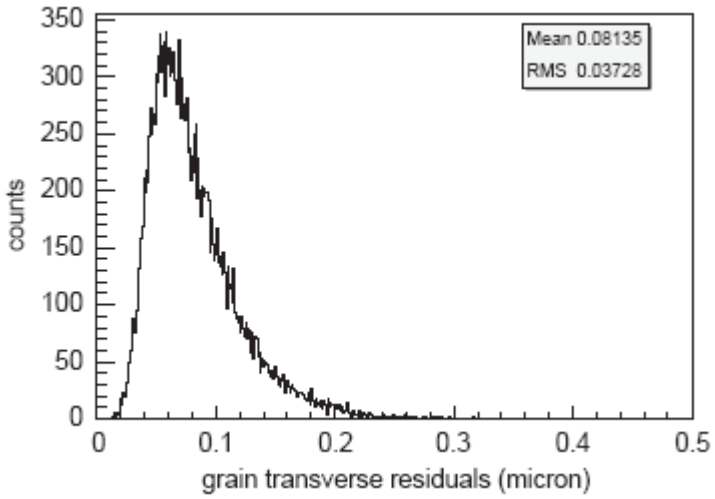

Fig. 6.3 – Grain transverse residuals with respect of the fitted micro-track trajectory.

After micro-track reconstruction the off-line task began; first of all micro-tracks belonging to top and bottom emulsion sides must be connected to build base-tracks (Fig 6.4). Each micro-track is extrapolated to the corresponding Z level of the plastic support and position and slope tolerances are applied to select correlated pairs.

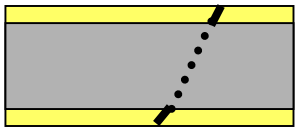

Fig. 6.4 – Base-track linking along plastic base.

By defining the quantity:

$$\sigma = \sqrt{\left(\frac{\Delta s_{t\perp}}{s_{\perp tol}}\right)^2 + \left(\frac{\Delta s_{t\|}}{s_{\|tol}}\right)^2} + \sqrt{\left(\frac{\Delta s_{b\perp}}{s_{\perp tol}}\right)^2 + \left(\frac{\Delta s_{bt\|}}{s_{\|tol}}\right)^2}$$

where $\Delta s_{t\perp} / \Delta s_{t\|}$ is the transverse/longitudinal slope difference between top/bottom micro-track and base-track and $s_{\perp tol}$ is the corresponding tolerance, it is possible to select good tracks having also an high number of grains; the usual quality cut used to discard the signal from instrumental or physical background tracks is, $\sigma < n \times 0.13 - 1.3$ where n is the number of grains. The resulting base-track finding efficiency is above 90% over the angular range (0; 700) mrad and the micro-track finding efficiency is above 95%. Correspondingly, the instrumental background, estimated by visually inspecting tracks of different angles found by the automatic system, is about 1 fake base-track/cm^2.

The off-line event reconstruction continues with plate to plate alignment that is performed by means of affine transformations taking into account emulsion relative translations, rotation and shears. Long tracks reconstructed along an emulsion volume are called volume tracks and can

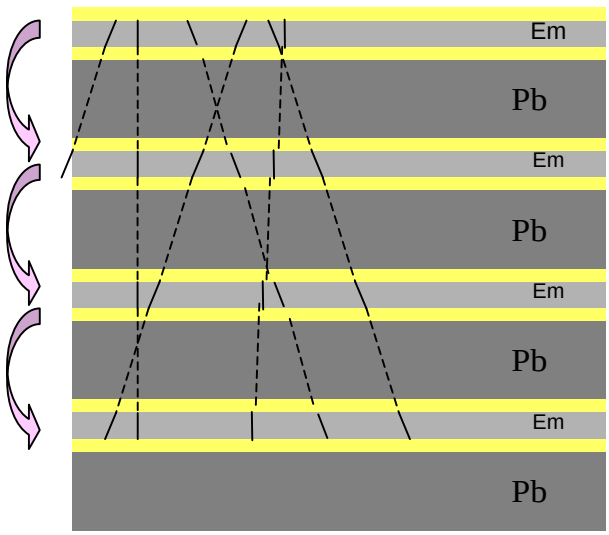

Fig. 6.5 – Alignment iterative procedure.

be used to locate interaction vertices and primary particles decays. The alignment procedure is accomplished by iterative mapping of two different plates, affine transformation parameters are computed in order to maximize the number of matching base-tracks within tight position and angular thresholds (Fig. 6.5). Alignment precisions achieved by this technique are well inside few microns threshold and are enough to permit momentum measurement by Multiple Coulomb Scattering and event location and reconstruction (Fig. 6.6).

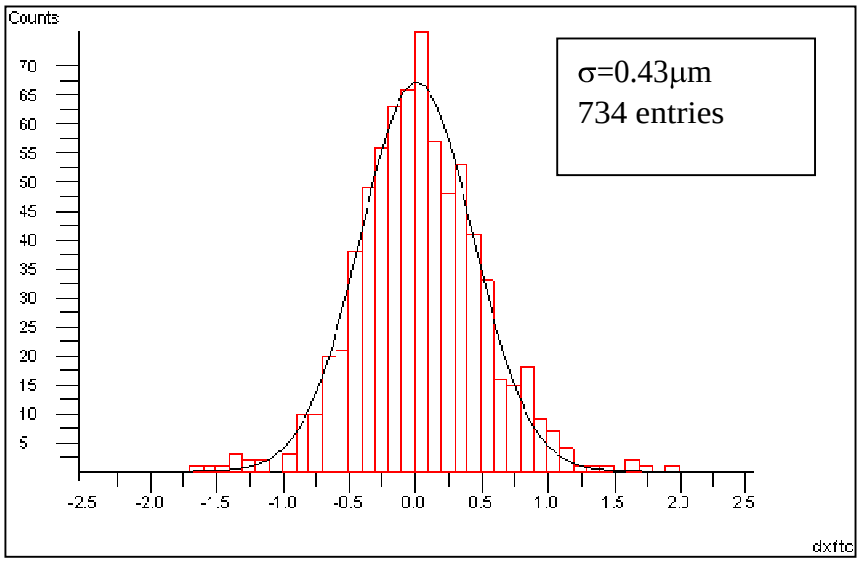

Fig . 6.6 – Alignment position residuals on 8 GeV pion tracks.

Event location is performed by selecting long stopping tracks intersecting one each other within custom thresholds; vertex reconstruction proceed among a selected emulsion volume and can be achieved by two different strategies. One strategy implies the computation of impact parameters between couple of stopping tracks; the other one implies the evaluation of bunches of tracks approaching a common point in a more restricted region. The precision obtained in the vertex point determination is affected by particle scattering trough lead plates and can be evaluated by Monte Carlo simulations. The IP determination allows the study of decays because it is a powerful tool to assign a track to a primary vertex without manual check inspection; furthermore in OPERA interaction point will be in lead so the IP correct determination will be crucial for vertex reconstruction. In order to tune this procedure and evaluate scanning system performances there have been several test exposures to an 8 GeV pion beam at CERN; the purpose was to train microscopes and algorithms to volume scanning and event reconstruction using pion interactions.

Pion exposures at CERN (June 2004)

The brick I analyzed in Salerno has been exposed to a 8 GeV pion beam at CERN, the track density was very low in order to simulate OPERA conditions; around 700 pion were accumulated during the exposure and their angles were (110; 0) mrad. Soon after the exposure the ECC has been exposed to cosmic rays for 24 hours and then depacked and developed. All

the plates have been scanned at 20 cm^2/h/side speed on a central area 36 cm^2 wide. From Monte Carlo simulations it is expected a pion interaction rate of 30% and the mean multiplicity of high energy tracks at vertex was 2; that means that around 60 pion interactions could be found in that brick. Due to a large amount of background tracks accumulated during the cosmic rays exposure the number of base-tracks was huge and the alignment has been performed in four different towers. Nevertheless the procedure was successful and it has been possible to align the whole brick. Vertex reconstruction software, AΩ Reconstruction, found hundreds of vertex candidates and I developed custom software to perform event selection. The basic criteria adopted to select interesting vertex topologies were the following:

- the mother track should have pion beam direction within 25 mrad tolerance
- daughter tracks should have a direction at least 50 mrad far from the mother one
- maximum Z distance of each track from the reconstructed vertex should be smaller than 3 emulsion-lead cells
- daughter tracks slope should be within 600 mrad
- tracks should consist of two base-tracks at least
- tracks should have at maximum a two cells hole between base-tracks
- tracks closest approach distance from the vertex should be less than 100 μm
- tracks IP at vertex should be less than 30 μm

Using this selection less than fifty topologies were tagged as interesting and I performed a visual inspection in emulsion. I searched for beam tracks in the downstream emulsion layer with respect of the vertex computed cell and for daughter tracks in the upstream layer. In case of a genuine pion interaction none of those tracks should have been found in emulsion. After this manual checks 31 interactions were located and confirmed as correctly reconstructed. Below are shown some examples (Fig. 6.8 & 6.9).

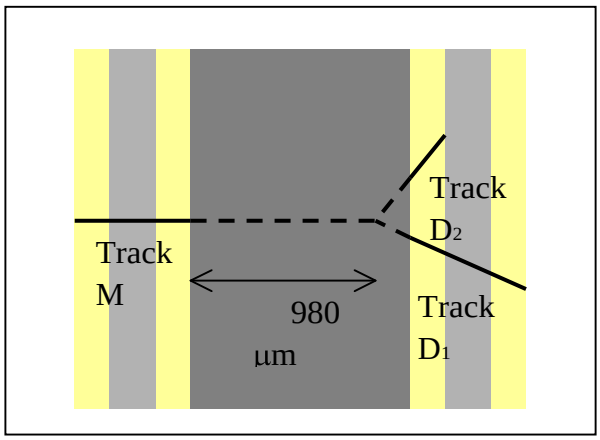

Fig. 6.8 – This vertex topology has two daughter tracks and the interaction point is near to the downstream emulsion.

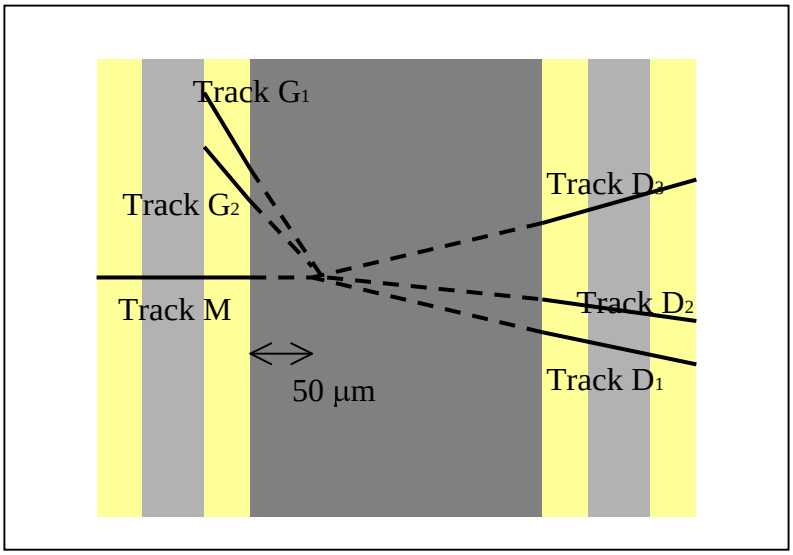

Fig. 6.8 – This vertex topology has three daughter tracks and the interaction point is near to the upstream emulsion; it has been possible to detect also two grey tracks emitted backwards.

OPERA scanning and event reconstruction strategy

After that first trial it has been planned a second pion beam exposure in order to test the OPERA scanning and event reconstructed strategy that implies CS doublet use and Data Base-driven scanning. The conceptual strategy is the following:

- General Scan on CS1: all micro-tracks will be picked up and recorded into the scanning Data Base
- Prediction Scan on CS2: tracks found on CS1 will be searched on CS2 one by one, in this case the software acting as scanning driver will read already found track positions and angles related to CS1 in the DB and schedule the CS2 scanning computing expected position on the downstream plate.
- CS doublet alignment: an off-line software will map CS1 on to CS2 and found matching tracks. At this stage tight alignment (<50μm) provided by X ray marks will be crucial to reduce random coincidence and avoid false scan-back candidates.
- Scan-back on ECC plates: selected scan back tracks will be searched along the whole ECC. The scanning will proceed trough intercalibration and scanning phases continuously checking with the DB. Preliminary plate intercalibration will be done acquiring the fiducial grid and three zones 1cm^2 wide and following cosmic long and straight selected tracks. In order to speed up this procedure that will take several minutes per plate it is needed a cosmic tracks density of 2-4 tracks/mm^2. Intercalibration will give affine transformation parameters used to follow selected tracks up to their

stopping point. A track will be searched for two more plates before declaring the stopping point has been found.

- Total Scan: a small area (Fig. 6.10) volume scanning will be applied around the stopping point in order to classify the vertex and confirm the presence of neutrino interaction. The volume area will be 5×5 mm^2×10 plates, skewed with primary scan-back track slope. The aim of this scanning is to filter out events with no sign of possible decay

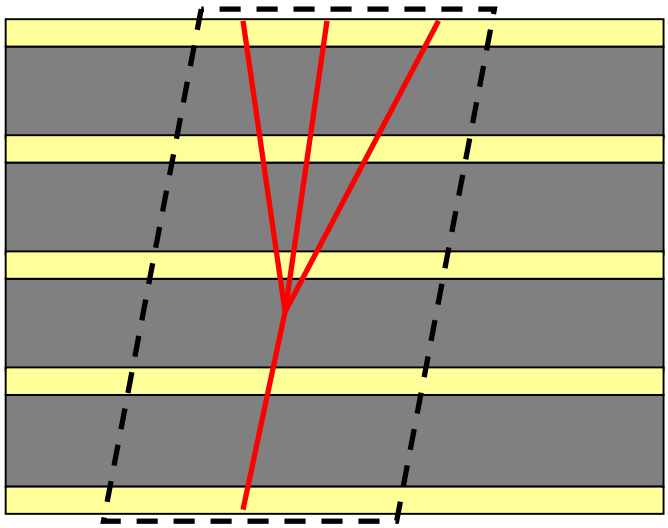

Fig. 6.10 – Total Scan volume.

topology and thus to reduce the number of events to be fully analyzed. The selection is mainly based on topological information; momentum measured by multiple scattering along the brick is only used to reject kink like topologies due to low momentum particles. Long decays, defined as decay topology where both parent and daughter tracks are recorded in at least one emulsion film, can be selected by requiring that both tracks converge within the errors and form between them a significant kink angle according to measurement errors. Short decays are those occurring in one cell and they are selected only by IP method. Interesting topologies will undergo more accurate and precise measurements and eventually visual inspections.

All those steps, apart from the last one, will be accomplished by fast and quasi on-line scanning, whose direction and low level selections are completely accomplished by the DB and its interface with the prediction and area scan drivers. In this scenario it is crucial to be able to take fast and reliable decision and to monitor the scanning quality; several of these tasks can be also accomplished by the DB routines. Several test are needed to tune this complicate procedure and that is why several test exposure have been planned to pion beam at CERN and to NuMI neutrino beam line at Fermi Lab. In the following pages I will report about the vertex location test realized at CERN PS pion beam and related scanning results in Salerno.

Pion exposure at CERN (November 2004)

This exposure was carefully planned in order to reproduce OPERA-like conditions as much as possible and 20 bricks were exposed and shared among 9 European Scanning laboratories. All the films used were refreshed at CERN small facility till the day before the exposure, spider brick packing was tested and the CS doublet was settled in custom boxes clipped to the ECC downstream face. Special care was devoted to prevent background tracks on CS doublet and they have been detached and developed soon after the exposure. The pion exposure was a very low density one and around 1200 pions (Fig 6.10) have been accumulated during each brick exposure. The cosmic rays exposure lasted 6 hours, giving a number of tracks available for plate intercalibration and alignment equal to 1 tks/mm^2.

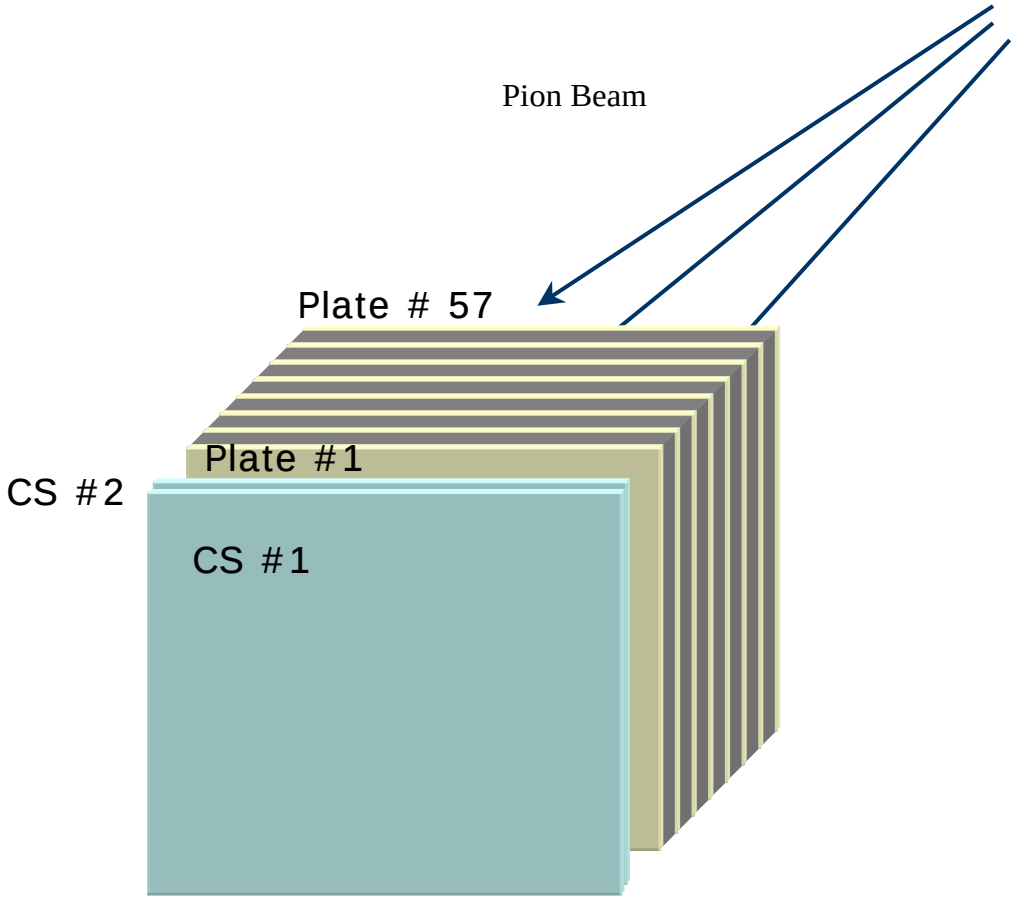

Fig. 6.11 – Beam exposure set-up; the beam track angle was (110;0)mrad.

CS doublet alignement

The first step was CS doublet alignment; track density on CS1 film was very high and it was more convenient to perform a general scan also on CS2 and then look for matching micro-tracks. High track density was unavoidable because refreshing and beam exposure were accomplished on the ground, anyway low momentum tracks were rejected using a quality cut selection on the basis of top-bottom linking quality as shown in Fig. 6.12.

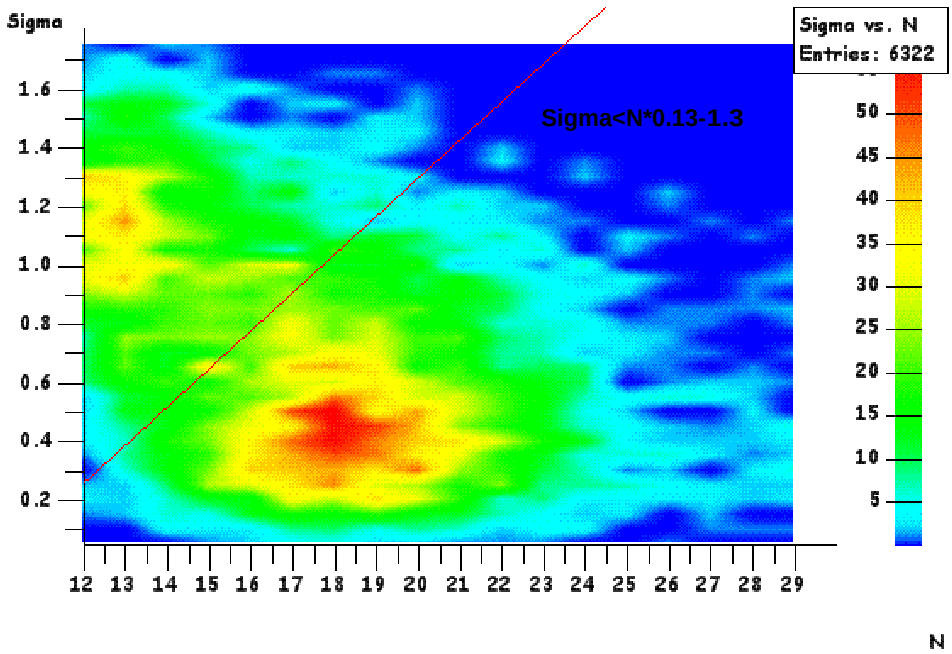

Fig. 6.12 – Quality cut among signal and background tracks population.

Alignment has been accomplished mapping CS1 on CS2 and computing translation and rotations along X and Y axes, as it is possible to see in the following plots (Fig. 6.13 & 6.14) that a considerable rotation should be applied between the two data sample to let them match.

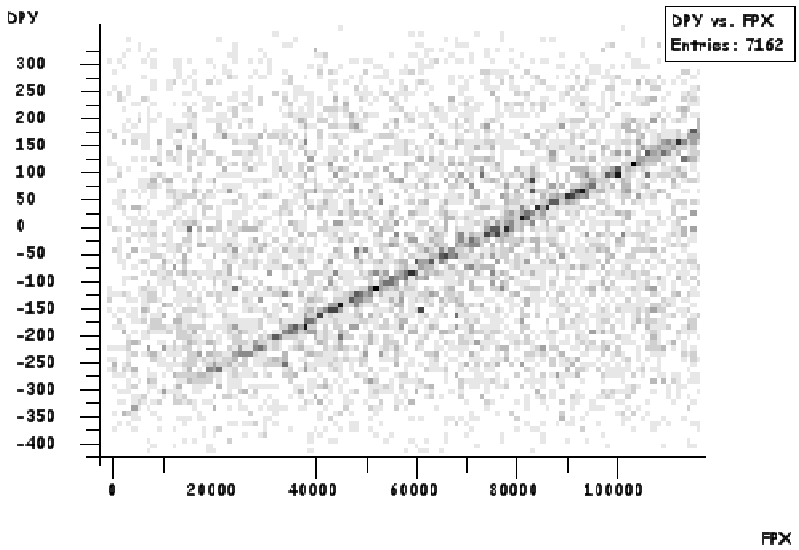

Fig. 6.13 – Y displacement versus X coordinate.

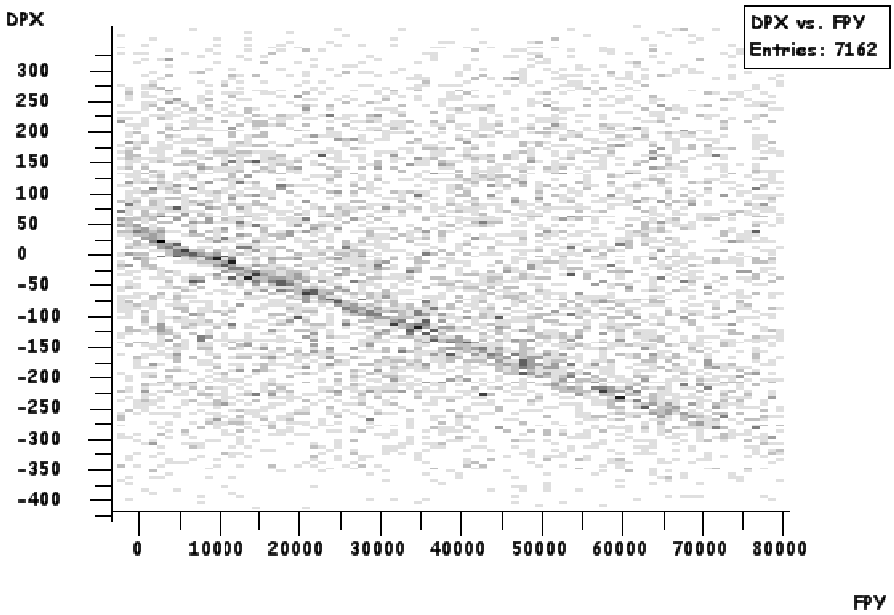

Fig. 6.14 – X displacement versus Y coordinate.

Selecting only tracks having beam direction it was possible to avoid bad alignment due to low momentum tracks, a cut is applied 50 mrad within the beam slope and the residuals tracks alignment was successful and background free as it is possible to see in the following plots. The position tolerance threshold chosen was 300 μm and the angular one was 0.01 rad; applying these cuts I got 7162 tks ->(57 tks/cm^2) matching tracks and 722 tks ->(5.7 tks/cm^2) of them were beam like. Even if the alignment was successful I found that apparently CS films have a relative distance of 900 μm, this result is really strange because CS doublet was vacuum packed and no air leakages were detected inside the box.

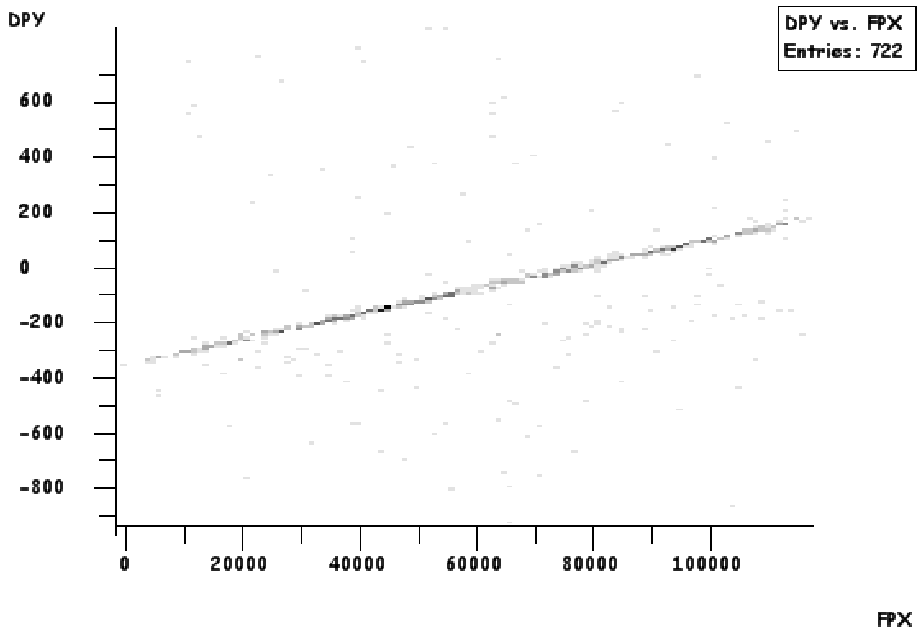

Fig. 6.15 – Y displacement versus X coordinate.

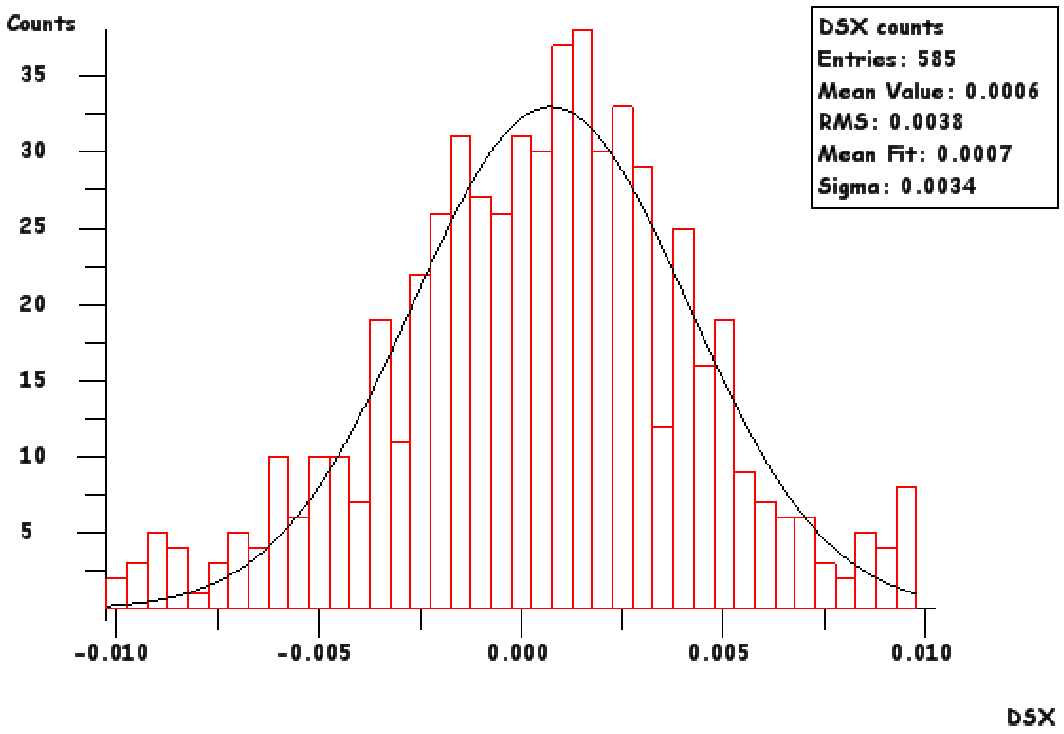

Fig. 6.16 – Angular residuals on aligned beam tracks.

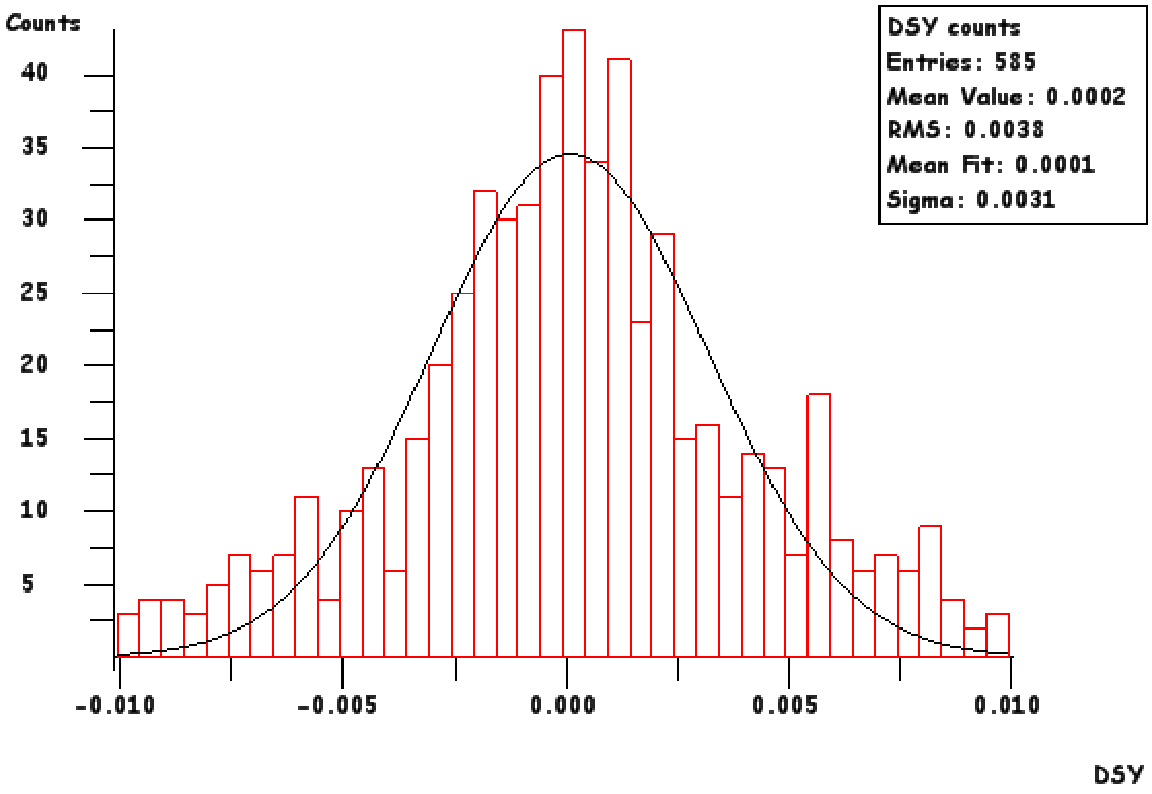

CS doublet to ECC alignment

The second step was CS doublet to ECC alignment; in this case the longitudinal distance was nominally around 5 mm and the matching procedure should be driven by beam tracks. Affine transformation parameters were computed on the basis of good tracks and then propagated to the whole sample having 500 μm position tolerance and 10 mrad angular tolerance. In this case the film distance found was 4700 μm, in agreement with experimental set-up.
1247 matches -> (9.9 tks/cm^2) could be found on plate 1, this number was in good agreement also with beam exposure specifications.

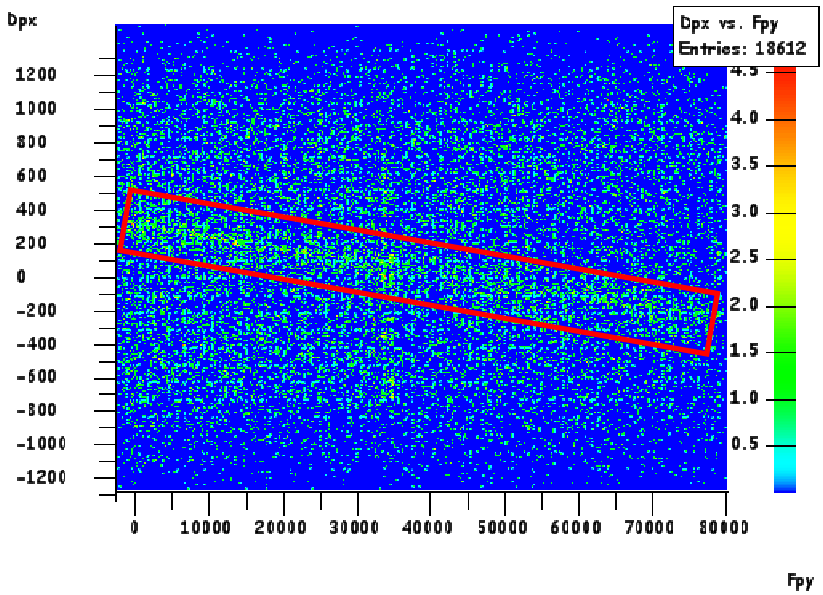

Fig. 6.17 – Good tracks selection on the basis of residual rotation computing.

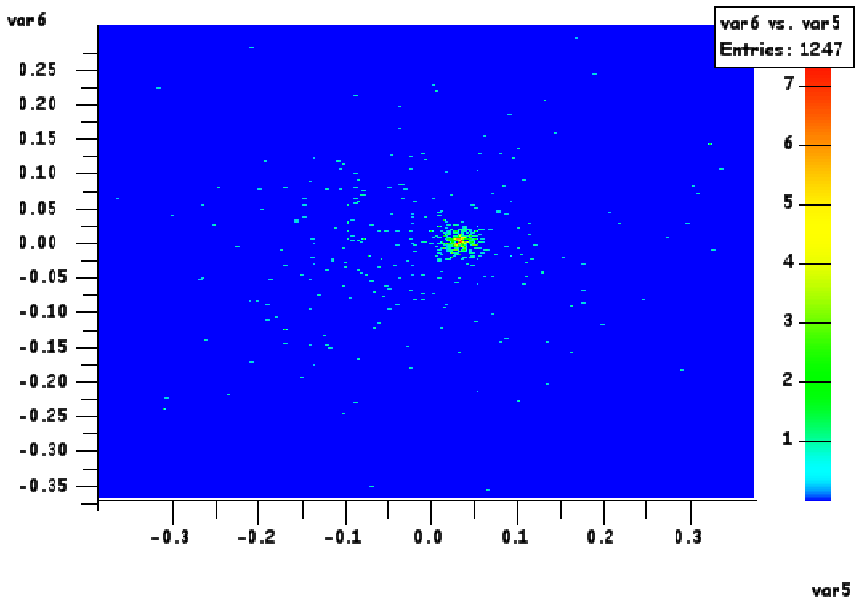

Fig. 6.18 – Selected tracks angular distribution.

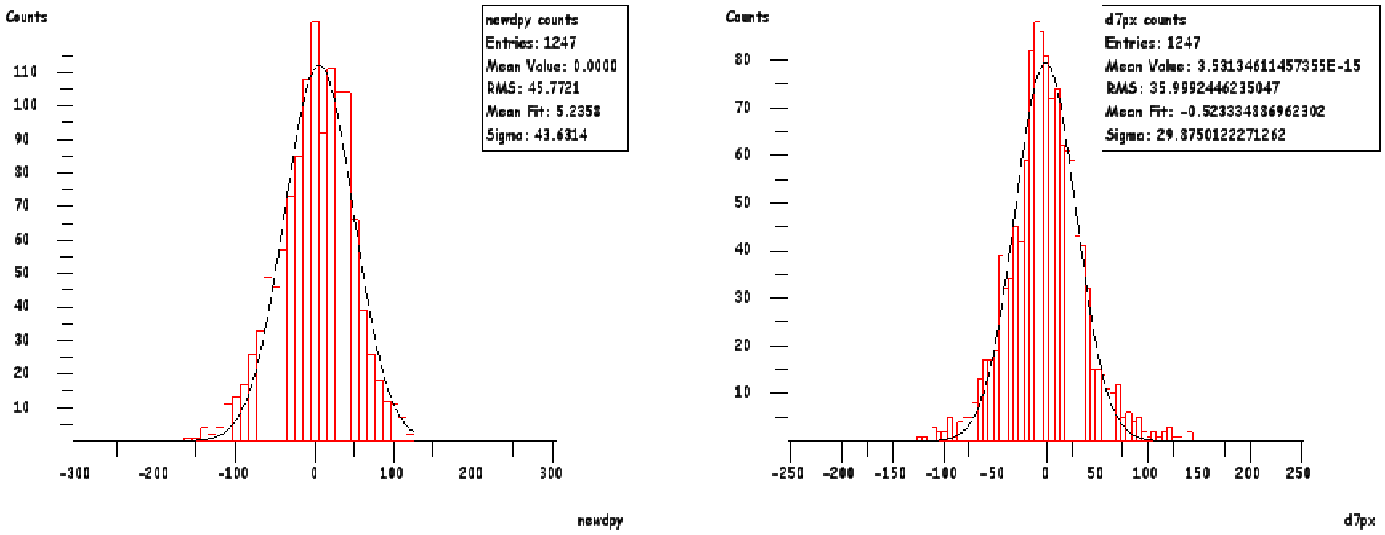

Fig . 6.19 – Position and angular residuals for all the matched tracks.

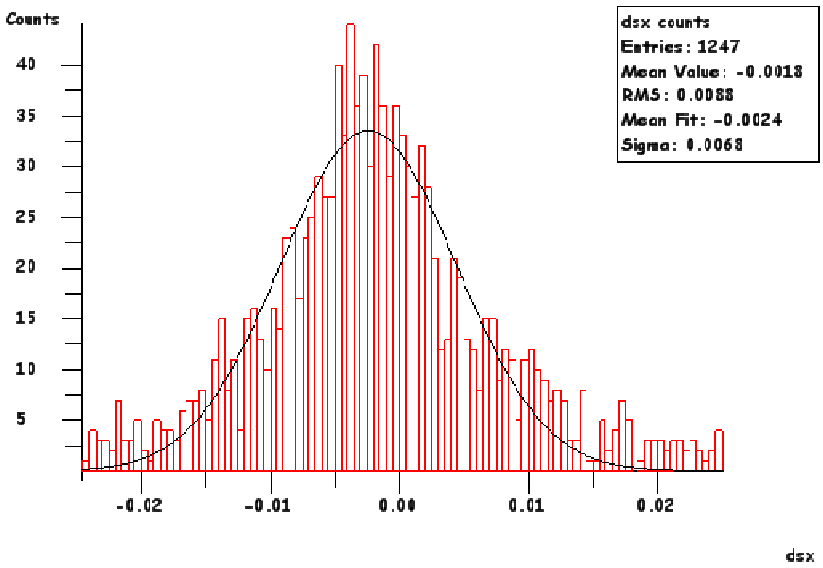

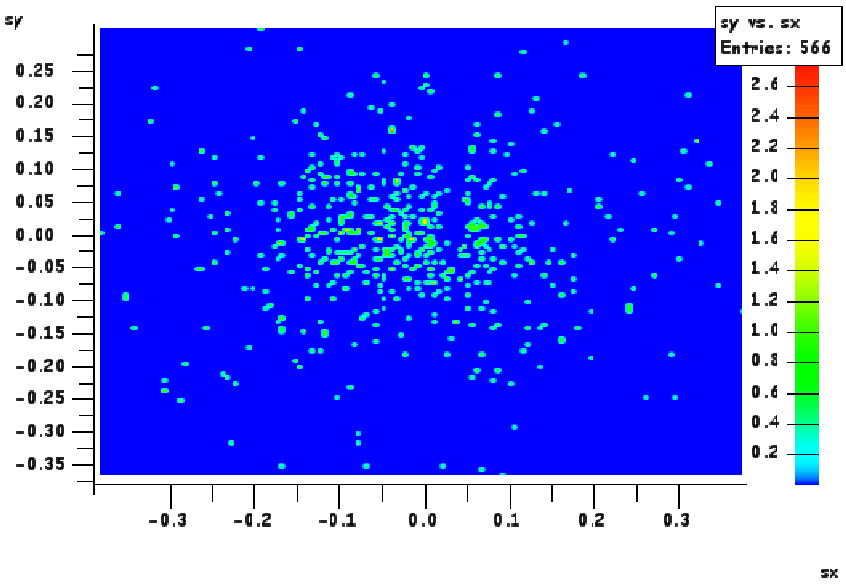

Fig. 6.20 – Angular distribution of out of beam tracks.

The angular distribution of out of beam tracks (Fig. 6.20) shows a sample of 566/1247 tracks having a high GD (Fig. 6.21), this result confirmed that low momentum particles have been rejected by the alignment procedure and that a scan-back could be started using that sample.

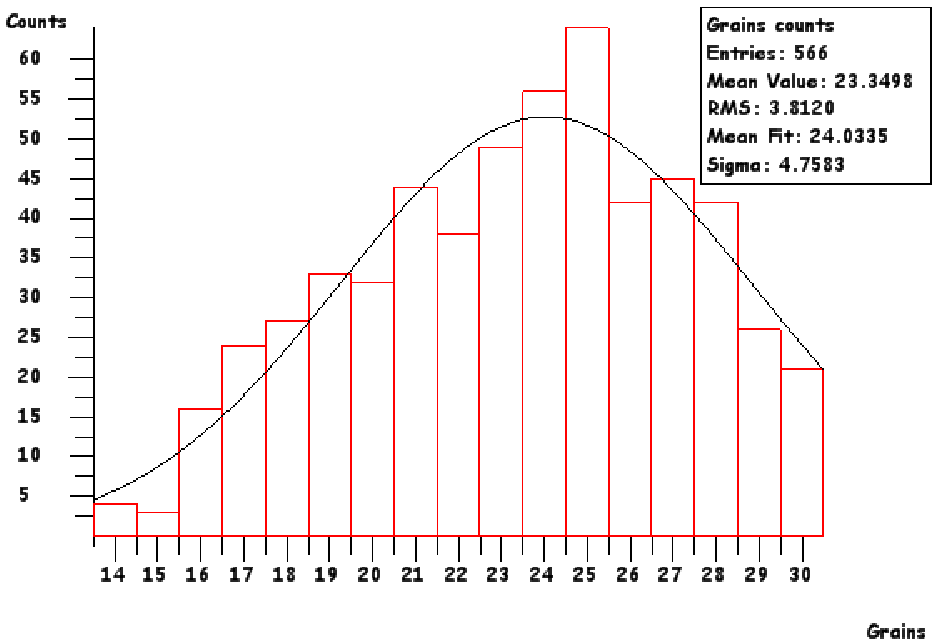

Fig. 6.21 – GD distribution for aligned out of beam tracks.

Scan back/Scan forth

All the selected tracks were followed back via the usual DB driven scan back procedure. The intercalibration procedure failed in few cases because of the old CHORUS grid was damaged but it has been possible to perform the entire brick scan. Analyzing position and angular resolution on long tracks I noticed a difference between high energy punch trough cosmic tracks and low energy pions interaction products; in both cases there were Gaussian residuals distributions but in the case of low energy tracks the angular alignment was worse and there are tails due to random multiple Coulomb scattering (Fig. 6.22).

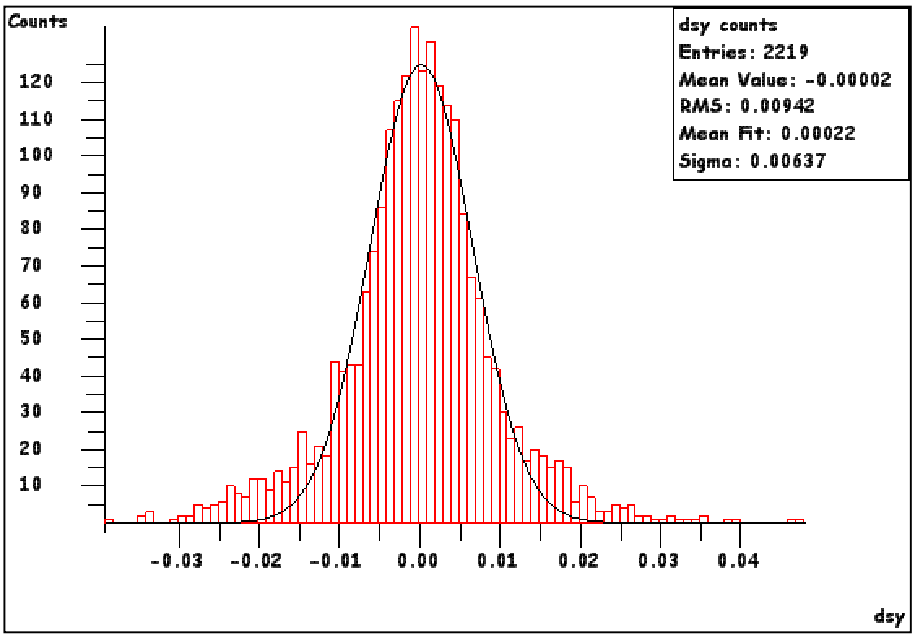

Fig. 6.22 - Angular residuals for all scan-back tracks, large tails are due to MCS of low momentum tracks produced in pion interactions.

Since the scan-back procedure was at its early beginning test phase it was accomplished also a reverse scan-back procedure called scan-forth; in this case plate 57 (most upstream) has been scanned and all the good tracks were followed up to plate 1. In this procedure also beam tracks can be followed and, since they are straighter than interaction products because of their higher momentum, better resolutions were achieved and also stopping points had a better repeatability (Fig. 6.23). In Figure 6.24 a longitudinal distribution of stopping plates is reported, most of the tracks stopped in the upstream plates and most likely they were beam or cosmic tracks, otherwise stopping points have a constant spread along the ECC depth and only the three plates affected by unsuccessful intercalibration showed different behavior.

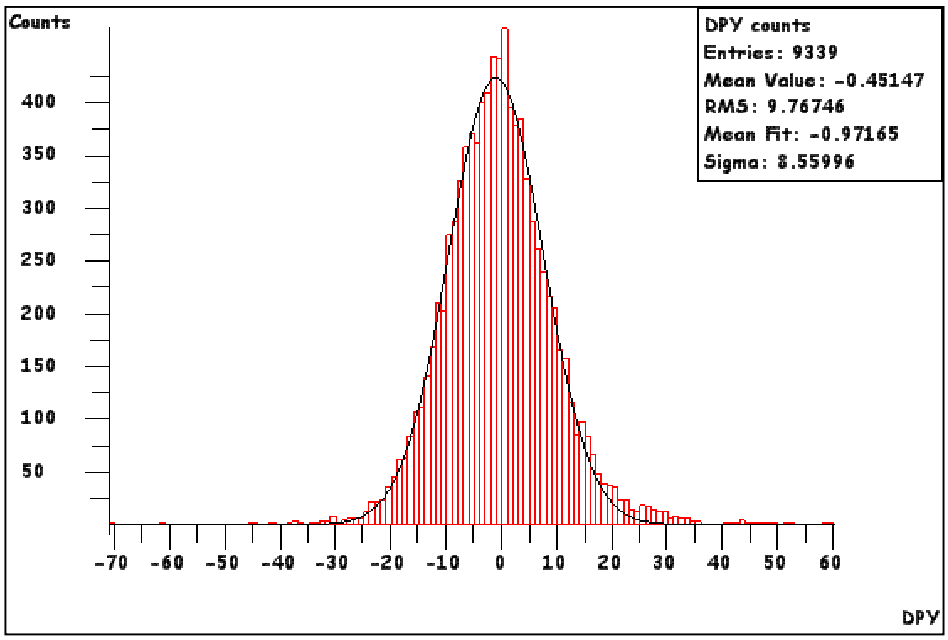

Fig. 6.23 – Position alignment residuals for scan-forth tracks.

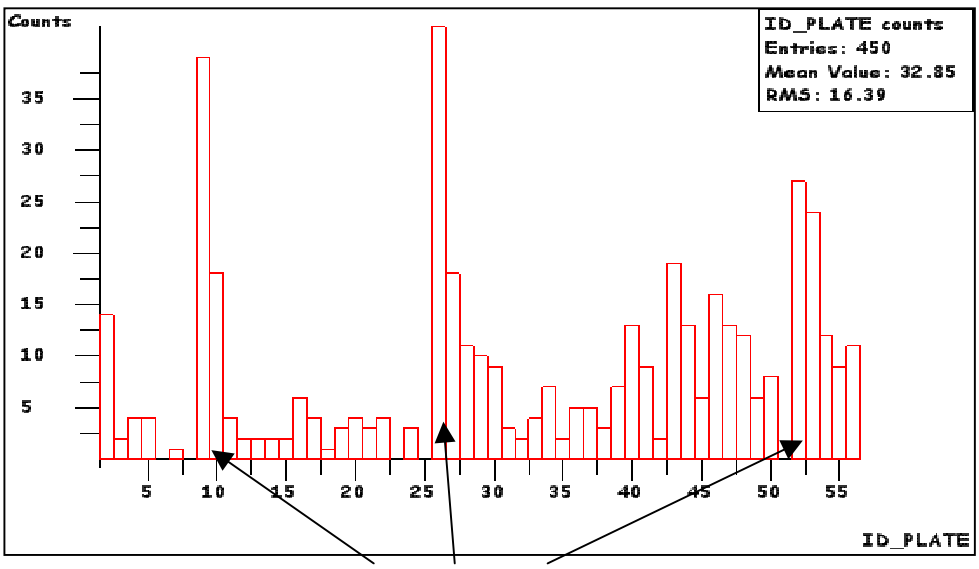

Intercalibration problems on damaged plates (old CHORUS grid)

Fig. 6.24 – Stopping points distribution along the ECC depth.

There have been found 450 stopping points and defining the Fill factor as the ratio between the number of plates where base track has been found and available plates it was possible to compare Scan-back and Scan-forth performances (Fig. 6.25 & 6.26). A track was flagged as seen if was within ΔSlope < 0.03 rad and ΔPosition < 50 μm/70 μm (depending on the number of consecutive missing plates); it there were several candidates resembling to the same tracks the one having a better position agreement was chosen. Fill factor in case of scan-back was 89% and in case of scan-forth was 92%; the difference could be explained by the different track momentum giving different scattering behavior

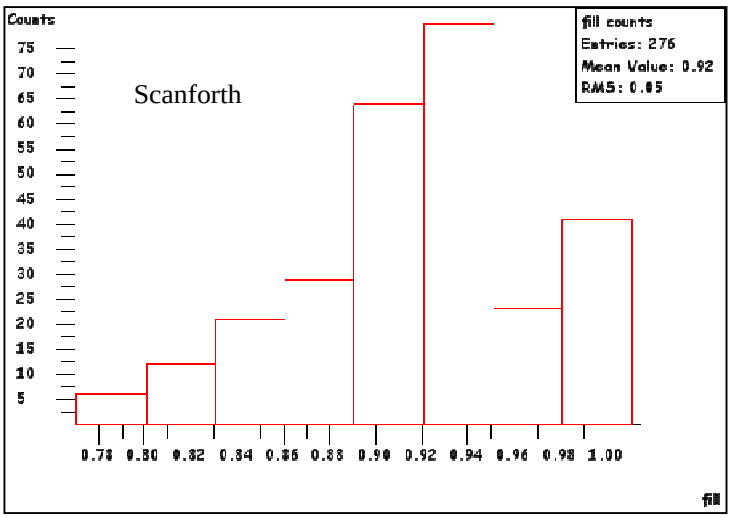

Fig. 6.25 – Scan-forth fill factor.

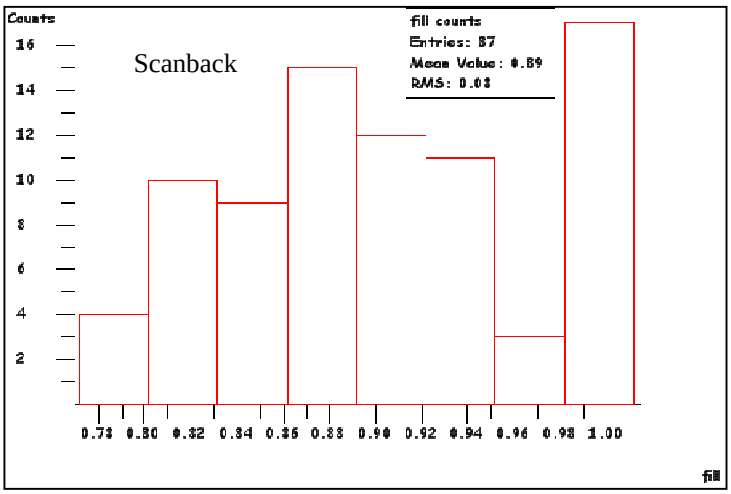

Fig. 6.26 – Scan- back fill factor.

Total Scan and vertex confirmation

Total Scan has been performed around all 450 stopping points over the usual volume. Aligned areas were processed by AΩ Reconstruction software and, after event selection based on the criteria previously described, 125 vertices were found and fully reconstructed. Stopping tracks have been visually inspected in emulsion and then all the interactions were confirmed.
In Fig. 6.27 there is the track average distance from the fitted vertex point, the mean value is 8 μm but there is a long tail due to severe scattering in lead plates containing the pion interaction.

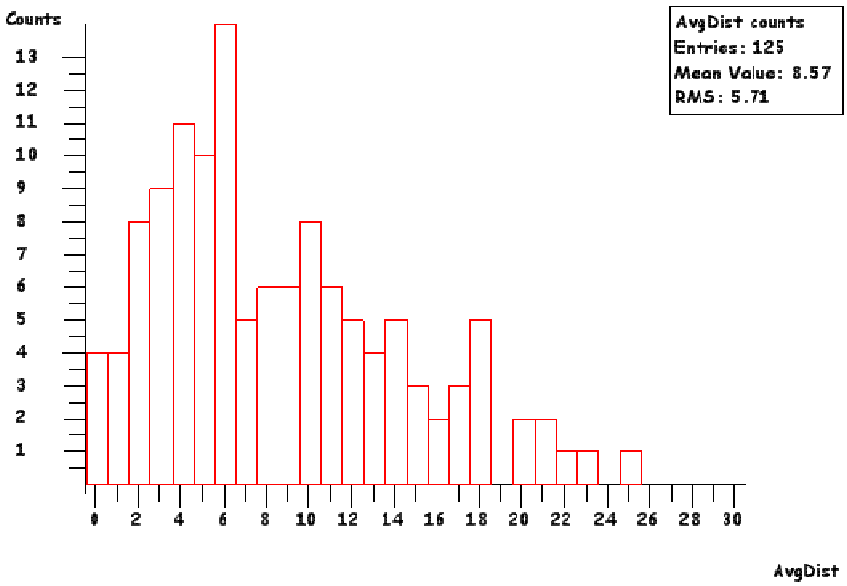

Fig. 6.27 - Average distance of track extrapolations from vertex point

This vertex reconstruction precision allows full event study and decay search as well if needed. Reconstructed vertices have been compared with MC truth events and it has been possible to evaluate the track multiplicity ratio between real data and simulated ones. The number of charged prongs is strictly dependent on pion energy and high multiplicity events could be easily found and better reconstructed. Thus a correct prong shape distribution should be correct with European Scanning System vertex location and reconstruction efficiency. Presently in Salerno we are evaluating those efficiencies; for this purpose it is possible to store simulated data as emulsion data and perform on that alignment and vertex reconstructions.
In conclusion this vertex location test showed that the most crucial point in terms of scanning load and time will be the vertex location step; that is strictly related to CS detector efficiency and relies on good track selection. In case of CERN exposure CS had a large number of background tracks so several fake scan-back paths were followed arising heavy scanning load; furthermore among scan-back procedure the plate to plate intercalibration procedure is the longer and it is demanded to tune in a proper way the cosmic ray exposure in order to minimize the

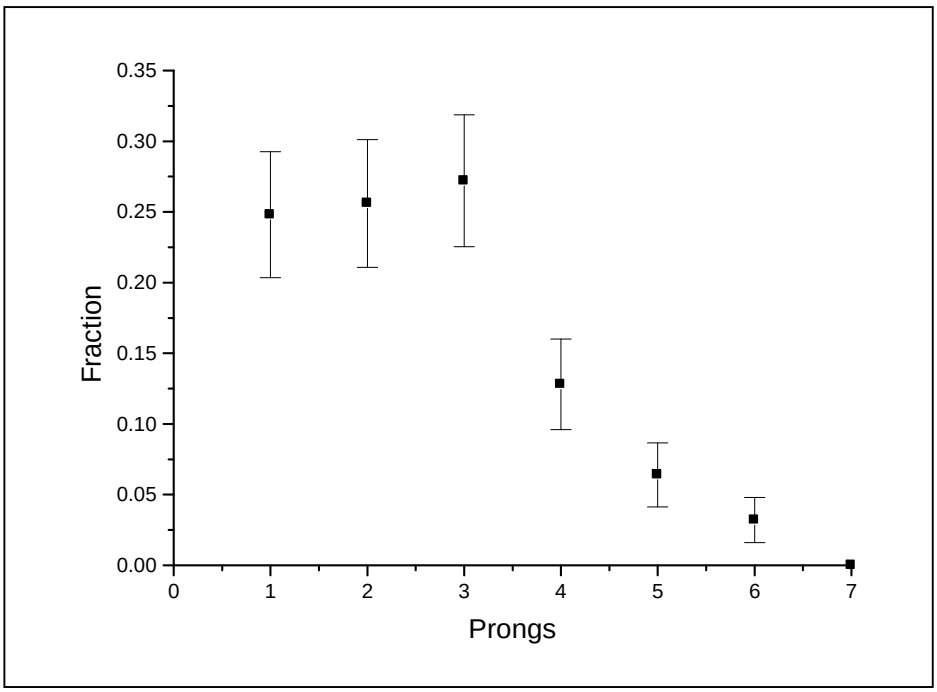

Fig. 6.28 – Number of charged prongs at reconstructed vertices.

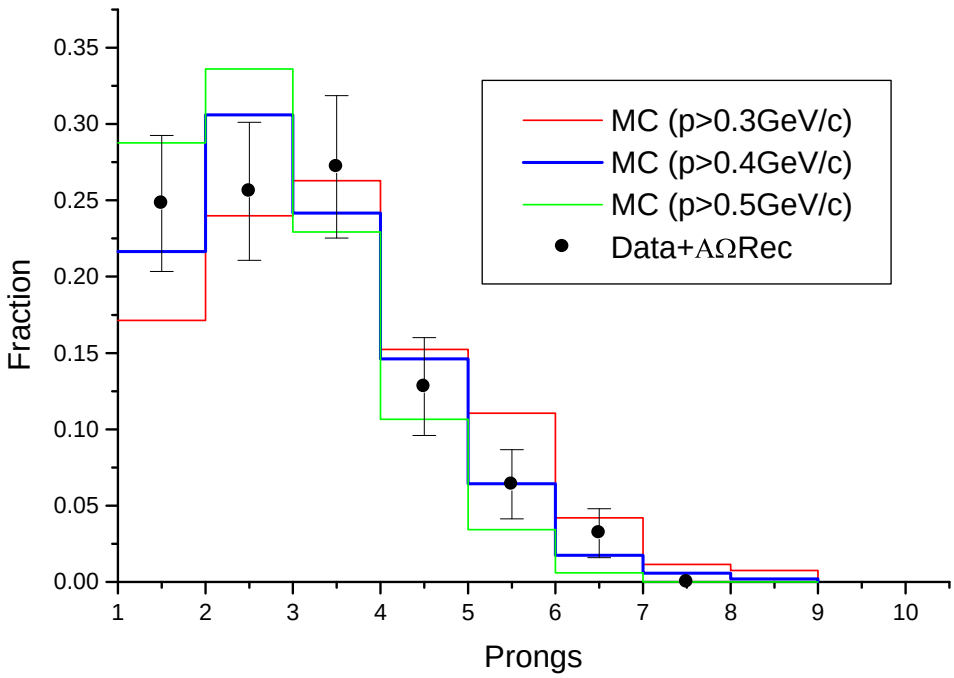

Fig. 6.29 -Prong number distribution: shape comparison between Salerno data sample and MC truth data.

intercalibration scanning areas and provide precise alignment as well.
Meanwhile the whole scanning procedure has been accomplished and several pion interactions were correctly reconstructed; this test shows that the European Scanning system is well on route for OPERA physical run.
The scanning and computing infrastructure has proven also to be strong and reliable enough to handle the huge amount of emulsion data coming from ECC scanning; both on-line and off-line reconstruction tasks can be accomplished without delays or problems.

Conclusions

The OPERA experiment is presently close to physical run and data acquisition, the detector construction in LNGS underground laboratory is well advanced and the emulsion/lead target will be assembled in ECC modular structure within few months. All the R&D activities described in this thesis were fundamental to ensure the experiment feasibility and success. OPERA aim is to locate, reconstruct and precisely analyze neutrino interactions, the searched signal is very rare and so everything must be well tuned and carefully planned.

In this scenario it is vital to guarantee long term stability and quality of all precious emulsion films; thus the large number of test performed on emulsion/lead/plastic compatibility and on emulsion refreshing and development was deserved; the availability of custom software tools described here made this kind of R&D fruitful and meaningful.

Remarkable improvements were reported on ECC packing option and mechanical specifications reached will allow precise emulsion measurements and excellent plate to plate alignment.

All emulsion related activities were performed in Europe and in Japan and continuous cross-check and collaboration were needed; my stay in Japan was very important in order to share experiences and to plan wisely the development of more than three thousands of films per day at LNGS. The development and refreshing procedure have been fixed and emulsion quality gained in terms of fog density and sensitivity will lead to a signal/background ratio suitable for fast emulsion scanning.

The early step of a fast and precise neutrino interaction location is the plate to plate intercalibration; the gridding and labeling machine that I designed and realized accomplished successfully this task and has been validated by several scanning laboratories among Europe.

In the last section I described a first attempt to perform event location and reconstruction; from the significant number of located pion interactions it turns out that the European Scanning System is working properly and can afford the OPERA challenge. Both speed and precision requested have been fulfilled and there is still room for improving our efficiency and purity, tuning event reconstruction algorithms on the basis of Monte Carlo simulations and experimental data.

The System structure is flexible and robust and the Data Base approach chosen will afford the management of a huge amount of data.

References

1. Walter H. Barkas – “Nuclear research emulsion” - 1963 Academic Press, New York and London.
2. http://cwp.library.ucla.edu/articles/blau/blau-rosenz.html
3. http://www.ilford.com/html/us_english/prod_html/nuclear/ParticlePhysics.html
4. W. F. Berg – “Latent image formation in photographic silver halide gelatine emulsions”- 1946 Rep. Prog. Phys. 11 248-297.
5. S. Stapnes – “Instrumentation for high energy physics” – Oslo University Lectures
6. G. Romano – “Emulsioni Nucleari”- 1978 , Rome University.
7. W. Pauli's bold suggestion of the existence of a new particle, the neutrino, was never published. The idea was put forth in a letter dated December 4, 1930, to the attendees of a Conference in Tubingen. It was addressed to "Dear Radioactive Ladies and Gentlemen." Pauli himself was not able to participate in the meeting because of a prior commitment to attend a ball in Zurich.
8. N. Solomey, “The Elusive Neutrino”- Scientific American Library, 1997- pp. 16-17.
9. F. Reines and C. L. Cowan., Phys. Rev. 92, 830 (L) (1953).
10. M. Goldhaber, L. Grodzins, and A. W. Sunyar, Phys. Rev. 109, 1015 (L).
11. G. Danby et al., Phys. Rev. Lett. 9, 36 (1962).
12. R. Davis, Jr., Phys. Rev. Lett. 12, 303 (1964).
13. DONUT collaboration, Nuclear Physics B, 77 (1999) 259-264.
14. B. Pontecorvo,Zh. Eksp. Theor. Fiz. 33, 549 (1957).
15. G. S. Abrams et al., Phys. Rev. Lett. 63, 2173 (1989).
16. S. Hegarty, K. Potter, and E. Quercigh (World Scientific, 1992), pp. 1-26.
17. Fleischmann L. et al., J.Low. Temp. Phys., 119 (2000) 615.
18. Assamagan K. et al., Eur. Phys. Rev. , 53 (1996) 6065.
19. Barate R., et al., Eur. Phys. J. C, 2 (1998) 3.
20. E. Bellotti and L.Zanotti – “Experimental aspects of solar neutrino physics” – 2002, Varenna – Course CLII on Neutrino Physics
21. Fukuda et al., Phys. Rev. Lett., 86 2001) 5651.
22. Gallex collaboration, Phys. Lett. B, 314 (1993) 445.
23. Gallex collaboration, Phys. Lett. B, 490 (2000) 16.
24. SNO collaboration, Phys. Rev. Lett., 89 (2002) 011301.
25. Inoue. K., Nucl. Phys. B, 145 (2005) 11-16.
26. Super Kamiokande collaboration, Nucl. Phys. B, 145 (2005) 112-115.
27. K2K collaboration, Nucl. Phys. B, 149 (2005) 114-121.
28. Thomson M.A. , Nucl. Phys. B, 143 (2005) 246-256.
29. De Lellis G., Nucl. Phys. B, 142 (2005) 109-114
30. Ushida et al., Phys. Rev. Lett., (1981) 47,24
31. CHORUS collaboration, NIM ,A 401 (1997), 7-44.

32. CHORUS collaboration , CERN- SPSC/90-42 (1993) Geneva.
33. G.Rosa et al., NIM A 394 (1997) 357-367.
34. C. Bozza – Ph.D. Thesis (2000) Salerno University.
35. C.Sirignano – Degree Thesis (2001) Salerno University.
36. CHORUS collaboration, CERN- EP/2000- 147.
37. CHORUS collaboration, Physics Letters B, 613, (2005), 105-117.
38. CHORUS collaboration, Physics Letters B, 555, (2003), 156-166.
39. CHORUS collaboration, Nuclear Physics B, 718, (2005I, 35-54.
40. CHORUS collaboration, Physics Letters B, 604, (2004), 11-21.
41. OPERA collaboration, Experiment proposal (2000).
42. C.Sirignano, Opera collaboration meeting (2002).
43. S.Buontempo, Opera collaboration meeing (2003).
44. T.Nakamura - Ph.D. Thesis (2004) Nagoya University
45. OPERA collaboration, "The CS detector in OPERA" –CERN/SPSC/2002-021
46. G. Rosa et al., "Automatic development of OPERA emulsion films", (2004).
47. C.Sirignano, Opera collaboration meeting (2005).
48. C.Bozza et al., NIM A (2005),

Contents